SELF-EXCITED OSCILLATIONS OF THE IMPINGING PLANAR JET

Self-Excited Oscillations of the Impinging Planar Jet

By

DAVID ARTHURS, M.A.SC., B. ENG.

A Thesis

Submitted to the School of Graduate Studies

in Partial Fulfillment of the Requirements

for the Degree

Doctor of Philosophy

McMaster University

DOCTOR OF PHILOSOPHY (2012)	McMaster University
(Mechanical Engineering)	Hamilton, Ontario

TITLE:	Self-Excited Oscillations of the Impinging Planar Jet
AUTHOR:	David Arthurs, M.A.Sc., B.Eng. (McMaster University)
SUPERVISOR:	Professor Samir Ziada
NUMBER OF PAGES:	xxv, 271

“*Success is not the result of spontaneous combustion.*
You must first set yourself on fire”

Fred Shero

ABSTRACT

This thesis experimentally investigates the geometry of a high-speed subsonic planar jet impinging orthogonally on a large, rigid plate at some distance downstream. This geometry has been found to be liable to the production of intense narrowband acoustic tones produced by self-excited flow oscillations for a range of impingement ratio, Mach number and nozzle thickness. Self-excited flows and acoustic tones were found to be generated in two distinct flow regimes: a linear regime occurring at relatively low Mach number, and a fluid-resonant regime occurring at higher Mach numbers. The linear regime has been found to generate acoustic tones exhibiting relatively low pressure amplitudes with frequencies which scale approximately linearly with increasing Mach number, and is produced by a traditional feedback mechanism which couples the jet instabilities with the impingement of the flow at the downstream surface. The fluid-resonant regime produces tones as a result of coupling between the unstable hydrodynamic modes of the jet and trapped acoustic modes occurring between the nozzle and the plate, and produces tones at significantly larger amplitudes, and at frequencies which are relatively invariant with increasing Mach number and impingement ratio. Coupling with these trapped acoustic modes was found to dominate the self-excited response of the system in the fluid-resonant regime, with the frequencies of these acoustic modes determining the unstable mode of the jet being excited, and with the impingement ratio of the flow having only minor effects related to the convection speed.

Phase-locked PIV measurements have revealed that self-excited flow oscillations in the linear regime are produced by a single flapping mode of the jet column, whereas tones in the fluid-resonant regime are produced by a series of five anti-symmetric modes of the jet, along with a single symmetric mode occurring for small impingement ratios. Fluctuating velocity amplitudes in the fluid-resonant regime have been found to be very large, with peak-to-peak fluctuation amplitudes in excess of 70% of the initial jet velocity for flow configurations with high Mach number. The behavior of large coherent flow structures forming in the flow has been investigated, and the structures have been found to convect relatively slowly, at ~40% of the initial jet velocity in the initial region, and with significant slowing in the downstream region. Measurements of structure circulation have revealed that vortices begin to interact with the plate surface after travelling approximately 75% of the total impingement distance. Results of these measurements have been used to develop new expressions for the effective impingement length and convection velocity of coherent flow structures for planar impinging jets. These expressions have been implemented in a feedback model for the impinging planar jet, which has been found to predict the oscillation frequency accurately for the complete range of impingement ratio, Mach number and nozzle thickness examined in this work.

ACKNOWLEDGEMENTS

The work presented in this thesis would not have been possible but for the contributions of the many people in my life, both in personal and professional relationships, who have supported me over the course of my career.

I would like to express my sincere gratitude to my supervisor, Samir Ziada, for his support, guidance and advice as I have completed my graduate studies. His actions as a mentor, supervisor and friend have benefited me enormously, and I will forever be grateful for his help.

My accomplishments would not have been possible without the love and support of my family and friends, especially my wife Clare, whose love and understanding has been the rock that has anchored me these past seven years.

Finally, I wish to extend my sincere gratitude to my colleagues at McMaster, members of my committee, and to the university staff, particularly Ron Lodewyks, Mark McKenzie, Jim McLaren, Joe Verhaeghe and JP Talon, whose technical expertise proved invaluable in my work.

TABLE OF CONTENTS

LIST OF FIGURES

LIST OF TABLES

CHAPTER 1

Introduction

1.1 Motivation

Impinging jets represent a class of flow that have found widespread use in many industrial applications as a result of their many useful properties, which include:

1. High Nusselt numbers (Nu) at the impingement surface in the impingement and wall-jet regions of the flow, resulting in high rates of heat transfer, making these flows useful in thermal processing applications.
2. High levels of shear stress at the impingement surface in the impingement and wall-jet regions of the flow, allowing these flows to be used for various coating control applications, such as gas-wiping of galvanized sheet steel, as well as for part drying and blow-off.
3. Intense turbulent mixing in the developing, impingement and wall-jet regions of the flow, leading to these geometries being used in various reactor geometries used in chemical processing.
4. High Sherwood numbers (Sh) at the impingement surface, a measure of the flows effectiveness for mass-transfer applications, resulting in impinging jets

being useful for a variety of material deposition processes, such as plasma-spray and cold-spraying applications.

As a result of the very high Nusselt numbers produced in the impingement regions of these flows, impinging jet flows are widely used in thermal processing applications, including the production and tempering of plate glass (Lee & Viskanta, 2012)[1], where these flows are used for both heating and cooling operations, thermal processing of stock material used in forming operations (Ferrari et al., 2003), and the cooling of electronics (El-Shiekh & Garmiella, 2000) and turbine blades (Li et al., 2011), among may others. These applications use axisymmetric and planar jet nozzles both alone and in banks, with single axisymmetric nozzles often used where spot cooling is required, and planar nozzles and banks of axisymmetric nozzles used for cooling of larger areas.

These flows also produce very high shear stresses at the impingement surface, making them attractive for use in coating control, part drying and blow-off applications, with one major application being the gas-wiping process used for galvanization of sheet steel (Arthurs & Ziada, 2012), where a pair of planar impinging jets are used to control the coating thickness of molten Zinc applied to a continuously moving steel sheet. Similar processes are often used in the production of polymer films (Steinberg, 1974), where these flows are used in a hybrid coating control/heat transfer application.

Impinging jets are also used in various applications for mixing enhancement, as in the case of various combustion geometries such as impinging flame jets (Schuller et al.,

[1] References in Chapters 1 and 2 are contained in the References Section at the end of this thesis. References in each journal article are self-contained in their respective chapter.

2002) and reactors used in chemical processing (Liu et al., 2009). Impinging jet and cross flow jet reactors are known to produce efficient micromixing, resulting in homogenous chemical reactions and small particle size of resulting precipitates, and combustion geometries employing impinging jets are known to produce very high rates of heat transfer that may be improved by external excitation or promoting self-excited flows.

Due to their high Sherwood number, impinging jets using supersonic flows are frequently used for particle deposition in the cold-spray process (Gärtner et al., 2006), which are used to apply thin coatings of materials that are difficult to deposit using other methods. In this process, microscale particles are added to the impinging flow, which upon impacting the downstream impingement surface, plastically deform and are fused to the impingement surface, resulting in the mechanical deposition of the seeded material to the substrate. This process is used extensively in the repair of turbine blades (Ogawa & Seo, 2006) to deposit material to areas of significant wear, and is attractive in this application because unlike other repair techniques such as thermal spraying or welding, this process does not involve significant heating that may impact the metallurgy of the substrate.

Under certain conditions, impinging jet flows are known to be liable to the production of very intense narrowband acoustic tones generated by a feedback mechanism between instabilities in the jet free shear layer and pressure perturbations produced by the impingement of the flow. The instabilities in the initial shear layer grow exponentially as they convect downstream, eventually rolling up to form large-scale coherent flow structures. The structures organize themselves in a pattern defined by the hydrodynamic mode of the jet, with both axisymmetric and helical modes having been documented for impinging axisymmetric jets, and symmetric (varicose) and anti-symmetric (sinuous) modes having been observed in the planar case. The structures then impinge on the downstream surface, with the modification of the structure vorticity giving rise to pressure fluctuations which travel back upstream to the leading edge of the nozzle, enhancing the instabilities in the initial shear layer, completing the feedback cycle.

The very intense acoustic tones and strong velocity fluctuations resulting from this feedback mechanism can be problematic in many practical applications, with high levels of noise leading to issues in industrial processes due to ergonomic restrictions related to noise exposure. In addition, acoustic fluctuations produced in the impingement zone can excite acoustic modes in surrounding components in confined systems, or can induce mechanical vibrations if the frequency of the mechanical modes is close to that of the acoustic fluctuations. One practical example of this phenomenon with which the author has first hand experience, is that high-amplitude acoustic tones near f=10.5kHz have been found to excite mechanical modes in the actuator arm of laptop hard disk drives. Exposure to acoustic fluctuations at this specific frequency prevented reading or writing of any data from the drives. However, a slight shift in the tone frequency, either higher or lower, resulted in the drive resuming normal operation. The drives were found to be excited entirely by acoustic waves propagating in air, as the problem persisted even after significant steps were taken to eliminate the propagation of structure-borne sound and vibration.

The feedback mechanism also produces strong periodic velocity fluctuations in the jet column, impingement region, and wall-jet regions of the flow, which can also be problematic in many cases, with oscillation of impinging flame jets often associated with incidents of extinguished combustion. The large dynamic pressure oscillations at the impingement surface may also present a potential source of mechanical vibrations at the impingement surface, though the author is not aware of any cases currently documented in the literature.

The effect of acoustic and velocity fluctuations in the self-excited flow has also been shown to have beneficial effects; with many authors having observed increased heat transfer rates for self-excited and externally excited flows in thermal processing applications. Impinging axisymmetric jets using both self-excited and externally-excited flows have been observed to produce significantly higher local Nusselt numbers in the area of structure impingement compared with equivalent cases using steady flows, and increases in overall heat transfer rate on the order of 10-15%. Oscillating planar impinging jets have shown even more promising results, with Camci & Herr (2002) finding increased local heat transfer rates in excess of 75% for a low Mach number impinging jet with a relatively large impingement ratio using a mechanically-excited jet flow. These effects would also be beneficial for applications requiring enhanced mixing.

Of the work that has been performed on self-excited impinging jet flows, the vast majority has focused on jets using axisymmetric or round nozzles, with robust coverage of both subsonic and supersonic flows, but with relatively little work having been performed on the planar case. Of the studies that have been performed on the planar impinging jet, most studies have examined these flows at low Mach numbers, which are not strongly self-excited and do not produce appreciable acoustic tones or strong flow fluctuations. Several studies by Krothapalli (1985), Norum (1991) and Tam & Norum (1992) have examined the behavior of impinging planar jets using supersonic flows, however the subsonic self-excited case has gone largely unstudied, with only one recent paper by Arthurs & Ziada (2011) examining this case. Because of the relatively wide use of these geometries in industrial practice, and because of the implications of both the positive and negative effects of these self-excited flows, there is a strong incentive for further study in this area.

1.2 Scope of Work

The collection of articles composing this thesis represents the first significant experimental investigation of the self-excited impinging planar jet using subsonic flows, and examines three different aspects of the behavior of this system: the self-excited aeroacoustic response of the system, the development and characteristics of the self-excited flow oscillations, and the fluid-resonant character of the system. The following sections give a brief description of each of these three articles, and how each of the works fits into the overall structure of the thesis.

1.2.1 Self-Excited Oscillations of the Impinging Planar Jet

The first article addresses the self-excited response of the planar impinging jet for the complete range of Mach number (M) and impingement ratio (x_o/h) for which self-excited flows are encountered, for a single nozzle thickness of h=3mm. This study thoroughly documents and analyzes the aeroacoustic response of the system, including the identification of the different hydrodynamic modes of the jet responsible for the generation of acoustic tones. This examination reveals that the planar jet-plate system is self-excited over two distinct regimes: a linear regime where the feedback mechanism exemplifies a typical Rossiter instability, consisting of downstream propagating flow fluctuations and upstream propagating acoustic disturbances, and a fluid-resonant regime, where the jet instability couples with trapped acoustic modes between the nozzle and the impingement surface. The linear regime occurs for relatively low Mach number ($M<0.6$), and produces relatively low acoustic pressures. The jet oscillation in this regime consists of a single flapping mode of the jet column, and tone frequencies are similar to those measured in earlier work by Arthurs & Ziada (2011 & 2012). The fluid-resonant regime occurs at higher Mach numbers and produces acoustic tones at significantly higher sound pressure levels, with these tones being excited by a series of five anti-symmetric hydrodynamic modes of the jet, along with a single symmetric mode. Each of these different hydrodynamic modes is found to couple with a series of resonant acoustic modes occurring between the nozzle and the impingement surface. Finite element methods have been used to predict the frequency and mode shape of these trapped modes, and results of these simulations show a good agreement with experimentally observed behavior.

1.2.2 Evolution of the Self-Excited Impinging Planar Jet

The second article examines the behavior of the self-excited flow oscillations for the third anti-symmetric hydrodynamic mode of the jet in the fluid-resonant regime as a function of both Mach number and impingement ratio, for a single jet thickness of *h*=3mm. The flow has been found to develop over three distinct ranges: an initial region where the growth of disturbances and formation of coherent structures occurs, a developing region where the structures grow rapidly as they convect towards the impingement surface, and an impingement region where the structures interact with the plate, producing the acoustic pressure fluctuations. The fluctuating velocity components have been found to be very large, with peak-to-peak amplitudes in excess of 70% of the flow velocity at the nozzle outlet, and with distributions of the fluctuating components that are qualitatively similar for varying Mach number and impingement ratio. The amplitudes of the fluctuating components of the self-excited flow are found to intensify with increasing Mach number, showing more rapid development in the initial region for the higher Mach number cases. The amplitude of flow oscillations have been shown to vary significantly over the range of each resonant acoustic mode, with fluctuations having relatively low amplitudes for the smallest impingement ratios for which the trapped mode is excited, and gradually increasing as the impingement ratio is increased within the range of each mode. The results of the phase-locked PIV measurements have been used to measure the behavior of coherent structures within the flow, to quantify their convection speed, path and their interaction with the impingement surface, and this information has been used to develop a feedback model for the impinging planar jet, which has been found to accurately predict the frequency response of the system.

1.2.3 Effect of Nozzle Thickness of the Impinging Planar Jet

The third and final article examines the effect of varying nozzle thickness on the self-excited response of the system. An investigation was carried out for a constant Mach number, but with varying impingement distance for a series of seven nozzle thicknesses from h=1mm to 4mm. The response of the system has been found to be excited predominantly by a fluid-resonant mechanism, for which coupling with trapped acoustic modes controls the aeroacoustic response of the system, with the acoustic tone frequency and hydrodynamic mode of the jet being largely a function of the total impingement distance, and the *impingement ratio* having only a small effect due to changes in the convection speed of the coherent flow structures. Flow visualization images reveal that the same hydrodynamic mode of the jet is excited at a constant impingement distance regardless of the impingement ratio, due to coupling with resonant acoustic modes whose frequency is related to the stream-wise length scale of the air volume between the nozzle and the plate. As a result of the coupling with these resonant modes, the aeroacoustic response of the jet-plate system for a given jet thickness can be used to predict the response of the system at other jet thicknesses, and it is likely that nozzles could be designed to reduce acoustic radiation to the surroundings to promote the formation of trapped acoustic modes and enhance the self-excited flow oscillations where the effects of these flows is desired.

1.3 Thesis Outline

This thesis is made up of a collection of three journal articles outlined previously that comprise the results portion of this thesis along with a collection of supplementary chapters which provide a survey of related literature and context for the research, as well as conclusions and recommendations. Chapter 2 provides the reader with a more comprehensive overview of past research in this area. Chapter 3 contains the first journal article titled "Self-Excited Oscillations of the Impinging Planar Jet", which focuses on characterizing the self-excited response of the planar impinging jet for a single nozzle thickness of h=3mm, as well as identifying the nature of the hydrodynamic modes of the jet responsible for tone generation, and the fluid-resonant character of the system response. Chapter 4 contains the second journal article titled "Evolution of the Self-Excited Impinging Planar Jet", which uses phase-locked PIV measurements to examine the nature of the self-excited flow oscillations in greater detail, and to develop a feedback model to predict the oscillation frequency. Chapter 5 contains the third and final journal article "The Effect of Nozzle Thickness on the Impinging Planar Jet", which investigates the effect of changing the initial jet thickness over the range h=1mm to 4mm on the self-excited response of the system, and characterizes the fluid-resonant nature of the system response. Chapter 6 contains the conclusions and recommendations for future work, including a list of the contributions to the state of knowledge. Appendix A provides an analysis of the uncertainty of the experimental measurements performed in during the course of this thesis, Appendix B provides a schematic of the electronic circuit used for generating the trigger used in phase-locked PIV measurements, and Appendix C provides phase measurements performed to assess the degree of span-wise correlation of the self-excited flow oscillations, as well as measurements to quantify the radiating acoustic field.

1.4 A Note to the Reader

As a result of the editorial requirements of publishing a series of three separate journal articles, there is some overlap of materials contained in this thesis. In particular, the sections of each journal article pertaining to the design and construction of the experimental apparatus and measurement techniques contain significant repetition. The literature review sections of each article also contain similar material, in particular relating to the early works on high-speed impinging jet flows that have laid much of the foundation for later more specialized research. However, each of these review sections is targeted, and do contain more specific references related to the work presented in each paper. In addition, some of the preliminary results related to the basic self-excited response of the system is repeated in each of the three papers, which is largely a consequence of the very limited amount of research on the self-excited planar impinging jet available in the literature. Finally, the conclusions reached in Chapter 6 are largely repeated from the conclusions contained in each of the three articles.

CHAPTER 2

Literature Review

2.1 Introduction

This section of the thesis is intended to give the reader a comprehensive review of the literature pertaining to the impinging planar jet. As a result of the editorial requirements of journal articles, the literature reviews provided in the introduction of each paper is relatively brief, giving only a synopsis of the work to date in a form which has been written for an audience well versed in work in this field. This section of the thesis has been provided to the reader to give a more seamless and thorough treatment of the relevant literature, to provide greater context to the work performed in this thesis. The work covered in this review can be split into three sections: a review of i) shear layer instability, ii) impinging axisymmetric jet flows and iii) impinging planar jet flows.

2.2 Instability of Free Shear Layers

Free shear layers, which are formed by the merging of two parallel flow streams moving at different flow velocities, are known to be inherently unstable flows, where small perturbations in the initial region will tend to grow and be amplified as they travel downstream, eventually rolling up to form large-scale vortical structures. Figure 2.1

shows a pair of flow visualization images (Brown & Roshko, 1974) showing a side and top view of shear layer instability, with small structures forming in the initial shear layer at the left hand side of the images, and growing as they travel downstream, rolling up to form vortical flow structures which are initially two-dimensional, and show a strong correlation in the span-wise direction. The linear stability theory based on inviscid flow developed by Rayleigh (1880) has shown an accurate prediction in both the frequencies over which the shear layer is unstable, as well as the growth rates of instabilities.

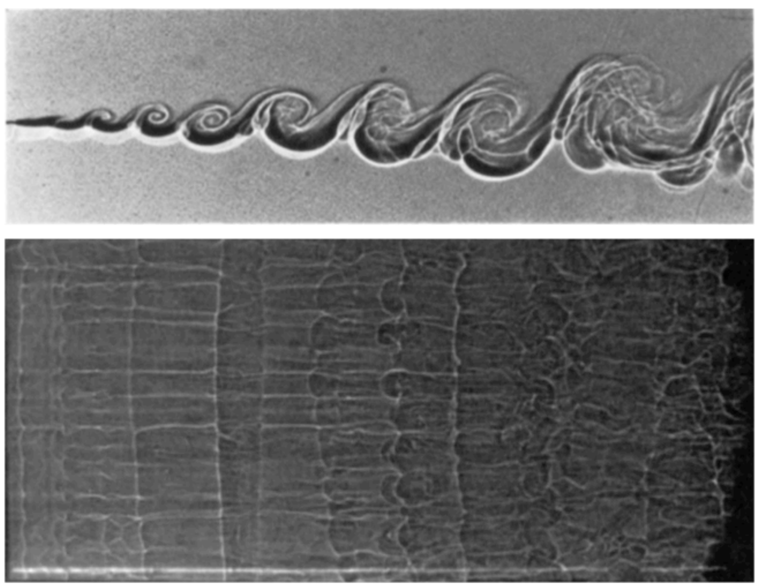

Figure 2.1: Flow visualization images of instability of a free shear layer using a shadowgraph technique (Brown & Roshko, 1974).

Work by Michalke (1964 & 1965) applied the inviscid linear stability theory developed by Lord Rayleigh to a shear layer having a hyperbolic-tangent velocity profile, who computed the stability characteristics of both spatial and temporal waves, and showed that the shear layer is unstable to a band of frequencies related to its thickness, with both very high and very low frequencies being damped (i.e. stable), and frequencies within this band being unstable. Freymuth (1966) examined shear layer instability using laminar axisymmetric and planar jets under the influence of external acoustic excitation in order to investigate the effect of both frequency and amplitude of initial disturbances on the response and evolution of flow instabilities. It was found that fluctuations in the shear layer experienced an initial region of exponential growth, whose growth rate was related to the frequency of the external excitation. Figure 2.2 shows a plot of the growth of transverse velocity fluctuations in the initial region for a variety of different excitation frequencies, where the frequency is given in the dimensionless form of the Strouhal number based upon momentum thickness as given in the following equation:

$$\mathrm{St}_\theta = \frac{f \cdot \theta}{U_\mathrm{o}} , \tag{2.1}$$

where f is the excitation frequency, θ is the momentum thickness of the initial shear layer, and U_o is the jet velocity.

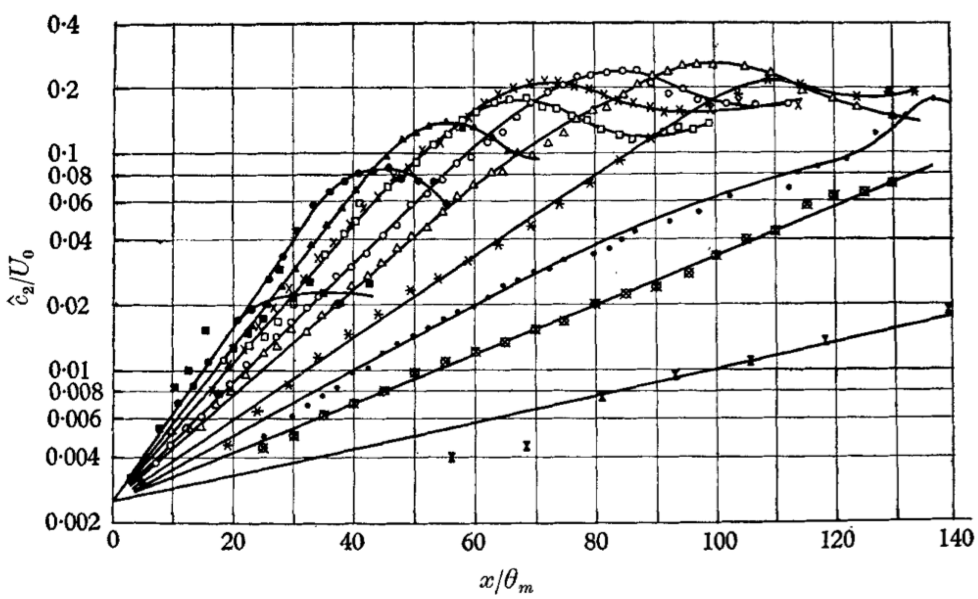

Figure 2.2: Amplitude of cross-stream flow instabilities normalized by jet velocity as a function of downstream position for an acoustically excited axisymmetric jet with varying forcing frequencies: □ St_θ=0.0118, ▲ St_θ=0.0148, ● St_θ=0.0176, ■ St_θ=0.0234, ▲ St_θ=0.002, ⊠St_θ=0.004, • St_θ=0.005, * St_θ=0.007, Δ St_θ=0.008, ○ St_θ=0.009, × St_θ=0.010. U_o=16m/s, D=0.075m, Re_θ=244 (Freymuth, 1966).

Each of the trend lines fitted to each data series in Figure 2.2 illustrates that the initial development of fluctuations occurs at an exponential rate as a function of downstream position, with the rate of growth being related to the excitation frequency, and with the growth of the excited component eventually saturating at some distance downstream as the fluctuations roll up to form vortical flow structures. The resulting exponential growth rate of instabilities, often referred to as the linear growth region, are plotted as a function of Strouhal number in Figure 2.3, along with the predictions of Michalke (1965) for spatial and temporal instabilities. The comparison between the theoretical prediction for the generic shear layer and the experimental results for both the planar and axisymmetric jet shows an excellent agreement, with the shear layers being most unstable for a dimensionless frequency near $St_\theta \approx 0.0167$ for all cases.

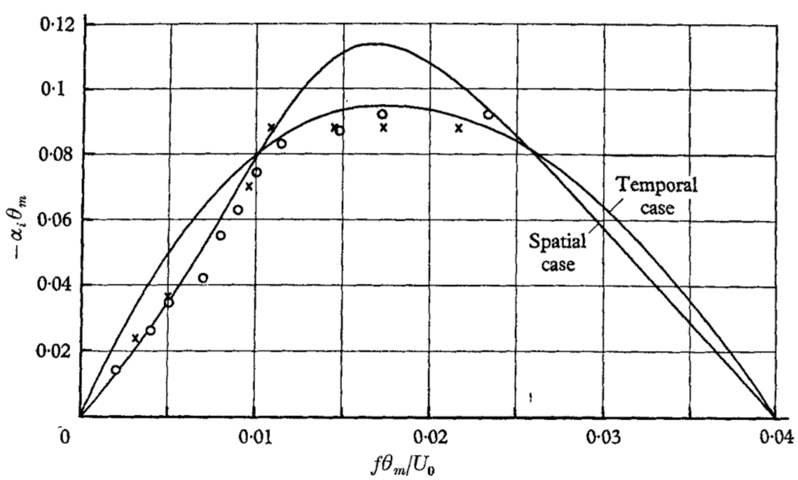

Figure 2.3: Growth rate ($-\alpha_i\theta_m$) as a function of Strouhal number for × planar and ○ axisymmetric free jets (Freymuth, 1966).

The effect of the amplitude of acoustic excitation on the growth of fluctuations is illustrated in Figure 2.4, which shows the results of an acoustically excited axisymmetric jet excited at a number of different sound pressure levels between 70 and 100dB at a constant Strouhal number of St_θ=0.0118. The initial fluctuation amplitude is found to be proportional to the level of excitation, however the growth rates for each of the four cases is identical, as are the maximum fluctuation levels occurring after exiting the exponential growth region as coherent structures are formed.

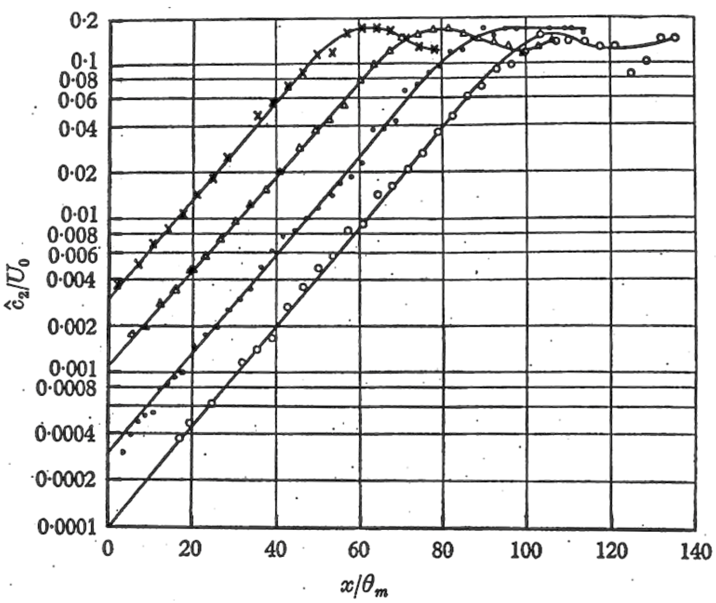

Figure 2.4: Growth of cross-stream instabilities in an acoustically excited axisymmetric jet for varying forcing levels: o 70dB; • 80dB; □ 90dB; × 100dB. U_o=8m/s, D=0.075m, Re_θ=122, St_θ=0.0118 (Freymuth, 1966).

Miksad (1973) investigated the development of the mixing layer in the non-linear region occurring after the saturation of the fundamental component, specifically the rise of various sub-harmonic components produced as a result of merging of structures formed at the fundamental frequency. These effects were found to be important as the fluctuation levels exceed ~3% of the jet velocity, with a series of the sub-harmonic component (½β) becoming the most unstable mode of the flow after the fundamental component has reached its maximum amplitude, as shown in Figure 2.5. Further work by Ho & Huang (1982) and others showed that a series of these sub-harmonic components are excited as a result of a series of distinct merging events, with the amplitude of successively lower frequency sub-harmonic components increasing after the saturation of higher frequency components, giving rise to larger, lower frequency vortical structures as the flow progresses downstream.

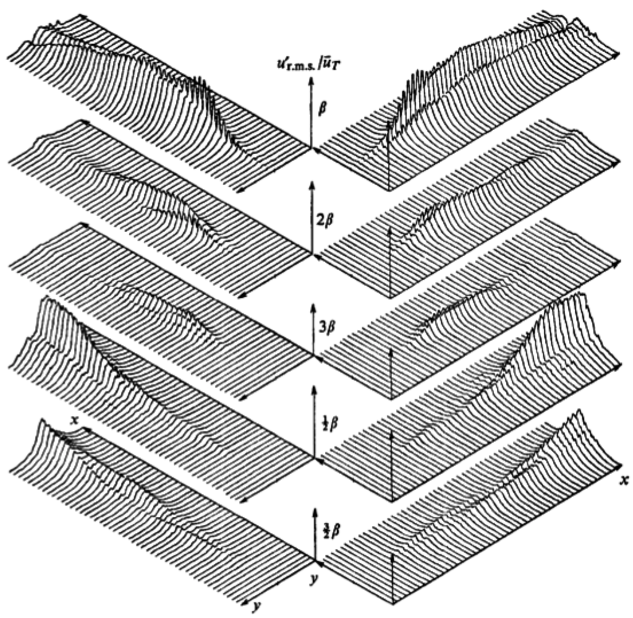

Figure 2.5: Profiles of the RMS intensity of the fundamental (β), harmonic (2β & 3β) and sub-harmonic components (½β & $^3/_2$β) for a plane mixing layer excited near its most unstable frequency. *y*-axis scale: u'_{rms}/u_T=0.155 for β, 2β & ½β, and u'_{rms}/u_T=0.055 for 3β & $^3/_2$β (Miksad, 1973).

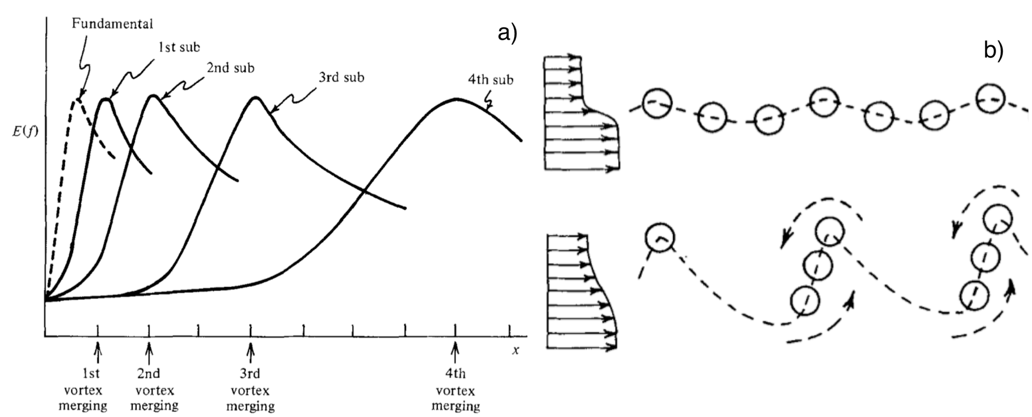

Figure 2.6: a) The evolution of sub-harmonic components in the plane mixing layer as a result of vortex merging and b) a schematic of a vortex merging process (Ho & Huang, 1982).

Turbulence levels in the initial shear layer have also been found to have a significant effect on the most unstable frequency of the shear layer, with laminar shear layers being most unstable at a Strouhal number of St_θ=0.0167, whereas turbulent shear layers show their highest growth rates at a higher dimensionless frequency of $St_\theta \approx 0.023$. Increasing Mach number and compressibility have also been shown to have an effect on the most unstable frequency of the shear layer as shown in Figure 2.7, with increasing convective Mach number resulting in less unstable flows, with their most unstable frequencies occurring at lower dimensionless frequencies. Part a) of Figure 2.7 taken from Kennedy & Chen (1998) shows the results of a linear stability analysis for a laminar planar jet with varying Mach number for both symmetric and anti-symmetric modes of the jet, with the anti-symmetric modes being far more unstable than the symmetric modes for the same flow conditions.

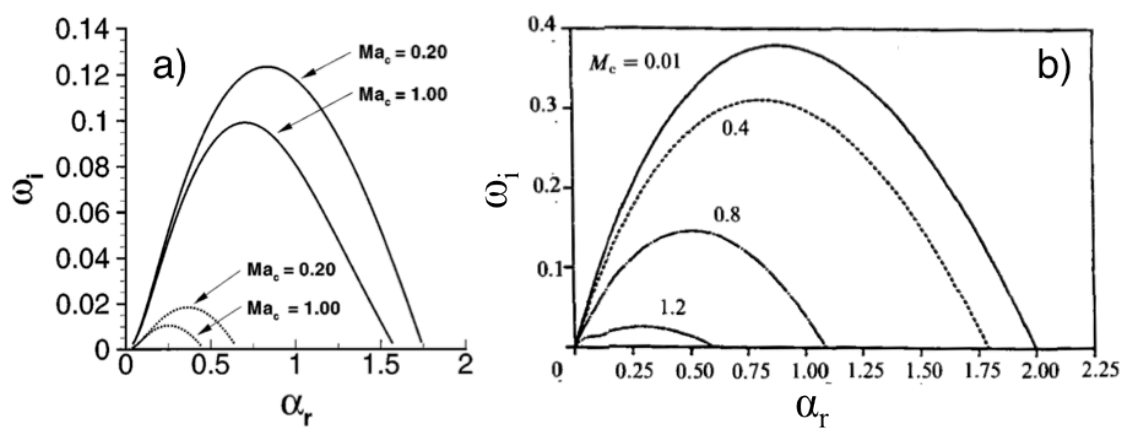

Figure 2.7: Temporal growth rates for a compressible a) planar jet and b) shear layer for varying convective Mach numbers. Dashed and solid lines in Part a) illustrate the receptivity of symmetric and anti-symmetric modes respectively (Kennedy & Chen, 1998 and Sandham & Reynolds, 1991).

2.3 Impinging Jet Flows

The impinging jet flow is part of a larger class of impinging shear layer flows which are known to be self-excited by a feedback mechanism between instabilities in the jet shear layer(s), and acoustic disturbances produced by the impinging jet flow at the downstream surface. The impinging jet flow can be classified by a number of a characteristics of the flow geometry including:

i) The geometry of the nozzle, including axisymmetric or round nozzles, planar or slot nozzles, elliptical nozzles, as well as other, more complex geometries.

ii) The downstream geometry on which the jet impinges, with more common examples including large plates, edges, surfaces with slots or holes, or small bluff bodies such as cylinders.

iii) The type of flow exiting the nozzle, including incompressible and compressible subsonic flows, as well as supersonic flows.

This thesis will investigate the case of a planar subsonic jet in the compressible flow regime impinging on a large flat plate at some distance downstream, shown in a basic schematic in Figure 2.8. As a result, this section of the literature review will focus primarily on jets with both planar and axisymmetric nozzles impinging on plates. However, because of the relative lack of research examining the planar case, some other lower Mach number cases using planar jets such as the jet-edge and jet slot geometries will be examined, as they show some similarities to the present planar case.

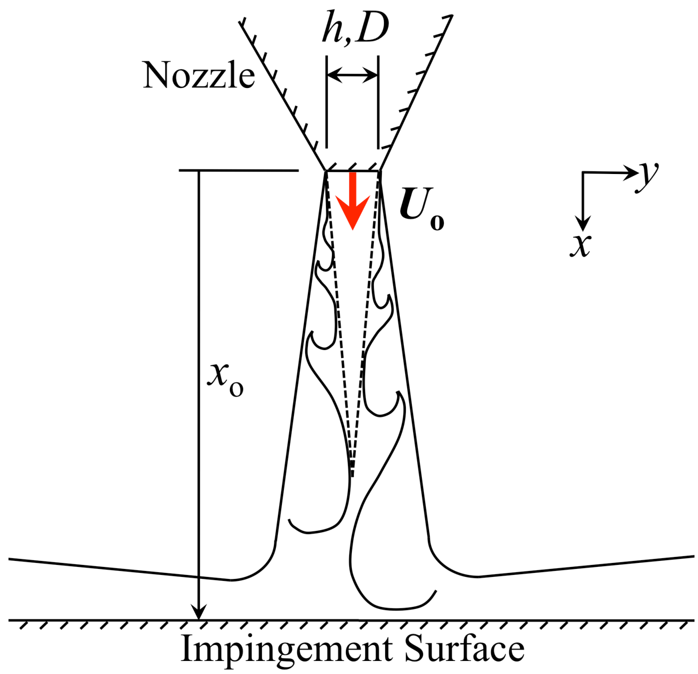

Figure 2.8: Schematic of the impinging jet flow including the nozzle dimension: *D* or *h* for axisymmetric and planar jets respectively, the flow velocity at the nozzle outlet (U_o) and impingement distance (x_o).

Many authors have investigated the steady-state fluid-dynamic and heat transfer properties of impinging jet flows using both axisymmetric and planar nozzles. The fluid-dynamic features have been examined experimentally by numerous authors such as Donaldson et al. (1971a&b), Nishino et al. (1996), Fairweather & Hargrave (2002a&b), Yuceil et al. (2002), Cooper (2003) and Guerra & Su (2005) for the axisymmetric case, and by Gutmark et al. (1978), Looney & Walsh (1984), Maurel & Solliec (2001), Akansu et al. (2008) among others for the planar jet case. In addition, many authors have used numerical tools to investigate these flows, with Chung & Luo (2002) having performed simulations of the impinging axisymmetric case, and Beaubert & Viazzo (2003) and Akiyama et al. (2005) being two examples of numerical investigations of the planar impinging jet. The heat transfer properties of these flows have also been thoroughly documented, with Huang (1984), Liu & Sullivan (1996), Hwang & Lee (2001), Angioletti et al. (2003), Hwang & Cho (2003), O'Donovan & Murray (2007a&b), and Roux et al. (2011) providing some examples of studies on the axisymmetric case, and Haneda et al. (1998), Camci & Herr (2002) and Narayanan et al. (2004 & 2007) having investigated the heat transfer properties for the planar impinging jet case.

2.3.1 Self-Excited Subsonic Impinging Axisymmetric Jets

Of the impinging jet flow geometries examined in previous studies, cases involving axisymmetric jets have received the bulk of attention in the literature, with significant coverage of impinging jets using both subsonic and supersonic flows. Marsh (1961) first documented the generation of discrete acoustic tones and increased overall sound pressure levels for the subsonic case of the impinging axisymmetric jet, and the early works of Wagner (1971) and Neuwerth (1972) characterized the nature of acoustic tone generation, including the range of impingement ratio and Mach number for which tones are generated, as well as performing measurements with variety of different nozzles. The impinging axisymmetric jet flow produces strong acoustic tones due to self-excited flow oscillations over a range of impingement ratio beginning near $x_o/D\approx1.5$ and persisting to $x_o/D\approx5.0$-7.0, depending on the nozzle design and initial conditions of the jet. Tones are excited beginning at a Mach number of M≈0.6, and are excited at increasing amplitudes as the Mach number increases, with some authors reporting sound pressure levels in the acoustic near-field in excess of 170dB. These authors found that tones were generated by a jet-staging phenomenon, with each stage brought about by the impingement of flow structures associated with distinct unstable mode of the jet. The acoustic tone frequency was shown to vary continuously within each stage as the Mach number and impingement ratio are varied, but with discontinuous jumps in tone frequency occurring sporadically as the jet switches between different unstable hydrodynamic modes.

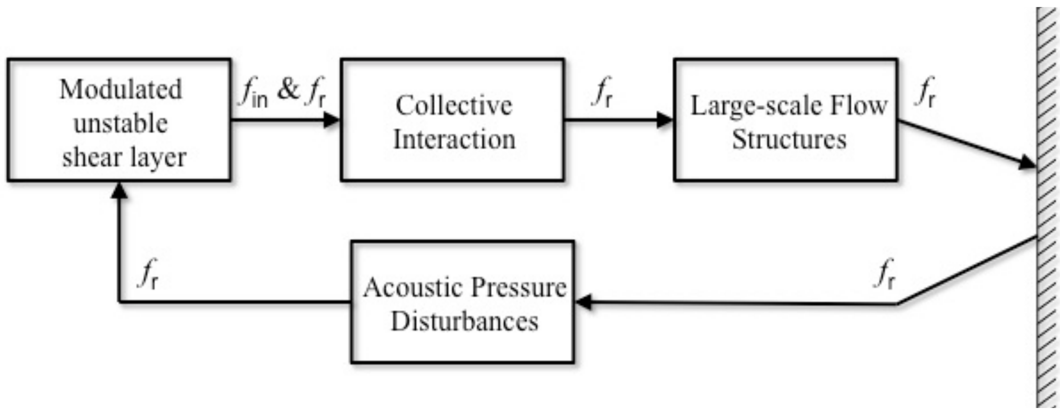

Figure 2.9: The feedback model, as proposed by Ho & Nosseir (1981), for the high-speed impinging axisymmetric jet. f_{in} and f_r are the frequencies of Helmholtz instability and the resonant tone respectively.

Ho & Nosseir (1981) and Nosseir & Ho (1982) examined the noise generation and feedback mechanism in their two-part study on the impinging axisymmetric jet, and attributed the generation of acoustic tones to a feedback mechanism shown in the schematic of Figure 2.9. The feedback mechanism occurs between flow instabilities in the jet free shear layer, which grow into large-scale coherent structures, and pressure fluctuations generated by the impingement of these structures at the downstream surface, which travel back upstream to the location of the instabilities in the jet initial shear layer, completing the feedback cycle. The number and distribution of coherent flow structures is dependent on the particular hydrodynamic mode of the jet being excited by this feedback mechanism, with different types of modes, such as axisymmetric and helical modes of the jet, being excited over different ranges of Mach number and impingement ratio, as well as higher and lower modes of a particular type consisting of a different number of vortical structures between the nozzle and the impingement surface.

Figure 2.10 shows a plot of Strouhal number of the dominant acoustic tone as a function of impingement ratio for an impinging axisymmetric jet with a Mach number of M=0.9, which clearly illustrates this jet-staging behavior, with discontinuities in frequency corresponding to jumps to successively higher hydrodynamic modes of the jet as the impingement ratio is increased. The hydrodynamic modes producing the acoustic tones were found to be entirely axisymmetric in nature for this case, and occur at a nominally constant Strouhal number of $\mathrm{St_D} \approx 0.36$, where the Strouhal number is given by the following expression:

$$\mathrm{St_D} = \frac{f \cdot D}{U_\mathrm{o}}, \qquad (2.2)$$

where D is the nozzle diameter and U_o is the flow velocity at the nozzle outlet. Part b) of the figure shows the jet-stage number (n), which illustrates that the tones are excited by the impingement of five different axisymmetric modes of the jet, given by modes n=2 through n=6, where the mode number is proportional to the number of flow structures formed between the nozzle and the plate.

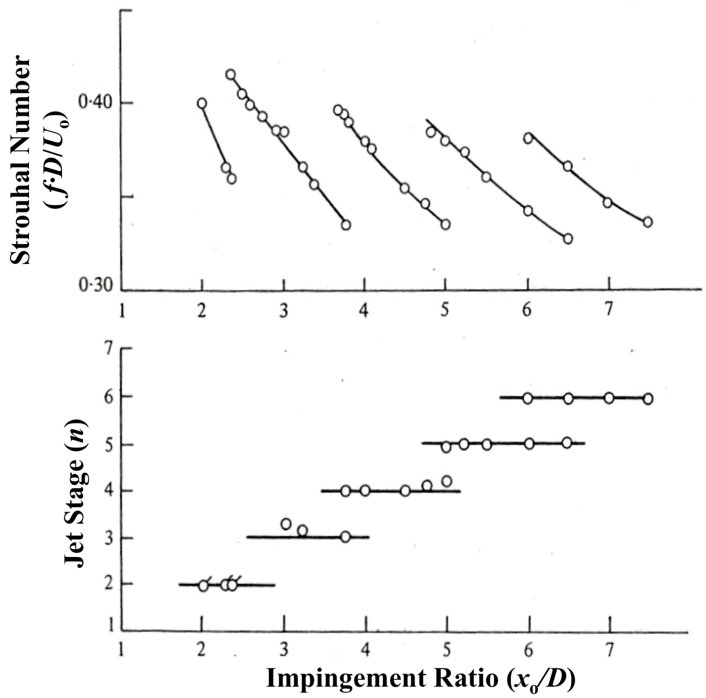

Figure 2.10: Dimensionless frequency (St_D) and mode number (n) of the dominant oscillation mode as a function of impingement ratio (x_o/D) for an impinging axisymmetric jet with a Mach number of M=0.9 (Ho & Nosseir, 1981).

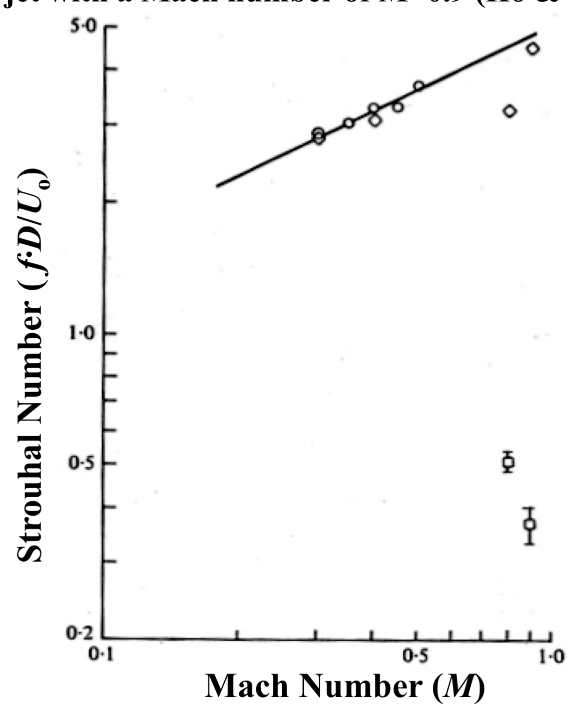

Figure 2.11: Comparison of the dimensionless frequencies for the Helmholtz instability of a free jet (○), the Helmholtz instability frequency of an impinging jet (◊) and the resulting resonant mode (□) (Ho & Nosseir, 1981).

The frequency of the resonant acoustic tones excited by the impinging jet flow are far lower than the most unstable frequency of the initial shear layer of the jet, or the so-called Helmholtz instability outlined in the previous section, with the frequency of resonant tones typically being less than 10kHz, and the frequency of the Helmholtz instability being far greater, often in excess of 100kHz. Figure 2.11 shows the results of frequency measurements of both phenomena performed by Ho & Nosseir (1981), with the Helmholtz frequency of both free and impinging jets showing excellent agreement, occurring over a range of Strouhal number from $3.0 \leq St_D \leq 5.0$ with frequencies tending to increase with increasing Mach number. The frequency of the self-excited flow occurs at frequencies more than an order of magnitude lower, with axisymmetric modes of the jet occurring at an approximately constant Strouhal number near $St_D \approx 0.36$. The authors resolved this disparity between these two frequencies by proposing a process known as collective interaction, illustrated in the schematic shown in Figure 2.12a), whereby a series of small wavelength disturbances associated with Helmholtz instability are modulated by the much longer acoustic waves at the resonant frequency, and merge to form a much larger flow structure at frequencies approximately an order of magnitude lower. Kopiev et al. (2003) captured this collective interaction process in flow visualization images of an acoustically excited axisymmetric jet, shown for comparison in Figure 2.12b), which shows numerous smaller structures forming in the initial shear layer merging to form a much larger flow structure at the wavelength associated with the low frequency acoustic excitation.

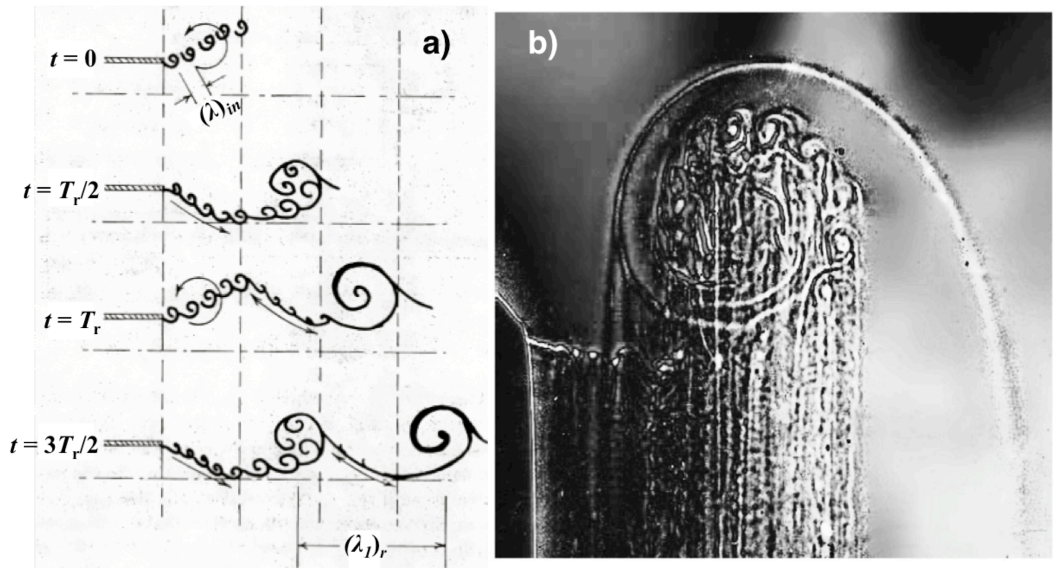

Figure 2.12: A schematic and flow visualization image of the collective interaction process (Ho & Nosseir, 1981 and Kopiev et al., 2003).

Later works by Tam & Ahuja (1990) and Panickar & Raman (2007) investigated aeroacoustic tone generation of the impinging axisymmetric jet for a series of sub-critical transonic Mach numbers, and identified the presence of helical hydrodynamic modes for flow velocities approaching choked flow by examining the phase relationship of an array of microphones placed in the near-field. Figure 2.13, which shows a series of plots taken from Panickar & Raman (2007), depicts the characteristics of aeroacoustic tone generation for Mach numbers of M=0.8, 0.85, 0.9 and 0.95 in Parts a) through d) respectively. The figure illustrates that axisymmetric modes are exclusively excited at the lower Mach numbers tested, and over a similar range of impingement ratio to that encountered in previous studies ($1.5 \leq x_o/D \leq 5.0$), with helical modes beginning to be excited at Mach numbers equal to or exceeding M=0.9, and at relatively small impingement ratios.

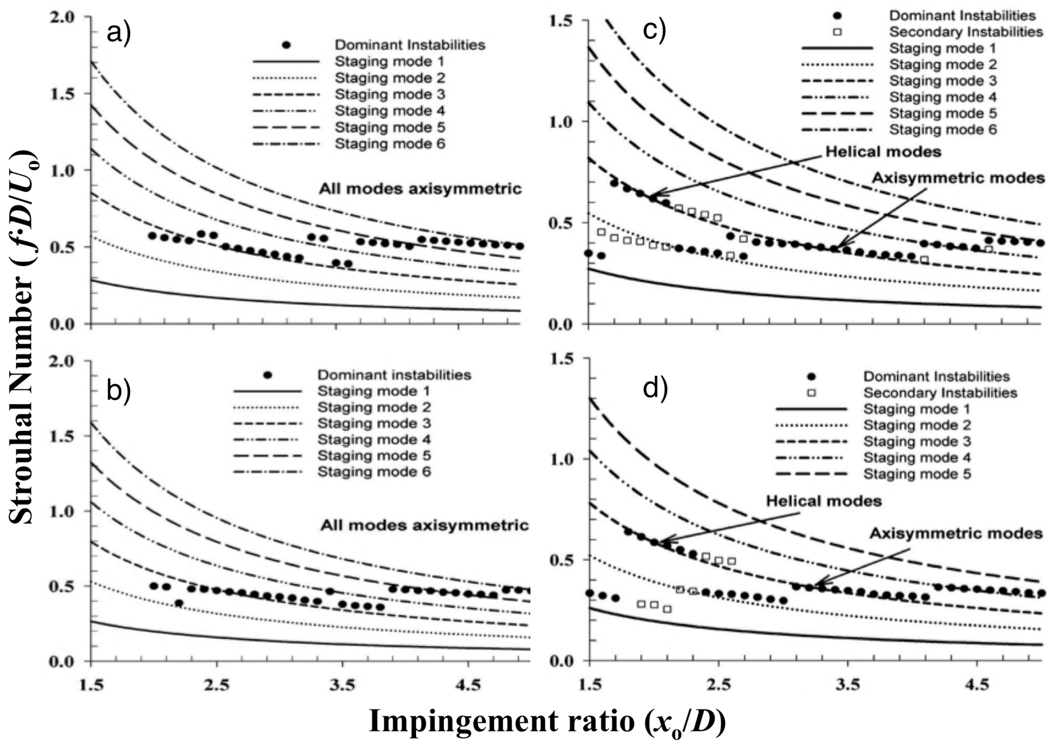

Figure 2.13: Strouhal number based upon jet diameter (*D*) of the (●) dominant and (□) secondary acoustic tones as a function of impingement ratio for Mach numbers of a) M=0.8, b) M=0.85, c) M=0.9 and d) M=0.95 (Panickar & Raman, 2007).

2.3.2 Self-Excited Supersonic Impinging Axisymmetric Jets

Numerous authors, such as Krothapalli et al. (1999), Elavarasan et al. (2000) and Henderson et al. (2005), have also investigated the axisymmetric impinging jet using supersonic flows, which have been shown to have a qualitatively similar response to the subsonic case, however the behavior of these systems often involve more complex interaction with shocks not present in the subsonic case. Figure 2.14 shows a series of three shadowgraph flow visualization images taken from Henderson (2002) of an underexpanded impinging axisymmetric jet for three impingement ratios, showing the general structure of the flow, including the presence of shocks in the jet column and standoff shocks occurring just above the plate surface. Figure 2.15 shows a plot of the aeroacoustic response of a similar impinging jet (Henderson & Powell, 1993), which shows a typical aeroacoustic response for these systems, with the tones being excited by a number of successive jet-stages, but with tone frequencies tending to be organized around jet screech tones, shown in dotted horizontal lines on the figure.

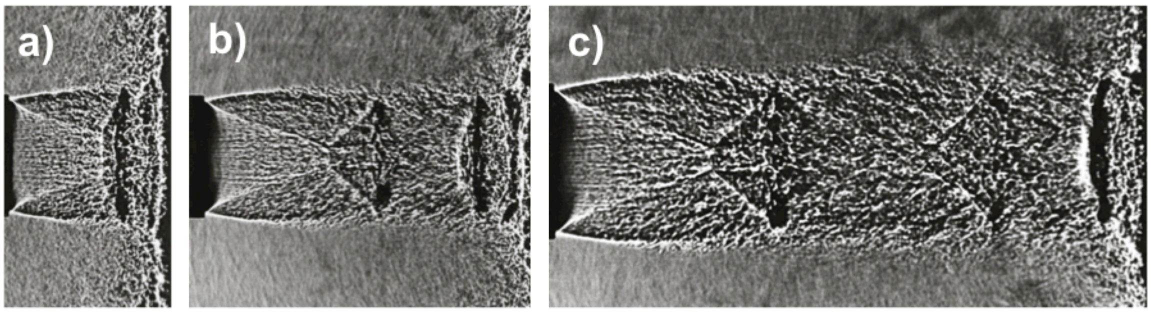

Figure 2.14: Shadowgraph flow visualization images showing the shock structure of a supersonic axisymmetric impinging jet flow with a pressure ratio of p_o/p_a=4.15 for impingement ratios of a) x_o/D=1.27, b) x_o/D=2.60 and c) x_o/D=3.8. Plate surface located at the extreme right of each image (Henderson, 2002).

PIV based flow measurements of a similar supersonic jet configuration were performed by Henderson et al. (2005), and revealed that the acoustic tones were produced as a result of impinging coherent flow structures produced in the annular flow region between the high-speed outer flow, and the recirculation region occurring upstream of the standoff shock. The formation and behavior of these structures were found to be strongly affected by the motion of the standoff shock itself, which was found to oscillate in both the stream-wise direction, as well as in a helical pattern depending on the geometric and flow parameters being examined.

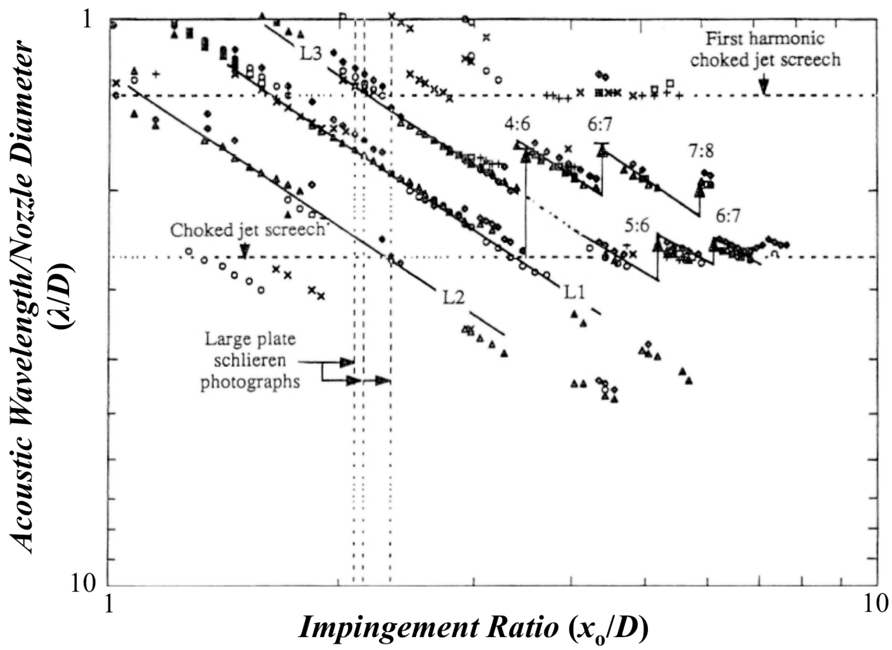

Figure 2.15: Discrete frequency tones as a function of impingement ratio for a supersonic axisymmetric jet with a pressure ratio of P_s/P_∞=2.70 impinging on a surface (Henderson & Powell, 1993).

2.4 Self-Excited Impinging Planar Jets

The case of the self-excited subsonic planar jet impinging on a plate has received far less attention in the literature, with only a few studies having been performed to assess their behavior, despite their widespread use in industrial applications. This section of the review is broken down into three sections which address research performed on self-excited impinging planar jet systems involving: i) low Mach number jet flows in the incompressible flow regime, ii) jet flows at larger subsonic Mach numbers in the compressible flow regime, and iii) supersonic impinging jet flows.

2.4.1 Self-Excited Low Mach Number Planar Impinging Jets

Numerous authors have addressed a number of similar systems such as the jet-edge and jet-slot systems, which are strongly self-excited at low Mach numbers within the incompressible flow regime. The jet-slot system has been the subject of many experimental and numerical investigations, with Nyborg (1954) and Powell (1961) performing the initial investigations, and later works by Lucas & Rockwell (1984), Ziada (1995), Kwon (1998) and Lin & Rockwell (2001) having built on these early works to provide flow visualization and quantification of the self-excited flow, as well as refinement of the feedback model. The jet-slot system has also been thoroughly investigated, with some relatively recent examples being provided by Ziada (1995), Ziada (2001), Billon et al. (2005) and Glesser et al. (2008).

The response of these two systems is qualitatively similar to the response of the high-speed planar jet impinging on a plate, with the frequency of self-excited oscillations being proportional to jet velocity, and scaling inversely with impingement distance, and with tones being produced in a series of distinct jet-stages, as illustrated in Figure 2.16. As a result of the use of a planar jet, the form of the self-excited flow instabilities is different from those in the axisymmetric case, with a series of anti-symmetric stages of the jet being observed for the jet-edge geometry, and both symmetric and anti-symmetric stages of the jet being excited in the case of the jet-slot geometry. Examples of flow visualization images showing each of these flow patterns are given in Figure 2.17, which shows the first two anti-symmetric modes of the jet-edge system in Parts a) and b), as well as a symmetric and anti-symmetric mode of the jet-slot geometry in Parts c) and d), respectively.

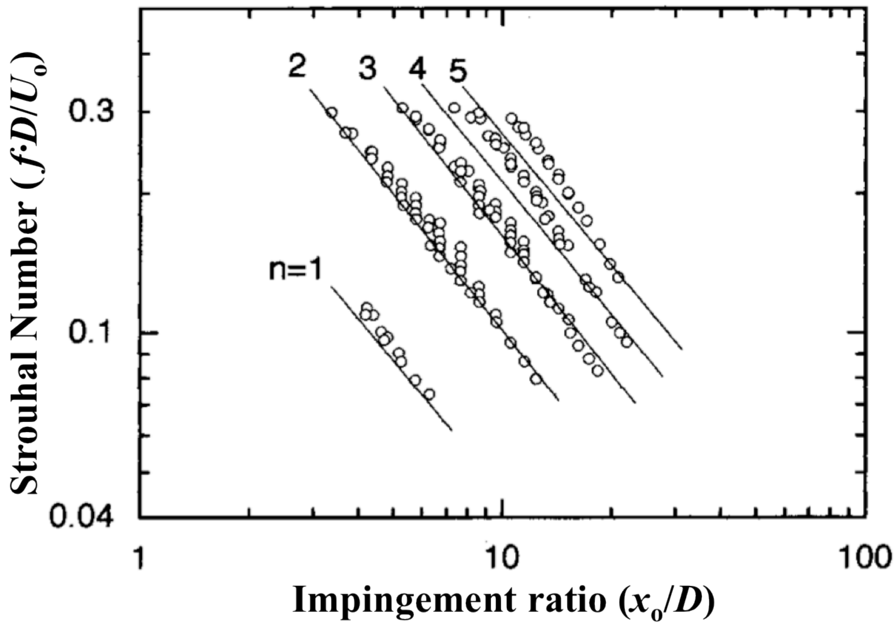

Figure 2.16: Strouhal number of acoustic tones as a function of impingement ratio of the jet-slot system, along with the prediction of a feedback model (Kwon, 1998).

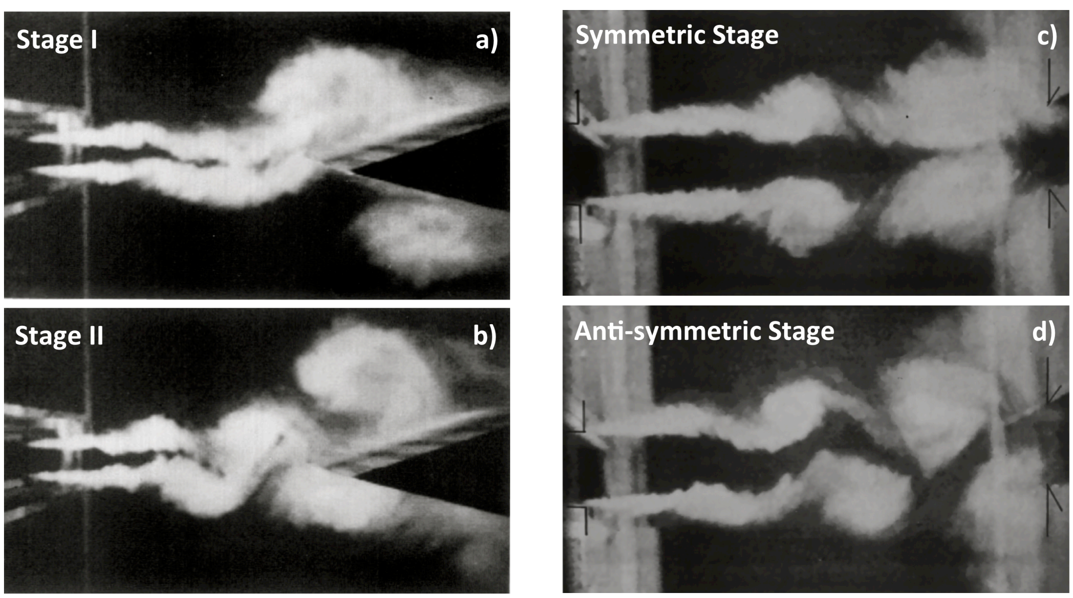

Figure 2.17: Flow visualization images of the self-excited flow patterns in the (a & b) jet-edge and (c & d) jet-slot systems (Ziada, 1995).

As with the higher-speed axisymmetric impinging jet flow, flow oscillations are excited by a feedback mechanism between instabilities in the flow and upstream propagating acoustic fluctuations, but the modeling attempts by various authors have generally neglected the acoustic propagation time, as the flows are self-excited at low Mach number, and therefore the acoustic propagation time is small compared to the oscillation period. In contrast with the high-speed systems outlined earlier, the frequency of the various jet-stages are found to organize themselves around a dimensionless frequency of $St_\theta \approx 0.0167$, corresponding to the most unstable frequency of the initial jet shear layer as illustrated in Figure 2.18 taken from Ziada & Rockwell (1982), whereas systems involving significantly higher Mach number flows tend to excited resonant tones at frequencies far lower than those of the most unstable frequency of the shear layer, with the collective interaction process participating in the feedback mechanism.

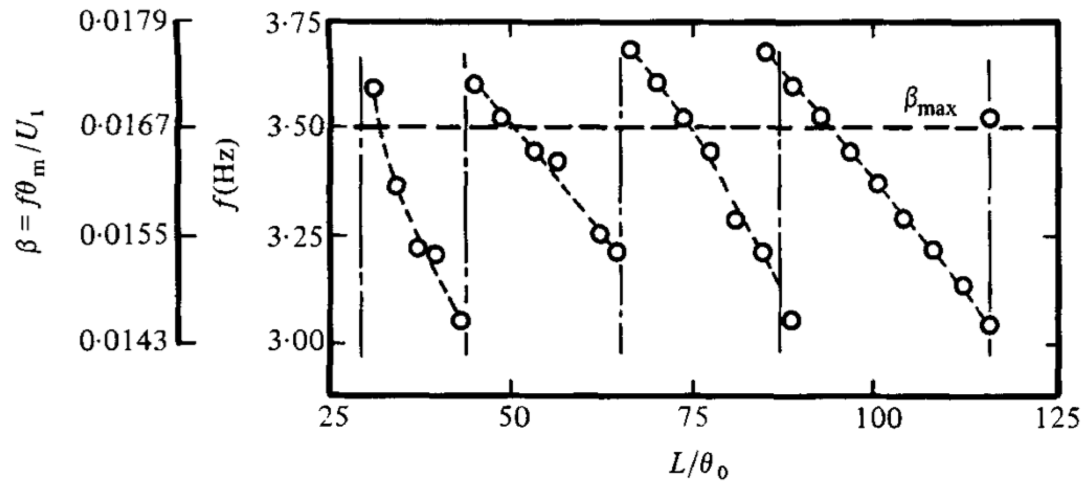

Figure 2.18: Frequency of self-excited flow oscillations of a shear layer impinging on an edge, showing the dimensionless frequency for the most unstable frequency of the shear layer at $St_{\theta m}=\beta=0.0167$, where θ_o and θ_m are the momentum thicknesses of the shear layer at separation and in the idle of the linear region, respectively (Ziada, & Rockwell, 1982).

2.4.2 Self-Excited Subsonic Impinging Planar Jets

The geometry of the planar jet impinging on a plate using high-speed subsonic flows has received very little attention in the literature, with only a few studies addressing this geometry using both experimental and numerical techniques. Hourigan et al. (1996)

performed numerical simulations of an impinging planar jet for two flow velocities of M=0.98 and 1.29 and a single impingement ratio of x_o/h=10 using an inviscid Euler based CFD scheme, and found that in both cases strong self-excited flows were generated by a series of symmetric and anti-symmetric hydrodynamic modes of the jet. The frequencies of these modes were found to scale with a so-called loop velocity, consisting of a combination of downstream and upstream velocity scales related to the velocity of the jet and the speed of sound. More recent work on this geometry has been performed by Arthurs & Ziada (2011 & 2012), who performed an experimental investigation of this flow over a range of intermediate Mach numbers ($0.28 \leq M \leq 0.6$), and found that acoustic tones of significant amplitude were generated over a relatively large range of impingement ratio ($4.0 \leq x_o/h \leq 25.0$) compared to other related geometries. Phase measurements performed at the impingement surface revealed that the acoustic tones were generated by an anti-symmetric hydrodynamic mode of the jet. Sample pressure spectra in the form of a series of waterfall plots are given in Figure 2.19.

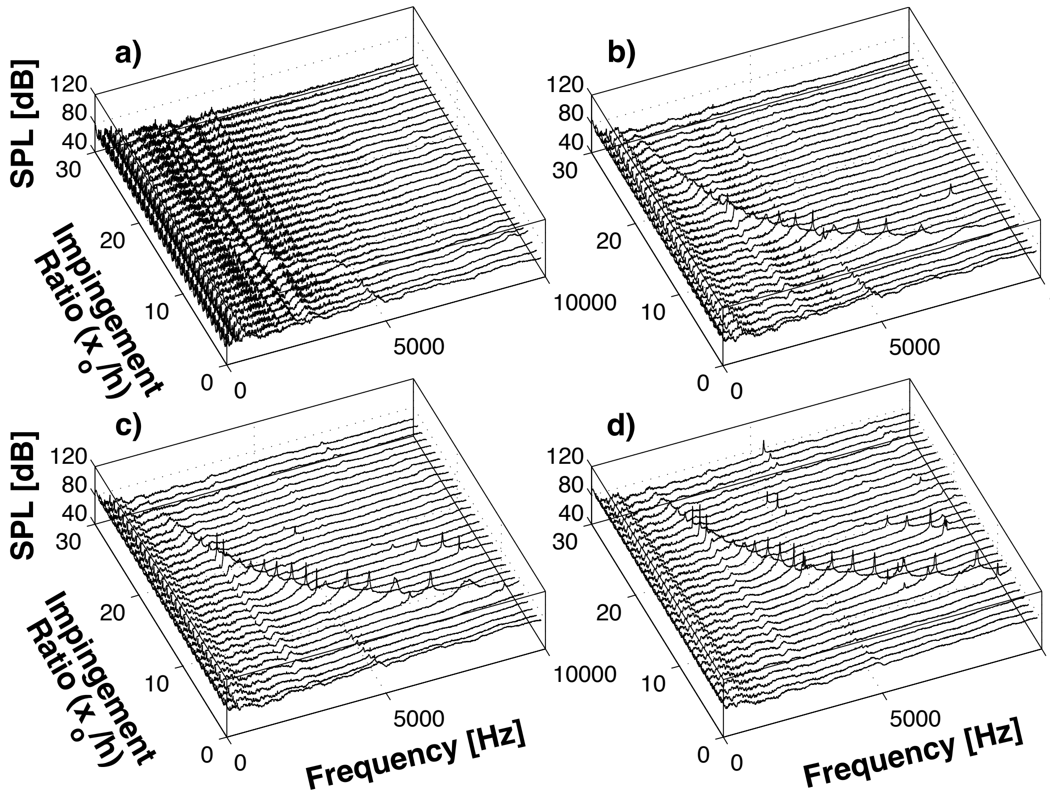

Figure 2.19: Aeroacoustic response of planar jet-plate impingement as a function of impingement ratio for isentropic jet velocities of (a) M=0.28, (b) M=0.41, (c) M=0.49, (d) M=0.56 (Arthurs & Ziada, 2011).

One additional study on high-speed impinging slot jets has been performed by Norum (1991), who investigated the aeroacoustic response of a rectangular jet with a relatively small aspect ratio for a single transonic Mach number of M=0.98, as well as for several cases involving supersonic flows. Results of this study, which are shown in part a) of Figure 2.20, illustrate that tones were excited by a series of five distinct jet stages over a relatively small range of impingement ratio of $2.0 \leq x_o/h \leq 10.0$, with higher jet stages excited as the impingement ratio increased. It is likely that the reduced range of impingement ratio for self-excited oscillations in this case is associated with the relatively small aspect ratio of the jet used in this study ($L/h \approx 4.25$), with measurements presented later in this thesis showing that the maximum impingement ratio for self-excited flow oscillations is reduced as the aspect ratio decreases.

2.4.3 Self-Excited Supersonic Impinging Planar Jets

A number of studies for a planar jet impinging on a plate have been performed using supersonic flows, such as Krothapalli (1985), Norum (1991) and Tam & Norum (1992), who investigated these geometries experimentally, as well as Hourigan et al. (1996) who examined this geometry numerically. The response characteristics have been found to have similar qualities, with measurements showing that a series of different jet-stages are excited as the Mach number and impingement ratio are varied. However, there is also significant evidence of interaction with shocks occurring in the flow and above the plate surface, and jet screech tones produced by a flapping mode of the jet column. These trends can be clearly identified in Parts b) and c) of Figure 2.20, which show the results of Norum (1991), illustrating the aeroacoustic response of impinging planar jets with a Mach number of M=1.29 and 1.49 respectively. These parts of the figure show that the frequencies of the various jet-stages interact with the frequencies of jet screech, shown using the linear fit through the origin, with the stages excited for the supersonic cases being organized by these screech tones.

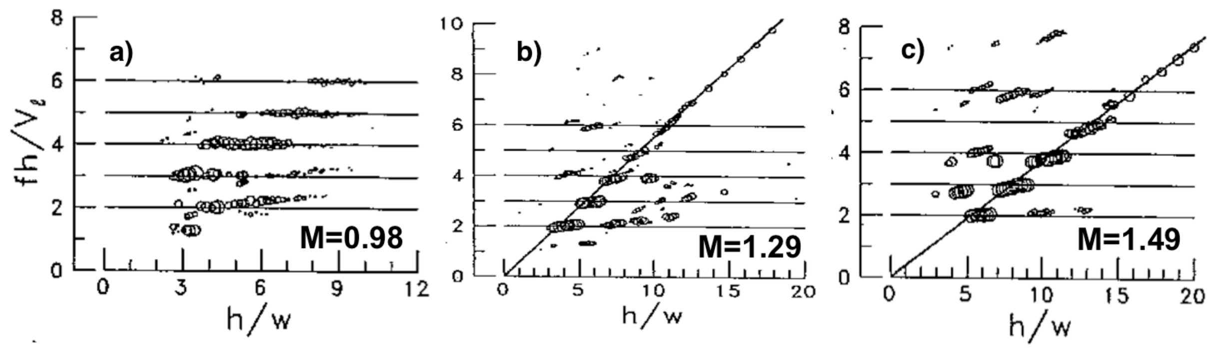

Figure 2.20: Acoustic tone frequency as a function of impingement ratio for a planar jet flow (Norum, 1991).

Flow visualization measurements have also been performed by Krothapalli (1985), and are shown in Figure 2.21, with six images having been obtained at consecutive points in the phase of the flow oscillation. The images clearly show an anti-symmetric flapping motion of the jet column similar to the motion observed by other authors for jet screech in free supersonic planar jets (Alkislar et al., 2003).

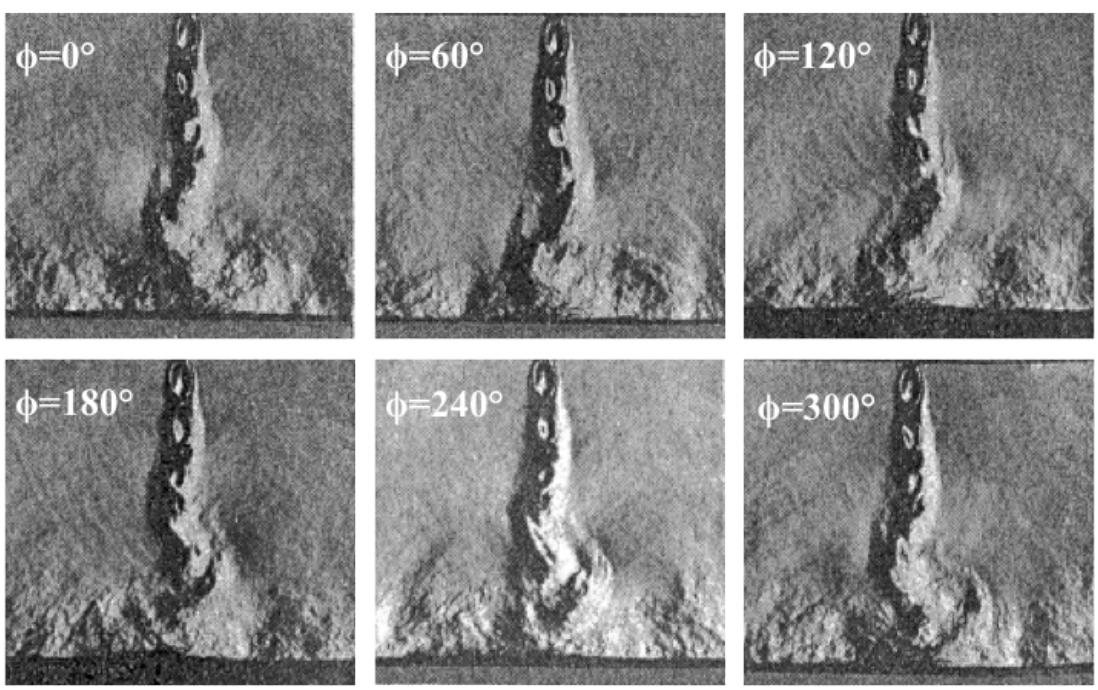

Figure 2.21: Flow visualization of a supersonic impinging planar jet flow for a pressure ratio of P_s/P_∞=5.07 and an impingement ratio of x_o/h=16.7 (Krothapalli, 1985).

2.5 Research Motivation

As the preceding literature survey has shown, the geometry of the self-excited impinging planar jet using subsonic flows has received relatively little attention in the literature, and there is a strong need for further research in this area. Preliminary work has revealed that these systems are liable to produce strong acoustic tones and self-excited flow oscillations as a result of a flow-acoustic feedback mechanism, and that the behavior of this system is substantially different from other related systems, exciting tones over a larger range of impingement ratio and beginning at lower Mach numbers than the equivalent axisymmetric case. Because these flows are used in a wide variety of different industrial applications where these self-excited phenomena could be either beneficial or a hindrance, there is a strong incentive for further study in this area, in order to quantify the nature of the system response and the physical mechanisms responsible for self-excitation, and eventually to develop techniques to control the system response, to enhance the self-excited behavior when these phenomena are desired, or to suppress them when they are not. This thesis contains the first substantial investigation of the self-excited planar jet-plate system using subsonic jets, and will quantify the self-excited response of the system, and investigate the nature of the oscillating flow field.

CHAPTER 3

Self-Excited Flow Oscillations of the Impinging Planar Jet

Complete Citation:

D. Arthurs, S. Ziada, 2012. Self-Excited Flow Oscillations of Impinging Planar Jets, Journal of Fluids and Structures, Submission #: YJFLS-1431, Accepted, Currently in-press.

Copyright

Preface

At the present time, the response characteristics of the self-excited planar impinging jet are largely unknown, as demonstrated in the literature review of the previous chapter, with only two significant experimental studies having been completed on this system. Norum (1991) performed a study on the impinging planar jet which focused largely on supersonic jets, but contained a single subsonic case with a Mach number of M=0.98, with the system showing strong self-excited acoustic tones by a variety of unknown modes of the jet, excited over a larger range of impingement ratio compared to similar axisymmetric cases. More recently, Arthurs & Ziada (2011) performed a study of the impinging planar jet for a range of relatively low Mach number

($0 \leq M \leq 0.6$), and found that acoustic tones were produced beginning at relatively low Mach numbers ($M > 0.4$), and over a relatively large range of impingement ratio ($5.0 \leq x_o/h \leq 25.0$). The acoustic tones tended to intensify as the Mach number was increased, but limitations of the experimental apparatus prevented the testing of Mach number in excess of $M=0.6$. Self-excited flow instabilities producing the acoustic tones were found to be anti-symmetric in nature by means of phase measurements obtained at the plate surface on either side of the jet profile, and a review of these measurements in light of the results in this thesis reveals that acoustic tones were excited entirely within the linear regime.

The journal article contained in this chapter is titled "Self-Excited Flow Oscillations of the Impinging Planar Jet" and contains the results of the first comprehensive examination of the self-excited response of the impinging planar jet. This initial investigation examines the nature of the aeroacoustic response, the form of the self-excited flow oscillations, and an investigation into the nature of the fluid-resonant nature of the self-excited flow for a single nozzle thickness of h=3mm. The planar jet-plate system has been found to produce strong discrete frequency acoustic tones and self-excited flow oscillations over a wide range of impingement ratio and Mach number, from $1.5 \leq x_o/h \leq 32.0$ and $0.4 \leq M < 1.0$, respectively. These self-excited flow oscillations are produced over two distinct regimes: a linear regime occurring for relatively low Mach number, from $0.4 < M < 0.6$, with the flow being self-excited by a traditional Rossiter feedback mechanism between instabilities in the jet free shear layers and acoustic disturbances produced by the impinging flow, and the fluid-resonant regime resulting from a Rossiter instability coupled with a trapped acoustic mode occurring between the plate surface and the nozzle. Acoustic tones produced in the linear regime have a significantly lower acoustic pressure amplitudes than those excited in the fluid-resonant regime, with tone frequencies which vary approximately linearly with changing Mach number, and inversely with varying impingement distance, and is accurately predicted by a feedback model proposed in this paper. Tones excited in the fluid-resonant regime have significantly higher RMS acoustic pressure levels than those in the linear regime, and tend to have tone frequencies which vary less as a function of both impingement ratio and Mach number, as a result of the coupling with three-dimensional resonant acoustic modes occurring in the air volume between the nozzle and the plate. Acoustic tones in both regimes tend to be most strongly excited for intermediate impingement ratios near $x_o/h \approx 10$, with tone amplitude decreasing as the impingement ratio is increased or decreased, and with acoustic tone amplitudes and overall sound pressure levels increasing as the Mach number increases.

The jet-staging phenomenon, consisting of distinct jumps in tone frequency as either the impingement ratio or Mach number is varied, is produced by the impingement of various hydrodynamic or shear layer modes of the jet. Phase-locked PIV measurements revealed that the acoustic tones in the linear regime are produced by a single flapping mode of the jet, whereas self-excited flows in the fluid-resonant regime are produced by a series of five anti-symmetric modes, along with a single symmetric mode occurring only for small impingement ratios. The anti-symmetric modes consist of a columnar flapping mode of the jet, along with an anti-symmetric distribution of coherent flow structures that convect from the nozzle to the plate surface, impinging on the plate to produce the intense acoustic pressure fluctuations, and convecting parallel to the plate surface in the wall-jet region of the flow.

Extensive measurements of the aeroacoustic response, along with a thorough dimensionless analysis of the resulting data, revealed that acoustic tones in the fluid-resonant regime are produced by different combinations of unstable modes of the jet coupled with trapped acoustic modes occurring in the air volume between the nozzle and the plate. The mode diagram, shown in Figure 3.14, illustrates the distribution of different hydrodynamic and acoustic modes as a function of both Mach number and impingement ratio. Finally, acoustic tone frequencies observed in the fluid-resonant regime are compared to the prediction of numerical simulations of the acoustic modes obtained using finite element analysis for a quiescent air volume, and a reasonable agreement is observed, considering the simplicity and assumptions of the numerical model.

The resulting article presents the reader with a comprehensive overview of the self-excited response of the planar jet-plate system, the form of the self-excited flows sustaining the feedback mechanism, as well as the nature of the fluid-resonant coupling occurring at higher Mach numbers.

All experimental measurements, numerical simulations, analysis of the resulting data, and the writing of the published article were completed by the current author, under the supervision of my advisor: Professor Samir Ziada.

Self-Excited Oscillations of a High-Speed Impinging Planar Jet

David Arthurs & Samir Ziada

McMaster University
1280 Main Street West
McMaster University – Dept. of Mech. Eng. JHE 316
Hamilton, ON, Canada
L8S 4L7

Abstract

This paper examines aeroacoustic tone generation of a high-speed *planar* gas jet impinging normally on a flat, rigid surface. Experiments are performed over the complete range of subsonic jet velocities for which tones are generated, and over the complete range of impingement distance for which tones occur, for a single nozzle thickness of h=3mm. The behavior of the planar impinging jet case is compared to that of the axisymmetric case and found to be significantly different, with tones being excited at much larger impingement ratios and lower flow velocities. The acoustic tones have been found to be generated by both symmetric and anti-symmetric jet instabilities, coupled with resonant acoustic modes occurring between the nozzle and plate surface. The nature of the flow instabilities has been investigated using phase-averaged Particle Image Velocimetry measurements. The frequency behavior of the resulting tones is predicted using a simple feedback model, which allows the identification of the various shear layer modes of the instabilities driving tone generation. Finally, a thorough dimensionless analysis is performed in order to quantify the system behavior in terms of the appropriate length and velocity scales.

3.1 Introduction

High-speed impinging jet flows are known to be liable to excitation of very intense acoustic tones generated by a feedback mechanism between instabilities in the free shear layers of the jet, and pressure fluctuations produced by the flow at the impingement surface. These effects can limit the usefulness of these geometries in many applications, however several studies (e.g. Lui & Sullivan, 1996; Vejrazka et al., 2005; O'Donovan & Murray, 2007a and 2007b; and Roux et al., 2011) have shown that local heat transfer rates for impinging jets can be enhanced by as much as 30% through the application of low-level acoustic excitation which produces flow oscillations within the jet flow, providing evidence of potentially useful effects of this phenomenon. Various forms of impinging jet flows have been the subject of a relatively intense research effort in the literature, and those which have been investigated to date can be broadly grouped as those using axisymmetric jets, and those using planar jets.

Of the geometries consisting of jets impinging on flat, rigid surfaces, the majority of the research in the literature has been devoted to the axisymmetric case. Various aspects of the feedback excitation mechanism for the subsonic axisymmetric case have been investigated by Ho & Nosseir (1981), Nosseir & Ho (1982), Tam & Ahuja (1990) and Panickar & Raman (2007), among many others. Extensive work on the axisymmetric case involving supersonic flows has been performed by Henderson & Powell (1993), Krothapalli et al. (1999) and Henderson (2001). In addition, the planar impinging jet case using supersonic jets has also received some attention in the literature, e.g. Krothapalli (1985), and others. In comparison to axisymmetric jets, the impinging planar jet case using *subsonic* flows has received relatively little attention in the literature, despite being widely used in a myriad of practical and industrial applications such as thermal processing in both heating and cooling applications, the production of sheet glass and polymer films and coating control applications.

There has also been considerable work performed on related geometries that use impinging planar jets, such as the jet-edge and jet-slot systems. Two recent studies examining the jet-slot system are Billon et al. (2005) and Glesser et al. (2008), which examined the coupling of a planar jet-slot oscillator with resonant longitudinal acoustic modes of the flow supply duct for Mach numbers up to M=0.1. In addition, there are many other studies in the literature documenting the response of the jet-slot oscillator such as Rockwell & Naudascher (1979), Ziada (1995) and Ziada (2001). There are also numerous examples of work performed on the jet-edge system such as Powell (1961), Karamcheti et al. (1969), Ziada (2002) and Ziada & Rockwell (1982). The response of the jet-edge and jet-slot systems is in some respects similar to the response of the planar jet impinging normally on flat, rigid surfaces; however, the range of flow velocity and impingement distance in the present investigation varies from these cases substantially.

The current study focuses on experimental results of a high-speed, subsonic planar jet impinging normally on a flat surface, as shown in Figure 3.1. A parametric study has been performed in which the impingement distance (x_o) and jet velocity (U_o) have been varied for a single nozzle thickness of h=3mm.

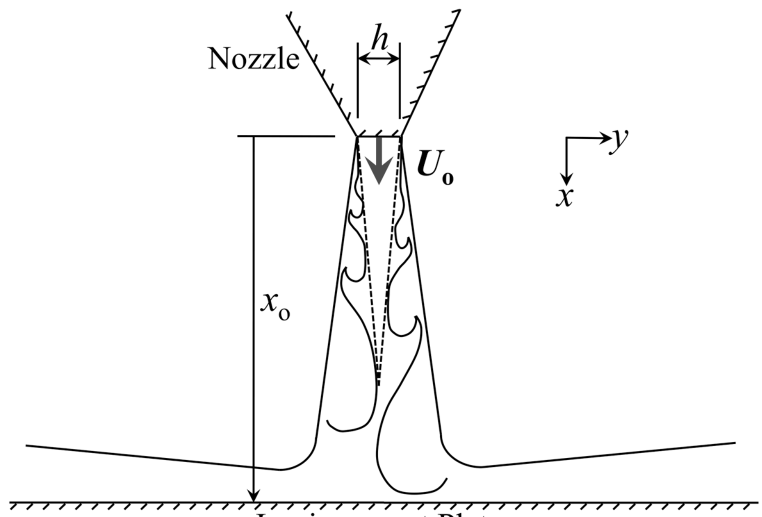

Figure 3.1: Basic schematic of the impinging planar jet geometry, showing the initial jet flow velocity (U_o), the impingement distance (x_o) and the nozzle thickness (h), as well as the downstream (x) and cross-stream (y) directions.

Table 3.1: Nomenclature of quantities and terms.

Nomenclature

c	Speed of sound in air [343 m/s]
d	Distance of the microphone from the stagnation point [m]
D	Nozzle diameter of an impinging axisymmetric jet [m]
f	Frequency [Hz]
h	Planar nozzle thickness [m]
L	Length of the planar jet in the span-wise direction [0.1m]
L/h	Nozzle aspect ratio
M	Mach number (U_o/c)
P_s	Supply pressure [Pa]
Re_h	Reynolds number based upon jet thickness ($U_o \cdot h/\nu$)
SPL	Sound pressure level in decibels [$20 \cdot \log_{10}(P_{RMS}/P_{ref})$ where P_{ref} =20μPa]
St_{xo}	Strouhal number ($f \cdot x_o/U_o$)
St_{eff}	Effective Strouhal number ($f \cdot x_o/U_{eff}$)
U_{eff}	Effective velocity [$U_{eff} = 2 \cdot U_d \cdot c/(U_d + c)$]
u_c	Velocity scale of the downstream portion of the feedback cycle [m/s]
U_o	Jet velocity at the centerline of the nozzle outlet [m/s]
x_o	Impingement distance (distance from the nozzle lip to the impingement surface) [m]
x_o/h	Impingement ratio
θ	Angle of microphone, as measured from the jet plane [degrees]
ζ	Distance from the nozzle flange to the nozzle lip [0.03 m]
λ	Acoustic wavelength [m]
$x_o+\zeta$	Distance from the plate surface to the nozzle flange (outer scale of the impinging jet flow) [m]
$(x_o+\zeta)/\lambda$	Number of acoustic wavelengths between the nozzle flange and the plate surface

3.2 Experimental Apparatus

The current study consists of an experimental investigation of a high-speed planar gas jet impinging on a plate at some distance downstream. In order to facilitate the study of this geometry, a planar nozzle and plate geometry was constructed. The planar nozzle and plenum geometry, shown in Figure 3.2, were machined out of Aluminum and has a span (L) of 100mm, and allows for adjustment of nozzle thickness (h) from 1.0mm to 5.75 mm in increments of +/-0.25mm using a precision dowel system. For the current study, results from a single nozzle thickness of h=3mm are presented, for an overall aspect ratio of the nozzle of L/h=33.3. The nozzle is pressurized using compressed air, which enters the plenum through 25.4mm diameter hole in top surface, at an angle perpendicular to the direction of the jet flow ultimately exiting the nozzle.

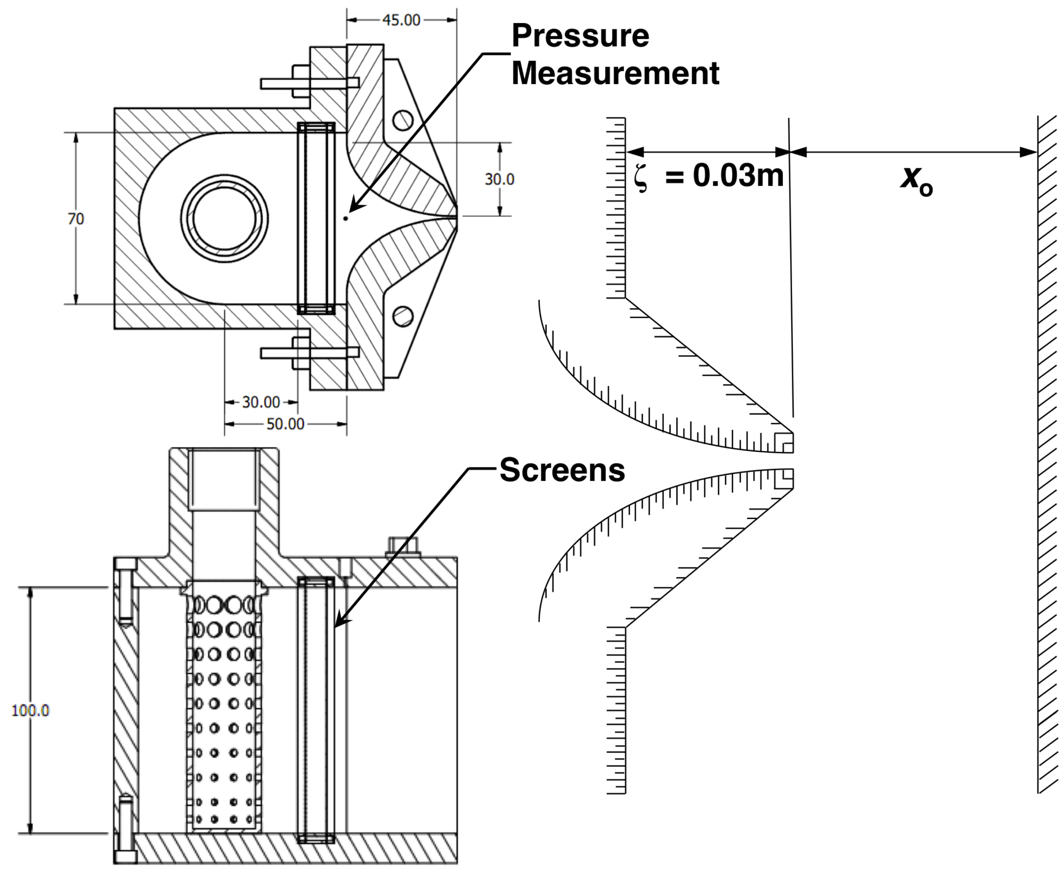

Figure 3.2: Sectioned views of the nozzle and plenum geometry showing the internal features such as the flow distribution tube, flow conditioning screens and adjustable nozzle thickness.

Air entering the plenum passes through a flow distribution tube, shown in Figure 3.2, which is mounted in the plenum and has been designed to evenly distribute the flow along the jet-span. The tube consists of a hollow tube with an inner diameter of 25.4mm that is sealed one end, and with holes distributed azimuthally in ten evenly spaced rings along its length. The size of the holes at each of the ten axial locations varies as a function of axial location, with the size of the holes being determined during the design process through the use of iterative CFD simulations, and subsequent physical testing of the nozzle. After entering the plenum through the flow distribution tube, the flow passes through a series of flow conditioning screens, consisting of a fine stainless steel cloth with a density of 70 wires per inch and an open area ratio of β=0.58, to break up any large turbulent structures (Mehta & Bradshaw, 1979). The jet nozzle uses an elliptical profile as shown in Figure 3.2, with dimensions of the major and minor axis of the ellipse of 45mm and 30mm respectively, providing a nozzle contraction ratio ~23 for a nozzle thickness of h=3mm. The use of elliptical profile for the nozzle facilitated changing the nozzle thickness h with relative ease without sacrificing the quality of the issuing jet.

Measurements of the initial velocity profile of the jet at the exit of the nozzle block were performed using a specially constructed stagnation pressure probe similar to that outlined in Arthurs & Ziada (2011), and a multi-axis traverse accurate to within ±0.01mm. Figure 3.3 shows a set of velocity profiles measured in both the span-wise (z) and cross-stream (y) directions for a nozzle thickness of h=3mm and flow velocities of U_o=150 and 300m/s. The figure shows that for both cases the flow is evenly distributed along the span of the jet, with a maximum variation of less than 1% across the nozzle span for the 300m/s case. Velocity profiles measured in the cross-stream direction show an even "top-hat" shaped velocity profile. Additional measurements of the velocity profiles in the in the cross-stream (y) and span-wise (z) directions were performed for a series of other flow velocities, all of which showed excellent flow distribution and similar velocity profiles. Table 3.2 lists the boundary layer thickness, disturbance thickness and momentum thickness at the outlet of the nozzle for each of the flow velocities tested. Static pressure in the plenum was measured at a location immediately upstream of the nozzle inlet at the nozzle centerline, as shown in Figure 3.2, and this pressure, referred to hereafter as the supply pressure (P_s), was used to estimate the flow velocity of the jet exiting the nozzle using the following equation:

$$U_o = c \cdot \sqrt{\frac{2}{\gamma - 1}\left[\left(\frac{P_s + P_\infty}{P_\infty}\right)^{\gamma-1/\gamma} - 1\right]}, \tag{3.1}$$

where P_∞ is the ambient pressure, γ is the ratio of specific heats of air, and c is the speed of sound. Subsequent PIV measurements confirmed that this expression, derived from equations of flow through a lossless nozzle, was accurate to within 2.5% for the conditions examined in this study, with the majority of the deviation occurring at high Mach numbers.

Table 3.2: Various measures of shear layer thickness at the mid-span of a planar jet with a thickness of *h*=3mm for varying flow velocities.

	Flow Velocity (U_o)			
	150m/s	**200m/s**	**250m/s**	**300m/s**
Disturbance Thickness (δ) [mm]	0.23	0.23	0.21	0.20
Displacement Thickness (δ^*) [mm]	0.077	0.077	0.076	0.071
Momentum Thickness (θ) [mm]	0.024	0.023	0.023	0.021

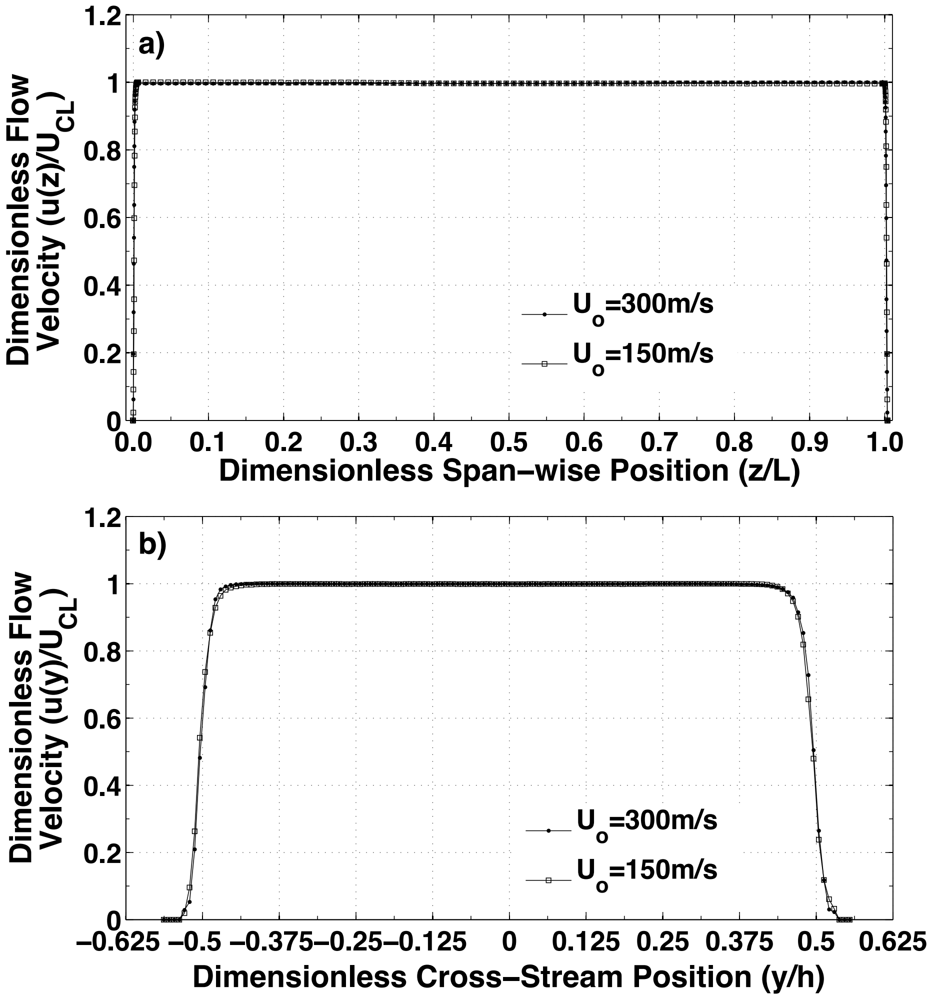

Figure 3.3: Profiles of a) the flow velocity at the nozzle centerline as a function of the span-wise position (*z*) and b) the flow velocity as a function of the cross-stream direction (*y*), for mean flow velocities of U_o= 150m/s (M=0.43, $Re_h=3\times10^4$) and 300m/s (M=0.87, $Re_h=6\times10^4$).

The flat surface used for jet impingement consists of a large, rigid plate machined out of Aluminum measuring 150mm×200mm and a thickness of 10mm. The plate surfaces have been machined using a single point fly-cut milling operation to provide the flattest surface possible. The plate has been machined to allow dynamic PCB 105C02 miniature dynamic pressure transducers to be flush mounted to the front surface of the plate at various locations to monitor fluctuating pressures at the plate surface.

Measurements in the acoustic free-field were obtained using a GRAS 40BP ¼" high-level microphone combined with a GRAS 26AC preamplifier and a GRAS 12AA power supply module. The microphone has a flat frequency response of 2Hz-70kHz (±1dB) and were calibrated using a GRAS Type 42AB sound calibrator. The microphone was located using an adjustable microphone boom assembly shown in Figure 3.4, and the measurements presented in this paper have been recorded at an angle of θ=60° as measured from the jet plane, and at a microphone distance of *d*=200mm as measured from the plate surface at the jet centerline at the midpoint of the jet-span. Acoustic damping foam was placed on reflective surfaces in the immediate area of the experimental setup, and measurements were performed to confirm that all acoustic measurements were completed in the acoustic free-field in non-reverberant conditions.

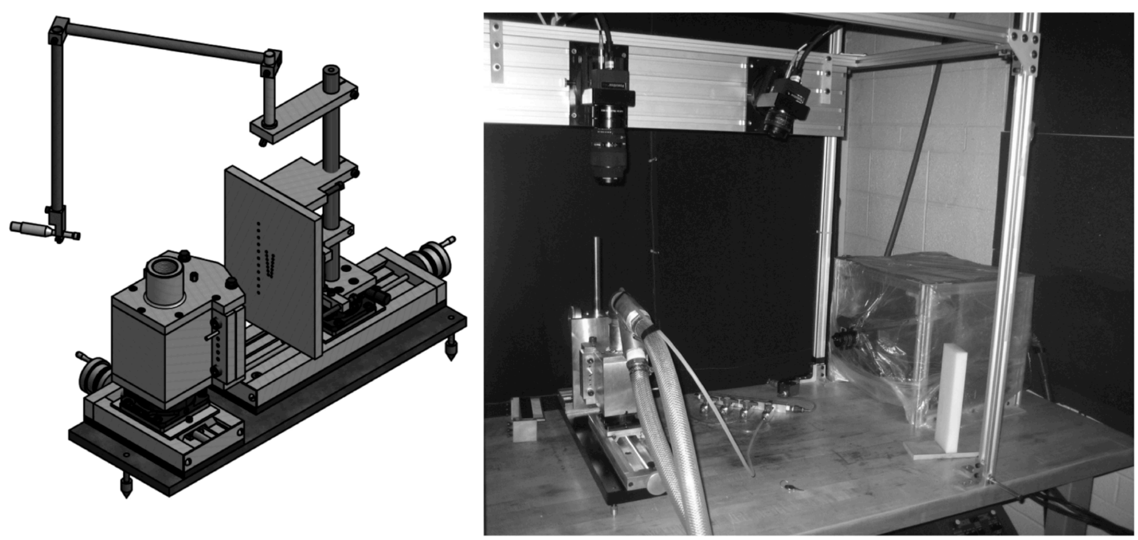

Figure 3.4: Isometric views of planar jet-plate apparatus and the layout of the jet-plate apparatus, PIV camera & supporting frame, and laser head unit & mounting frame.

Measurements were acquired using a National Instruments NI-4452 4 channel data acquisition card, which uses 4 simultaneously sampled channels, a maximum sample rate of 204.8kS/s, and hardware based anti-aliasing filters. Each acoustic measurement was obtained by recording the pressure-time signal using a sample rate of 204.8kHz for 15 seconds. Spectral analysis was performed by breaking the time signal into 60 equally sized blocks of 51,200 samples with no overlap, calculating the amplitude spectrum of RMS acoustic pressure for each block, and averaging the 60 spectra to produce an average acoustic spectrum. This results in an amplitude spectrum with a frequency range from 0Hz to 102.4kHz and a spectral resolution of 4Hz, which is truncated to a frequency range of 0Hz to 70kHz, corresponding to the linear response range of the microphone.

In order to measure the velocity fields of the impinging jet flow, particle image velocimetry was used. A 2-dimensional particle image velocimetry system using a single PowerView 4MP 12 bit digital camera with a resolution of 2048×2048 pixels was used for all flow measurements. For flow field illumination, a 532nm New Wave Solo 120XT pulsed Nd:YAG laser with a maximum output of 120mJ per pulse was used. The beam was focused to a sheet using a plano-cylindrical and spherical lenses. Camera optics were determined by the required field of view for each flow field being captured, with a Sigma 105mm f2.8 lens being used in combination with 1.4x and 2.0x teleconverters and extension tubes. Synchronization of the laser pulses and camera images was performed using a TSI LaserPulse Model 610035 synchronizer with external triggering and software adjustable time delay. The high-speed impinging planar jet flow produces a highly periodic flow oscillation which gives rise to the intense acoustic tones. This phenomenon occurs over a range of frequencies several orders of magnitude higher than the maximum image aquisition rate of the PIV system used in this study. In order to capture this relatively high-speed phenomenon using the current system, a phase-locked PIV measurement technique was employed. Measurements performed using the phase-locked technique utilize the highly periodic pressure signal obtained at the plate surface to trigger flow velocity measurements at a particular instant in the flow oscillation cycle using a custom designed trigger generator. Each PIV vector field was obtained using a deformation based scheme incorperating 24×24 pixel interrogation regions with 75% overlap in both the x and y-directions. All PIV measurements presented in this paper have a *minimum* validation rate of 99% for single instantaneous flow fields before incorperating vector replacement or interpolation schemes.

Seeding of the flow for PIV imaging was performed using a six-nozzle Laskin aerosol generator using olive oil as a seeding medium, producing 1μm mean diameter droplets. The Stokes number of seeding particles for all PIV cases shown in present work falls below Sk=0.1 and fall within the range of $0.05 \leq Sk \leq 0.1$, which will result in tracking error of less than 2% even for the relatively high frequency oscillations present in the impinging planar jet (Melling, 1997). To avoid laser reflections from the machined Aluminum surfaces of the nozzle and the impingment surface from appearing in the images and/or damaging the camera sensor, a clear acrylic paint infused with a laser fluorescing dye, Rhodamine Chloride ($C_{28}H_{31}N_2O_3Cl$), was applied to the exterior surfaces of the nozzle and to the impingement plate. Calibration of the PIV system was performed using a Starett machinists' grade straight edge, mounted to a fixture which is attached to the impingment surface temporarily during calibration.

3.3 Aeroacoustic Response

The high-speed impinging planar jet-plate system is known to produce large amplitude acoustic tones resulting from periodic flow oscillations occurring over a range of impinging jet velocities and impingement distances. For the current study, sound measurements have been performed in a grid for flow velocities from U_o=150m/s to ~343m/s (*choked flow*) in increments of ±2.5m/s, and for a range of impingement ratios, defined as the distance from the nozzle lip to the plate surface divided by the nozzle thickness, from x_o/h=2.0 to 32.0 in increments of ±0.5, a total of ~4,800 distinct acoustic measurements. Figure 3.5 shows a single acoustic spectrum for an impingement ratio of x_o/h=7.0 and a flow velocity of U_o=300 m/s. A dominant acoustic tone is generated at a frequency of f =10,452 Hz, and an amplitude in sound pressure level of 137.4dB. Three super-harmonics of the dominant tone frequency are clearly visible on the spectrum, as well as one sub-harmonic, and a variety of other acoustic tones of smaller amplitudes. The dominant acoustic tone is more than 20 dB greater than the next largest acoustic tone amplitude, in this case the 1st super-harmonic of the dominant tone, and more than 40 dB greater than nearby broadband noise levels. This behavior is indicative of the typical response of the planar jet-plate oscillator, which tends to generate an acoustic response with a large amplitude dominant acoustic tone, with a series of sub and super-harmonics of lesser amplitudes, and relatively high broadband noise levels. For the purposes of this paper, the threshold defining a "tone generating condition" shall be any configuration producing an acoustic spectrum having a spectral peak of greater than, or equal to, 20dB above the associated broadband noise level.

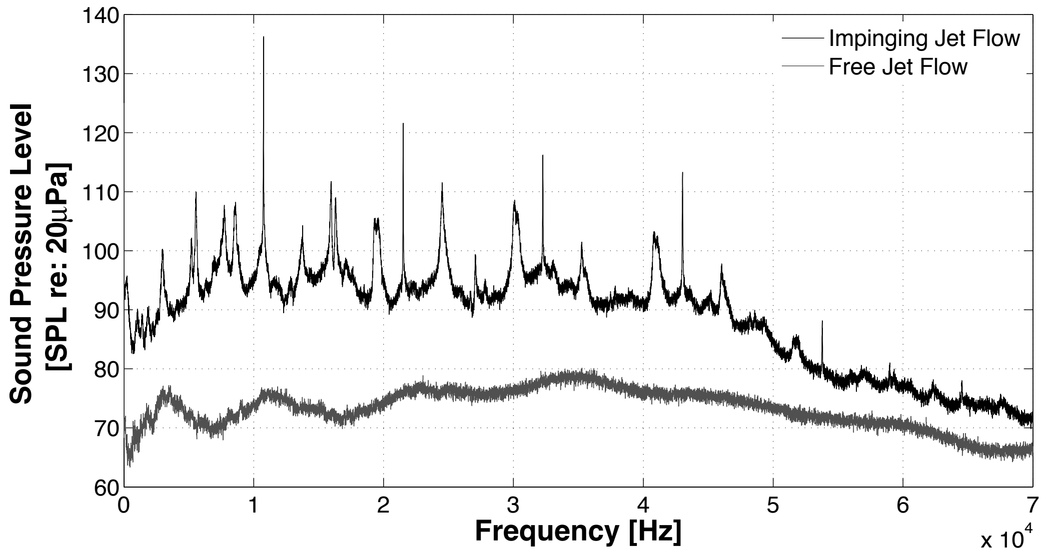

Figure 3.5: A pair of acoustic spectra showing the aeroacoustic response of a free and impinging planar jet for a flow velocity of U_o=300m/s (M=0.87). Impingement ratio of x_o/h=7.0 for the jet-plate case.

Figure 3.6 shows a contour plot which shows a collection of acoustic spectra taken at a range of flow velocities between U_o=150 m/s to 343 m/s. The contour plot clearly shows the presence of a distinct jet-staging phenomenon common to impinging shear layer flows, with the jet-plate oscillator switching between jet-stages at a flow velocity of U_o=265 m/s. Both the lower frequency jet-stage, which occurs for relatively low flow velocities, and the higher frequency stage show strong super harmonics, although the behavior of both the tone frequency and amplitude appears to be different for the two stages. Figure 3.7 shows a plot of both the frequency and amplitude of the dominant acoustic tone as a function of flow velocity at the nozzle exit. The initial jet-stage, which is excited for flow velocities of less than U_o=265m/s, appears to have tone frequencies which increase approximately linearly with increasing flow velocity, varying between 3,198Hz to 4,858Hz, and has relatively low acoustic pressure amplitudes, which increase monotonically with increasing flow velocity. The dimensionless frequencies excited within the linear regime of the current study are in agreement with previous work performed by Arthurs & Ziada (2011), which was performed on a separate experimental apparatus utilizing a different nozzle design and nozzle thickness. In contrast, the higher jet-stage, excited for flow velocities greater than U_o=265 m/s, has a tone frequency which is approximately constant, and nearly invariant with increasing flow velocity (10,196Hz to 10,648Hz). The acoustic pressures of this stage are significantly higher than those found in the first jet-stage. The difference in the behavior is thought to arise as a result of the lower jet-stage being produced by a traditional Rossiter mode, consisting only of upstream and downstream propagating disturbances between the nozzle lip and the plate surface, whereas the higher jet-stage is a Rossiter mode coupled with a resonant acoustic mode. These resonant modes will be discussed in a later section of this paper.

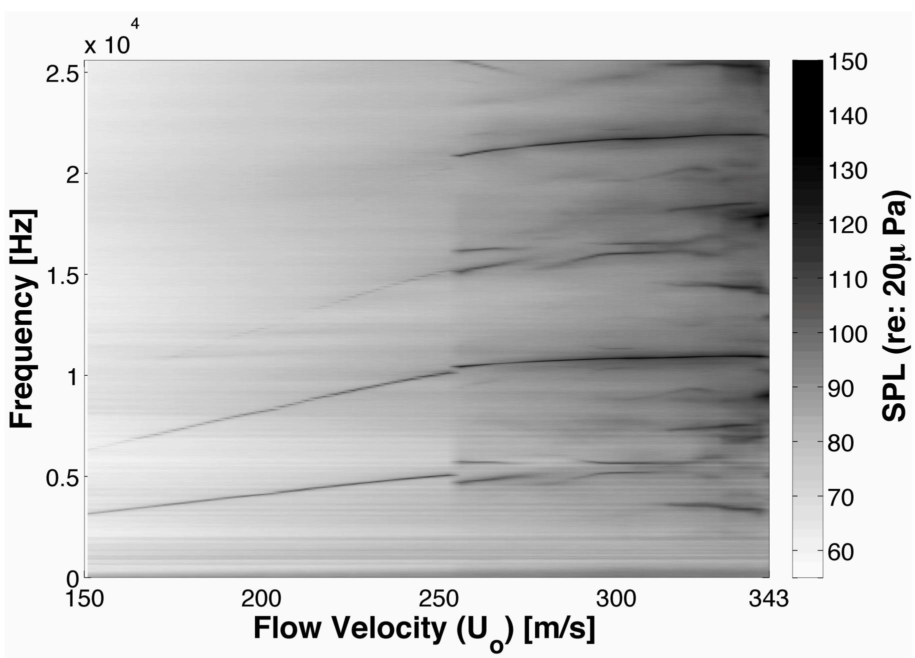

Figure 3.6: Contour plot showing the aeroacoustic response of the planar jet-plate system as a function of flow velocity at the nozzle exit (U_o) for a nozzle thickness of h=3mm and an impingement ratio of x_o/h=7.0.

One interesting trend found in Figure 3.7 is that after the onset of the fluid resonant mode at a flow velocity of U_o=268m/s, the acoustic pressure amplitude decreases to a local minimum at a flow velocity U_o=280m/s, to an amplitude comparable to those found in the linear regime, and subsequently increases as the flow velocity is increased further. This minimum in acoustic pressure corresponds to the coincidence between a pair of linear fit lines fitted to the tone frequency of the linear regime (f_{lin}), and to the sub-harmonic of the resonant tone frequency (f_r /2). After the onset of the fluid-resonant jet stage, the amplitude of the resonant tone (f_r) is shown to decrease monotonically as the coincidence point is approached. Concurrently, a pair of sub-harmonic components, f_a and f_b, which are symmetrically located about $f_r/2$, such that $(f_a+f_b)/2=f_r/2$, are found to increase in amplitude over the same range, reaching a maximum at the coincidence point. Post-coincidence, the resonant tone amplitude increases monotonically, and the sub-harmonic components decrease, eventually disappearing altogether at a flow velocity of $U_o \approx 290$m/s and replaced by a single sub-harmonic component, $f_r/2$. Huang & Hsiao (1999) observed a similar phenomenon in their work on acoustically excited planar jets, where two symmetrically positioned sub-harmonic components were observed and attributed to a "parametric resonance" phenomenon. The authors attributed the formation of two peaks to the relative phase between the waves of the fundamental (f_r) and the sub-harmonic ($f_r/2$) frequencies, which resulted in a sub-harmonic peak not at $f_r/2$, but $f_a = f_r/2 - \Delta f$, where Δf is related to the phase difference. Non-linear interaction produces a second, weaker peak, symmetrically located at a frequency of $f_b = f_r/2 + \Delta f$, and in the case of the current measurements which involves much higher sound pressure levels, a further peak at $f_r - 2\Delta f$. Figure 3.8 shows a series of five acoustic spectra taken at varying flow velocities both above and below the flow velocity marking the onset of fluid-resonant jet-stages. The various frequency components of interest have been labeled including the frequency of the linear and fluid-resonant tones (f_{lin} and f_r, respectively) as well as the sub-harmonic components (f_a, f_b and $f_r/2$).

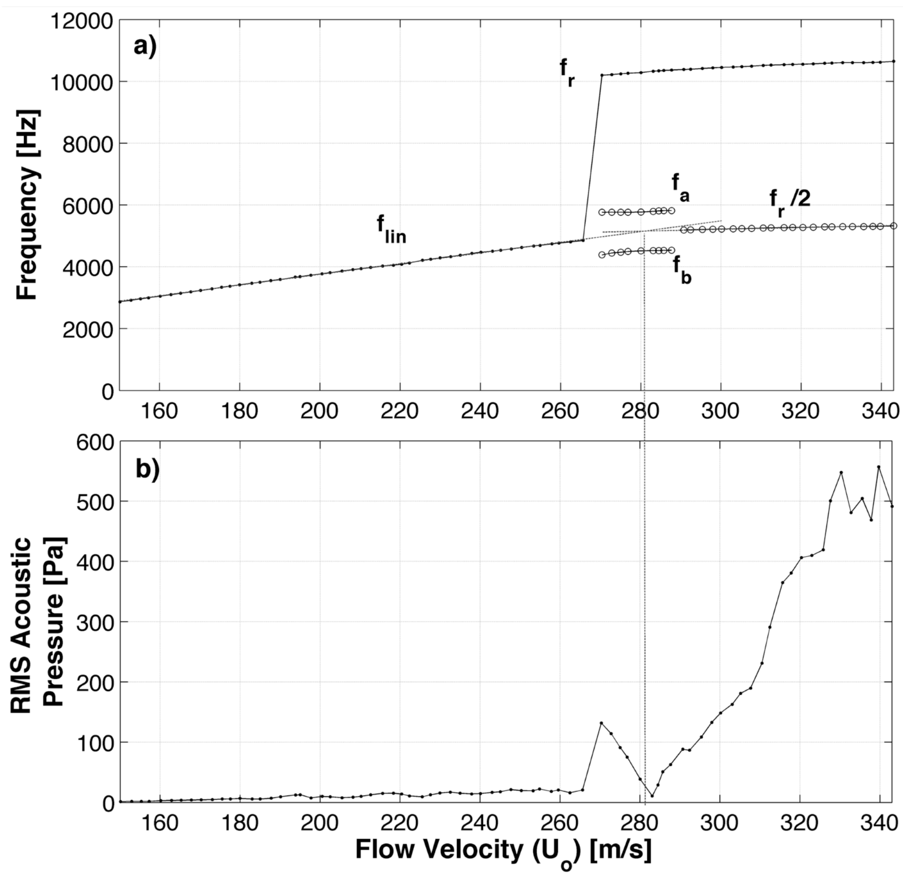

Figure 3.7: Frequency and amplitude of the dominant acoustic tone (•), and sub-harmonic frequencies (o) as a function of flow velocity of the planar jet-plate system for an impingement ratio of x_o/h=7.0.

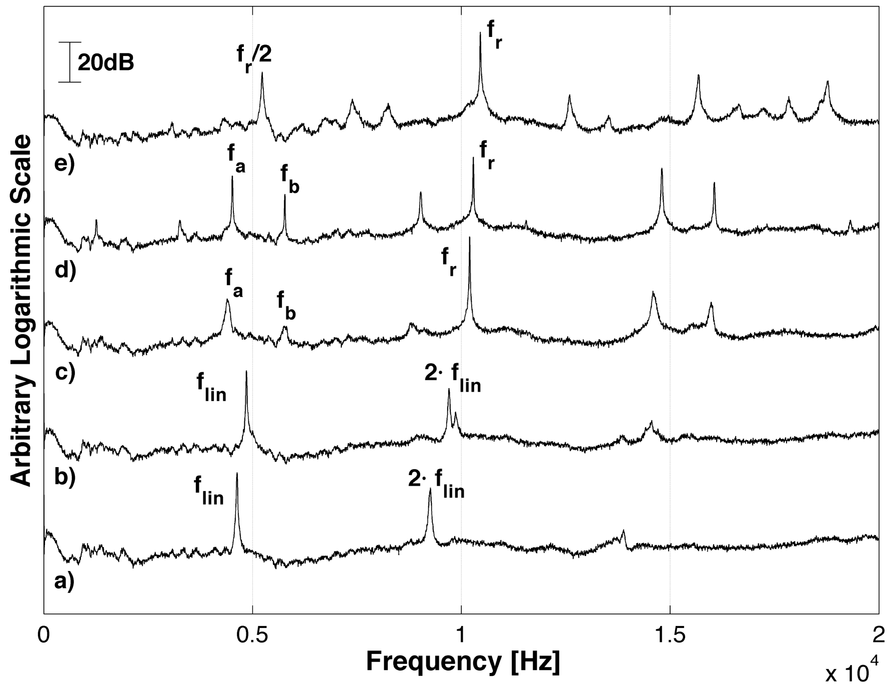

Figure 3.8: A series of acoustic spectra taken prior to and after the onset of fluid resonant tone generation (Each subsequent spectrum shifted by 50dB). a) U_o=250m/s, b) U_o=265m/s, c) U_o=268m/s, d) U_o=280m/s & e) U_o=300m/s.

Figure 3.9 shows the frequency and amplitude of the dominant acoustic tone as a function of varying impingement ratio for a constant flow velocity of U_o=300m/s (M=0.87). These results show that the planar jet-plate oscillator responds in a large number of distinct jet-stages, which generate dominant acoustic tones over a wide range of frequencies, in this case from f=4.0kHz to more than 30kHz. Each dominant tone has one or more clear super-harmonics, which are not included in the figure for clarity. Further, these tones occur over a large range of impingement ratios, from $x_o/h\approx 2$ up to $x_o/h\approx 28$, with frequent switching to both higher and lower jet-stages as the impingement ratio is increased. This range of excitation is significantly wider than the impingement ratio range of other similar geometries, such as the impinging axisymmetric jet flow. For instance, the high-speed subsonic impinging axisymmetric jet flow has been found to excite tones only over an impingement ratio range from $1.5 \leq x_o/D \leq 7.0$, or within the range of the potential core of a free axisymmetric jet, whereas the planar impinging jet is found to excite tones over a range of both the jet's potential core in free planar jets, as well as the transition region, and the beginning of the self-similar regime. Furthermore, the planar impinging jet case begins generating tones at lower flow velocities than the axisymmetric case, with the planar case exciting tones at Mach numbers as low as M=0.4, whereas the axisymmetric case begins exciting tones at M=0.6. Comparison of the current measurements with recent measurements of the impinging axisymmetric jet case performed by Panickar & Raman (2007) show that the amplitude of tone generation for planar and axisymmetric impinging jet cases is comparable when normalized for the total flow area of the two nozzles. It is clear from inspection of Figure 3.9 that the frequencies of the various stages display an approximately hyperbolic behavior, with tone frequency being inversely proportional to the impingement ratio. The amplitude of the dominant acoustic tones can be very high, with strongest tone excitation occurring for an impingement ratio falling near the middle of the range of excitation (x_o/h=10.2) at an amplitude of 144 dB, and with abrupt changes in amplitude occurring when the system switches between stages. The acoustic tone amplitude tends to decrease as the impingement ratio is increased or decrease from this impingement ratio, but amplitude of the dominant acoustic tone remains above 120dB for a range of impingement ratios from x_o/h=3.5 up to 23.0.

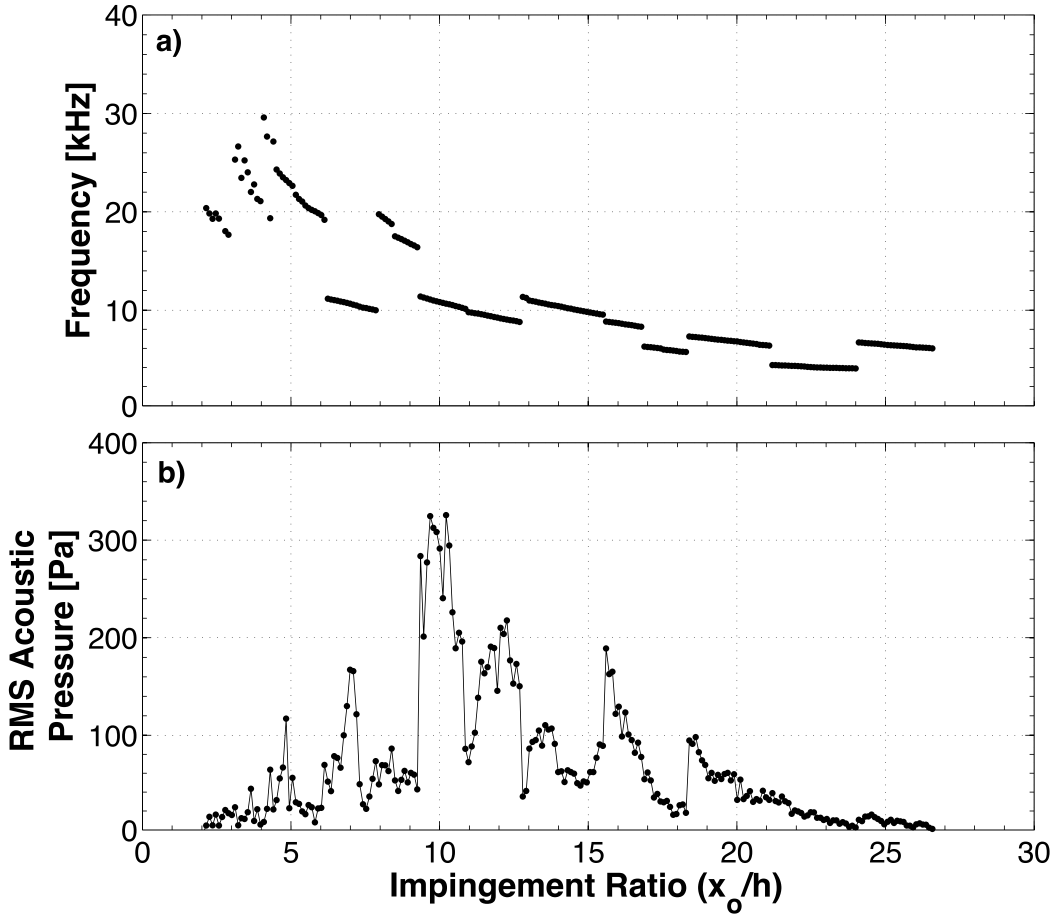

Figure 3.9: Frequency of the dominant acoustic tone as a function of the impingement ratio (x_0/h) of the planar jet-plate system with a nozzle thickness of h=3mm for a flow velocity at the nozzle exit of U_o=300m/s.

3.4 Dimensional Analysis

The results shown in the preceding section have shown that the planar jet-plate oscillator produces large amplitude acoustic tones that manifest in a series of distinct jet-stages as the impingement ratio and flow velocity are varied. In order to gain further understanding of the various stages excited by jet impingement, a thorough dimensional analysis will be applied. The Strouhal number is a dimensionless frequency comprised of f, the frequency in Hertz of the dominant acoustic tone, a length scale, L, and a velocity scale, U. Previous authors, such as Ho & Nosseir (1981), Nosseir & Ho (1982), Tam &

Ahuja (1990) and Panickar & Raman (2007) who investigated the tone generation process in the impinging *axisymmetric* jet flow, have used the diameter of the nozzle outlet (D) as the relevant length scale, and the flow velocity of the jet at the nozzle outlet (U_o) as the velocity scale. The same authors have attributed the generation of acoustic tones in impinging jet flows to a feedback cycle, consisting of a coupling between instabilities in the free shear layer and acoustic perturbations provided by impingement of coherent structures on the plate. Based on this heuristic model of the tone generation phenomenon, a more appropriate for the length scale would seem to be the impingement distance x_o, defined as the distance from the nozzle lip to the plate surface, as it is the distance traversed by both the coherent flow structures as well as the acoustic perturbations and as such, x_o has a direct impact on defining the frequency of the acoustic tones. The velocity scale chosen for the preliminary analysis will be U_o, the flow velocity at the centerline of the nozzle outlet. As reviewed by Rockwell & Naudascher (1979), this Strouhal number scale has been applied by many researchers to similar geometries, such as the jet-slot (Ziada, 2001 & Billon et al., 2005) and jet-edge geometries (Karamcheti et al., 1969 & Ziada, 1995), and is given in the following equation:

$$\mathrm{St}_{xo} = \frac{f \cdot x_o}{U_o} \quad . \tag{3.2}$$

Figure 3.10 shows the results of the Strouhal number as a function of Mach number for an impingement ratio of x_o/h=7.0, the same case shown in Figures 3.6 and 3.7. The initial jet-stage, occurring for Mach numbers of M<0.78, shows a Strouhal number which is approximately constant at $\mathrm{St}_{xo} \approx 0.4$ with a slight decreasing trend with increasing Mach number, indicating that the tone frequency of this stage is approximately proportional to the flow velocity at the jet outlet. The higher jet-stage on the other hand, which is excited for M>0.78, shows a strong decreasing trend in the Strouhal number as a function of increasing Mach number, as the tone frequency of this stage was found to be approximately constant as the Mach number is increased within this range.

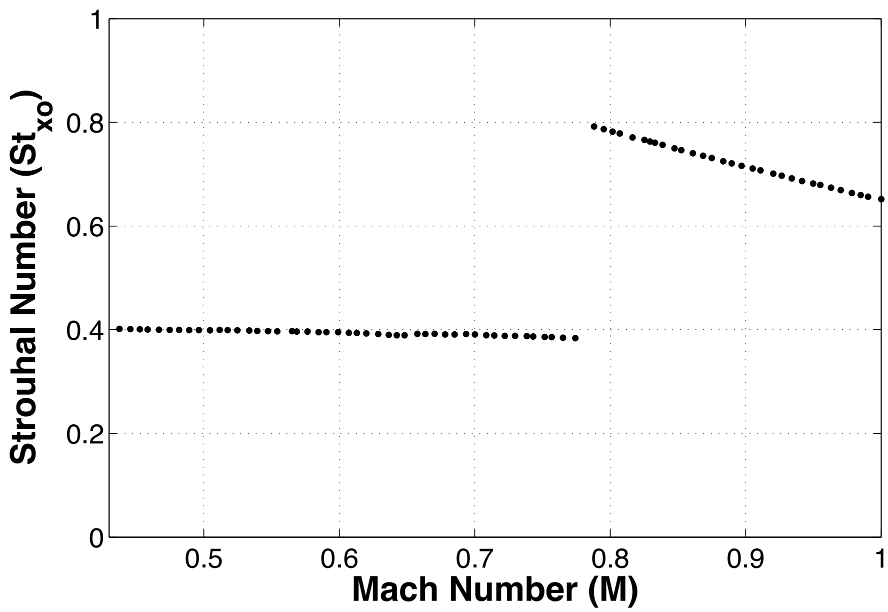

Figure 3.10: The Strouhal number (St_{xo}) based upon impingement distance (x_o) and jet velocity (U_o) of the dominant acoustic tone as a function of Mach number for an impingement ratio of x_o/h=7.0 and a nozzle thickness of h=3mm.

Figure 3.11 shows the same Strouhal number scale applied to the complete data set of tone generating conditions collected for all impingement ratios and Mach numbers tested. These measurements consist of a range of Mach numbers between 0.44≤M<1.0 and impingement ratios of $2.0 \leq x_o/h \leq 32.0$. Inspection of the plot shows a good collapse for the linear jet-stage, for which the data for each impingement ratio shows a nearly constant Strouhal number near $St_{xo} \approx 0.4$ for Mach numbers from M=0.44 to 0.77. There is some variation in the mean Strouhal number of the linear stage as the impingement ratio is varied, particularly for the larger impingement ratios, with the mean Strouhal number decreasing as the impingement ratio is increased. All other data points shown on this figure correspond to tones excited within the fluid-resonant regime and show a fair collapse, but no overall trend is distinguishable.

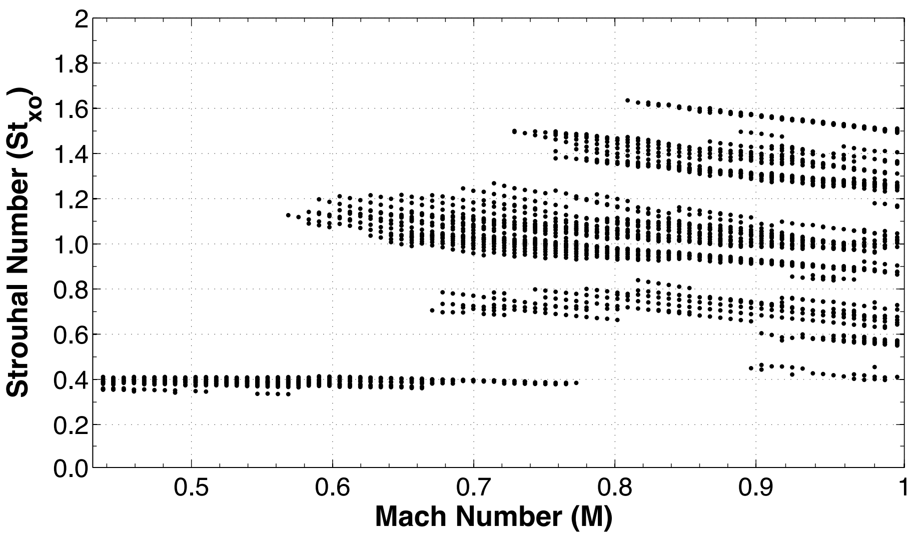

Figure 3.11: The Strouhal number (St_{xo}) based upon impingement distance (x_o) and jet velocity (U_o) of the dominant acoustic tone as a function of Mach number for all tone generating conditions of the impinging planar jet for impingement ratios between x_o/h=2.0 and 32.0.

In order to better understand the behavior of the frequency data, and to identify the various jet-stages generating the tone for the planar case, a more appropriate velocity scale has been developed. The use of the flow velocity at the nozzle outlet (U_o) as a velocity scale is common in many related geometries, such as the jet-slot and jet-edge cases. These geometries are typically self-excited at Mach numbers far lower than the current impinging planar jet case, with the flow velocity typically being less than 10% of the speed of sound. As a result, in these geometries the time taken for an acoustic perturbation to traverse the distance between the downstream geometry and the nozzle lip is a small fraction of the time taken for a coherent flow structure to travel the same distance, so that the acoustic propagation time has a relatively small effect on the frequency, typically less than 5%. Therefore, the acoustic propagation time is typically neglected altogether for these lower speed geometries, an assumption often referred to as a "hydrodynamic model", which results in significant simplification of the model, and still yields excellent prediction for low Mach number systems.

The current geometry however, involves flows at Mach numbers at or approaching the speed of sound. Consequently, the propagation time of acoustic disturbances and coherent structures are comparable, and thus the velocity scale should represent an *effective velocity* for the *complete* feedback cycle, considering both downstream propagating flow structures, as well as upstream propagating acoustic disturbances. This effective velocity scale, U_{eff}, is given in the following equation:

$$U_{\mathrm{eff}} = \frac{2 \cdot u_{\mathrm{c}} \cdot c}{u_{\mathrm{c}} + c}, \tag{3.3}$$

where u_{c} is the convection velocity of downstream propagating coherent flow structures and c is the speed of sound. The effective flow velocity scale takes this form as it is not simply an average of the downstream and upstream velocities, but reflects the total time taken for the feedback cycle. A similar velocity scale has been used in the feedback models proposed by a number of authors examining the axisymmetric impinging jet case, including Ho & Nosseir (1981) Nosseir & Ho (1982), Tam & Ahuja (1990) and Panickar & Raman (2007). In these studies, the downstream velocity scale (u_{c}) has been approximated by the flow velocity at the nozzle outlet, multiplied by a convection coefficient κ, defined as the ratio of structure convection speed to flow speed, and is typically in the range of $0.5<\kappa<0.7$. The application of this effective velocity scale in the axisymmetric jet models resulted in accurate predictions of frequency of the n^{th} shear layer mode as a function of both flow velocity and impingement ratio.

The present planar jet configuration requires some modifications to the downstream portion of the effective velocity scale, due to the characteristics of tone excitation in the planar system, and the significant differences in the structure of the self-excited planar impinging jet flow compared to the axisymmetric case. The axisymmetric impinging jet case has been found to generate strong acoustic tones for impingement ratios from $1.5 \leq x_o/D \leq 7.0$, i.e. when the plate is positioned within the range of the potential core for free axisymmetric jets. Thus, the basic structure of the impinging axisymmetric jet flow for this range of impingement ratios involves an inner potential core between the nozzle and plate surface which travels at the same flow velocity as at the nozzle outlet, except for the impingement region. This high-speed inner core is surrounded by relatively stagnant entrained flow. Because of these structural characteristics of the axisymmetric impinging jet flow, coherent structures formed at the nozzle lip and convected in the shear layer are bound by the flow within the jet potential core, and the low-speed entrained flow surrounding the jet for virtually the entire impingement distance. These specific conditions allow for the application of the relatively simple model for the downstream velocity component described earlier.

The impinging planar jet case, on the other hand, generates acoustic tones over a much larger range of impingement ratio, from $x_o/h \approx 2$ up to $x_o/h \approx 31$, a range that not only encompasses the potential core structure for planar jets, but which also extends well beyond. For impinging jet flows with relatively large impingement ratios, a bulk slowing of the jet flow will occur as the flow enters the transition region, occurring downstream of the jet potential core. As a result, modifications to the downstream component of the effective velocity scale are required to account for this effect. Measurements of the mean flow field of the present case were made using Particle Image Velocimetry (PIV) for a range of impingement ratios from x_o/h=3 up to x_o/h=32, and an empirical expression was developed to estimate the downstream component of the effective velocity scale. These expressions approximate the mean flow velocity along the centerline of the impinging jet flow between the nozzle lip to the edge of the impingement zone ($0 \le x/x_o \le 0.9$), multiplied by the convection coefficient κ, and are given in the following equations:

$$u_c = \kappa \cdot U_o \qquad \text{for } x_o/h < 8.5 \text{, and} \tag{3.4}$$

$$u_c = \kappa \cdot U_o \cdot 1.6 \cdot \left(x_o/h \right)^{-0.26} \qquad \text{for } x_o/h \geq 8.5 \text{.} \tag{3.5}$$

Equation 3.4, which applies to impingement ratios occurring near the range of the potential core, has an identical form as the expression used by Panickar & Raman (2007) and others, and both Equations for downstream velocity component the same value of convection coefficient of κ=0.58 as determined by fitting to the current data, compared to κ=0.55 used by Panickar & Raman (2007) for the axisymmetric case.

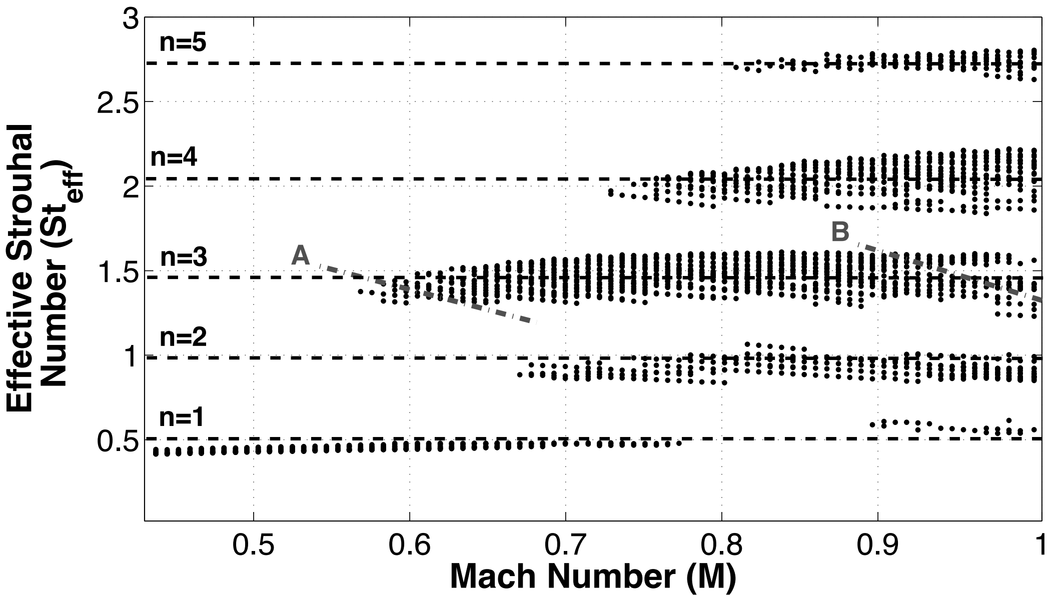

Figure 3.12: The effective Strouhal number (St_{eff}) of the dominant acoustic tone as a function of Mach number for all tone generating conditions of the impinging planar jet for impingement ratios between x_o/h=2.0 and 32.0. Dotted lines correspond to the mode number (n) of the shear layer instability.

When this effective Strouhal number scale, which given in the following equation:

$$\mathrm{St}_{x_{\mathrm{eff}}} = \frac{f \cdot x_{\mathrm{o}}}{U_{\mathrm{eff}}}, \tag{3.6}$$

is applied to the dominant tone frequency data for all tone generating conditions tested, as shown in Figure 3.12, a much more effective collapse of the data is observed compared with the initial Strouhal number scale. Data points corresponding to the linear jet-stage, which now occur at a mean Strouhal number of $St_{xeff} \approx 0.47$, show a better collapse than for the initial Strouhal number scale, which showed some variation for larger impingement ratios. The effective Strouhal number scale compensates for the slowing of the jet flow at larger impingement ratios, resulting in a better collapse of the data. The collapse of the data corresponding to the higher fluid-resonant stages of the jet has improved significantly through the use of the new velocity scale, with the data now collapsing to five distinct bands, indicated on the figure by their stage number, n=1 through n=5. The most prevalent of these fluid-resonant modes is the n=3 jet-stage, which occurs for Mach numbers as low as M≈0.55, with other modes occurring at a range of impingement ratios as the Mach number is increased. It is clear from the figure that for the higher Mach numbers tests, numerous jet-stages can occur depending on the impingement ratio.

Figure 3.13 shows the dimensionless pressure P^* as a function of the effective Strouhal number for all tone generating conditions, with dimensionless pressure being given in the following equation:

$$P^* = {P_{\text{rms}}}/{P_s} \,, \tag{3.7}$$

where P_{RMS} is the RMS acoustic pressure of the dominant acoustic tone and P_s is the supply pressure. This scale is similar to the dimensionless pressure commonly used in may related geometries such as the jet-edge and jet-slot using incompressible flows, which normalize the RMS acoustic pressure by the dynamic pressure for the flow. The supply pressure is the most physically analogous pressure scale for the current compressible flow case, and provides the most relevant comparison. The figure shows that modes n=2 and n=3, occurring at Strouhal numbers of St_{xeff}≈1.0 and ~1.5 respectively, respond most strongly, with the other fluid-resonant tones and tones generated by the linear stage responding at lesser amplitudes.

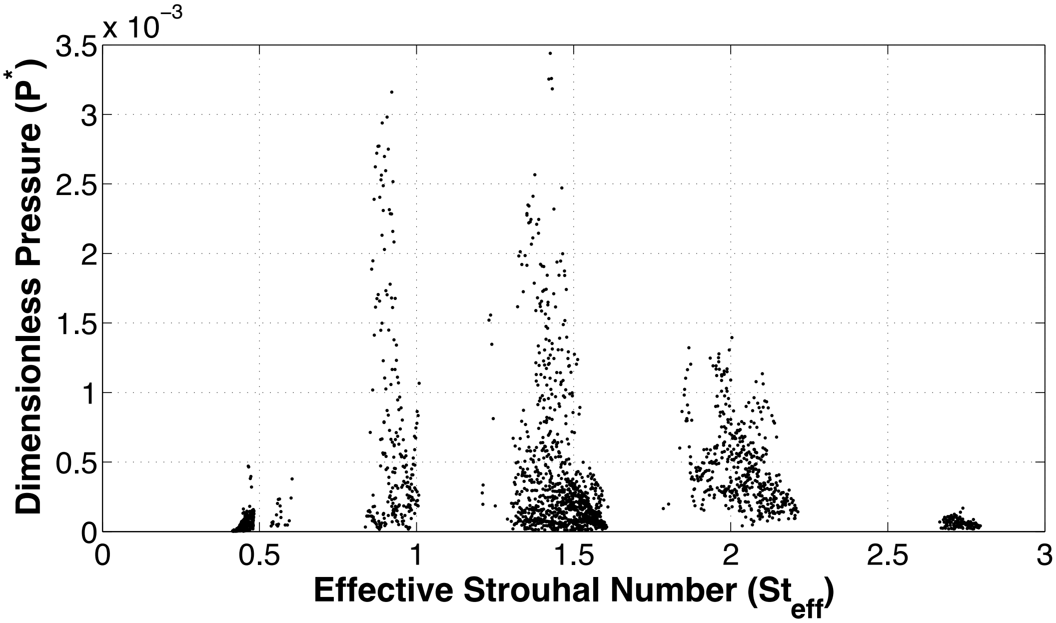

Figure 3.13: Dimensionless pressure (*P) as a function of Effective Strouhal number (St_{eff}).**

Figure 3.14 shows a contour plot illustrating the distribution of the various jet-stages as a function of both the Mach number and the impingement ratio. This figure shows that the different jet-stages (*n*), denoted by Arabic numbers, occur in a series of distinct bands occurring for concurrently increasing Mach number and impingement ratio. These jet-stage bands are further sub-divided into smaller bands, denoted with roman numerals, corresponding to the various sub-stages (*m*) of each jet-stage. The jet-stage number (*n*) refers to the form of the shear layer instability driving tone generation, i.e. a certain number of structures occurring between the nozzle and the plate, whereas each sub-stage number (*m*) corresponds to a coupling with a given *resonant acoustic mode* occurring in the air volume between the nozzle and the plate. As will be shown in a subsequent figure, each sub-stage occurs over a discrete range of frequency, with jumps in frequency occurring between changes in both jet-stage and sub-stage. Inspection of this figure shows that the critical flow velocity: the lowest flow velocity for which appreciable acoustic tones are excited, varies depending on the impingement ratio under consideration. For configurations with larger impingement ratios, near x_o/h=30, the critical flow velocity required to generate acoustic tones is near choked flow (U_o=343m/s). As the impingement ratio is decreased, the critical flow velocity tends to decrease progressively, and the amplitude of the tones for a given flow velocity tends to be greater than for those generated at larger impingement ratios. This trend of decreasing critical flow velocity with decreasing impingement ratio continues until the impingement ratio range of $7.0 \leq x_o/h \leq 10.5$, for which tones are excited for the complete range of flow velocity tested. The impingement ratio corresponding to the largest acoustic amplitude for a given Mach number also tend to occur in this range, with an example if this characteristic having been shown earlier in Figure 3.9. As impingement ratio is decreased further to impingement ratios of less than x_o/h=7.0, the critical flow velocity begins to increase once more, with tones eventually ceasing at a minimum impingement ratio of x_o/h=2.2 for a flow velocity of $U_o \approx 343$m/s. For the sake of clarity, the behavior of the sub-stages belonging to the n=3 jet-stage will be explained in the following example with reference to both Figures 3.12 and 3.14.

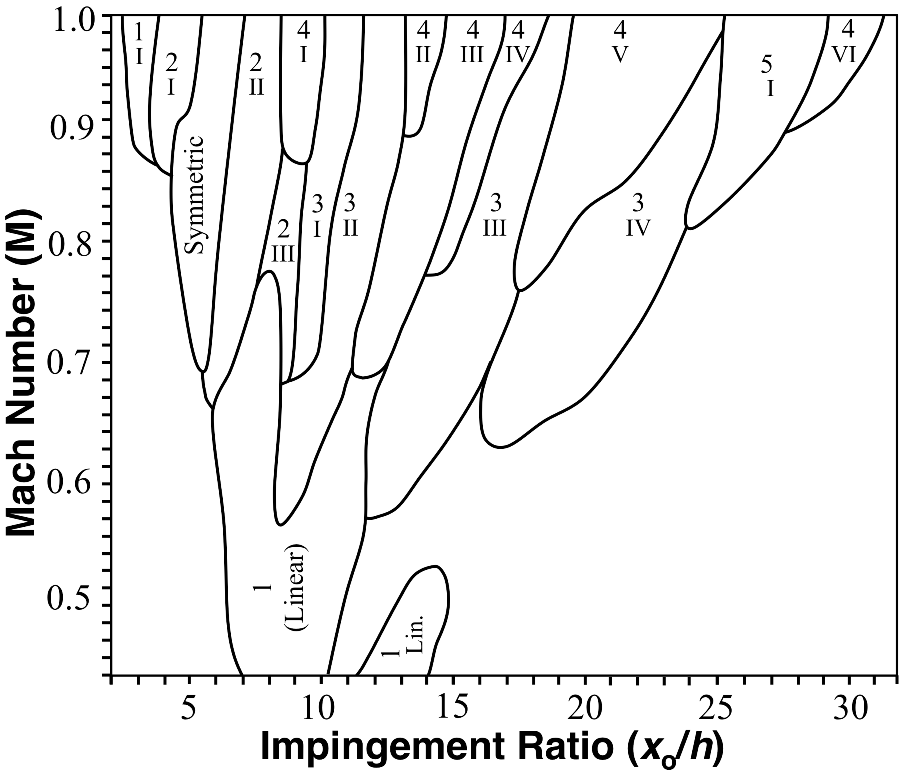

Figure 3.14: The jet-stage diagram for the planar jet-plate system with a nozzle thickness of h=3mm. Measurements taken in a grid pattern from 0.44≤M<1.0 in increments of ±0.007 and 2.0≤x_o/h≤32.0 in increments of ±0.5.

Beginning at low impingement ratios, the n=3 jet-stage is first excited in the m=II sub-stage at impingement ratios of x_o/h=8.5 for Mach numbers between M=0.6 and 0.7. On Figure 3.12, the data of this sub-stage will fall nominally along line A, with a clear decreasing trend in effective Strouhal number occurring as the Mach number is increased. As the impingement ratio is increased, the m=II sub-stage is excited over a range of progressively higher Mach numbers, with each data series showing a very similar downward sloping trend as shown by line A, but with the data moving progressively towards line B shown in Figure 3.12 as the impingement ratio is increased. The data belonging to the next sub-stage (m=III) of n=3 jet-stage is excited beginning at impingement ratios of x_o/h=11.5, will also fall near line A, and as the impingement ratio is increased will move back towards line B, in a similar fashion as the previous sub-stage. Thus, the change from one sub-stage to another, within the same jet-stage, as the impingement ratio is increased is associated with a jump back from line B to line A, illustrated in Figure 3.12. Each of the various sub-stages excited by jet-stages in the fluid-resonant regime shows this characteristic trend, with the sub-stages being initiated at relatively low Mach number for small impingement ratios, being excited at progressively higher ranges of Mach number as the impingement ratio is increased, and eventually ceasing or shifting to supersonic jet velocities as the impingement ratio increases.

The linear jet-stage is shown as the n=1 mode at the lower end of range of Mach number in Figure 3.14, for a range of impingement ratios from $5.5 \leq x_o/h \leq 15.5$. The n=1 jet-stage is also excited in the fluid-resonant regime for higher Mach numbers and relatively small impingement ratios. Jet-stages n=2 through n=5, are excited exclusively within the fluid-resonant regime and there is a general trend for the system to be excited at lower stages for smaller impingement ratios, such as the n=1 and n=2 stages, and at higher jet-stages as the impingement ratio increases. This is only a general trend however, and there is also frequent switching to lower modes as the impingement ratio is increased. As revealed by means of PIV measurements, the jet oscillates in an anti-symmetric pattern except for a single *symmetric* stage which is excited for Mach numbers greater than M=0.7 and for an impingement ratio range from x_o/h=4.5 to 6.5. The excitation of this symmetric jet-stage is thought to be produced by fluid-resonant coupling with a symmetric acoustic mode, as opposed to anti-symmetric acoustic modes which couple with anti-symmetric jet stages.

3.5 Application of a Modified Rossiter Model

The model developed by Rossiter (1964), for use with transonic and supersonic flows over rectangular cavities, is a relatively simple heuristic model based on the principle of a feedback mechanism between instabilities in the free shear layer, and acoustic perturbations generated by the impingement of coherent flow structures. The model assumes that the downstream and upstream propagating disturbances travel at approximately constant velocities of u_c and c, respectively over the impingement distance x_o, and that the frequency of the n^{th} stage is determined by the total propagation time divided by the stage number, n. The model is given in the following equation:

$$f_n = \frac{n \cdot u_c \cdot c}{x_o \left(u_c + c \right)}, \tag{3.8}$$

and provides an estimate of the frequency of the n^{th} shear layer stage based on the convection velocity (u_c), convection coefficient (κ), and impingement distance. Many authors have utilized this model for low Mach number systems such as the jet-edge and jet-slot systems under the so-called hydrodynamic assumption, and others authors, such as Ho & Nosseir (1981) and Panickar & Raman (2007), have applied the model successfully to the high-speed impinging axisymmetric jet system. In this section, the Rossiter model is applied to the current high-speed impinging planar jet system, using the empirical expression developed to estimate the downstream velocity component (u_c) given in Equations 3.4 and 3.5.

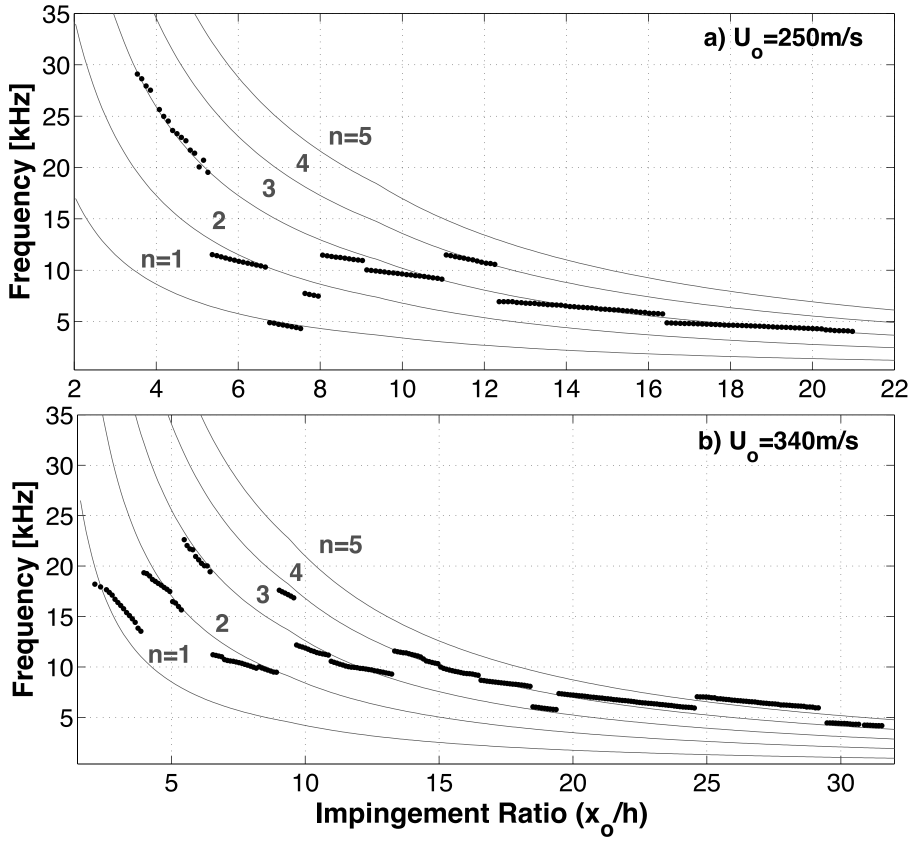

Figure 3.15: Frequency of the dominant acoustic tone as a function of impingement ratio compared with the prediction of first five jet-stages of the Rossiter model of Equation 3.8.

Figure 3.15 shows the prediction of the first five Rossiter stages as a function of impingement ratio for two cases with fixed flow velocities of U_o=250m/s and 340m/s respectively. The model has been found to predict tone frequency of the n^{th} mode well. The fit of the model to the frequency data of impingement ratios near the range of the potential core, x_o/h<8.5, where the downstream velocity scale is defined by Equation 3.4, is similar to that used by Panickar & Raman (2007) for an impinging axisymmetric jet. The empirical relation used to approximate the downstream convection velocity for larger impingement ratios, given by Equation 3.5, has also been found to produce good agreement over a wide range of impingement ratios. Thus, the Rossiter model provides a relatively simple and robust set of expressions to estimate the potential frequency of acoustic tones that may be generated, and the jet-stage responsible for tone generation. The majority of the discrepancy between the data and the Rossiter model is due to the fluid-resonant coupling that is not accounted for in the model.

3.6 Shear Layer Modes

In order to reveal the flow oscillation pattern, i.e. the shear layer mode of each jet-stage, extensive flow measurements have been performed using PIV. The flow oscillations for the present impinging planar jet case range in frequency from 4kHz to more than 30kHz, and typical commercial high-speed PIV systems currently available are not capable of producing a time resolved image series with an adequate number of frames over a given cycle at even the low end of this frequency range. The PIV measurements have instead been performed using standard speed PIV system with a maximum acquisition rate of ~7Hz by utilizing a phase-locked measurement technique, in which a series of images of the flow are captured at a series of specified points within the phase of the flow oscillation in order to reconstruct a time series of the flow oscillation cycle. The individual measurements are triggered using the signal obtained by a pressure transducer flush mounted to the surface of the plate in the impingement zone. By adding and manipulating a time delay between the trigger point and the flow measurement, sets of images can be collected at any point in the phase of the cycle. This technique allowed for the reconstruction of periodic flow oscillations in excess of 20kHz, yielding results not possible using other methods.

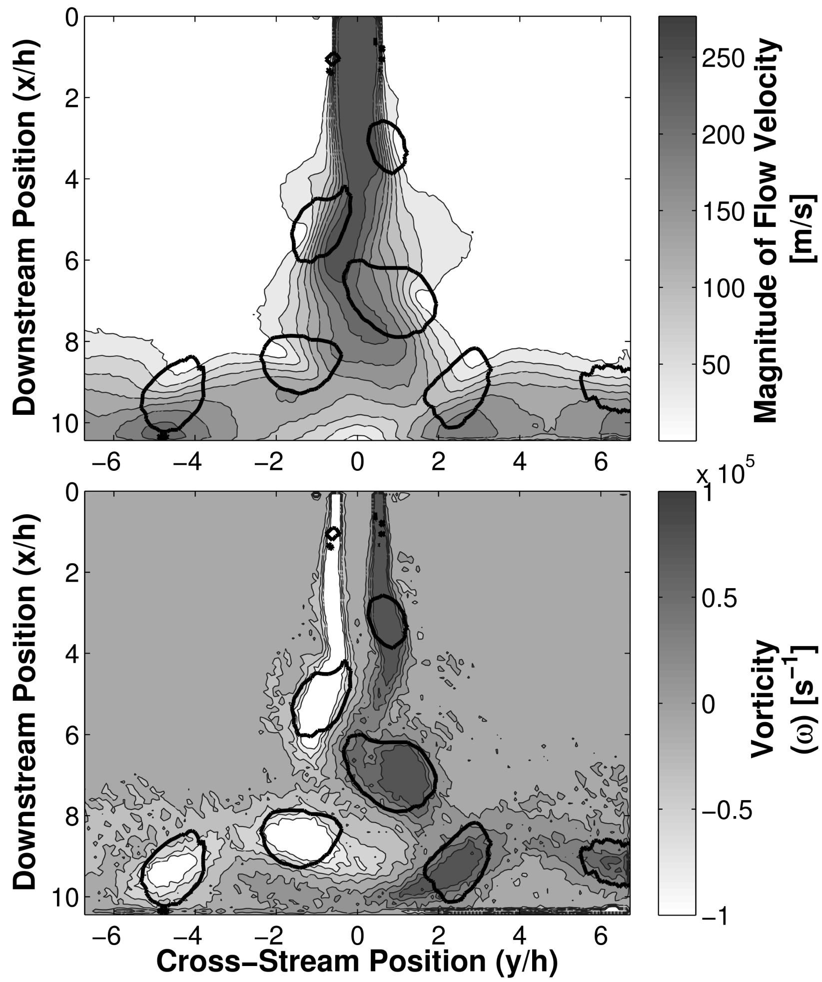

Figure 3.16: a) The velocity and b) vorticity fields of the *n*=3 anti-symmetric shear layer mode generated using the average of 100 instantaneous images obtained at a constant phase in the oscillation cycle. The vorticity field has ben superimposed with the coefficient d_2 for identifying coherent structures in the shear layers. x_o/h=10.5, U_o=275m/s (M=0.8), *f*=9.5kHz.

Figure 3.16 shows a flow field produced using the phase-locked measurement technique, which was composed using the average of 100 instantaneous velocity fields acquired at the same point in the phase of the flow oscillation. The impinging jet case shown has an impingement ratio of x_o/h=10.5 and a flow velocity of U_o=275m/s, which produces an n=3 anti-symmetric flow oscillation at a frequency of f=9.5kHz. The phase-averaged field shows the same general form and characteristics as any of the 100 instantaneous fields, but with a smoother image, which allows for more effective interpretation of the flow field, as well as less noise in the calculation of velocity gradient terms. Inspection of the flow field shows that for the n=3 anti-symmetric flow oscillation, a columnar displacement or flapping motion of the jet is shown, which ultimately produces alternating high and low velocity pockets of flow at the plate surface in the wall jet region. Note that similar PIV images, together with measured tone frequency were used to identify the other jet-stages outlined in Figure 3.14.

One of the most important characteristics of the flow field is the presence of coherent flow structures, and the manner in which they propagate between the nozzle lip and the plate surface. One of the traditional methods used to identify these structures is the use of the vorticity field, as shown in the lower image of Figure 3.16, which corresponds to the velocity field shown in upper image of the same figure. Unfortunately, impinging planar jet flows have a number of other features that generate very high levels of vorticity, such as the initial shear layers near the nozzle lip, as well as the boundary layers formed at the impingement surface. These regions contain vorticity magnitudes that are typically greater than those found in the coherent structures, which can result in significant difficulty in structure identification using the vorticity field. Another method, which has been developed by Vollmers (2001), uses the discriminant of the velocity gradient tensor, and is given in the following equation:

$$d_2 = \left(\frac{\partial u}{\partial x} + \frac{\partial v}{\partial y}\right)^2 - 4\left(\frac{\partial u}{\partial x}\frac{\partial v}{\partial y} - \frac{\partial u}{\partial y}\frac{\partial v}{\partial x}\right). \qquad (3.9)$$

This quantity, also commonly referred to as the “swirl” of the flow field, uses a non-linear combination of velocity derivative terms to identify areas of strong vorticity that have a particular shape characteristic, i.e. round or near-round structures. Other features of the flow with high vorticity, such as boundary layers and shear layers, are not typically identified by this parameter because of their non-circular shape characteristics. The discriminant parameter d_2 is a scalar, and will give a negative value when a structure is detected, and a positive value if no structure is detected. As a result, this parameter is used only to indicate the presence or absence of a coherent vortical structure, and cannot be used to assess the sign or direction of rotation of the structure.

A single contour level of the swirl parameter has been superimposed on the flow fields shown in Figure 3.16, with a contour level of d_2=0. The swirl parameter clearly identifies the presence of an anti-symmetric pattern of coherent structures on either side of the centerline of the jet flow, with each identified structure being centered over areas of high vorticity on either side of the jet column. The parameter also produces much better fidelity in structure identification than the vorticity field at locations further upstream in the vicinity of the initial shear layer, and does not mistakenly identify structures at other high vorticity areas of the flow, such as the boundary layers at the plate surface. The presence of the structures near the plate surface occurring post-impingement in the wall-jet region is also apparent; although the strength of the structures do begin diminish after impingement on the plate surface.

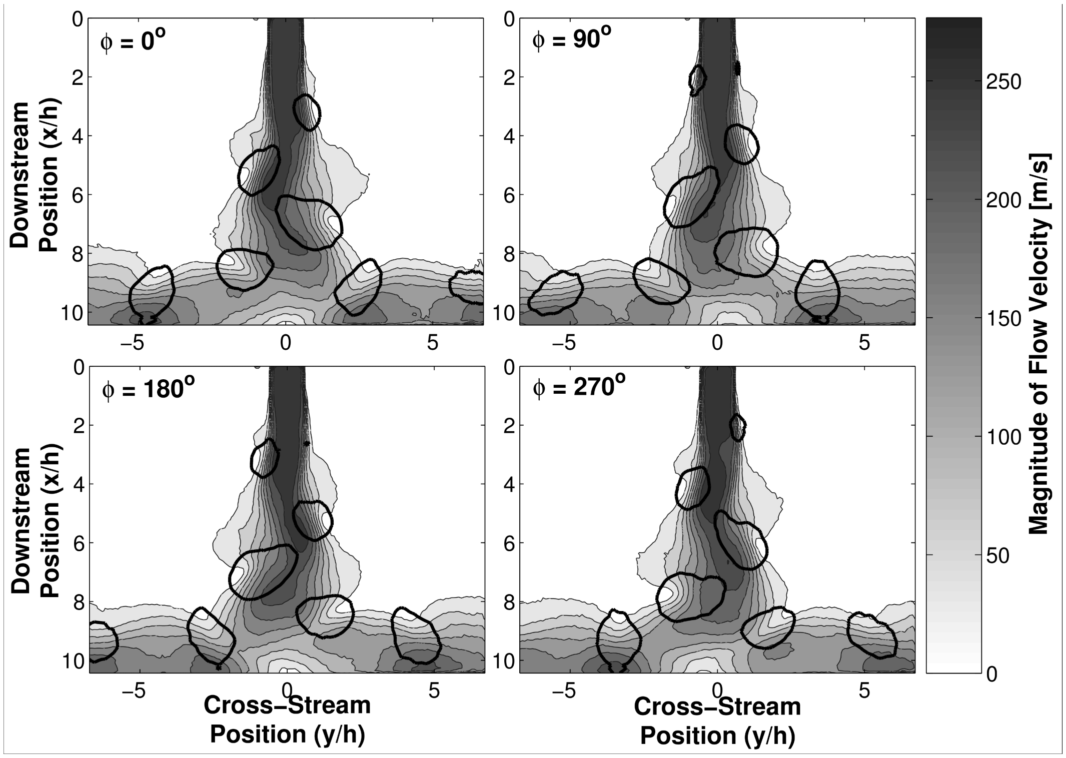

Figure 3.17: Phase-averaged velocity fields showing one cycle of the flow oscillation with phase increments of ϕ=±90° for the n=3 anti-symmetric shear layer mode, showing the formation, convection and impingement of coherent structures. x_o/h=10.5, U_o=275m/s (M=0.8), f=9.5kHz.

In order to visualize the flow oscillation over a complete cycle, a series of four phase-averaged velocity fields taken at phase angle increments of 90° are shown in Figure 3.17. Inspection of this figure clearly shows that the impinging jet flow oscillates in a columnar instability, with the jet flow displaced from the centerline in a wave-like pattern, and with coherent flow structures positioned nominally at the saddle points of the wave pattern. The columnar oscillation appears to propagate downstream in time as the phase of the oscillation progresses, with the structures located near the saddle points of the wave pattern also propagating downstream, and ultimately impinging on the downstream surface. The flow oscillation appears to have two structures in each shear layer on either side of the jet appearing between the nozzle and the plate, although this assessment is somewhat ambiguous as it is not entirely clear at which point in the cycle the structure has "impinged" on the plate surface, and detection of relatively small structures in the initial shear layer is difficult using this method. A high-velocity pocket of flow occurs near the impingement surface between the plate and the coherent structure, with the rotation of the structure contributing to the increased velocity at these locations. These high velocity pockets propagate with the structure as it travels along the surface of the plate. For the current case, these periodic high-velocity pockets are more than 25% larger than the mean flow in this region, and represent a large fluctuating flow component at the surface of the plate. The impinging jet flow also shows a stationary stagnation region in the impingement zone near the plate surface at the jet centerline, a feature also found in non-fluctuating impinging jet flows.

The results of the preliminary dimensionless analysis performed in this paper have shown that the use of the impingement distance and an effective flow velocity scale in the Strouhal number results in a collapse of the frequency data to a series of distinct jet-stages. By assigning the different groups of Strouhal number a distinct stage number, and displaying the stage number as a function of Mach number and impingement ratio, as shown in Figure 3.14, it has been shown that each of the various stages occurs in a series of distinct recurring bands. In order to confirm that the recurring bands of each jet-stage identified in the earlier dimensionless analysis do in fact, correspond to the same jet-stage, PIV measurements were performed for approximately 55 configurations distributed throughout the range of impingement ratio and Mach number for which tones are generated, with measurements being performed at multiple locations within each band, and for each stage.

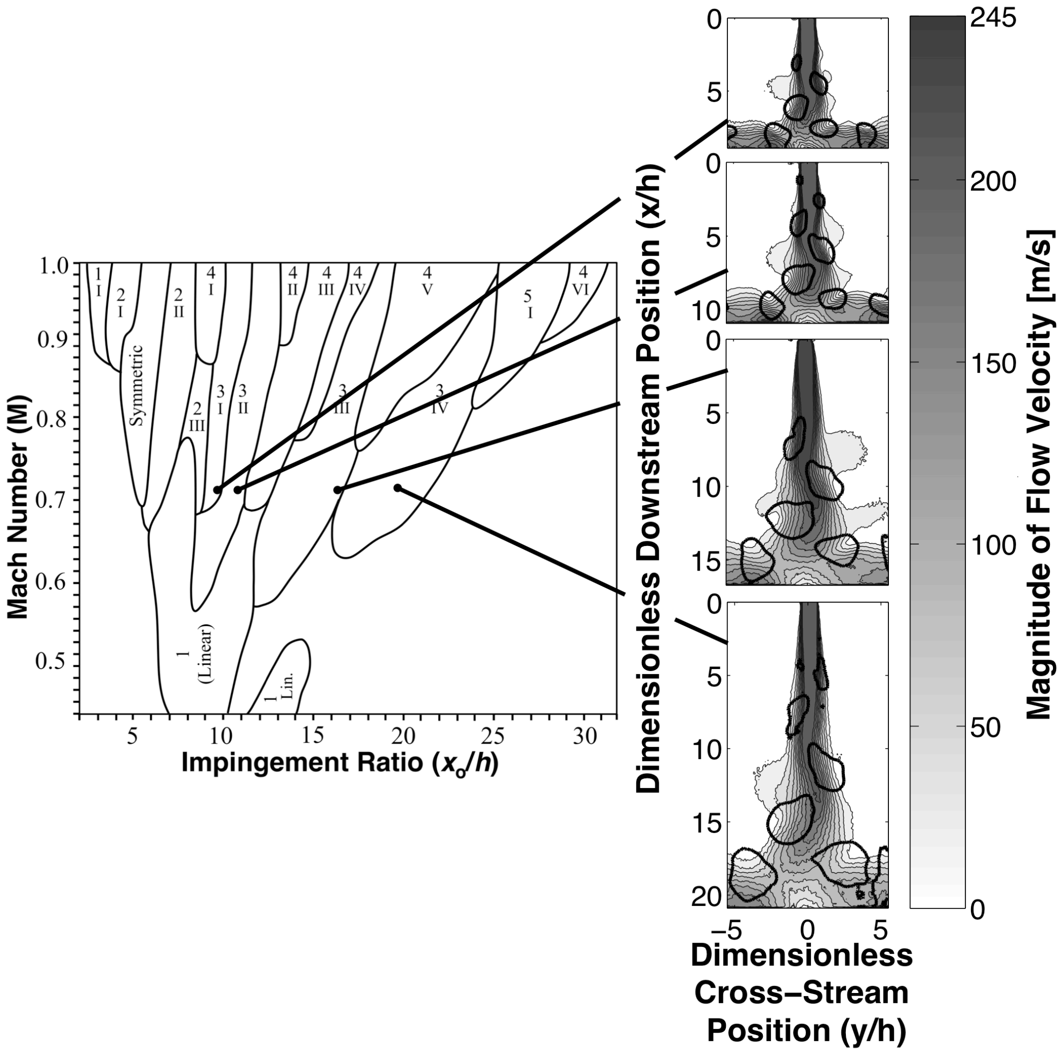

Figure 3.18: Velocity field of the *n*=3 anti-symmetric shear layer mode measured at the same point in the phase of the oscillation for impingement ratios of (top plot) x_o/h=9.15, (second plot) x_o/h=10.5, (third plot) x_o/h=17.0 and (bottom plot) x_o/h=20.4. U_o=245m/s (M=0.71) for all cases.

Figure 3.18 shows a series of four phase-averaged flow fields at a constant flow velocity and for varying impingement ratios occurring at locations within each of the four distinct bands for the *n*=3 anti-symmetric mode. Each of the four flow fields shown are at the same instant in the phase of the flow oscillation, and the flow fields within each of the four bands shows a very similar distribution of flow and coherent structures. The number of structures occurring on either side of the jet, as well as the general form of the flow oscillation is comparable for each case, indicating that the same jet stage is in fact excited in a series of repeating bands occurring at different combinations of Mach numbers and impingement ratios. PIV measurements performed in the separate bands of all other jet-stages showed similar results, with the same jet-stage being excited in the multiple distinct bands.

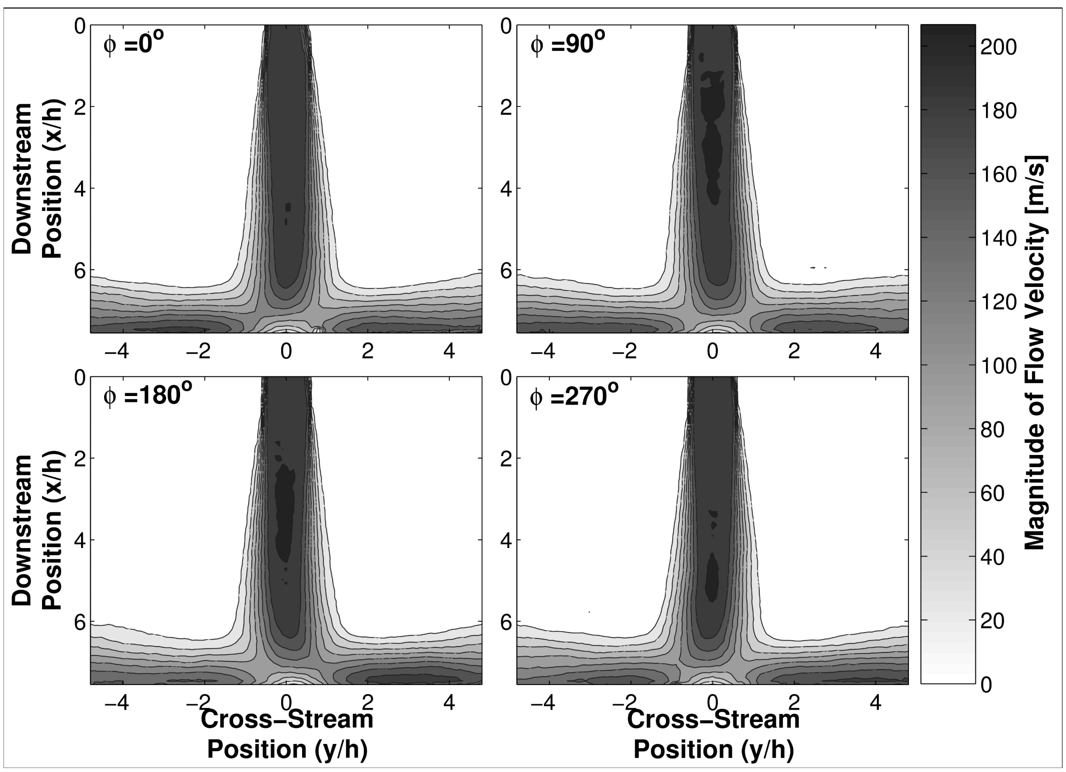

Figure 3.19: Phase-averaged velocity fields showing one cycle of the flow oscillation with phase increments of ϕ=±90° for the n=1 anti-symmetric shear layer mode in the linear regime, showing the form of the flow oscillation. x_o/h=7.0, U_o=210m/s (M=0.61), f=4.5kHz.

As has been discussed in the previous portions of this paper, the impinging planar jet flow excites tones in two separate regimes produced by two related, but distinct mechanisms: a linear response regime, which is excited by a traditional Rossiter mode, and a fluid-resonant response regime, consisting of a Rossiter mode coupled with a resonant acoustic mode. Figure 3.19 shows a series of flow fields for a flow oscillation occurring in the linear regime, for a flow velocity of U_o=210m/s and an impingement ratio of x_o/h=7.0, which generates a tone at a frequency of f=4.5kHz. The flow oscillation observed in the linear regime appears to be significantly different from the stages driven by the fluid-resonant mechanism. The magnitude of both the flow fluctuations and the resulting acoustic pressure fluctuations are significant, but are much smaller than those generated by the fluid-resonant mechanism, even for similar flow velocities of the impinging jet. Furthermore, the presence of large-scale coherent flow structures that dominated the flow field of the fluid-resonant case are not present in the case of the linear regime. For the linear stage, the jet flow oscillates in a flapping pattern, similar to the first mode of vibration of a cantilever beam, with the fixed end located at the nozzle outlet, and the free end at the plate surface. This flow oscillation appears to occur in a pure rocking mode, with no coherent vortical structures being formed in the initial shear layers and the pronounced convective flapping phenomenon that was present in the fluid-resonant case is not found in the linear jet-stage flow oscillation.

Figure 3.20 shows a series of PIV flow fields obtained for some of the remaining modes of the jet. The figure shows the n=2, 3 and 4 anti-symmetric stages, as well as an n=2 *symmetric* jet stage.

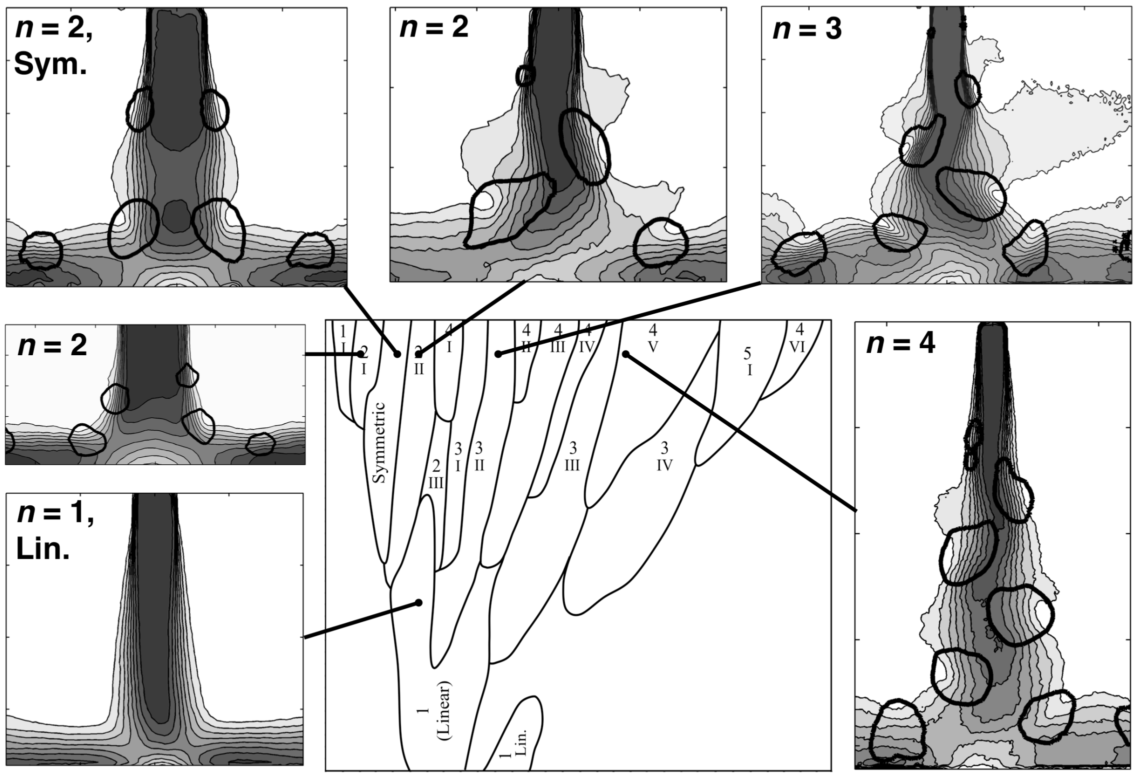

Figure 3.20: Phase-averaged velocity fields showing a series of different jet-stages excited during planar jet-plate impingement.

3.7 Fluid-Resonant Coupling

In this section, the nature of the fluid-resonant regime will be investigated, and the physical mechanisms responsible for the behavior of the various jet-stages will be explored. The current system is comprised of a planar jet nozzle with a large, flat flange set back ζ=30mm from the nozzle outlet and a large flat plate positioned at some distance downstream, as shown in Figure 3.2. This geometry forms an open acoustic system, with nominally parallel solid surfaces at the plate and nozzle, and openings to surroundings at the either end of the nozzle span, as well as at the two edges of the plate and nozzle flange. This system is geometrically similar to a single occurrence of a flat plate cascade in an open environment and as a result, it is expected to possess trapped acoustic modes occurring between the nozzle and plate surface as shown in Koch (1983). A number of authors have investigated the phenomenon of trapped modes in various geometries such as ducts containing splitter plates and various bluff bodies (Hein et al., 2004), axisymmetric and rectangular cavities in ducts (Aly & Ziada, 2010 & Ziada et al., 2003) as well as rectangular cavities in an open environment (Hien & Koch, 2008 & Duan et al., 2007), and airfoils with leading-edge slats (Hein et al., 2007). These geometries, which all represent relatively unconfined acoustic systems, have been found to be liable to the excitation of trapped acoustic modes occurring between solid boundaries, especially at high frequencies as the acoustic wavelength becomes small and radiation to the surroundings diminishes.

The onset of the fluid-resonant regime in the impinging planar jet is marked by a significant increase in the sound pressure levels compared to tones excited within the linear regime, and tone frequencies that tend to couple with resonant acoustic modes consisting of standing waves between the exterior of the nozzle and the impingement surface. The frequency of the acoustic resonance varies with changing impingement distance, but is relatively invariant with changing flow velocity. The resulting fluid-resonant jet-stages have been shown to be excited in bands, as shown in Figure 3.14 of the previous section, with any particular jet-stage being excited over a series of distinct ranges of both Mach number and impingement ratio.

Figure 3.21 shows the same effective Strouhal number data as in Figure 3.12 of the previous section, but now as a function of impingement ratio. Because the effective Strouhal number scale shown on the *y*-axis is identical to that shown in Figure 3.12, the data shows a collapse to the same mean Strouhal numbers for each stage however, viewing the data as a function of impingement ratio reveals a series of distinct clusters or bands related to the impingement ratio. The majority of these bands show a nominally linear, upward sloping trend, with the spread of the data in Figure 3.12 at each mean Strouhal number being accounted for by the trends found in these clusters. Furthermore, the upward sloping bands found in this figure correspond to the distribution of bands shown in the jet-stage diagram of Figure 3.14 of the previous section.

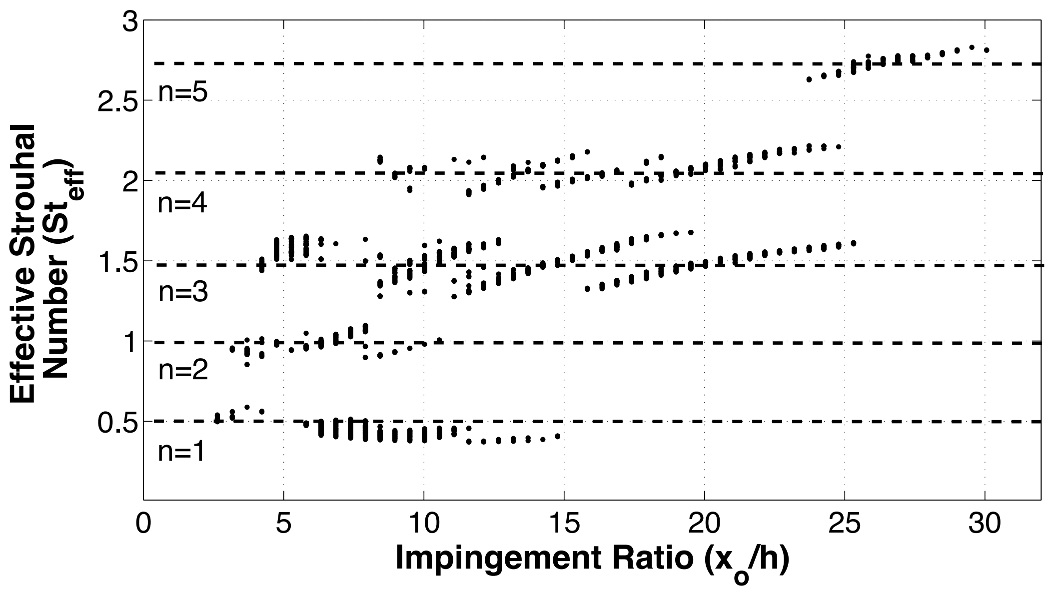

Figure 3.21: Effective Strouhal number (St_{eff}) as a function of impingement ratio for Mach numbers from $0.44 \leq M < 1.0$.

Figure 3.22 shows the tone frequency and effective Strouhal number data of the *n*=3 anti-symmetric jet stage as a function of impingement ratio. Part a) of this figure, which shows the tone frequency as a function of impingement ratio for a range of Mach numbers, shows that each sub-stage is excited within a distinct cluster or band of frequencies that is separated from the other sub-stages, and that the higher frequency *m*=I and *m*=II sub-stages are excited for relatively small impingement ratios, with the lower *m*=III and *m*=IV sub-stages being excited at progressively larger impingement ratios and thus lower frequencies. Part b) of this figure shows the Strouhal number of the various sub-stages as a function of impingement ratio. This figure shows a clear collapse of the four separate sub-stages into four distinct bands, with each band showing a similar upward sloping trend. The small spread in the data points occurring at each impingement ratio in parts a) and b) in this figure are the result of varying Mach number within each sub-stage. The upward sloping trend of effective Strouhal number as a function of impingement ratio suggests that the tone frequency does not drop in proportion with increasing impingement distance, x_o. This is to be expected because as shown later, the excited modes are 3-dimensional acoustic modes for which the frequency is dependent on a number of length scales related to the acoustic volume between the nozzle and the plate (Kinsler et al., 2000). Analysis of the frequency data of all sub-stages of the n=3 anti-symmetric, as well as the data of the other stages and sub-stages, has revealed that the tone frequencies scale with the distance between the plate surface and flange of the nozzle, ($x_o+\zeta$), as shown in Figure 3.2. As the impingement distance is changed, both the frequency of the trapped resonant mode, as well as the Rossiter frequencies given by Equation 3.8 will change, but at different rates. The resonant mode frequency will change in proportion with the outer length scale ($x_o+\zeta$), whereas the Rossiter frequency of the jet will change in proportion with the impingement distance, x_o. At certain impingement distances, frequency jump occurs to a frequency that allows optimal coupling between a Rossiter mode and a resonant acoustic mode, where such jumps may occur by maintaining the same jet-stage, but jumping to a different resonant mode, or by jumping to a different jet-stage and different resonant mode.

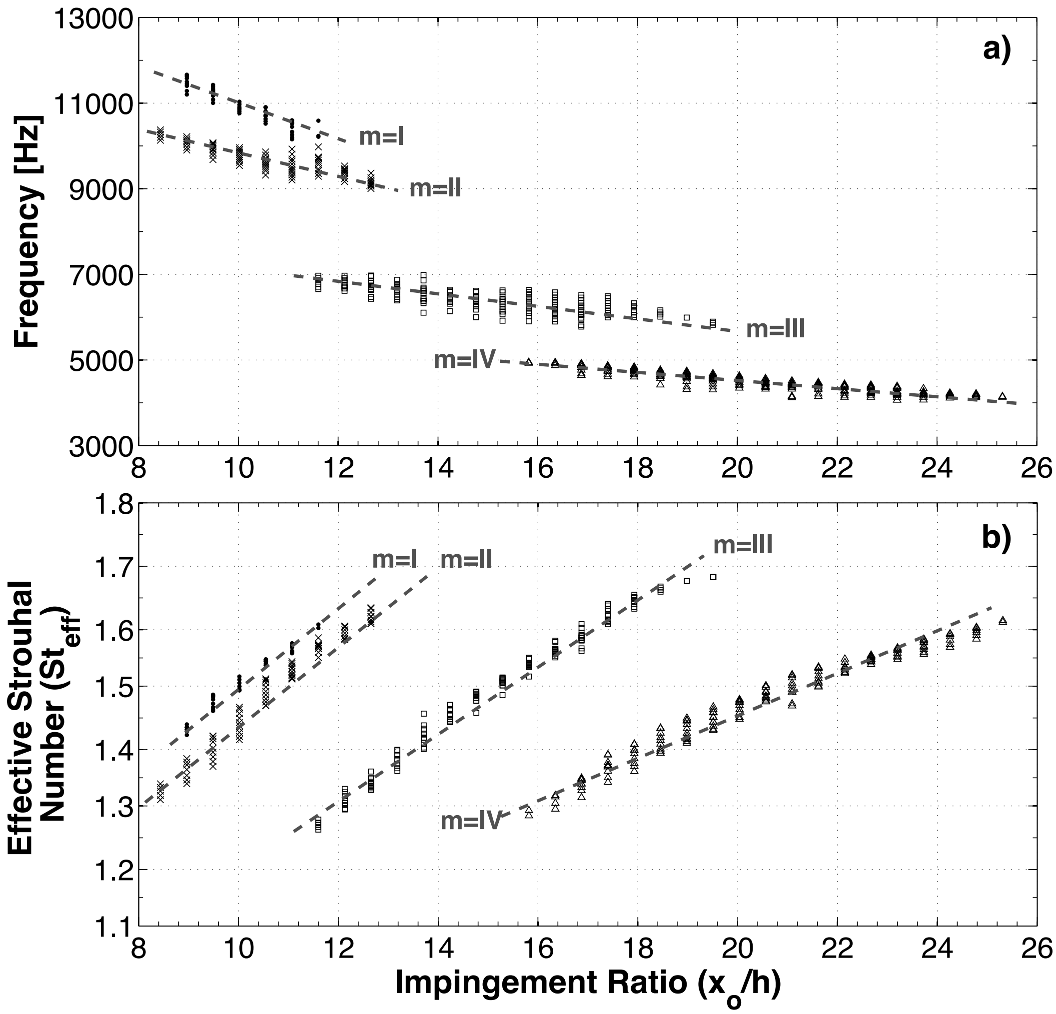

Figure 3.22: a) Frequency and b) effective Strouhal number of the dominant acoustic tone of the four distinct sub-stages of the *n*=3 anti-symmetric shear layer mode as a function of impingement ratio for Mach numbers from 0.44≤M<1.0.

Figure 3.23 shows both the tone frequency data, as well as the number of wavelengths of a resonant mode having the measured frequency and assumed to exist between the nozzle flange and the impingement plate. The data presented in this figure is for the *m*=II sub-stage of the *n*=3 anti-symmetric jet-stage. Part a) of this figure indicates that at each fixed impingement ratio, the sub-stage is excited at frequencies which increase slightly as the Mach number of the jet is increased. The total variation in resonant tone frequency as a function of Mach number at each particular impingement ratio is relatively small, typically less than 5% of the mean value. This phenomenon of increasing tone frequency vs. Mach number has been observed in a number of geometries undergoing flow-acoustic resonance, and has been attributed to the reduction in added mass effect generated by the shear layer oscillations on the resonant mode frequency (Graf & Ziada, 2010). When the impingement ratio is increased, this qualitative trend is maintained, but the mean frequency for the sub-stage decreases, indicating that the impinging jet must be coupled to acoustic modes that are trapped between the nozzle flange and the impingement surface. In light of this trend, Part b) of this figure shows a dimensionless parameter illustrating the ratio of distance between the nozzle flange and the impingement plate to the wavelength of the resonant acoustic mode, and clearly shows a collapse of the frequency data to a well-defined increasing linear trend. The trend shows an excellent collapse at Mach numbers below M=0.9, and a fair collapse at transonic Mach numbers, with approximately constant ratio between the length scale and wavelength. The increasing linear trend of this ratio associated with the variation in mean flow jet velocities at the plate surface produced by the impinging jet flow, which can cause some variation in resonant mode shape, and thus the mode frequency.

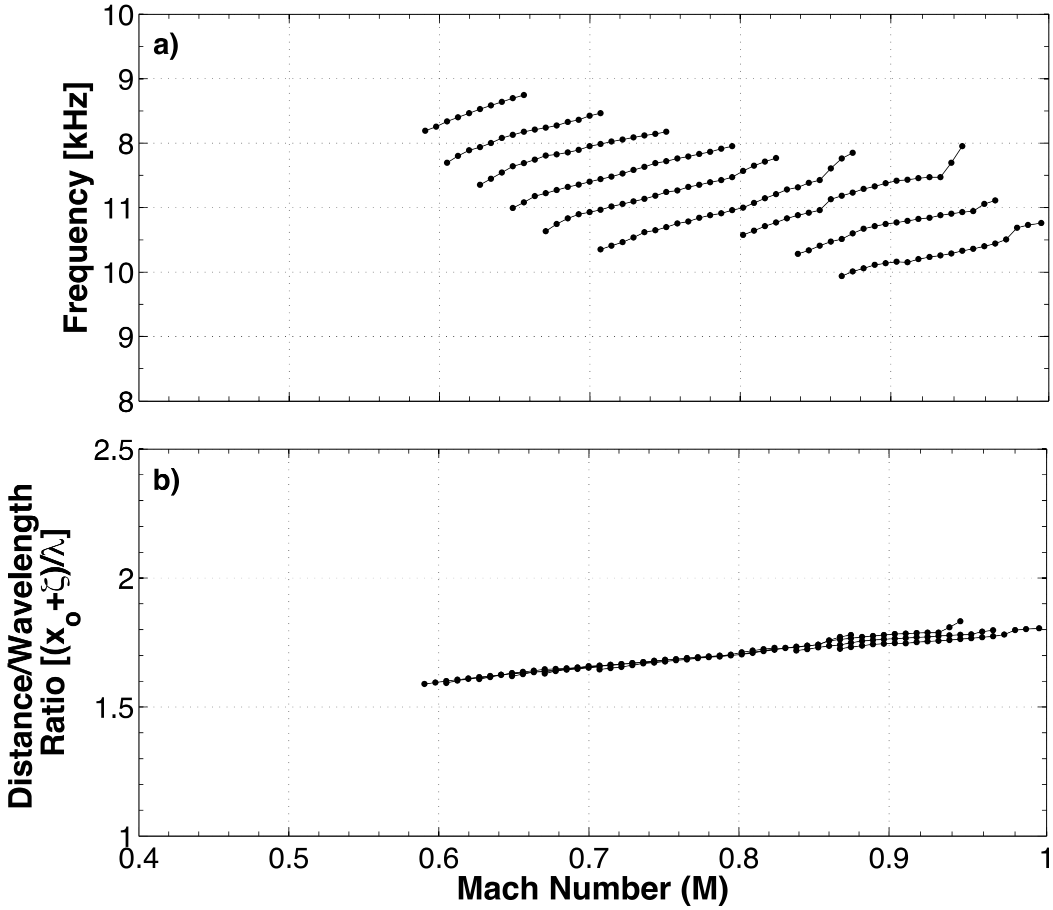

Figure 3.23: a) Frequency dominant acoustic tone and b) number of wavelengths in the outer scale of the nozzle of the *m*=II sub-stage of the *n*=3 anti-symmetric shear layer mode as a function of Mach number.

To investigate the possibility of trapped acoustic modes occurring between the nozzle and the plate, and to assess the effect of varying impingent ratio on resonant tone frequency, a series of acoustic simulations were carried out using Finite Element Analysis. Results in the domain were calculated using a 4-node tetragonal, unstructured mesh in the commercial FEA software package Abaqus, with a minimum of 15 elements per acoustic wavelength, defined by the frequency range of interest. A sample volume and mesh are given in part a) of Figure 3.24. The finite element model treats the air volume within the domain as stagnant, and does not include the effects of the mean flow on the frequency or mode shape of the trapped modes. One of the difficulties encountered in modeling trapped acoustic modes in open systems is the placement of the opening boundaries and the form of the boundary conditions. Typical "opening" type boundary conditions impose a zero acoustic pressure at the domain boundaries, and thus fix the location of acoustic pressure nodes in the creation of the domain, which may affect the frequency and mode shape of the resulting trapped modes. Other authors have avoided these effects using a variety of techniques such as the use of a so-called perfectly matched layer (PML), which provides a perfectly non-reflecting boundary (Koch, 1983; Hein et al., 2004; Hein et al., 2007; Hien & Koch, 2008 & Duan et al., 2007), or by adding a sufficiently large volume of air at the opening boundaries (Aly & Ziada, 2010).

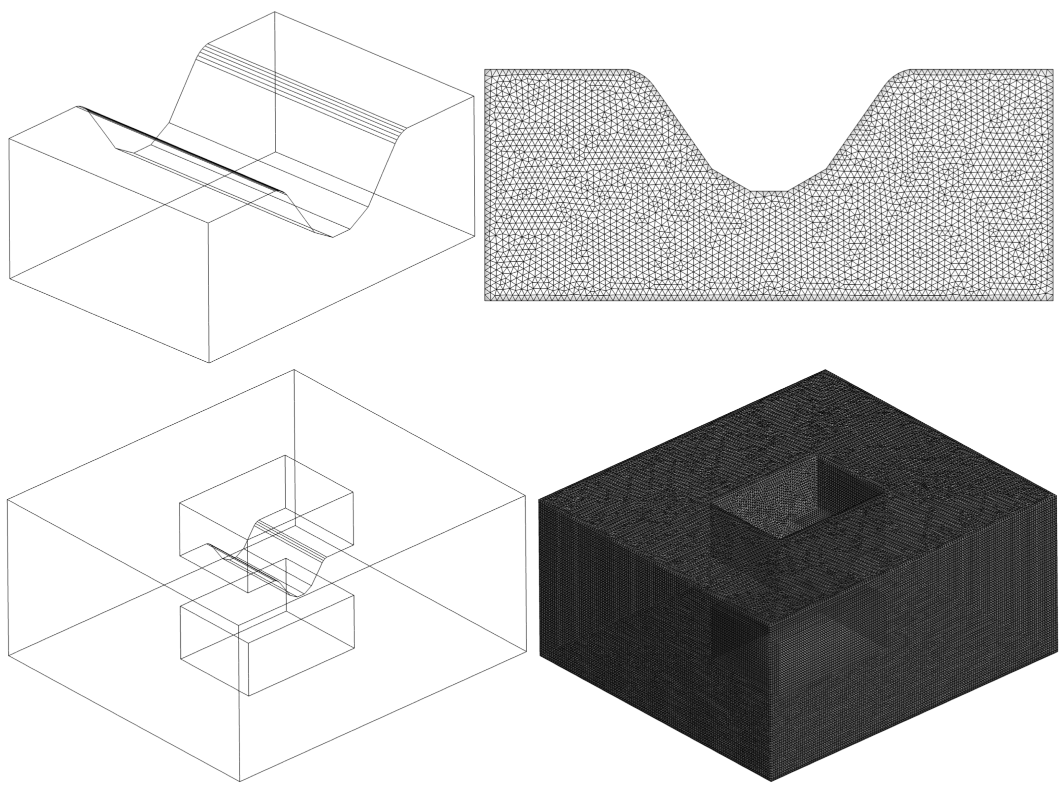

Figure 3.24: Domain volume and mesh for the planar jet-plate system for an impingement ratio of x_o/h=9.0 with (upper part) no additional volume at acoustic openings and (lower part) with additional volume at acoustic openings.

A series of simulations were carried out using only the air volume between the nozzle and plate, as shown in upper part of Figure 3.24, and additional simulations were performed with a large air volume surrounding the openings at either end of the nozzle span and at each end of the plate, as shown in part b) of Figure 3.24. It was found that the placement of the opening boundary condition at the edge of the nozzle and plate had a relatively small effect on both the frequency and mode shape of the resultant acoustic modes, with a difference in frequency of any given mode of less than 3% between simulations using the jet-plate air volume and those with additional air volumes placed at the openings.

The Finite Element simulations solve the Helmholtz equation in 3-dimensions for the air volume under consideration, and as a result, return a multitude of acoustic modes. Eigenvalues corresponding to the resonant acoustic modes encountered in the current geometry were identified by selected modes that are i) correlated along the jet-span, i.e. no pressure nodes occurring along the jet span in the *z*-direction, and ii) symmetry properties which match the flow oscillation under consideration, i.e. a symmetric acoustic mode for symmetric flow oscillations, and an anti-symmetric acoustic mode for anti-symmetric flow oscillations. These criteria were effective in eliminating many of the spurious eigenvalues, and allowed effective identification of the relevant trapped acoustic modes that were observed during the experiments. Figure 3.25 shows the acoustic pressure distribution of all four sub-stages of the n=3 jet-stage, along with the experimentally obtained average tone frequency compared to the tone frequency prediction of the finite element model. The simulations confirmed the presence of acoustic modes that occur primarily between the nozzle flange and the plate surface, resulting in tone frequencies that change in proportion with the longer length scale between the nozzle flange and plate. The prediction of the finite element model for each of the m=I, II & III sub-stages shows excellent agreement, with an average deviation of approximately 3%, and average deviation of approximately 9% for the m=IV sub-stage. In addition, the good qualitative agreement in tone frequency as a function of impingement ratio between the experimental and the numerical model show that the sub-stage phenomenon is produced as a result of coupling between a particular shear layer mode and a trapped resonant acoustic mode. It should be noted that the objective of the computing the frequency of resonant acoustic modes was to validate the existence of trapped modes with frequencies and mode shapes compatible with the results obtained during experiments within the fluid-resonant regime. A relatively simple model was therefore selected for this study because even if the boundary conditions were accurately modeled (i.e. using PML), the resonance frequencies and mode shapes would still be approximate because the effect of the high Mach number flow would still not be taken into account. For example, Aly & Ziada (2010) demonstrated the effect of mean flow on the resonance frequency and mode shape of trapped modes occurring in axisymmetric cavities.

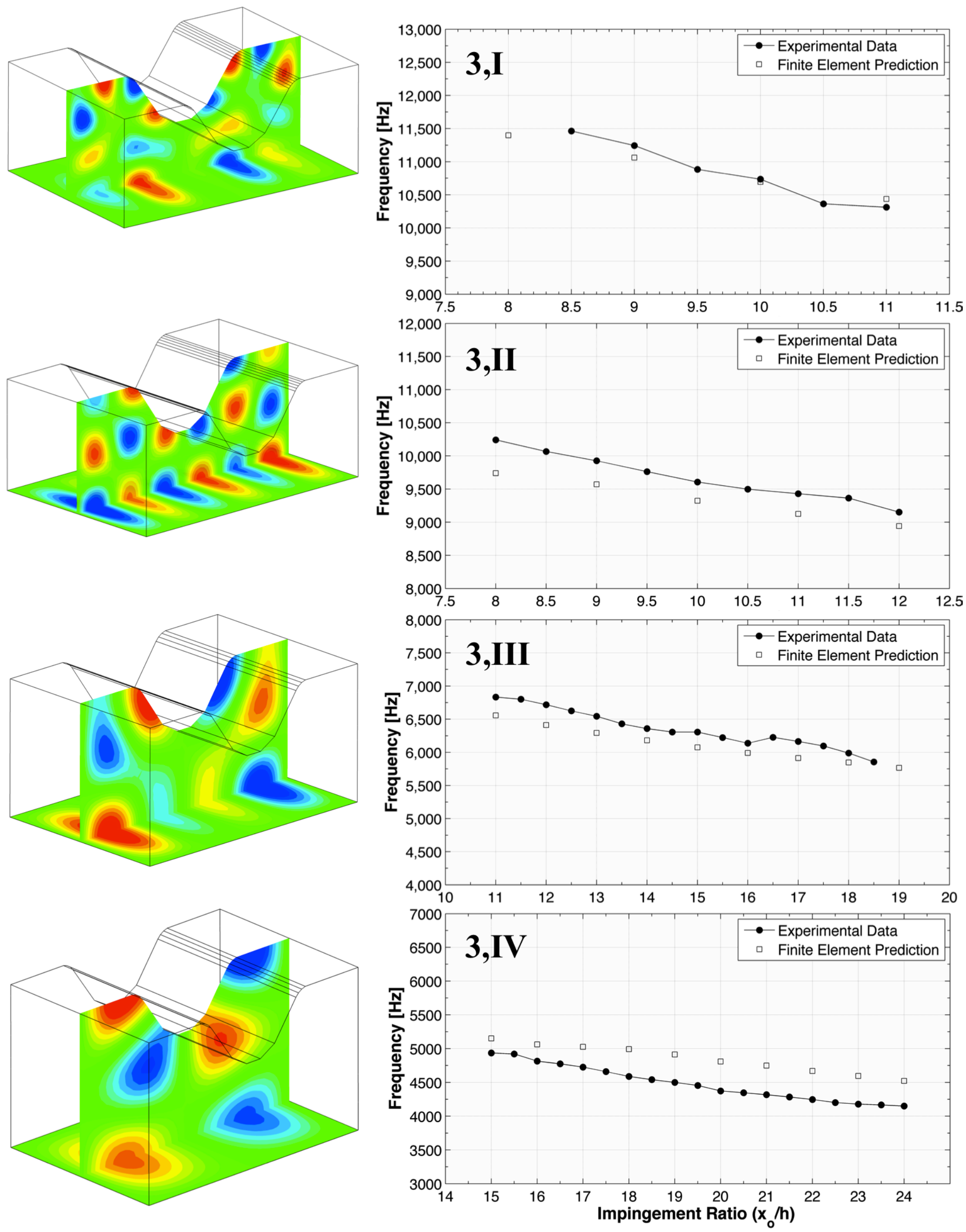

Figure 3.25: Comparison of trapped acoustic mode frequencies as a function of impingement ratio of finite element analysis vs. experimental data showing average tone frequency.

In summary, in examining the response of the current planar jet-plate system, a variety of factors suggests that for lower Mach number cases tested, a traditional Rossiter mode is excited, which displays moderate sound pressure levels and linearly increasing frequency as the Mach number is increased, and tone frequencies which are inversely proportional to impingement distance, x_o. For higher Mach numbers the system exhibits evidence of a resonant acoustic coupling, with an abrupt change in both the aeroacoustic response and the flow structure. When entering this regime, sound pressure levels increase dramatically, tone frequency becomes relatively invariant with increasing Mach number, and the frequency of the acoustic tones varies with a length scale related to the volume between the nozzle flange and the impingement plate, as shown by the FEA computations. In addition, the flow structure changes from a columnar rocking mode found in the linear regime, to a pronounced convective flapping flow oscillation, with large-scale coherent structures forming in both symmetric and anti-symmetric jet-stages depending on the flow conditions. In this fluid-resonant regime, the various fluid-resonant jet-stages are excited in bands, or sub-stages, with the frequency data of each sub-stage showing a strong collapse with the length scale between the nozzle flange and the plate surface. These fluid resonant sub-stages are each associated with a separate trapped acoustic mode occurring in the volume between the nozzle flange and the plate surface.

3.8 Conclusions

A comprehensive experimental study of the high-speed planar jet-plate geometry has been performed for Mach numbers from M=0.44 to 1.0 and impingement ratios between x_o/h=1.6 and 32.0, for a single nozzle thickness of h=3.0mm. The planar jet-plate system has been shown to excite strong, narrow band acoustic tones over a wide range of Mach numbers and impingement ratios. These tones have been found to be excited within two distinct ranges, a lower speed linear regime, where tones are excited by a Rossiter mode consisting of downstream propagating flow structures and upstream propagating acoustic disturbances, and a higher speed fluid-resonant regime, in which a Rossiter mode couples with a resonant acoustic mode occurring between the nozzle flange and the plate surface. The flow oscillations driving tone generation within the linear regime has been identified as a rocking mode of the jet core, whereas higher fluid-resonant tones are generated predominantly by an anti-symmetric wave-like instability of the jet core, with varying numbers of large-scale coherent structures occurring between the nozzle and the plate, depending on the jet-stage excited. Further, the planar jet-plate system has also been shown to be self-excited in the fluid-resonant regime by a single symmetric jet-stage, occurring for relatively small impingement ratios. The various jet-stages have been found to be excited in distinct recurring bands, with each band being associated with a particular resonant acoustic mode between the plate surface and the nozzle flange.

3.9 References

Aly, K., Ziada, S., 2010. Flow-excited resonance of trapped modes of ducted shallow cavities. Journal of Fluids and Structures. 26, 92–120.

Arthurs, D., Ziada, S., 2011. The planar jet-plate oscillator. Journal of Fluids and Structures. 27, 105–120.

Billon, A., Valeau, A., Sakout, A., 2005. Two feedback paths for a jet-slot oscillator. Journal of Fluids and Structures. 21, 121–132.

Duan, Y., Koch, W., Linton, C.M., McIver, M., 2007. Complex resonances and trapped modes in ducted domains. Journal of Fluid Mechanics. 571, 119–147.

Glesser, M., Valeau, A., Sakout, A., 2008. Vortex sound in unconfined flows: application to the coupling of a jet-slot oscillator with a resonator. Journal of Sound and Vibration. 314, 635–649.

Graf, H., Ziada, S., 2010. Excitation source of a side-branch shear layer. Journal of Sound and Vibration. 329, 2825–2842.

Hein, S., Hohage, T., Koch, W., 2004. On resonances in open systems. Journal of Fluid Mechanics. 506, 255–284.

Hein, S., Hohage, T., Koch, W., 2007. Acoustic resonances in a high-lift configuration. Journal of Fluid Mechanics. 582, 179–202.

Hein, S., Koch, W., 2008. Acoustic resonances and trapped modes in pipes and tunnels. Journal of Fluid Mechanics. 605, 401–428.

Henderson, B., 2001. The connection between sound production and jet structure of the supersonic jet. Journal of the Acoustical Society of America. 111 (2), 735–747.

Henderson, B., Powell, A., 1993. Experiments concerning tones produced by an axisymmetric choked jet impinging on flat plates. Journal of Sound and Vibration. 168 (2), 307–326.

Ho, C., Nosseir, N. S., 1981. Dynamics of an impinging jet. Part 1: The feedback mechanism. Journal of Fluid Mechanics. 105, 119–142.

Huang, J-M., Hsiao, F-B., 1999. On the mode development in the developing region of a plane jet. Physics of Fluids. 11(7), 1847–1857.

Karamcheti, K., Bauer, A.B., Shields, W.L., Stegen, G.R., Woolley, J.P., 1969. Some features of an edge-tone flow fields. NASA SP-207.

Kinsler, L.E., Frey, A.R., Coppens, A.B., Sanders, J.V., 2000. Fundamentals of acoustics, fourth ed. Wiley, New York.

Koch, W., 1983. Resonant acoustic frequencies of flat plate cascades. Journal of Sound and Vibration. 88(2), 233–242.

Krothapalli, A., Rajkuperan, E., Alvi, F., Lourenco, L., 1999. Flow field noise characteristics of a supersonic impinging jet. Journal of Fluid Mechanics. 392, 155–181.

Krothapalli, A., 1984. Discrete tones generated by an impinging under-expanded rectangular jet. AIAA Journal. 23 (12), 1910–1915.

Liu, T., Sullivan, J., 1996. Heat transfer and flow structures in an excited circular impinging jet. International Journal of Heat and Mass Transfer. 39, 3695–3706.

Maurel, S., Solliec, C., 2001. A turbulent plane jet impinging near and far from a flat plate. Experiments in Fluids. 31, 687–696.

Mehta, R., Bradshaw. P., 1979. Design Rules for Small Low-Speed Wind Tunnels. Aeronautical Journal of the Royal Aeronautical Society. 83, 443–449.

Melling, A., 1997. Tracer particles and seeding for particle image velocimetry. Measurement Science and Technology. 8, 1406–1416.

Nosseir, N.S., Ho, C., 1982. Dynamics of an impinging jet. Part 2: The noise generation. Journal of Fluid Mechanics. 116, 379–391.

O'Donovan, T.S., Murray, D.B., 2007a. Jet impingement heat transfer – Part I: Mean and root-mean-square heat transfer and velocity distributions. International Journal of Heat and Mass Transfer. 50, 3291–3301.

O'Donovan, T.S., Murray, D.B., 2007b. Jet impingement heat transfer – Part II: A temporal investigation of heat transfer and local fluid velocities. International Journal of Heat and Mass Transfer. 50, 3302–3314.

Panickar, P., Raman, R., 2007. Criteria for the existence of helical instabilities in subsonic impinging jets. Physics of Fluids. 19, 106103–1.

Powell, A., 1961. On the edge tone. Journal of the Acoustical Society of America. 33, 395–409.

Rockwell, D., Naudascher, E., 1979. Self-sustained oscillations of impinging free shear layers. Annual Review of Fluid Mechanics. 11, 67–94.

Rossiter, J. E., 1964. Wind tunnel experiments on the flow over rectangular cavities at subsonic and transonic speeds. Royal Aircraft Establishment. TR No. 64307.

Roux, S., Fenot, M., Lalizel, G., Brizzi, L.E., Dorignac, E., 2011. Experimental investigation of the flow and heat transfer of an impinging jet under acoustic excitation. International Journal of Heat and Mass Transfer. 54, 3277–3290.

Tam, C., Ahuja, K., 1990. Theoretical model of discrete tone generation by impinging jets. Journal of Fluid Mechanics. 214, 67–87.

Vejrazka, J., Tihon, J., Marty, P., Sobolik, V., 2005. Effect of an external excitation on the flow structure in a circular impinging jet. Physics of Fluids. 17, 105102.

Vollmers, H., 2001. Detection of vortices and quantitative evaluation of their main parameters from experimental velocity data. Measurement Science and Technology. 12, 1199–1207.

Ziada, S., 1995. Feedback control of globally unstable flows: Impinging flows. Journal of Fluids and Structures. 9, 907–923.

Ziada, S., 2001. Interaction of a jet-slot oscillator with a deep cavity resonator and its control. Journal of Fluids and Structures. 15, 831–843.

Ziada, S., 2002. Active stabilization of a planar jet impinging on a flexible wedge. Journal of Fluids and Structures. 16, 613–626.

Ziada, S., Ng, H., 2003. Flow excited resonance of a confined shallow cavity in low Mach number flow and its control. Journal of Fluids and Structures. 18, 79–92.

Ziada, S., Rockwell, D., 1982. Oscillations of an unstable mixing layer impinging upon an edge. Journal of Fluid Mechanics. 124, 307–334.

CHAPTER 4

On the Evolution of the Self-Excited Impinging Planar Jet

Complete Citation:

D. Arthurs, S. Ziada, 2012. Evolution of the Self-Excited Impinging Planar Jet, Journal of Fluid Mechanics, Submitted: 23/07/2012, Submission #: JFM-12-S-0698.

Copyright:

Preface

This article investigates the nature of the self-excited flow oscillations of the impinging planar jet in detail, using phase-locked PIV measurements to examine the structure of the impinging flow, the distribution and properties of fluctuating velocity components, and the behavior of coherent structures which sustain the feedback mechanism. This article examines these characteristics for a single n=3 anti-symmetric hydrodynamic mode of the jet as a function of both Mach number and impingement ratio, for a single nozzle thickness of h=3mm.

The self-excited flow has been found to develop in three distinct regions: the initial, developing and impingement regions. The initial region, which contains the initial small disturbances of the jet shear layers, extends over the first 20% of the impingement length, and has been shown to have velocity fluctuations which are predominantly in the stream-wise direction, with significant fluctuation levels in both the entrainment and jet-core regions of the flow, and with the transverse fluctuating velocity component being relatively low in this region. The stream-wise velocity fluctuations in the entrainment and jet core regions of the flow have been found to be 180° out of phase with respect to one another, leading to very high fluctuating velocity levels in the shear layers, with this intense shearing action being the primary mechanism leading to the formation of the vortical structures near the end of this region.

The flow structures that form in the initial region grow rapidly and intensify as they convect downstream in the developing region, which occurs over a range of downstream positions from x/x_o=0.2 to 0.75. In this region, the transverse fluctuating velocity component grows rapidly due to the circulation of the coherent structures, which results in a transfer of flow energy from the stream-wise to the transverse direction. These transverse fluctuating velocity components grow continuously within this region, reaching a maximum amplitude of over 30% of the initial jet velocity near the end of this region at a downstream distance of $x/x_o \approx 0.75$. The pronounced flapping motion of the jet column in the self-excited impinging planar jet is a symptom of the large fluctuating transverse velocity component that develops in this region, with these fluctuations being distributed in a series of alternating positive and negative bands oriented in the cross-stream direction, with this pattern being produced by the rotation of the structures themselves. The anti-symmetric distribution of structures, along with the opposing direction of rotation on either side of the jet induces a type of pumping mechanism, where the rotation of the staggered structures drives the flow in the positive and negative cross-stream directions. The stream-wise fluctuating velocity component continues to grow early in the developing region of the flow, although at a slower rate than in the initial region of the flow, with the fluctuating velocity amplitude reaching a local maximum near the middle of this region, and then decaying to a local minimum at the end of the developing region.

The impingement region occurs over the last 25% of the impingement length, and marks the onset of interaction between the coherent flow structures and the impingement surface. As the flow progresses into the impingement region, the stream-wise fluctuating velocity component begins to increase as a result of the fluid-structure interaction, reaching a local maximum near $x/x_o \approx 0.85$, and then decaying rapidly to zero at the plate surface. The amplitude of the transverse component decreases continuously as the flow progresses towards the plate surface, but with this component maintaining a significant non-zero amplitude close to the plate surface due to the passage of coherent flow structures.

Increasing the Mach number of the impinging jet within the range of the n=3 anti-symmetric mode of the jet results in a similar distribution of flow patterns, fluctuating velocity components and coherent flow structures, but produces more intense flow oscillations. Significant variation in the amplitude of fluctuating components is also observed within each resonant mode as the impingement ratio is varied; with the strength of flow oscillations increasing as the impingement distance is increased, and decreasing upon the excitation of a new resonant mode.

A structure-tracking scheme using the velocity discriminant parameter was developed to investigate the behavior of coherent structures, including the path, convection velocity, size and strength of the vortices as they develop and evolve within the impinging jet flow. The structures were found to convect at 40% of the flow velocity at the nozzle outlet in the initial region, with evidence of slowing as the structure progress downstream beyond the extent of the jet potential core. This measured convection velocity is relatively low compared to other similar geometries, such as the impinging axisymmetric jet, which have been found to have convection coefficients in the range: $0.52 \leq \kappa \leq 0.65$ (Ho & Nosseir, 1981 and Krothapalli et al., 1999), or the free planar jet, for which $0.55 \leq \kappa \leq 0.7$ (Kerhervé et al., 2006 & 2010). This discrepancy is likely associated with both the anti-symmetric form of the hydrodynamic mode, as well as the large size of the structures, which have a diameter of several times the initial jet thickness. The convection velocity has been found to be relatively constant in the initial region as both the Mach number and impingement ratio are varied. Measurements of the structure circulation as a function of downstream position reveals that as a result of both the large size of the structures, and the highly two-dimensional structure path, vortices begin to interact with the downstream impingement surface after travelling ~75% of the total impingement distance.

A feedback model has been developed using the results of the measured convection speed and effective impingement distance to predict the oscillation frequency of the impinging planar jet as a function of both the impingement ratio and Mach number. The model has been found to accurately predict the oscillation frequency of the self-excited flows over the complete range of impingement ratio and Mach number examined in this study.

All experimental measurements, analysis of the resulting data, and the writing of the published article were completed by the current author, under the supervision of my advisor: Professor Samir Ziada.

On The Evolution of the Self-Excited Impinging Planar Jet

David Arthurs & Samir Ziada

McMaster University
1280 Main Street West
McMaster University – Dept. of Mech. Eng. JHE 316
Hamilton, ON, Canada
L8S 4L7

Abstract

The current study examines the flow evolution of a self-excited, high-speed planar jet impinging normally on a plate fixed at some distance downstream. Measurements of the flow field have been performed using a phase-locked PIV measurement technique to analyze the characteristics of the self-excited flow responsible for the generation of the intense acoustic tones. These measurements have been performed for self-excited oscillation at the third (n=3) anti-symmetric hydrodynamic mode of the jet, at a series of Mach numbers and impingement ratios within the fluid-resonant regime, where hydrodynamic modes of the jet couple with trapped acoustic modes between the nozzle and the plate. The amplitude of fluctuating velocity components have been found to be relatively large, often in excess of 30% of the initial jet velocity at the nozzle outlet. The behavior of fluctuating velocity components has been found to be intrinsically tied to the formation of the anti-symmetric pattern of coherent flow structures forming in each shear layer, whose impingement generates acoustic pressure fluctuations responsible for sustaining the self-excited flow. Measurements of the convection speed and path of the coherent structures have revealed that they travel at approximately 40% of the velocity at the nozzle outlet early in the developing region of the jet, with significant slowing

occurring in the transition region for impinging jet cases with large impingement ratios. Furthermore, measurements of the evolution of flow structure circulation have revealed that the plate begins to affect the circulation of approaching vortices at approximately 75% of the total impingement distance. The measured phase-speed and equivalent impingement distance have been used to develop a feedback model, which accurately predicts the frequency of flow oscillations over the complete range of impingement ratio and Mach number for which self-excited flows are observed.

4.1 Introduction

High-speed impinging planar jet flows, as shown in Figure 4.1, are commonly used in a variety of industrial processes and applications including thermal processing of stock material in forming applications (Ferrari et al., 2003), coating control processes, such as the production of hot-dipped galvanized sheet steel (Arthurs & Ziada, 2011 & 2012a), annealing and tempering of plate glass (Camci & Herr, 2002), as well as in the production of polymer films and paper products (Viskanta, 1993 and Chung & Luo, 2002). These geometries are liable to the production of very intense self-excited flow oscillations that are produced by a feedback mechanism between unstable hydrodynamic modes of the jet, which produce large-scale vortical flow structures, and acoustic fluctuations produced by the impingement of these structures at the downstream surface. In addition to the noise hazard posed by the generation of the intense acoustic tones, these flows can also produce large fluctuating velocities and pressures at the impingement surface, which may result in potential vibration and fatigue issues if the oscillation is allowed to couple with mechanical or acoustic modes of surrounding components. Both of these effects can adversely affect the usefulness of this geometry in many applications, however work by Camci & Herr (2002) has found that self-excited flow oscillations of an impinging planar jet of moderate Reynolds number resulted in increasing overall Nusselt numbers by more than 70% compared to an equivalent steady flow, and other researchers investigating this effect on the self-excited axisymmetric jets have reported similar findings (O'Donovan & Murray, 2007). In either case, there is a strong incentive to understand the mechanisms responsible for tone generation, to document their response characteristics, and for the development of models to accurately predict these self-excited flow phenomena.

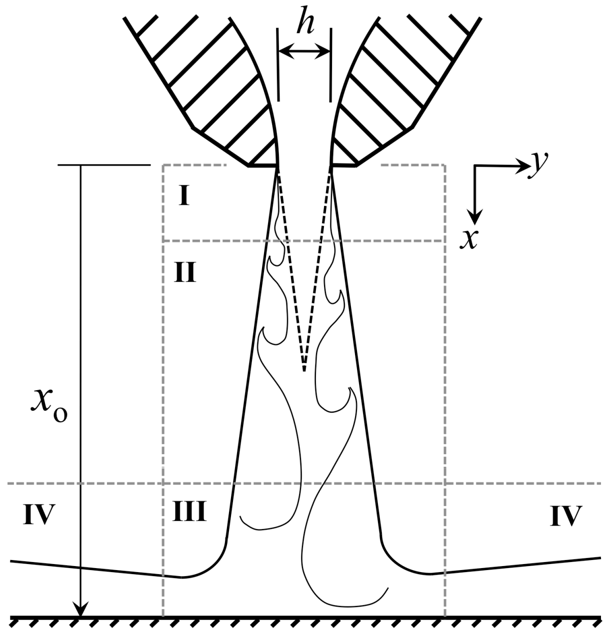

Figure 4.1: Basic schematic of the impinging planar jet geometry, showing the impingement distance (x_o) and the nozzle thickness (h), as well as the initial (I), developing (II), impingement (III) and wall-jet (IV) regions of the flow.

Impinging jet flows have been the subject of a relatively intense research effort, with the different jet geometries, including planar, axisymmetric or elliptical nozzles, each receiving varying amounts of attention in the literature. The subsonic impinging axisymmetric jet has received the bulk of the research in this area, with Wagner (1971) and Neuwerth (1972) performing the first comprehensive studies investigating the character of noise and tone generation, as well as some flow visualization to assess the nature of the self-excited flow oscillations driving tone generation. Ho & Nosseir (1981) and Nosseir & Ho (1982) further documented the noise generation, and proposed that tones were generated as a result of a feedback mechanism between instabilities in the jet free shear layer, and acoustic disturbances produced by impingement of these structures at the impingement surface. Tam & Ahuja (1990) and Panickar & Raman (2007) further expanded on these earlier works through the application of linear stability theory to predict the onset of various axisymmetric and helical stages of the jet. In addition, many authors have investigated the tone generation mechanism in *supersonic* impinging axisymmetric jets, whose features are similar to the subsonic case in some respects, but whose response is complicated by interaction with shocks and jet-screech (Krothapalli et al., 1999 & Henderson et al., 2005).

A myriad of studies have also been performed to examine the turbulence and heat transfer characteristics of steady, low Mach number impinging jet flows. Some examples include Gutmark & Wolfshtein (1978), Maurel & Solliec (2001) and Narayanan (2004) among many others, however the number of studies examining higher Mach number jet flows that result in self-excited flow oscillations are far fewer in number. Norum (1991) performed very limited measurements on a planar impinging jet flow at a single subsonic Mach number very close to choked flow (M=0.98), but the majority of the measurements performed in this study focused on supersonic planar jet impingement. Other authors such as Krothapalli (1985) and Tam & Norum (1992) have investigated the self-excited behavior of supersonic impinging planar jets, whose response is affected by jet screech and shock interaction. Studies performed on the subsonic self-excited impinging planar jets have primarily focused on geometries such as the jet-edge (Powell, 1961; Lucas & Rockwell, 1987, Ziada, 1995 and Lin & Rockwell, 2001) and jet-slot (Ziada, 2001, Billon et al., 2005 and Glesser et al., 2008), which tend to be self-excited at much lower Mach numbers within the incompressible flow regime.

For the case of self-excited flow oscillations of a subsonic planar jet impinging on a plate, Arthurs & Ziada (2011 & 2012b) have performed two studies, with the most recent addressing the self-excited response of the system over a wide range of Mach number and impingement ratio using the current experimental apparatus. The impinging planar jet flow was found to excite tones over a relatively wide range of impingement ratio ($1.5 \leq x_o/h \leq 32.0$), a much larger range than the equivalent axisymmetric case ($1.5 \leq x_o/D \leq 6.5$), and with tones also being excited over a wider range of subsonic Mach numbers, from M≈0.4 to 1.0. Acoustic tones were found to be generated in two distinct regimes: a linear regime occurring for lower Mach numbers ($0.4<M<0.6$), and a fluid-resonant regime occurring at higher Mach numbers ($M>0.6$), where the hydrodynamic mode of the jet was found to interact with trapped acoustic modes occurring in the air volume between the nozzle and the impingement surface. Preliminary flow measurements in these studies revealed that the acoustic tones are generated by a series of jet-stages corresponding to the 1st through 5th anti-symmetric hydrodynamic modes of the jet, as well as a single symmetric jet-stage occurring for small impingement ratios.

Of the studies performed on high-speed, self-excited impinging jet flows, very few have included significant measurements of the flow, such as characterizing the fluctuating velocity components, or performing measurements of the convecting flow structures responsible for sustaining the feedback mechanism. In addition, many studies have attempted to predict the behavior of the self-excited flows based on feedback models originally developed for flows with significant structural differences compared to impinging jet flows, and using estimates of flow behavior extrapolated from measurements of analogous free jets flows. The goal of the current study is to use the results of phase-locked PIV measurements to investigate the nature of the self-excited flow oscillations driving tone generation in the fluid-resonant regime, to both qualitatively and quantitatively characterize the steady and fluctuating components of the flow, as well as the behavior of convecting vortical flow structures. Results of these measurements will offer new insights into the structure and flow evolution of self-excited impinging planar jets, and will be used to develop a feedback model, which will allow for accurate predictions of the frequency of self-excited flow oscillations.

Table 4.1: Nomenclature of quantities and terms.

Nomenclature	
c	Speed of sound in air [343 m/s]
d_2	Discriminant of the velocity field
D	Nozzle diameter of an impinging axisymmetric jet [m]
D_s	Diameter of coherent flow structure [m]
f	Frequency [Hz]
h	Nozzle thickness [m]
L	Length of the planar jet in the span-wise direction (100mm)
L_d	Lagrangian structure displacement [m]
L/h	Nozzle aspect ratio
M	Mach number (U_o/c)
P_s	Supply pressure [Pa]
P_∞	Ambient pressure [Pa]
Re_h	Reynolds number based upon jet thickness ($U_o \cdot h/\nu$)
SPL	Sound pressure level in decibels $20 \cdot \log_{10}(P_{RMS}/P_{ref})$ where P_{ref} =20μPa]
u	Stream-wise velocity component [m/s]
u_ϕ	Phase-averaged stream-wise velocity component [m/s]
u'_ϕ	Phase-averaged fluctuating stream-wise velocity component [m/s]
$\lvert u' \rvert$	Magnitude of fluctuating stream-wise velocity component [m/s]
u_c	Stream-wise convection velocity [m/s]
$\lvert U \rvert$	Magnitude of flow velocity [m/s]
U_c	Magnitude of structure convection velocity [m/s]
U_o	Jet velocity at the centerline of the nozzle outlet [m/s]
v	Transverse velocity component [m/s]
v_ϕ	Phase-averaged transverse velocity component [m/s]
v'_ϕ	Phase-averaged fluctuating transverse velocity component [m/s]
$\lvert v' \rvert$	Magnitude of fluctuating transverse velocity component [m/s]
v_c	Transverse structure convection velocity [m/s]
x_o	Impingement distance [m]
x_o/h	Impingement ratio
δ	Disturbance thickness of the shear layer/boundary layer [m]
δ^*	Displacement thickness of the shear layer/boundary layer [m]
θ	Momentum thickness of the shear layer/boundary layer [m]
κ	Convection coefficient (u_c/U_o)

4.2 Experimental Apparatus

The current study consists of an experimental investigation of a high-speed planar gas jet impinging normally on a plate at some distance downstream. In order to facilitate the study of this geometry, the planar nozzle and plate assembly shown in Figure 4.2 has been constructed. The planar nozzle, which has been CNC machined out of Aluminum, has a span of L=100mm and a thickness of h=3mm, for an overall aspect ratio of L/h=33.3. The nozzle is pressurized using compressed air, which enters the plenum through 25.4mm diameter hole in its top surface, at an angle perpendicular to the direction of the jet flow ultimately exiting the nozzle. Air enters a settling chamber in the interior of the plenum through a flow distribution tube, a device that has been designed to evenly distribute the flow along the jet span, and then passes through a series of flow conditioning screens mounted upstream of the nozzle contraction. The screens consist of a fine stainless steel cloth, with 70 wires per inch and an open area ratio of $\beta \approx 0.58$, to break up any large turbulent structures and smooth the flow prior to entering the nozzle contraction. The nozzle uses an elliptical profile, with dimensions of the major and minor axis of the ellipse of 45mm and 30mm respectively, and with the major axis aligned with the stream-wise direction of the flow exiting the nozzle, resulting in a nozzle contraction ratio ~23:1 for a nozzle thickness of h=3mm.

Flow velocity at the nozzle exit has been calculated using the following equation:

$$M = \eta \cdot \sqrt{\frac{2}{\gamma - 1}\left[\left(\frac{P_s + P_\infty}{P_\infty}\right)^{\left(\gamma-1/\gamma\right)} - 1\right]}, \tag{4.1}$$

where γ is the ratio of specific heats of air, P_s and P_∞ are the static pressure in the nozzle and the ambient pressure respectively, and η is the isentropic efficiency of the nozzle. Static pressure within the plenum was measured at the jet centerline immediately upstream of the nozzle contraction using a Validyne DP-15 pressure transducer with an accuracy of 0.25% of the full range of 1 bar, and calibrated to a known pressure source. The isentropic efficiency of the nozzle (η) was measured as a function of Mach number by comparing the actual Mach number measured at the nozzle outlet using Particle Image Velocimetry (PIV), to the Mach number predicted for a flow exiting a lossless nozzle. The isentropic efficiency was found to be in excess of η=0.97 for the complete range of Mach number tested, with the lowest efficiencies occurring for conditions near choked flow (M≈1.0). The results of these measurements are used in Equation (4.1) to calculate the actual Mach number at the nozzle outlet as a function of the static pressure within the plenum, and as a result, the Mach numbers given in this article reflect the actual conditions at the outlet of the nozzle, and not an estimate based on the assumption of an isentropic nozzle.

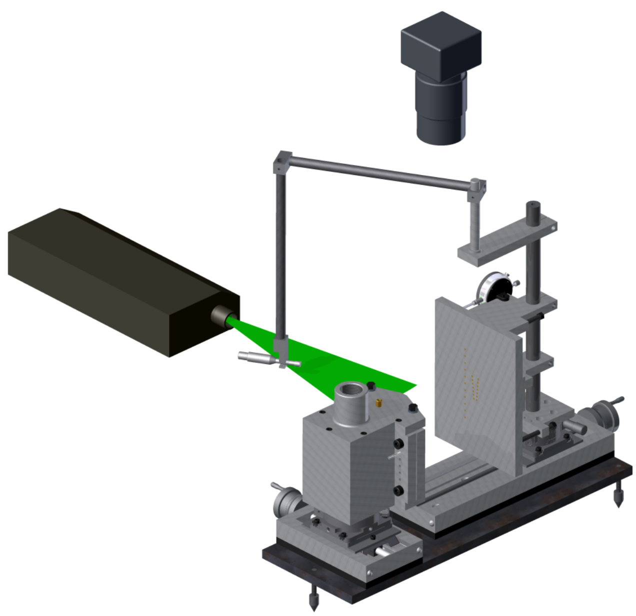

Figure 4.2: Isometric view of planar jet-plate apparatus and the layout of the PIV camera and laser head unit.

Measurements of the initial velocity profile of the jet at the exit of the nozzle were performed using a specially constructed total pressure probe similar to that outlined in Arthurs & Ziada (2011) and a multi-axis traverse accurate to within ±0.01mm, with the results of these measurements having been subsequently validated using subsequent PIV measurements. Figure 4.3 shows a series of velocity profiles measured in the transverse (*y*) direction at the nozzle exit for a series of Mach numbers of the exiting jet flow and a single nozzle thickness of h=3mm. Figure 4.3 shows an even "top-hat" shaped velocity profile, with relatively thin shear layers, and with Table 4.2 listing the boundary layer thickness, disturbance thickness and momentum thickness as a function of Mach number. The results show that the disturbance thickness of the shear layers is relatively constant at ~8% of the total jet thickness, and the shape factor of the boundary layer at the nozzle exit is relatively large for all Mach numbers tested at $\delta^*/\theta=3.0$, indicating that the boundary layer at the nozzle outlet is initially laminar. In addition, measurements of the velocity profile in the span-wise (*z*) direction have shown that the flow is evenly distributed along the span of the jet, with a maximum variation of flow velocity of less than 1% across the nozzle span for all Mach numbers examined in this study (Arthurs & Ziada, 2012b). The flat surface used for impingement consists of a large, rigid plate machined out of Aluminum measuring 150mm×200mm, with a thickness of 10mm. The front and rear surfaces of the plate have been machined using a single point fly-cut milling operation to provide the flattest surface possible, and the plate has been machined to allow dynamic PCB 105C02 miniature dynamic pressure transducers to be flush mounted to the front surface of the plate within the impingement zone to trigger the phase-locked PIV measurements.

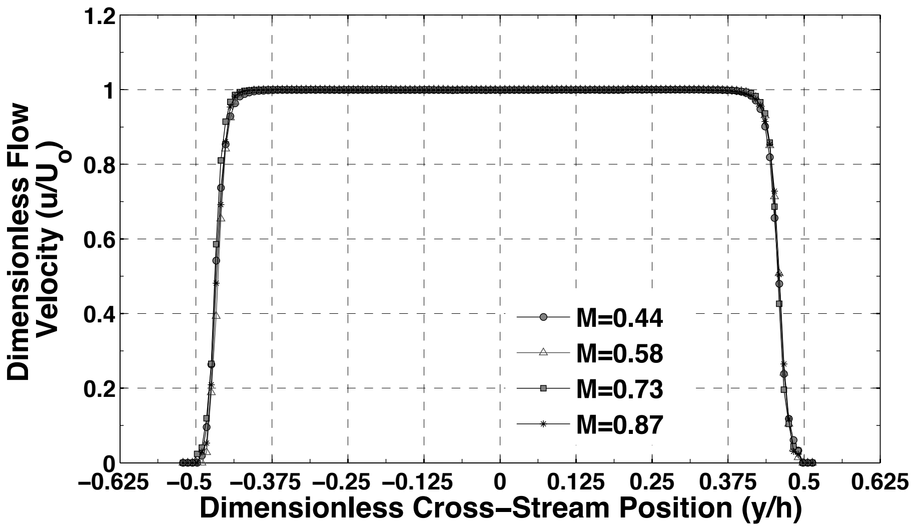

Figure 4.3: Dimensionless velocity profiles at the nozzle exit for a series of Mach numbers ($3.1\times10^4 \leq Re_h 7.0\times10^4$).

Table 4.2: Various measures of dimensionless shear layer thickness at the mid-span of a planar jet with a thickness of *h*=3mm for varying flow velocities.

	Mach Number (M)			
	0.44	**0.58**	**0.73**	**0.87**
Disturbance Thickness (δ) [mm]	0.25	0.25	0.24	0.23
Displacement Thickness (δ*) [mm]	0.075	0.075	0.073	0.072
Momentum Thickness (θ) [mm]	0.025	0.025	0.024	0.023

Measurements in the acoustic free-field were obtained using a GRAS 40BP 6.35mm high-level microphone combined with a GRAS 26AC preamplifier and a GRAS 12AA power supply module. The microphone has a flat frequency response of 2Hz-80kHz (±2dB) and was calibrated using a GRAS Type 42AB sound calibrator. The microphone was located at a distance of 200mm from the stagnation point at an angle of 60° as measured from the jet plane, and at the midpoint of the jet-span. Data acquisition was performed using a National Instruments NI-4452 data acquisition card, with each measurement consisting of the pressure time signal acquired at a sample rate of 204.8kHz for 15 seconds. Spectral analysis was performed by breaking the time signal into 60 equally sized blocks of 51,200 samples with no overlap, calculating the amplitude spectrum of RMS acoustic pressure for each block, and averaging the 60 spectra to produce a final average acoustic spectrum for each measurement case. The resulting amplitude spectrum has a frequency range from 0Hz to 102.4kHz and a spectral resolution of 4Hz, which is then truncated to a range of 0Hz to 80kHz, corresponding to the linear response range of the microphone.

In order to measure the velocity fields of the impinging jet flow, a phase-locked PIV measurement technique has been used. The 2-dimensional PIV system uses a single PowerView 4MP 12 bit digital camera with a resolution of 2048×2048 pixels, and a 532nm New Wave Solo 120XT pulsed Nd:YAG laser with a maximum output of 120mJ per pulse was used for flow field illumination. Camera optics and lenses consisted of a Sigma 105mm *f* 2.8 lens in combination with a variety of teleconverters and extension tubes, depending on the flow configuation being investigated. Synchronization of the system was performed by a TSI LaserPulse Model 610035 synchronizer with external triggering and adjustable time delay.

The high-speed impinging planar jet flow produces very intense acoustic tones that are generated by highly periodic, self-excited flow oscillations at frequencies several orders of magnitude higher than the maximum image aquisition rate of the PIV system used in this study. Flow measurements have been performed using a phase-locked technique that uses the periodic pressure signal obtained at the plate surface in the impingment region to trigger PIV measurements at a particular instant in the flow oscillation cycle using a custom designed trigger generator. Using this technique, a series of measurements can be obtained at a specific instant in the phase, which can be combined to produce a phase-averaged flow field for that particular point in the flow oscillation cycle. By adding and manipulating a time delay between the trigger point and measurement, flow fields at multiple points in the phase of the flow oscillation can be obtained, allowing for the reconstruction of an *average* flow oscillation cycle. For the current study, flow field measurements have been obtained at a series of eight phase angles distributed evenly over the flow oscillation cycle for each case, with 100 flow field images having been obtained at each point in the phase. The process of phase averaging has the effect of removing the random turbulent scales of the flow through a form of spatial smoothing, while leaving the larger scales associated with the periodic, self-excited flow unaffected. For this reason, it is understood that the magnitude of the fluctuating components shown in the later sections of this article are related to the periodic, self-excited flow, and that any fluctuations produced by turbulence, which are significant, will be in addition to those presented here.

Vector fields have been processed using multi-grid, 1st order defomation correlation scheme with guassain sub-pixel interpolation, similar to that employed in the work of Scarano & Riethmuller (2000). A pair multi-grid refinement steps was used in conjunction with a series of four iterative refinement steps for defomation of the interogation window. Window sizes of 64×64 and 24×24 pixels were used for the inital and final interogation regions, with an overlap of 75% for the final interogation region. Vector validation rates in excess of 99% were achieved for all measurements presented in this work, before the implementation of any vector replacement/interpolation schemes. Because of the relatively thin shear layers of the present geometry, the maximum displacement gradients corresponding to the $\partial u/\partial y$ velocity gradient near the nozzle outlet are quite high, in excess of 0.5 pixels/pixel, leading to some gradient truncation in these locations, however these levels are confined to the thin shear layers in the *immediate vicinity* of the nozzle outlet. The shear layers tend to thicken quickly as they convect downstream from the nozzle outlet, and the maximum displacement gradients quickly fall below the 0.5 pixels/pixel displacement gradient threshold required for no gradient truncation with the deformation scheme at a downstream position of $x/h \approx 0.25$.

Table 4.3: PIV acquisition parameters and error analysis.

Acquisition parameters		
Field of View (Masked Area)		29.7mm × 34.2mm
Total Sensor Size		2048 pixels × 2048 pixels
Total Image Size		1416 pixels × 1630 pixels
Spatial Calibration		20.97 μm/pixel
Pulse Seperation		350 ns
Number of Acquisitions		800 total, 100 per phase angle
Processing Parameters		
Initial Window Size		64 pixels × 64 pixels
Subpixel Interpolation Scheme		Guassian
Window Distortion Scheme		1st Order Deformation Scheme
Number of Grid Refinements		2 refinements
Final Window Size		24 pixels × 24 pixels
Final Overlap		75%
Number of Vectors	$[x \times y]$	[236 × 270] 63,700 per field
Spatial Resolution	$(\Delta x = \Delta y)$	126 μm
Validation Rate		>99%
Error Analysis		$(x=0.5 \cdot h,\ y=-0.9 \cdot h)$
Maximum Displacement Gradient	$(\partial u/\partial y)_{max}$	0.343 pixels/pixel
	$(\partial v/\partial x)_{max}$	0.051 pixels/pixel
Uncertainty in Particle Displacement	ε_u	0.11 pixel
	ε_v	0.02 pixel
Relative Uncertainty of Particle Displacement	ε_u/δ_u	1.9%
	ε_v/δ_v	1.0%
Uncertainty of Vorticity	$\varepsilon_{(\partial u/\partial y)} = 0.7 \cdot \varepsilon_u/\Delta X$	0.009 pixels/pixel
	$\varepsilon_{(\partial v/\partial x)} = 0.7 \cdot \varepsilon_u/\Delta X$	0.002 pixels/pixel
Relative Uncertainty of Vorticity	$\varepsilon_{(\partial u/\partial y)}/(\partial u/\partial y)_{max}$	2.80%
	$\varepsilon_{(\partial v/\partial x)}/(\partial v/\partial x)_{max}$	3.43%

The PIV error analysis provided in Table 4.3 was performed for the most challenging case examined in this work: an impinging jet case with an impingement ratio of x_o/h=10.5 and a Mach number of M=0.98 at the nozzle outlet, which produces very strong self-excited flow oscillations at a frequency of f=10.6kHz. The analysis uses velocity profiles at stream-wise and cross-stream positions of x/h=0.5 and y/h=-0.9 respectively, positions corresponding to the thin initial shear layer exiting the nozzle, and large, well-developed coherent structures in the jet shear layer, respectively. These locations also corresponded to the largest velocity gradients for $\partial u/\partial$y and $\partial v/\partial x$ respectively, for any of the measurements used in the analysis of the development of the self-excited flow. The $\partial u/\partial y$ component reaches a maximum displacement gradient of 0.343 pixels/pixel in the initial shear layer at the downstream poistion of x/h=0.5, corresponding to a relative uncertainty of particle displacement in the x-direction of 1.9%, whereas the $\partial v/\partial x$ displacement gradient is lower, with a maximum value of 0.051 pixels/pixel at a location further downstream at the location of a large, well-developed structure in the jet shear layer, corresponding to a relative uncertainty of particle displacement in the y-direction of 1.0%.

As will be shown in the forthcoming velocity measurements, the current geometry produces extremely intense self-excited flow oscillations and relatively large coherent flow structures and as a result, the ratio of the interrogation region size (W_s) to the size of the small structures in the initial shear layer (Λ) is quite low at $W_s/\Lambda \approx 0.05$. This yields a truncation error of ~2% of the peak azimuthal velocity found around the vortex core (Scarano & Riethmuller, 2000). Because of the intense circulation of the coherent structures found in this geometry, significant rarefication of the seeding particles within the structures is evident in the raw images. This rarefaction is evidence of an induced outward radial component of the particles with respect to the surrounding air due to their higher density, resulting in an error in the radial velocity component of the structure, but relatively little error in the azimuthal component (Raffel et al., 2007). As a result, measurement of vorticity and structure circulation remains unaffected, as the radial component does not contribute to these quantities. This rarefication was overcome by using increased seeding density and through the use of a 12-bit camera to provide particle detection in the core of vortices.

Seeding of the flow for PIV imaging was performed using a six-nozzle Laskin aerosol generator using olive oil as a seeding medium, producing 1μm mean diameter droplets. The Stokes number of seeding particles for all PIV cases shown in present work falls within the range of $0.05 \leq Sk \leq 0.1$, which will result in tracking error of less than 2%, even for the relatively high frequency oscillations of the present impinging planar jet (Melling, 1997). To avoid laser reflections from the machined Aluminum surfaces of the nozzle and the impingment surface from appearing in the images and/or damaging the camera sensor, a clear acrylic paint infused with a laser fluorescing dye, Rhodamine Chloride ($C_{28}H_{31}N_2O_3Cl$) was applied to these surfaces, and a 532nm bandpass filter was used for image acquisition. Calibration of the PIV system was performed using a Starett machinists' grade straight edge, mounted to a fixture which is then attached to the impingment surface temporarily during calibration.

4.3 Overview of the Planar Jet-Plate Oscillations

The high-speed planar impinging jet geometry is liable to a feedback mechanism between various unstable hydrodynamic modes of the jet, and acoustic fluctuations generated by the impingement of large-scale coherent structures associated with those modes at the impingement surface. This feedback mechanism produces strong self-excited velocity fluctuations in the jet column and at the impingement surface, as well as very intense, narrow-band acoustic tones. Figure 4.4 shows an example of a typical acoustic spectrum produced by the self-excited flow for an impinging planar jet with a Mach number of M=0.9, an impingement ratio of x_o/h=10.5, and a nozzle thickness of h=3mm. The spectrum gives a good qualitative representation of a typical response of the planar jet-plate system, with a strong fundamental tone occurring at a frequency of f=10.2kHz and an amplitude in excess of 140dB, a series of higher harmonics of smaller amplitudes occurring at integer multiples of the fundamental frequency, and relatively high broadband noise levels. An accompanying spectrum for a free planar jet under the same conditions is shown as a comparison, which illustrates that the analogous free flow has broadband acoustic pressure levels that are significantly lower compared to the self-excited flow, and without the presence of narrowband tones, indicating that the self-excited behavior is produced by the impingement of the jet on the plate.

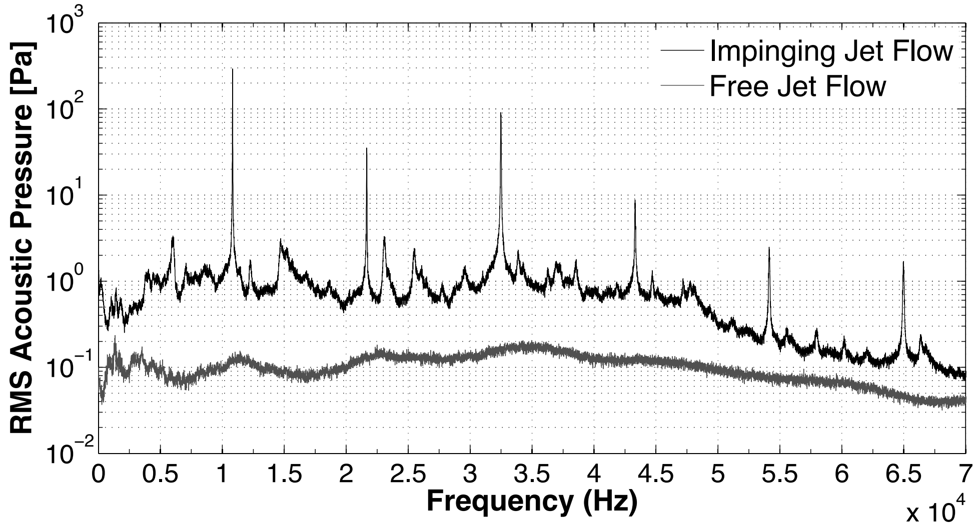

Figure 4.4: The aeroacoustic response of the planar jet-plate system with a thickness of *h*=3mm, an impingement ratio of x_0/h=10.5 and a Mach number at the nozzle exit of M=0.9, in comparison to the spectrum of a similar non-impinging jet.

The planar jet-plate system generates these acoustic tones in a series of discrete jet-stages, with each stage being produced by a distinct hydrodynamic mode of the jet. The tone frequency varies continuously within each stage as either the impingement distance or Mach number is changed, with distinct jumps in frequency marking a change in the hydrodynamic mode of the jet. Previous work by Arthurs & Ziada (2012b) showed that the planar jet-plate system was liable to excitation in two distinct regimes: a linear regime occurring at relatively low Mach number (0.4<M<0.6), where acoustic tones are excited by a traditional Rossiter instability (Rossiter, 1964 and Rockwell & Naudascher, 1979) consisting of downstream propagating flow instabilities and upstream propagating acoustic disturbances, and a fluid-resonant regime occurring at higher Mach numbers (M>0.6), which consist of Rossiter instabilities coupled with resonant acoustic modes occurring between the nozzle and the plate. Figure 4.5 shows the aeroacoustic response of the planar jet-plate system within the fluid-resonant regime that illustrates this jet-staging phenomenon, with the frequency of the dominant acoustic tone being plotted as a function of impingement ratio for a fixed Mach number of M=0.9. In addition, flow visualization images corresponding to the *n*=2, 3 & 4 hydrodynamic modes of the jet are also shown in the figure for three different impingement ratios. This figure clearly illustrates that the impinging planar jet oscillates in a myriad of different jet-stages over a large range of impingement ratio, with acoustic tones produced by the impingement of different hydrodynamic modes of the jet. As can be observed in Figure 4.5, the hydrodynamic mode number, *n,* indicates the jet oscillation pattern, or the number of instability waves between the nozzle and the plate.

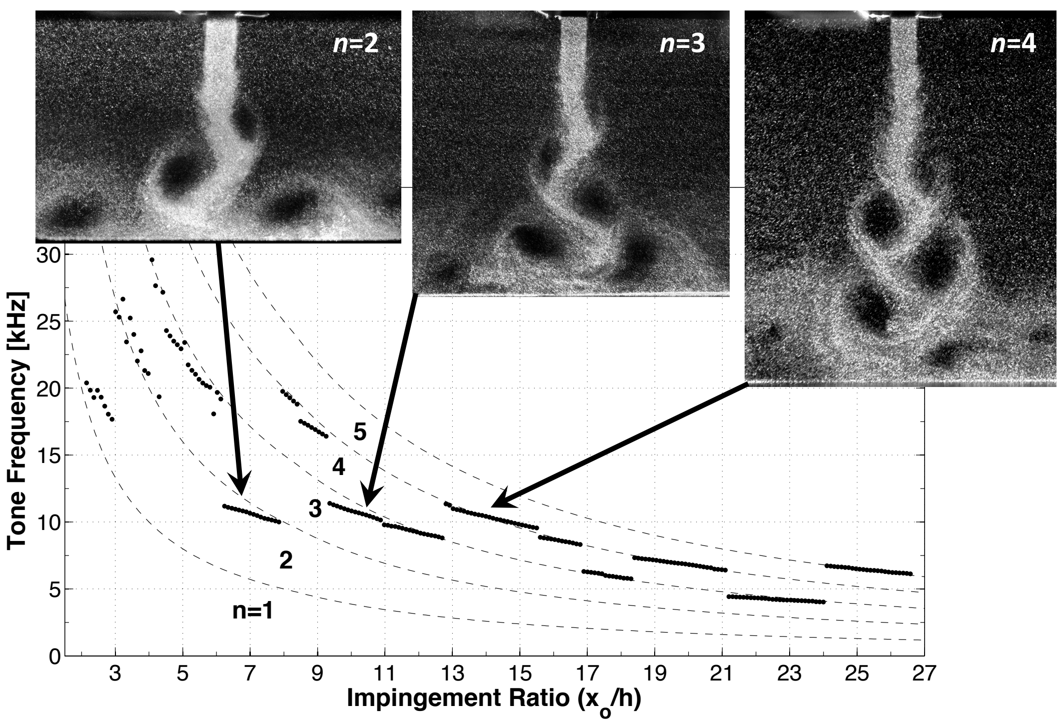

Figure 4.5: Acoustic tone frequency as a function of varying impingement ratio with a nozzle thickness of *h*=3mm and a fixed Mach number of M=0.9, along with flow visualization images showing the *n*=2, 3 & 4 hydrodynamic modes of the jet.

Figure 4.6 shows a schematic illustrating the distribution of different hydrodynamic modes of the jet as a function of both Mach number and impingement ratio for a single jet thickness of h=3mm. The schematic has been composed using the results of ~4800 distinct acoustics measurements performed in a grid pattern over a measurement domain, with a range of Mach number of $0.44 \leq M < 1.0$, and measurements having been performed at increments of ΔM=0.007*,* and a range of impingement ratio of $1.5 \leq x_o/h \leq 32.0$, with measurement increments of $\Delta x_o/h$=0.5. The figure gives the reader an overview of the complexity of the self-excited response of the system, with various hydrodynamic modes of the jet being excited in a series of bands occurring for concurrently increasing Mach number and impingement ratio. The hydrodynamic modes, excited for a particular combination of Mach number and impingement ratio, have been found to be strongly influenced by interaction with various resonant acoustic modes occurring between the nozzle and the plate (Arthurs & Ziada, 2012b).

The present study examines the flow evolution of the self-excited impinging planar jet for the n=3 anti-symmetric hydrodynamic mode of the jet in the fluid-resonant flow regime. This particular mode was selected as it is the most prolific of all jet instabilities for this system, occurring more often and over a wide range of both Mach number and impingement ratio. The evolution and development of the self-excited flow will be examined over a range of both Mach number and impingement ratio, and the resulting information will be incorporated into a feedback model to predict the oscillation frequency of the impinging planar jet.

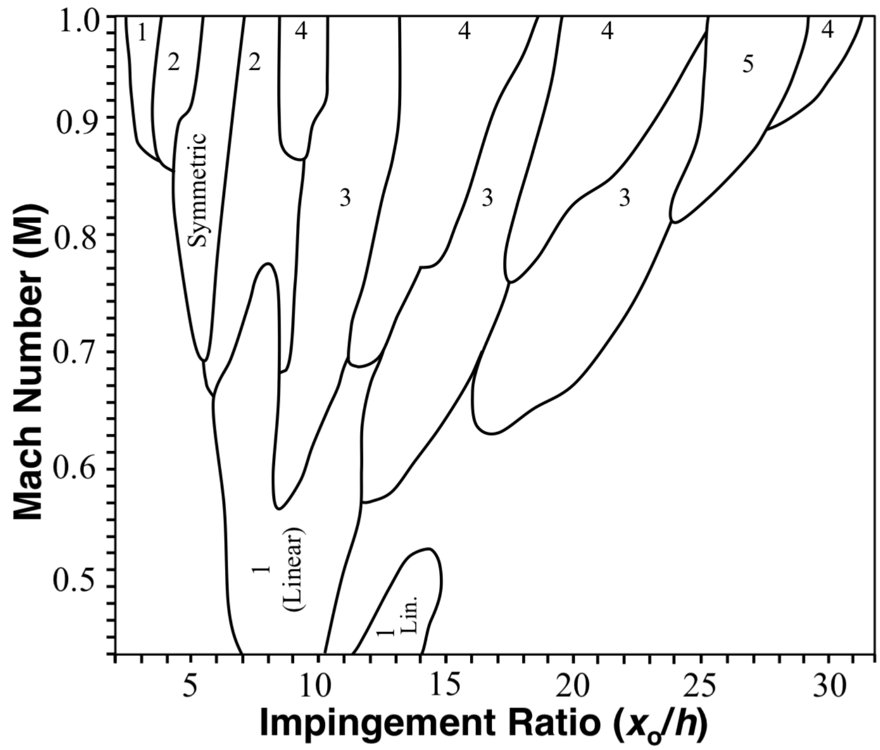

Figure 4.6: Schematic showing the distribution of hydrodynamic modes of the jet as a function of Mach number (M) and impingement ratio (x_o/h) for a nozzle thickness of h=3mm. Arabic numerals denote the hydrodynamic mode of the jet excited.

4.4 Development of the Self-Excited Flow

In order examine the characteristics of the self-excited impinging planar jet, PIV measurements of a single flow configuration corresponding to the n=3 anti-symmetric hydrodynamic mode of the jet will be presented in this section, and the effect of Mach number and impingement ratio on the development of this mode in later sections. The flow configuration examined in the present section is an impinging planar jet with a Mach number of M=0.9 (U_o=310m/s), an impingement ratio of x_o/h=10.5 and a nozzle thickness of h=3mm, with the jet being excited in the n=3 anti-symmetric hydrodynamic mode at a frequency of f=10.2kHz.

4.4.1 Characteristics of the Velocity Field and Flow Structures

Figure 4.7 consists of a pair of phase-averaged flow fields showing the velocity magnitude and vorticity, with the fields having been composed using the average of 100 instantaneous flow field measurements. The vorticity field has been computed using a second-order central difference scheme (Raffel et al., 2007), and spatially smoothed using a single pass of a Gaussian filter for ease of inspection. These two flow fields reveal that the acoustic tone is generated by the impingement of anti-symmetric oscillation of the jet exhibiting a flapping motion of the jet column. The vorticity field reveals an anti-symmetric pattern of vortical structures on either side of the jet centerline.

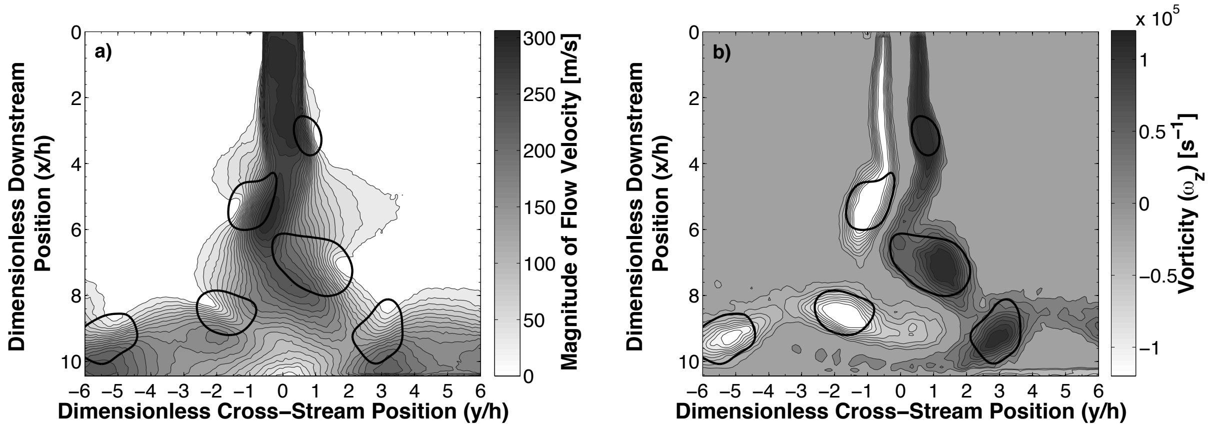

Figure 4.7: Phase-averaged flow fields showing a) magnitude of flow velocity and b) vorticity, along with a single contour of the velocity discriminant parameter (d_2) for M=0.9, x_o/h=10.5, f=10.2kHz and a phase of ϕ=0°.

The behavior of the large-scale coherent flow structures that form and convect in the jet shear layers is an integral part of the feedback mechanism that sustains the self-excited flow, and is one of the most important features of the impinging planar jet. Although inspection of the vorticity field does allow for visualization of the flow structures, accurate identification is obscured by the high vorticity levels in the initial shear layers, with distinct vortices only becoming evident in the later stages of the jet development after the structure has travelled a significant portion of the total impingement distance. In order to allow for enhanced identification of coherent structures, and to track the motion and behavior within the self-excited flow with greater precision, the velocity discriminant parameter (d_2) proposed by Jeong & Hussain (1995) and Vollmers (2001) has been used. The parameter is defined by the following equations:

$$d_2 = \left[tr(G)\right]^2 - 4|G|, \tag{4.2}$$

$$G = \begin{pmatrix} \frac{\partial u}{\partial x} & \frac{\partial u}{dy} \\ \frac{\partial v}{\partial x} & \frac{\partial v}{\partial y} \end{pmatrix}, \tag{4.3}$$

where u and v are the velocity components in the x and y-directions, respectively. This parameter, which has been used by other authors for vortex detection (Schram, 2003 & Schram et al., 2004), uses a non-linear combination of velocity gradient terms to identify regions in the flow with strong circulation that show *circular* shape characteristics, with the parameter returning a scalar field, where negative values indicate the presence of coherent flow structures. As a result of the conditional nature of this detection parameter, the discriminant is able to ignore the high vorticity levels in the jet initial shear layers and allow for enhanced structure detection not only in the initial region, but in all regions of the jet flow. The onset of negative values of the velocity discriminant parameter has been used to define the extent of coherent flow structures in the various regions of the flow (Hussain, 1986, Jeong & Hussain 1995), and a single contour level of d_2=0 has been superimposed over both flow fields shown in Figure 4.7. Inspection of Part b) of the figure illustrates a clear coincidence between areas of high vorticity and discriminant parameter in the developing region of the jet where the vorticity field shows distinct flow structures, indicating effective structure identification in this region.

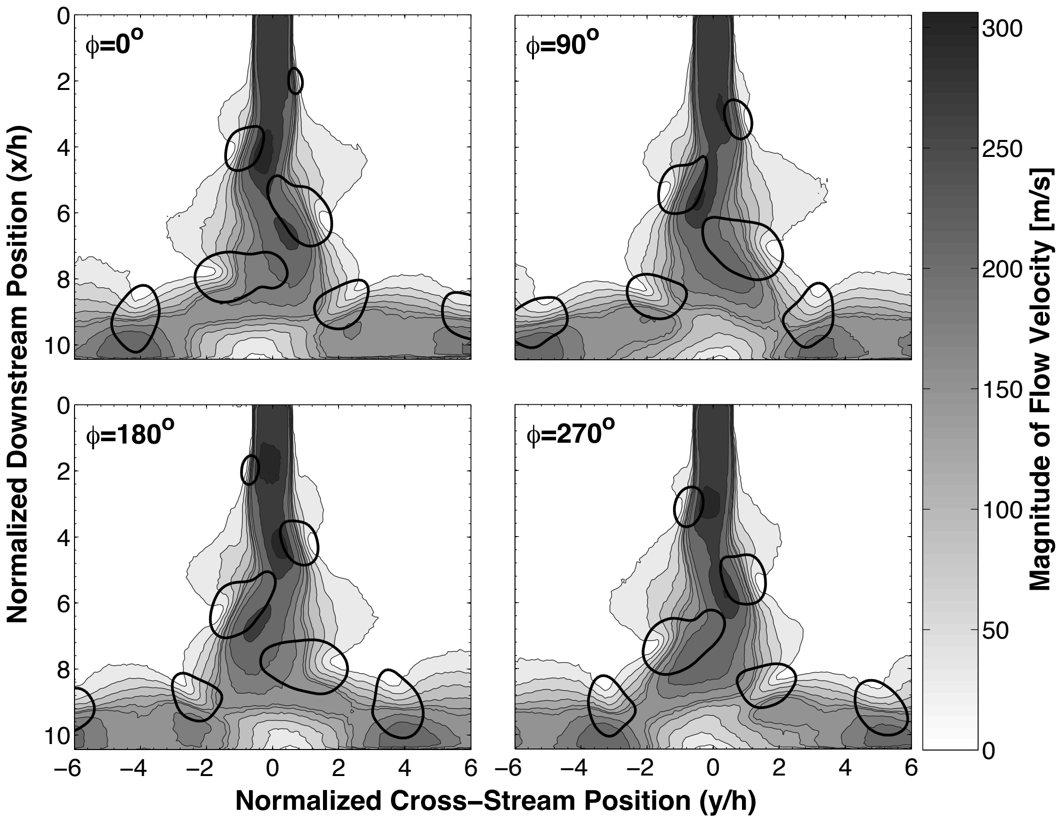

Figure 4.8: Phase-averaged velocity fields showing one cycle of the flow oscillation with phase increments of 90° for the *n*=3 anti-symmetric hydrodynamic mode, showing the formation, convection and impingement of coherent structures. x_0/h=10.5, M=0.9, *f*=10.2kHz.

To illustrate the evolution of the *n*=3 hydrodynamic mode of the jet over the complete flow oscillation cycle, a series of four phase-averaged velocity fields in increments of $\Delta\phi$=90° are shown in Figure 4.8. The flow fields illustrate that the oscillation takes the form of a pronounced flapping motion of the jet column, with coherent flow structures appearing in an anti-symmetric pattern about the jet centerline, near the saddle points of the columnar flapping pattern. The inclusion of images at additional points in the phase show that the flow structures, which are initially detected in the initial region at approximately 20% of the impingement distance, grow rapidly as they propagate downstream, and changing direction from the stream-wise to the transverse flow directions as they enter the impingement region, and eventually being convected parallel to the plate surface in the wall-jet region. This flapping motion of the jet column represents the *preferred mode* of the impinging planar jet oscillation, and exemplifies the preferred mode observed for other self-excited jet flows, such as jet screech in free supersonic planar jets (Krothapalli et al., 1986, Raman, 1997 and Walker, 1997), impinging supersonic planar jets (Krothapalli, 1985 Tam & Norum, 1992), as well as those suggested by the measurements of Antonia et al. (1983), Thomas & Goldschmidt (1986), Thomas & Chu (1989) and Thomas & Prakash (1990) for low Mach number free planar jets. The excitation of these preferred modes for different flow cases occurs over a similar range of Strouhal number of $0.1<St_h<0.4$, indicating that these hydrodynamic modes of the jet are liable to excitation in a number of different flow configurations and over a wide range of flow conditions.

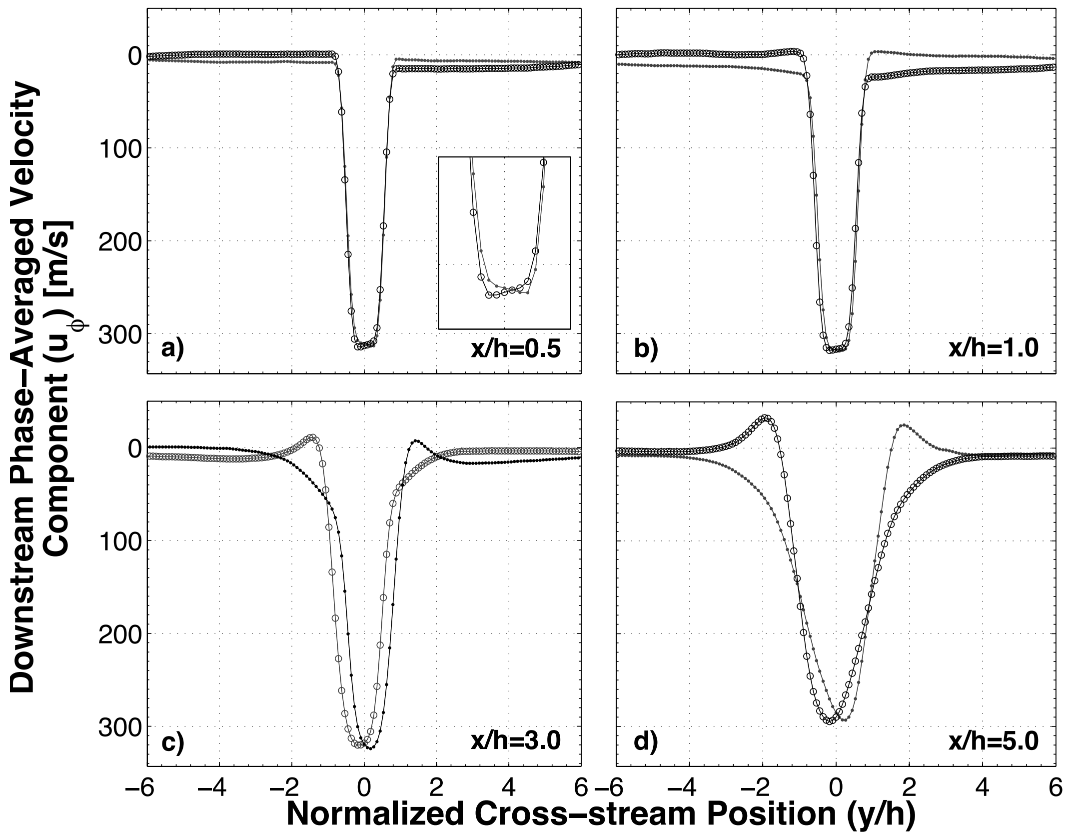

Figure 4.9: Phase-averaged stream-wise velocity profiles showing fluctuations in the flow in the jet column and entrainment regions at a series of downstream positions.

Figure 4.9 shows a series of velocity profiles of the stream-wise velocity component taken at four different downstream positions for the case shown in the previous figure, with the two profiles shown in each part of the figure having been selected at a phase difference of 180° to illustrate the extent and character of the velocity fluctuations occurring at each position. Part a) of the figure, which shows a pair of velocity profiles taken close to the upstream lip of the nozzle (x/h=0.5), illustrates two interesting features. First, there are significant fluctuations of the stream-wise velocity component in the entrainment region that extend a significant transverse distance from the jet column (y/h=±0.5). This fluctuating velocity component oscillates in phase along the complete cross-stream extent of the measurement domain on each side of the jet, and has a total fluctuation level of approximately 15m/s, with fluctuating velocities on opposite sides of the jet core being 180° out of phase. Secondly, the velocity profiles *within the jet core* at this location also show a significant fluctuating velocity component, resulting in significant fluctuating asymmetry of the two profiles, with a close up of the jet core shown in the inset portion of Part a) of the figure. Furthermore, the fluctuations in each entrainment regime on either side of the jet are 180° out of phase with respect to the fluctuations within the jet core region on the corresponding side of the jet centerline, providing an alternating shearing flow in the initial shear layers, with fluctuating velocities of opposite signs occurring in either shear layer. These fluctuations result in very high stream-wise fluctuation levels of over $|u'|$=30m/s that are confined to the relatively thin shear layers at this location, whereas the total fluctuation levels of the transverse velocity component are significantly lower, reaching a maximum fluctuating amplitude of $|v'|\approx$6m/s.

These trends are enhanced at the next downstream location of x/h =1.0, shown in part b) of the figure, with the stream-wise fluctuating amplitude in the entrainment region having increased to 25m/s and a similar asymmetrical fluctuation in the jet core, resulting in a maximum fluctuation level in the shear layers of $|u'|\approx$55m/s, with transverse fluctuation levels remaining low at this location. This intense shearing action produced by the opposing stream-wise velocity fluctuations in the entrained flow and jet core seems to be the primary mechanism that initiates the formation of coherent flow structures in the initial region of the jet. The areas of slight flow reversion occurring just outside the jet core at x/h=1.0 indicate the early development of the structures due to flow circulation. At the next two downstream locations of x/h=3.0 and 5.0 respectively, the anti-symmetric reversion pattern occurring on either side of the jet is much more pronounced as a result of the now fully formed coherent flow structures, whose strength and size increases as they convect downstream. In addition, significant lateral motion of the core produced as a result of the flapping motion of the jet is evident at these locations.

In order to examine the evolution of the flow oscillations within the self-excited flow, the fluctuating stream-wise and transverse velocity components in the x and y-directions respectively have been extracted from the PIV measurements. These components have been obtained by subtracting the time-averaged stream-wise and transverse velocity components from the phase-averaged stream-wise and transverse velocity components obtained at each phase angle, as given in the following equations:

$$u_\phi' = u_\phi - u_{avg} \quad , \qquad (4.4)$$

$$v_\phi' = v_\phi - v_{avg} \quad , \qquad (4.5)$$

where u_{avg} and v_{avg} are the time-averaged or mean x and y velocity components obtained by averaging the measurements performed at all phase angles, u_ϕ and v_ϕ are the phase-averaged velocity components, and u'_ϕ and v'_ϕ are the resulting fluctuating velocity components.

Visualization of the development of these fluctuating velocity components over a complete flow oscillation cycle is shown in Figure 4.10, with the transverse and stream-wise fluctuating components shown in the left-hand and right-hand columns of the figure, respectively. Analysis of these components will show that the formation and development of the coherent flow structures in the various regions of the flow are intrinsically tied to the development of these fluctuations. As a result, some insight into the behavior of flow structures can be made by examining the evolution of these components in the various regions of the flow. Considering first the transverse fluctuating component beginning at a phase angle of ϕ=0°, a pocket of positive transverse velocity begins to develop in the right shear layer near leading edge of the newly formed coherent flow structure. This pocket, which develops as a result of the counterclockwise rotation of the coherent flow structure, intensifies along with the structure as it convects downstream as shown in the flow fields corresponding to later phase angles, eventually producing a pocket of negative transverse velocity at the trailing edge of the structure. As the flow oscillation cycle progresses further, a subsequent structure forms in the opposing shear layer, first appearing at a phase angle near ϕ=180°, ultimately producing the same qualitative pattern of transverse fluctuating velocity components at the leading and trailing edges of the structure, but with opposing sign due the reversed direction of rotation.

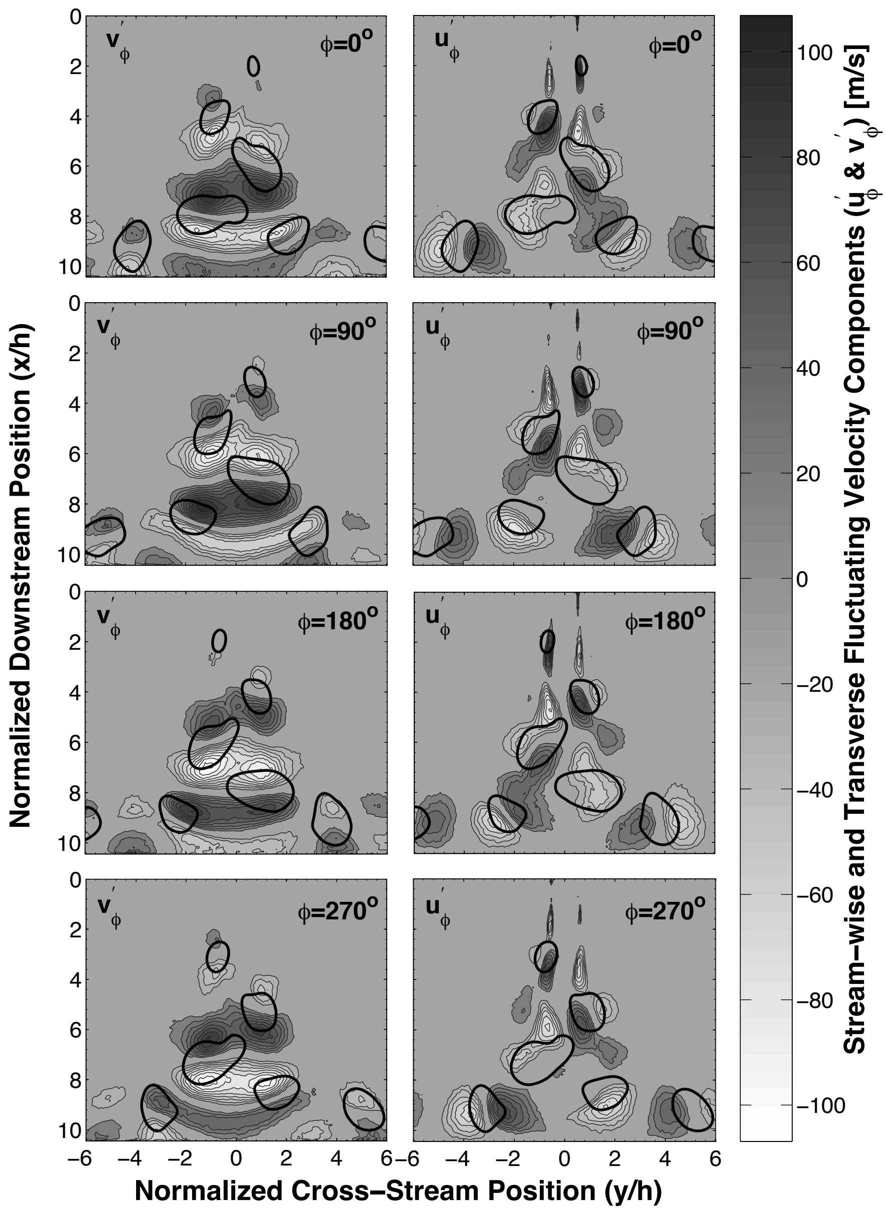

Figure 4.10: Phase-averaged velocity fields of the instantaneous fluctuating (left column) transverse velocity component (v'_{ϕ}) and (right column) stream-wise velocity component (u'_{ϕ}). The solid lines indicate a single level of the velocity discriminant parameter at d_2=0. x_o/h=10.5, M=0.9, f=10.2kHz.

During the development of the jet in the initial region, where the structures have travelled only a small fraction of the total impingement distance, the pockets of transverse fluctuating velocity on either side of the jet are localized in the shear layers near the flow structures, and remain relatively isolated due to the effect of the jet potential core. As the structures travel downstream beyond the range of the potential core, the pockets of transverse flow velocity on each side of the jet begin to merge, and in doing so intensify significantly, eventually forming the series of alternating bands of positive and negative transverse flow velocity, a pattern which is produced due to the anti-symmetric nature of the hydrodynamic mode of the jet, and because the structures formed in each shear layer have opposing directions of rotation. These alternating bands of cross-stream velocity produced by the vortical structures are responsible for producing the pronounced lateral flapping motion of the jet column, and produce very large fluctuating velocities in the developing region, alternating between maximum and minimum values of $|v_\phi'|\approx 105$m/s and −105m/s respectively, a peak-to-peak fluctuation of ~210m/s which represents more than 65% of the initial jet velocity at the nozzle outlet for this case. The transverse component of velocity fluctuations is also present in significant amplitudes in the wall-jet region of the flow, appearing above and below the coherent structures in this region as they convect along the impingement surface.

The stream-wise fluctuating velocity component, which is shown in the right-hand column of Figure 4.10, illustrates that this component has an anti-symmetric distribution about the jet centerline, with a nominally zero amplitude along the jet centerline over the entire impingement distance. This component begins to develop significant amplitudes in the initial shear layers of the jet at very small downstream distances, with alternating positive and negative fluctuations forming on either side of the jet as a result of the out of phase fluctuations in the entrainment and jet core regions shown earlier in Figure 4.9.

These fluctuating regions are initially confined to the thin initial shear layers, however as the flow structures form and convect downstream, they increase in width, producing positive fluctuations at the inside leading edge of the structure and negative fluctuations at the outside trailing edge due to the rotation of the structure. The maximum amplitude of the stream-wise fluctuating component is less than that of the transverse component for this case, with a maximum amplitude of approximately 140m/s (±70m/s) further downstream. As the structures convect downstream past the end of the jet potential core, both the flapping motion of the jet and the impingement of the structure on the plate surface produce significant distortion in this pattern, with the negative and positive pockets of stream-wise velocity fluctuation occurring at the leading and trailing edges of the structures respectively in the wall-jet region. The stream-wise component also maintains significant amplitudes in the wall jet region due to the rotation of the structures, with pockets of positive and negative velocity occurring at the trailing and leading edges of the structures respectively.

Figure 4.11 shows a contour plot of the magnitude and distribution of the stream-wise and transverse fluctuating velocity components, as well as the maximum fluctuation level of the two components as a function of downstream distance. The magnitude of the velocity fluctuations is obtained by calculating the difference between the maximum and minimum values of the velocity components at each point in the flow over the complete flow oscillation cycle, and normalizing this value using the jet velocity at the nozzle outlet, as given in the following equations:

$$\frac{|u'|}{U_o} = \frac{\left(|u_\phi|_{\max} - |u_\phi|_{\min}\right)}{2 \cdot U_o} \quad , \tag{4.6}$$

$$\frac{|v'|}{U_o} = \frac{\left(|v'_\phi|_{\max} - |v'_\phi|_{\min}\right)}{2 \cdot U_o} \quad , \tag{4.7}$$

where $|u_\phi|_{max}$, $|u_\phi|_{min}$ & $|v_\phi|_{max}$, $|v_\phi|_{min}$ are the maximum and minimum values of the fluctuating flow velocity components at each point measured over the entire flow oscillation cycle. The left and right halves of the contour plot shown in Part a) of the figure show stream-wise and transverse fluctuating velocity components, respectively. It is clear from inspection of part a) that the stream-wise component develops rapidly in the initial shear layers of the jet and has two local maxima occurring in two distinct regions of the flow, the first being in the developing region of the jet, just downstream of the potential core, and the second in the impingement region, near the impingement point of the coherent flow structures. The transverse component shows slower development in the initial region of the jet, with amplitudes increasing as the flow progresses past the end of the jet potential core, reaching a global maximum near the end of the developing region.

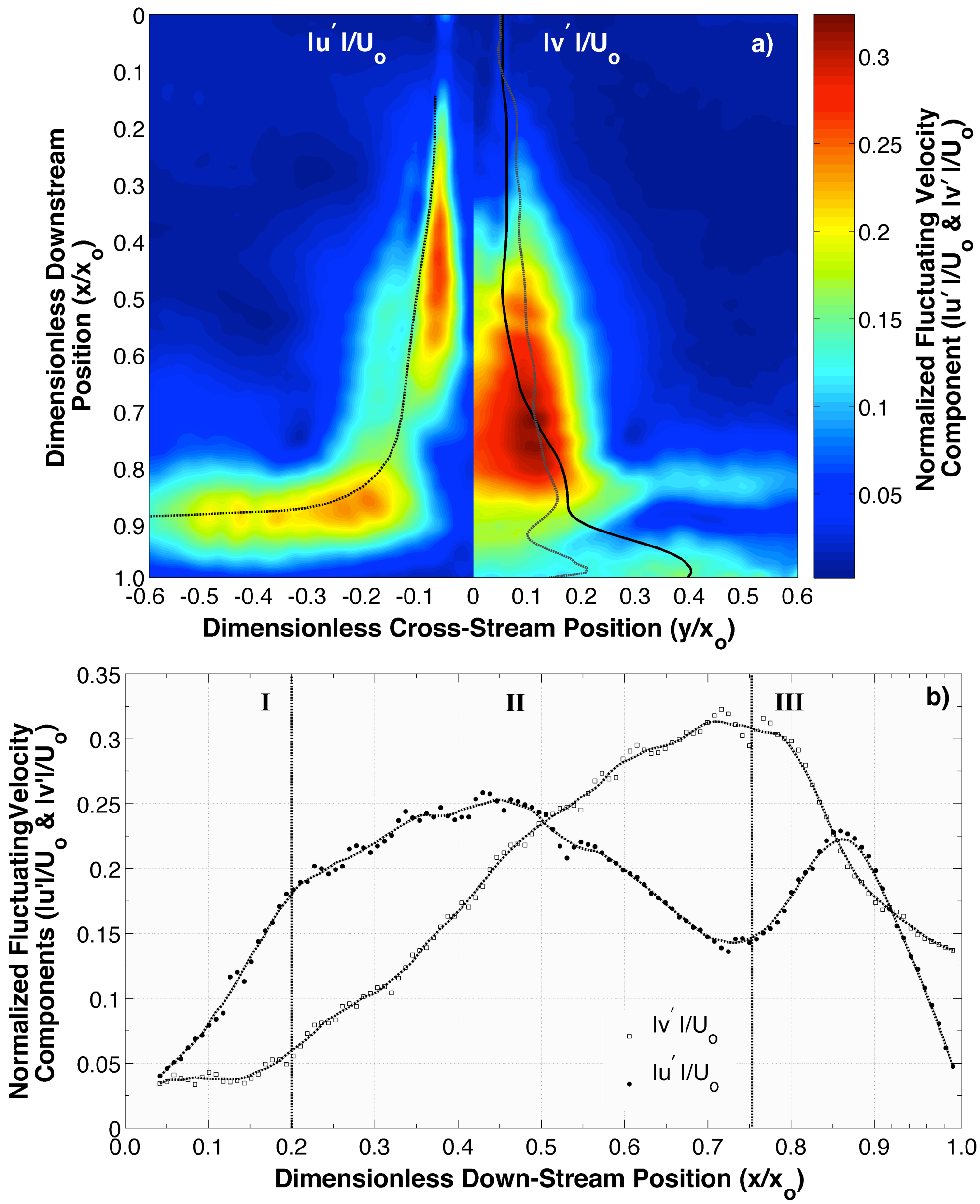

Figure 4.11: a) Contour plot of normalized amplitude of stream-wise and transverse fluctuating velocity components and b) stream-wise development of the maximum amplitude of fluctuating velocity components. Black line on the left-hand side of Part a) indicates the path of coherent flow structures, and grey and black lines on the right-hand side show the location of maximum amplitude of the transverse and stream-wise fluctuating velocity components. x_o/h=10.5, M=0.9, f=10.2kHz.

Part b) of the figure plots the maximum amplitude of the two fluctuating components as a function of downstream position, and illustrates that the evolution of the impinging flow can be divided into three distinct regions. The first region occurs over a range of downstream distance from $0.0 \leq x/x_o \leq 0.2$, or the so-called initial region, a section of the flow field that encompasses the initial shear layers near the nozzle outlet and the formation of coherent flow structures. In this region, the shearing of stream-wise fluctuations in the jet-core and entrainment regions initiates the formation of the coherent vortical structures in the shear layers, with the fluctuations eventually rolling up to form large-scale vortical structures near the end of this range at $x/x_o \approx 0.2$. This region of the flow corresponds to the largest growth rates for the stream-wise fluctuating component, and relatively low amplitude for transverse velocity fluctuations, which only begins to increase near the end of this range as the vortical structures begin to form. The increasing amplitude of the transverse component near the end of this region is associated with the rotation of the vortical structures in each shear layer, which have the effect of transferring energy stream-wise fluctuations to the transverse direction.

The second flow development region occurs for the developing region of the jet, over a range of downstream distances from $0.2 \leq x/x_o \leq 0.75$, where the coherent flow structures grow rapidly to produce the strong flapping motion of the jet column. Initially, the coherent flow structures in each shear layer remain relatively isolated due to the effects of the jet potential core, however as the flow progresses further downstream, the pockets of transverse fluctuating velocity begin to merge, and display rapid growth rates, producing the large-scale flapping motion of the jet column. The stream-wise component continues to grow in this region, but at a slower rate, reaching a local maxima at an amplitude of $|v'|/U_o \approx 0.25$ at a downstream position of $x/x_o \approx 0.45$, after which the amplitude decreases as a function of increasing downstream position as a result of transfer of energy into the transverse fluctuations and the flapping motion of the jet column. The transverse component continues to grow until reaching a maximum amplitude of $|v'|/U_o \approx 0.33$ at a downstream distance of $x/x_o \approx 0.75$, which marks the beginning of the impingement region.

The third and final flow development zone is the impingement region, occurring over the last 25% of the distance between the nozzle and the plate, where coherent flow structures interact with the plate. The beginning of this region is marked by the global maximum in the transverse fluctuating velocity component, and the onset of a secondary region of growth in the stream-wise fluctuating component. The transverse component decreases continuously within this region, but maintains a significant non-zero amplitude close to the plate due to the passage of coherent flow structures. The stream-wise fluctuating component encounters a region of secondary growth associated with the impingement of coherent flow structures, with amplitudes beginning to increase at the edge of the impingement region ($x/x_o \approx 0.75$), and reaching a local maxima of $|v'|/U_o \approx 0.23$ at a downstream position of $x/x_o \approx 0.85$.

4.4.2 Effect of Mach Number

In order to investigate the effect of flow parameters such as the Mach number and impingement ratio on the development and evolution of the flow oscillations, a series of measurements have been performed for a carefully selected set of flow configurations. The first set of measurements focused on the effect of Mach number, and have been completed for a constant impingement ratio of $x_o/h=10.5$, but for four separate Mach numbers varying between M=0.71 and 0.98. These four cases are shown by the open data points in Figure 4.12a), which illustrates the aeroacoustic response of the impinging planar jet as a function of Mach number, along with the predictions of the feedback model that will be developed in a later section of this article. This set of flow configurations has been selected because the jet-plate system responds in a constant n=3 hydrodynamic mode over a relatively large range of Mach number, and produces intense acoustic tones and flow oscillations over the majority of this range. Part a) of the figure shows that significant acoustic tones are generated beginning at a Mach number of M≈0.54, and are excited in two distinct stages as the Mach number is increased. The first jet-stage, which occurs at frequencies near ~2.5kHz for Mach numbers between M=0.54 and 0.68, is produced within the linear regime, and has a relatively low acoustic pressure and a tone frequency which varies linearly with increasing flow velocity. The higher jet-stage is excited in the fluid-resonant regime and is produced by a coupling between the n=3 anti-symmetric hydrodynamic mode of the jet and a resonant acoustic mode between the nozzle flange and impingement surface (Arthurs & Ziada, 2012b). This stage is excited continuously over a range of Mach number from M=0.71 to ~1.0 at frequencies near 10kHz, and produces acoustic tones which show less variation in tone frequency as a function of increasing Mach number and at significantly larger acoustic amplitudes than those in the lower stage, both due to the nature of the fluid-resonant coupling. Figure 4.12b) shows three acoustic spectra obtained at Mach numbers of M=0.71, 0.87 and 0.98, and are given as an example of the acoustic response over this range to illustrate that as the Mach number is increased the frequency of the dominant acoustic tone shows relatively little change due to the fluid-resonant nature of the coupling present in this regime, however the prominence of harmonics in the spectra increases dramatically as the Mach number is increased.

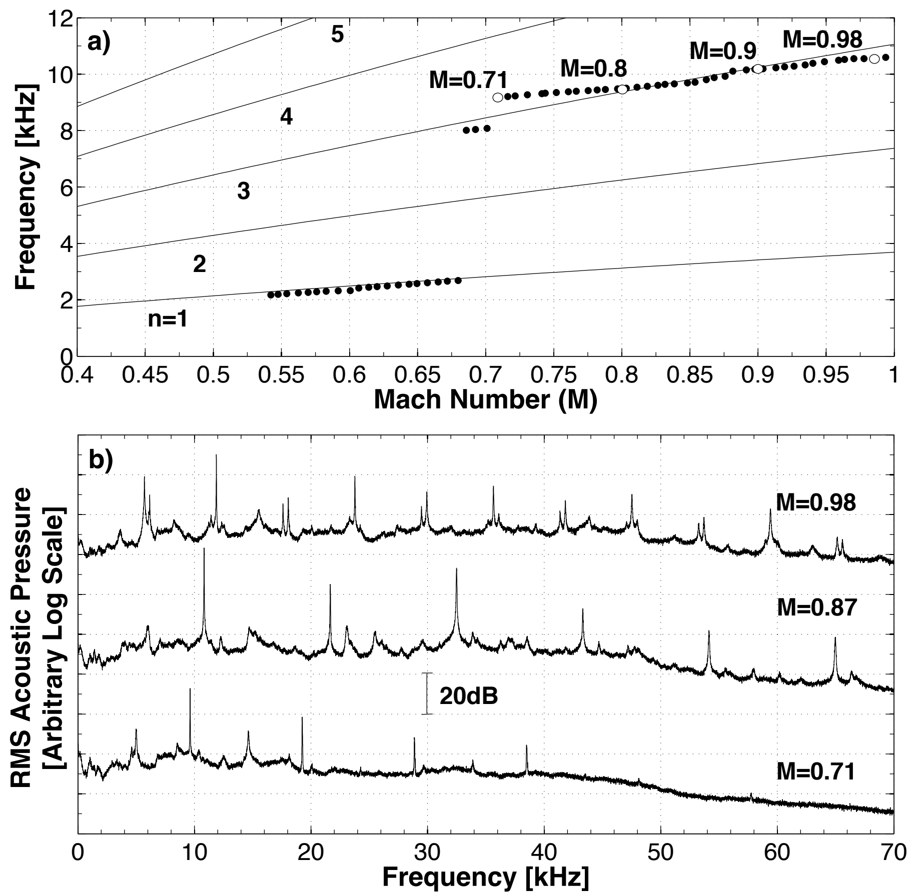

Figure 4.12: The aeroacoustic response of the planar jet-plate system as a function of Mach number for a constant impingement ratio of x_0/h=10.5.

Figure 4.13 shows four phase-averaged flow fields of the magnitude of flow velocity at the same point in the phase for each of the four Mach numbers cases outlined in Figure 4.12, along with a single contour level of the d_2 parameter showing the extent of coherent flow structures. The images show that the n=3 anti-symmetric hydrodynamic mode of the jet is excited for each of the four cases, with each flow field showing a qualitatively similar flapping pattern of the jet column about the centerline, and an analogous anti−symmetric distribution of coherent structures on either side of the jet centerline. It is also relatively clear that as the Mach number increases, the amplitude of the self-excited flow oscillation intensifies, resulting in a more pronounced flapping of the jet column about the centerline and larger coherent flow structures. One distinction in this behavior is evident for the M=0.98 case, which shows a different distribution of structures in the initial region of the jet at a downstream position near $x/x_o \approx 0.3$, with *two* adjacent structures in the left shear layer, and another in the right shear layer, whereas the M=0.71 through M=0.9 cases show a single, large structure in the left shear layer. The reason for these differences will be explored shortly.

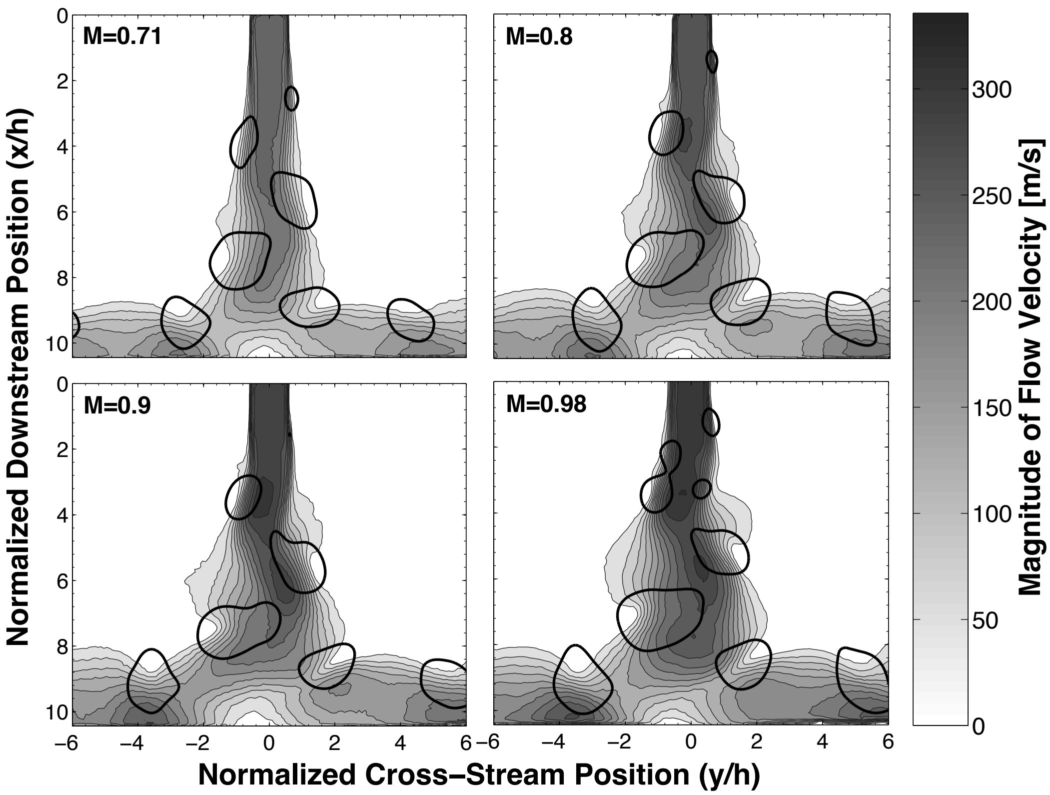

Figure 4.13: Phase-averaged flow fields showing the planar jet-plate system responding in the *n*=3 anti-symmetric jet-stage for Mach numbers of M=0.71, 0.8, 0.9 & 0.98, for an impingement ratio of x_o/h=10.5.

As a result of the same hydrodynamic mode being excited for all four Mach number cases, the spatial distribution of fluctuating components for each of the four cases is qualitatively similar to those shown in Figure 4.10, with the transverse component occurring in a series of alternating bands oriented in the cross-stream direction, and the stream-wise component showing a similar anti-symmetric pattern about the jet centerline, and with more rapid growth rates in the initial region and a nominally zero amplitude along the jet centerline. To examine trends in the magnitude and distribution of the fluctuating components as the Mach number is varied, Figure 4.14 shows a comparison of the maximum fluctuation levels of the transverse and stream-wise fluctuating components as a function of downstream position in parts a) and b) of the figure respectively, with the components of each case being normalized by the flow velocity at the nozzle outlet. Part a) of the figure shows the transverse fluctuating component, and reveals that similar qualitative trends are present for each of the four Mach numbers tested, with transverse fluctuations building relatively slowly in the initial region (I) of the jet, with spatial growth rates eventually increasing at a downstream location corresponding to the formation of the coherent flow structures, and then experiencing rapid growth and reaching a global maximum at the end of the developing region (II) ($x/x_o \approx 0.75$). Similarly, part b) of the figure shows the stream-wise fluctuating component, and illustrates similar qualitative trends for each of the four cases with two distinct local maxima occurring in the developing and impingement zones of the flow for each case, but with significant variation in the distribution and amplitude of these fluctuations, particularly for the upstream maxima, in the developing region of the jet.

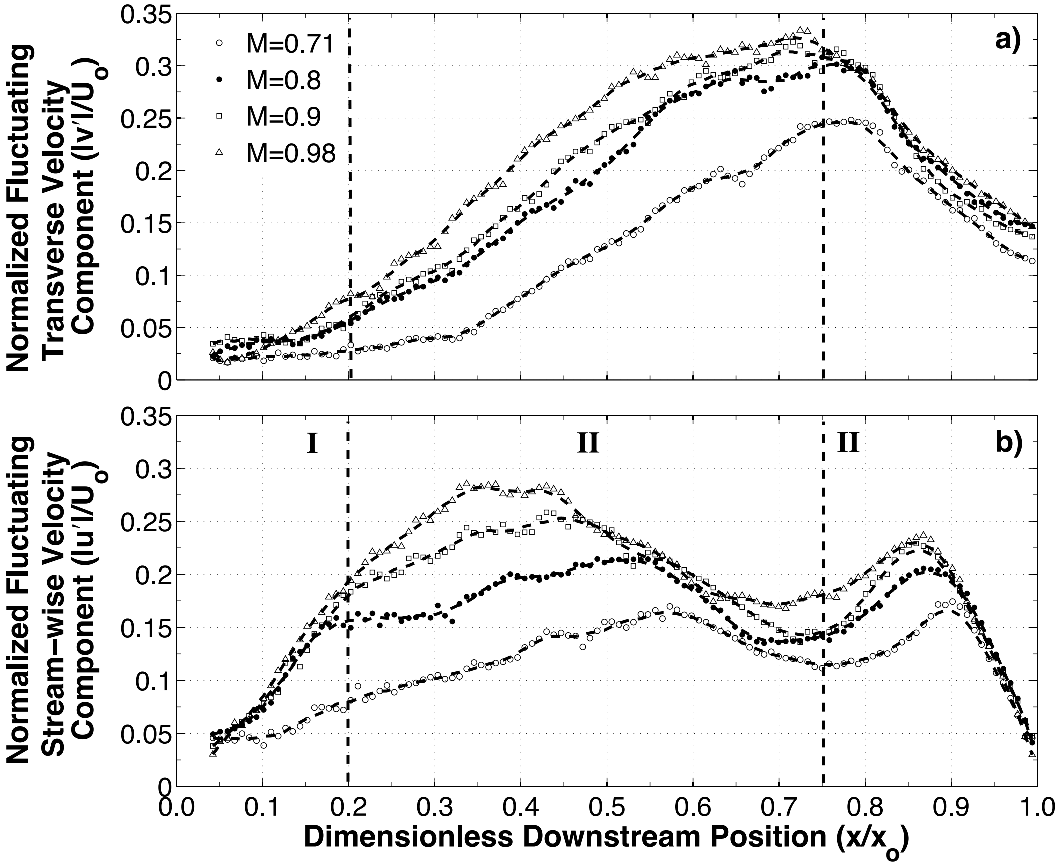

Figure 4.14: Amplitude of a) stream-wise and b) transverse fluctuating velocity component as a function of downstream position for the *n*=3 anti-symmetric jet stage for Mach numbers of M=0.71, 0.8, 0.9 and 0.98.

The fluctuating components of the M=0.71 case, which represents the lowest Mach number for which this hydrodynamic mode of the jet is excited, are shown to have significantly lower initial growth rates for both the transverse and stream-wise components, as well as lower maximum values in both the developing and impingement regions of the jet. These trends are thought to be the result of a relatively weak fluid-resonant coupling for this case, which produces lower acoustic pressure amplitudes and weaker self-excited flow oscillations compared to higher Mach number cases. The higher Mach number cases excite acoustic tones of greater amplitudes as a result of a more robust flow-acoustic coupling, and therefore show larger growth rates and maximum amplitudes of the fluctuating velocity components.

The location of the first local maxima of the stream-wise fluctuating component moves upstream and increases in amplitude as the Mach number increases, occurring at locations of $x/x_o \approx 0.57$, 0.54, 0.41 and 0.35 for the M=0.71, 0.8, 0.9 and 0.98 cases, respectively. All four cases show similar rates of decay for this component after passing through the first maxima in the developing region, with all four cases reaching a local minima near the edge of the impingement region at $x/x_o \approx 0.75$, and encountering a region of secondary growth as the flow enters the impingement region. The transverse fluctuating component also shows very similar trends among the different Mach number cases, with growth rates increasing near the end of the initial region and building to a global maximum at the edge of the impingement region at $x/x_o \approx 0.75$, where this component begins to decrease due to the interaction of the coherent flow structures with the downstream surface. The maximum amplitude of the transverse component is related to the Mach number of the impinging jet, with the dimensionless fluctuation levels reaching comparable amplitudes between all cases.

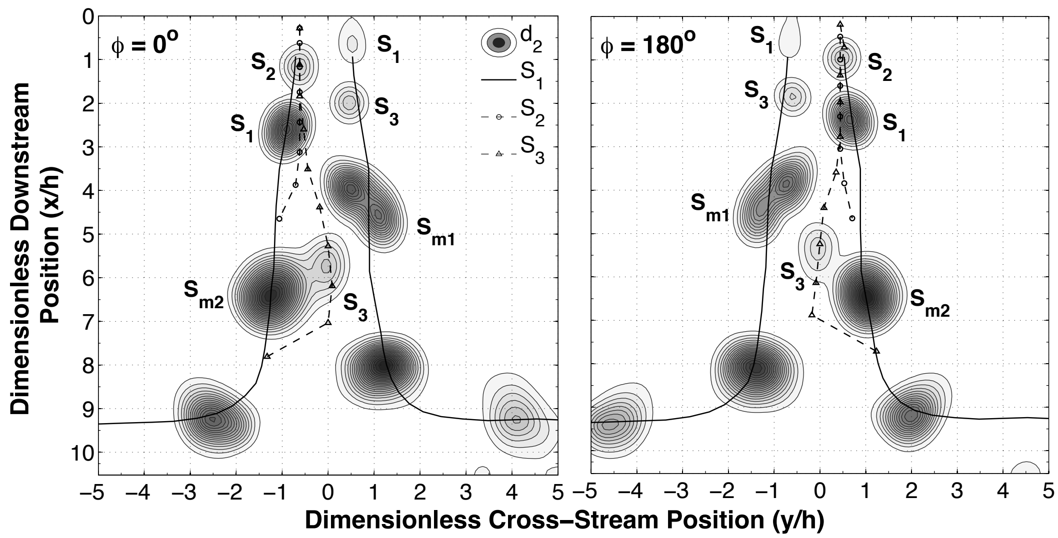

Figure 4.15: Structure amalgamation and paths for the transonic impinging planar jet with an impingement ratio of x_o/h=10.5 and a Mach number of M=0.98.

As the Mach number of the jet approaches choked flow at the nozzle outlet, substantial differences in the evolution of the coherent flow structures in the initial region are observed in Figure 4.15, which shows a pair of contour plots of the discriminant field (d_2), illustrating coherent flow structures for two time instants 180° apart in the phase of the flow oscillation. The fields have been spatially smoothed for ease of inspection using two passes of a Gaussian filter, and the x and y-positions of the coherent flow structures have been extracted by calculating a weighted average of the discriminant function for measurements performed at each phase angle in the following form:

$$\overline{x} = \frac{\iint_A \left\{ d_2(x,y) \cdot x \right\} dA}{\iint_A d_2(x,y)\, dA}, \tag{4.8}$$

$$\overline{y} = \frac{\iint_A \left\{ d_2(x,y) \cdot y \right\} dA}{\iint_A d_2(x,y)\, dA}, \tag{4.9}$$

where $\bar{x}$ and $\bar{y}$ are the resulting structure positions at each phase angle, and the functions are integrated within the bound of each structure whose extent is defined by negative values of the velocity discriminant. Similar structure tracking techniques have been employed by Scarano & Riethmuller (2000) and Schram et al. (2004), who examined structure propagation and merging in an acoustically excited free jet.

For this case, the shear layer on each side of the jet spawns three consecutive structures: S_1, S_2 and S_3, before repeating this pattern, with each shear layer forming these vortices simultaneously, but out of phase by 180°. Structure S_1 is the strongest of the three structures and will be denoted the primary flow structure, with S_2 and S_3 being weaker secondary structures which will later merge with S_1. These three structures move downstream along the paths shown in the figure and ultimately merge in a repeatable, anti-symmetric pattern on either side of the jet. After structures S_1 and S_2 have been formed in the initial shear layer, they convect downstream with structure S_2 convecting along a path closer to the jet centerline. Structure S_2, being smaller and convecting in a region with a higher mean flow velocity, travels at a greater convection speed than S_1, resulting in the structures ultimately merging at a downstream distance of approximately x/x_o=0.4 to form a new structure S_{m1}. Shortly after the formation of structures S_1 and S_2, a third structure S_3 forms immediately behind in the same shear layer, with this structure convecting along a path closer the jet centerline as it trails structures S_1 and S_2. Shortly after structure S_1 and S_2 merge to form S_{m1}, a second merging event involving structures S_{m1} and S_3 occurs at a downstream distance of approximately x/x_o=0.75 to form a second merged structure S_{m2}. In both instances of vortex merging, (S_1 & $S_2 \rightarrow S_{m1}$ and S_3 & S_{m1}

$\rightarrow S_{m2}$), the trailing structure convects along a path closer to the jet centerline than the leading structure(s), resulting in the trailing structure convecting at a higher velocity allowing the merging to occur. These merging events occur simultaneously in each shear layer, but with a phase difference of 180°.

This series of vortex amalgamations results in structures impacting the impingement surface and a resultant tone frequency of ⅓ of frequency of structure production in the initial shear layer. There is evidence that this merging process *does occur* in the lower Mach number cases presented in this paper; however, the secondary structures (S_2 and S_3) are not as strong over their entire paths, making visualization more difficult. In these lower Mach number cases, the merging events are more visible than the secondary structures themselves, with the S_{m1}&$S_3 \rightarrow S_{m2}$ merging event being the most visible event, which can be seen in Figure 4.13 by the irregular shape of structures in this location, and the S_1 & $S_2 \rightarrow S_{m1}$ merging event also being visible, but less obvious. It has been found in previous work on acoustically excited free jets at low Mach number that vortex merging events can be responsible for the generation of significant noise, in particular the production of strong sub and higher harmonics of the fundamental tone frequency (Schram & Hirschberg, 2003 and Schram et al., 2004). This agrees with the trends shown in Figure 4.12b), which shows increased prominence of harmonics in the acoustic spectra as the Mach number is increased. Similar merging events have been observed in other self-excited impinging jet flows such as Umeda el al. (1987), which investigated a high subsonic and supersonic axisymmetric jet impinging on a small cylinder at varying distances downstream. The authors of this paper also attributed this phenomenon to the production of harmonic components.

4.4.3 Effect of Impingement Ratio

This section will investigate the influence impingement ratio on the evolution of the impinging planar jet oscillations. Due to the complex response characteristics of the impinging planar jet outlined in Arthurs & Ziada (2012b), it is not possible to manipulate the impingement ratio over a significant range without impacting other response characteristics, such as coupling with different resonant acoustic modes which control the jet oscillation frequency. To examine the effect of varying impingement ratio on the flow evolution of the impinging planar jet, a set of seven flow configurations with constant Mach number of M=0.71 and impingement ratios varying in the range of $8.25 \leq x_o/h \leq 17.0$ have been selected, with these flow configurations being self-excited by the same n=3 hydrodynamic mode of the jet, but coupling with three distinct resonant acoustic modes over this range. The purpose of these measurements is to examine the effect of varying impingement ratio on the characteristics of a single hydrodynamic mode of the jet, and in addition the effect, if any, of the coupling of a constant hydrodynamic mode of the jet with different resonant acoustic modes.

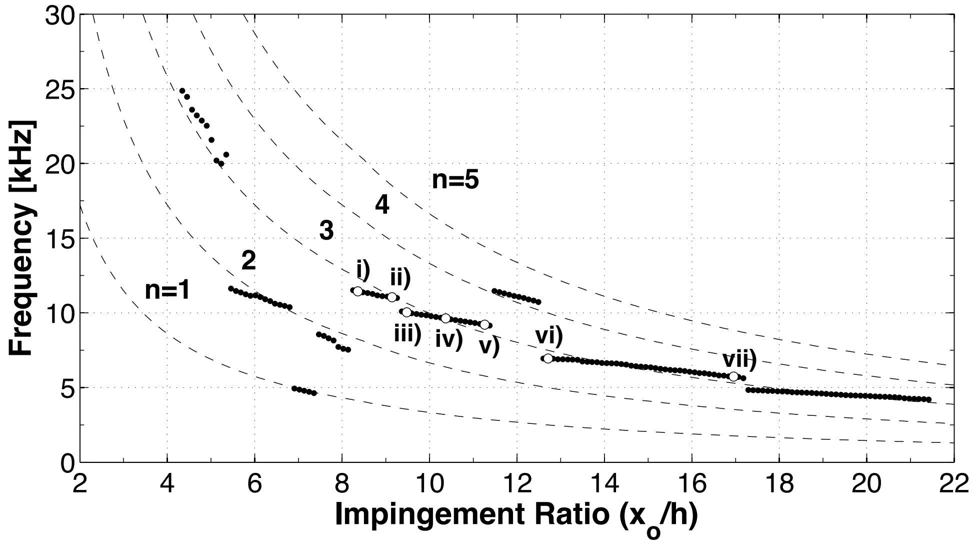

Figure 4.16: The aeroacoustic response of the planar jet-plate system as a function of impingement ratio for a constant Mach number of M=0.71 (U_o=245m/s). Cases i) through vii) shown by open data points represent the seven measured PIV cases.

Figure 4.16 shows the aeroacoustic response for a fixed Mach number of M=0.71, with the seven cases selected for PIV measurements denoted by open data points and labeled with Roman numerals i) through vii). Also shown in the figure are the predictions of the feedback model that will be developed later in this article, but shown now for clarity. The seven selected cases are from data that lies nominally along the prediction of the *n*=3 hydrodynamic mode of the jet, and are distributed over three distinct bands of data, with each band resulting from the jet oscillation coupling with a different resonant acoustic mode between the nozzle and the plate.

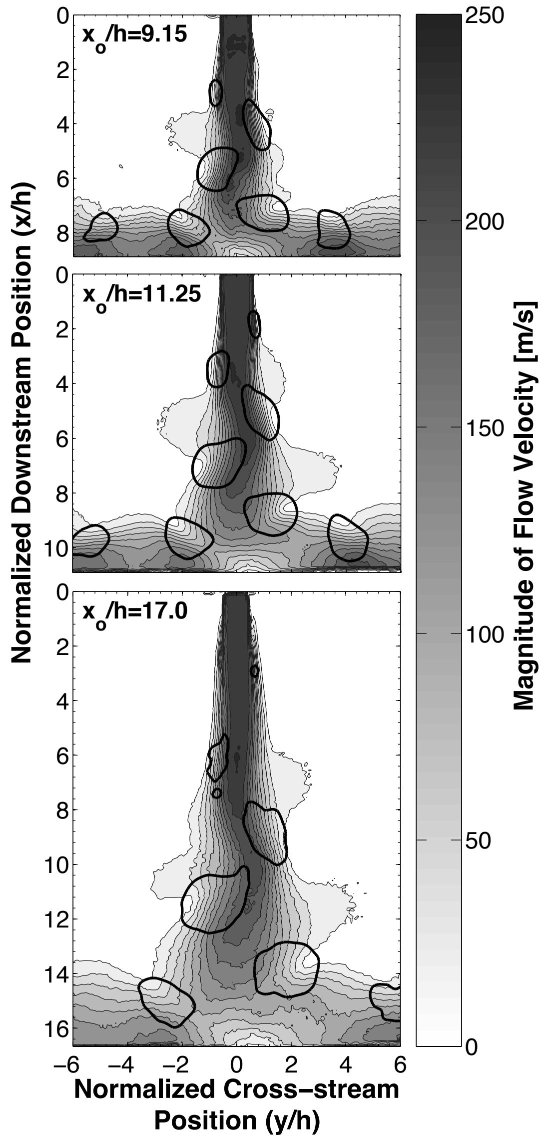

Figure 4.17: Magnitude of flow velocity of the *n*=3 anti-symmetric hydrodynamic mode for three separate impingement ratios. Flow fields taken at the same point in the phase of each flow oscillation cycle.

Figure 4.17 shows a series of three flow fields detailing the magnitude of flow velocity at the same instant in the phase for cases ii), v) and vii) in Figure 4.16, corresponding to impingement ratios of x_o/h=9.15, 11.25 and 17.0, or measurements taken at near the largest impingement ratio for each of the three resonant acoustic modes. The three flow-fields indicate that the general form of the flow oscillation is very similar, with the characteristics of the flapping mode of the jet and the number and distribution of coherent flow structures being comparable as the impingement ratio is varied within n=3 hydrodynamic mode, even as the jet couples with different resonant modes. The structure of the jet flow is elongated as the impingement distance increases, with the time-averaged flow fields of cases ii), iv) and vi) having successively longer potential cores extending to x/h=3.43, 4.12 and 4.82 respectively, and the size of the coherent structures being larger as the impingement ratio is increased. As would be expected from the qualitative similarity of the flow fields shown in Figure 4.17, the distribution of the stream-wise and transverse fluctuating velocity components is very similar to those shown earlier.

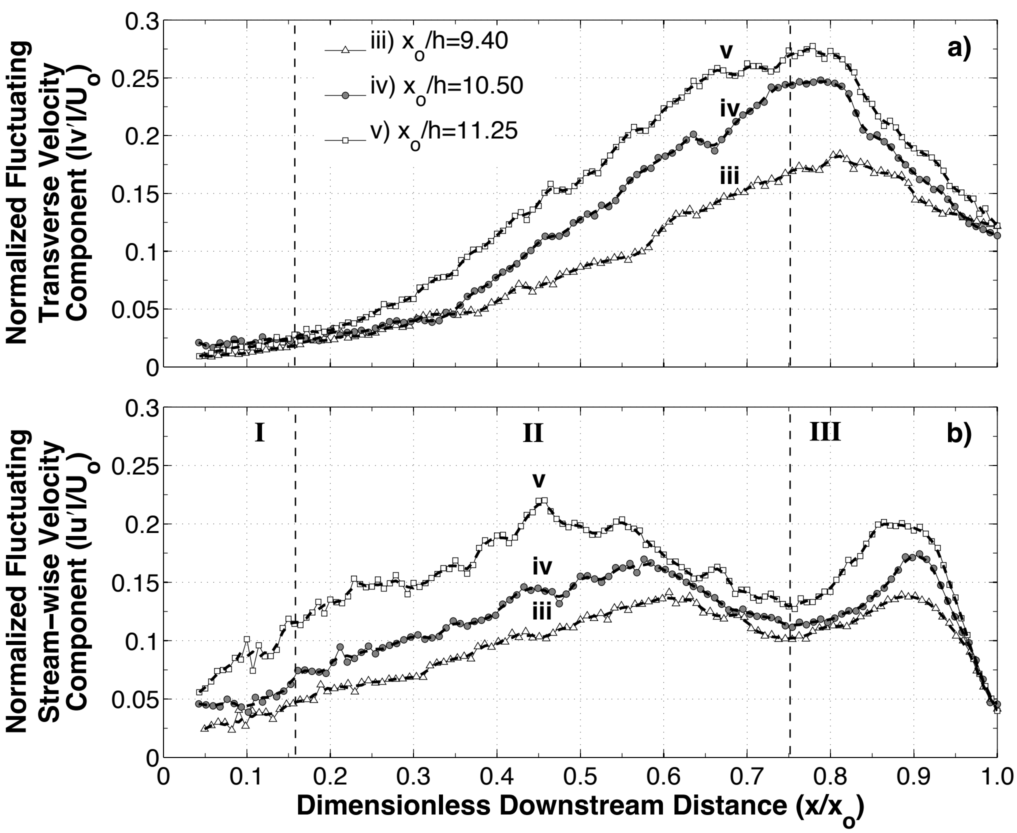

Figure 4.18: Maximum velocity fluctuation levels for flow measurements performed at three impingement ratios with a resonant acoustic mode. M=0.71 (U_o=245m/s).

Figure 4.18 shows the amplitude of fluctuating velocity components in the transverse and stream-wise directions for cases iii), iv) and v), taken at three impingement ratios of x_o/h=9.4, 10.5 and 11.25 distributed over a single resonant mode. The flow oscillations show similar characteristics within the resonant acoustic mode, but with increasing amplitudes of both the transverse and stream-wise components as the impingement ratio is increased. The transverse component shows a maximum amplitude at a dimensionless downstream position of x/x_o≈0.75 corresponding to the beginning of the impingement region, with the position of the global maximum moving upstream slightly as the fluctuation levels increase due to the increased size of the coherent flow structures. The amplitude of the stream-wise component shows similar trends as in the previously examined cases, with two local maxima occurring in the developing and impingement regions respectively, and with the location of the upstream maxima moving upstream in a similar fashion to the cases examining the effect of Mach number in the previous section.

This pattern of lower fluctuation levels at the small end of the impingement ratio range for a given resonant acoustic mode, and increasing as the impingement ratio is increased over the range of acoustic mode is repeated in each of the three separate bands of data shown in Figure 4.16. The amplitude of the transverse fluctuating component at the small and large ends of the impingement ratio range is shown in Figure 4.19 for each of the three resonant modes. Each of the six cases shown in this figure depict a qualitatively similar distribution to those found in earlier cases, with the transverse component starting at a very small amplitude, and growing to a maximum at approximately 70-80% of the impingement distance, but with the amplitudes being significantly larger at the end of the impingement ratio range of each resonant mode.

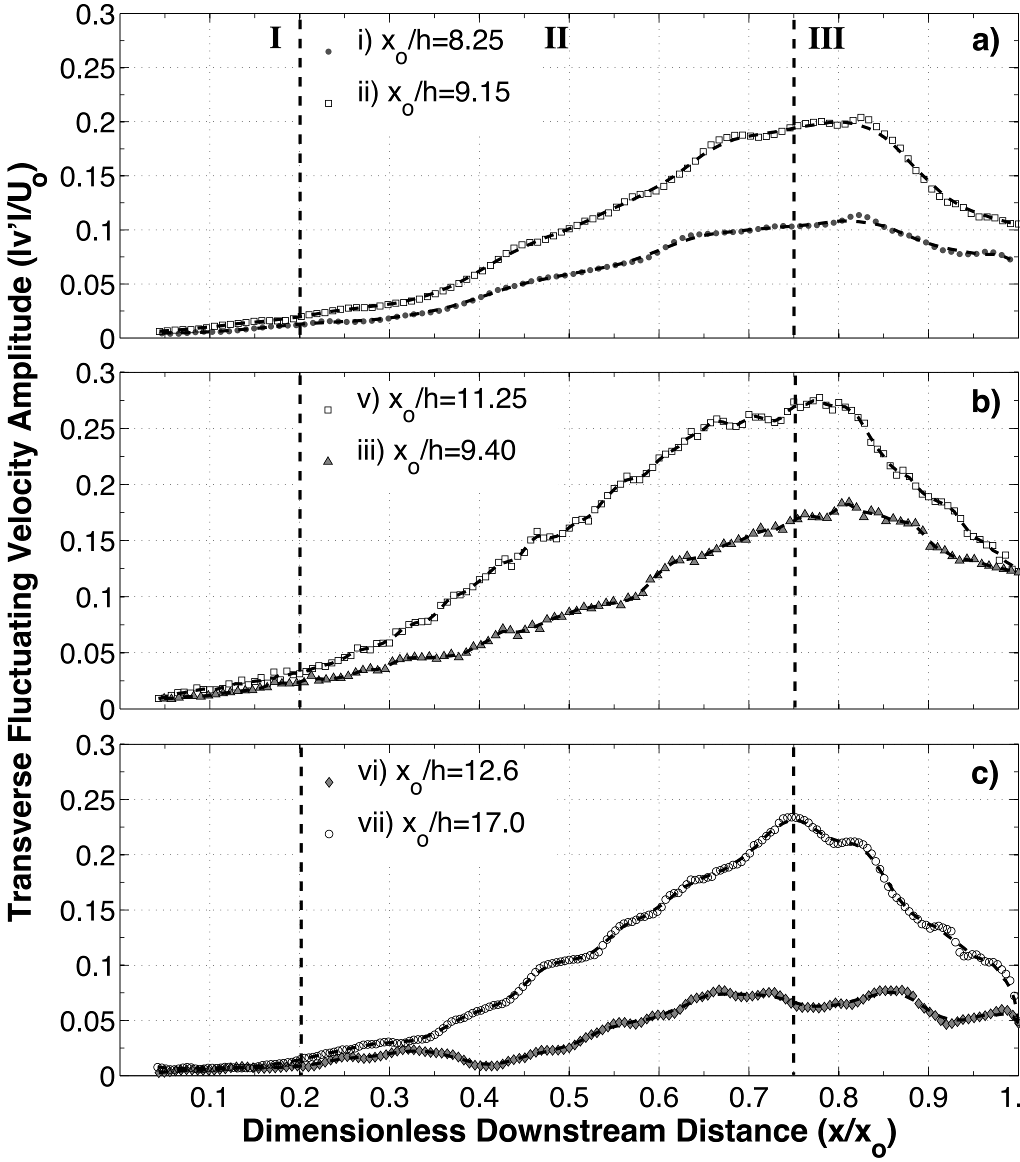

Figure 4.19: The maximum transverse fluctuating velocity component as a function of dimensionless downstream position for a) cases i & ii, b) cases iii & v an c) cases vi) & vii.

4.5 Development of a Feedback Model

Since the development of the Rossiter model in 1964 for use in high-speed cavity flows, the model has been applied to a wide variety of free and impinging systems to describe the feedback mechanism that produces self-excited flows. The model has been applied to a variety of low Mach number systems such as the jet-edge (Powell, 1961 & Kwon, 1998), jet-slot (Glesser et al., 2008) and free-jet geometries (Thomas & Prakash, 1991) under the so-called "hydrodynamic assumption", in which the propagation time of acoustic disturbances is neglected, and it has also been used to describe the behavior of higher Mach number systems where the acoustic propagation time is included, such as jet-screech in both planar and axisymmetric supersonic free jets (Tam, 1988 & Raman, 1999). Numerous authors have applied the model to the case of a high-speed jet impinging on a plate for subsonic axisymmetric jets (Ho & Nosseir, 1981, Nosseir & Ho, 1982, Tam & Ahuja, 1990, and Panickar & Raman, 2007), as well as supersonic axisymmetric jets (Krothapalli et al., 1999) and supersonic planar jets (Krothapalli, 1985). These models generally use some form of the following equation:

$$f_n = \frac{(n+d)\cdot c \cdot u_c}{x_o(u_c + c)}, \tag{4.10}$$

where n is the jet-stage number and related to the hydrodynamic mode of the jet, c is the speed of sound, u_c is the downstream convection velocity of flow disturbances and x_o is the impingement distance. An additional factor d has been added by many authors as an adjustable parameter, which has been most often attributed to variation in phase between the flow and the acoustic disturbances at the impingement point or nozzle (Krothapalli et al., 1999), and the values of this parameter has typically ranged from d=0 to d=−0.5. The majority of authors have approximated the downstream convection velocity (u_c) to be some fraction of the initial jet velocity at the nozzle outlet, typically in the range

$0.55 \leq \kappa \leq 0.7$ (Panickar & Raman, 2007), with the selected value typically being justified by measurements performed in analogous free jets. Often, minor changes to the convection coefficient and/or the adjustable parameter d have been adapted to obtain the best fit between experimental data and the theoretical model.

While the Rossiter model is conceptually correct in its application to self-excited jet flows, and can be very useful to predict the frequency of acoustic tones and explain their generation mechanism, the model utilizes a number of assumptions which can be misleading in their application to impinging jet flows, and in particular those impinging on plates, due to the significant structural differences between these geometries and the cavity flows for which the model was initially developed. These structural differences result in significant modifications being required for two key components of the model: the downstream velocity scale (u_c), related to the propagation of coherent flow structures, and the impingement distance (x_o) travelled by those structures. The following sections are devoted to examining the behavior of the coherent flow structures responsible for sustaining the feedback mechanism, and to use the present results to develop a feedback model that can accurately predict the behavior of the system.

4.5.1 Convection Speed of Coherent Flow Structures

Because of the inherent difficulty of performing measurements in high-speed flows, measurements investigating the convection speed and behavior of coherent flow structures are relatively uncommon. Measurements of this type have been performed in self-excited geometries at lower speed such as the jet-edge (Ziada & Rockwell, 1982 and Kwon, 1998), jet-cylinder (Hsiao et al., 1999 and Hsiao & Hsu, 2004), where measurement issues are not as problematic. On the other hand, measurements performed in higher-speed flows are generally confined to the widely studied case of compressible free jets, and are performed using a variety of optical techniques such as Laser-Doppler Velocimetry (LDV) (Kerhervé et al., 2006 and Kerhervé et al., 2010), Particle Image velocimetry (PIV) (Fleury et al., 2008) and Phase-Doppler Velocimetry (PDV) measurements (Thurow, 2005 and Thurow et al., 2008). There are some examples of convection speed measurements performed in high-speed impinging jet flows, such as Nosseir & Ho (1982), who indirectly measured the convection speed using a pair of microphones in the acoustic near-field and a cross-correlation technique using "pre-whitening" to extract the speeds of the upstream and downstream propagating disturbances. Umeda et al. (1987) used measurement of Schlieren photographs to estimate the convection speed for a supersonic jet impinging on a small cylinder, and Krothapalli et al. (1999) and Elavarasan et al. (2000) used PIV measurements of an impinging supersonic axisymmetric jet and a structure tracking technique to extract the convection speed of coherent structures. In these most recent examples, the authors found that the convection speed in impinging axisymmetric jets was significantly less than that of the equivalent free jet, being in the range $0.52 \leq \kappa \leq 0.6$, compared to the range of $0.6 \leq \kappa \leq 0.7$ commonly reported for free jet flows, and that the convection velocity changed as a function of both impingement ratio and flow velocity. In this section, measurements of the convection velocity of coherent flow structures will be made using the results of phase-averaged PIV measurements presented earlier. These measurements have been performed for a series of intermediate impingement ratio cases presented earlier, with all measurements corresponding to the n=3 hydrodynamic mode of the jet excited in the fluid-resonant regime.

Measurements of the convection velocity for the M=0.9 case have been obtained using two separate techniques. The first approach tracks the propagation of *velocity fluctuations* within the flow to indirectly track the motion of the structures in a method analogous to a two-point spatial correlational technique. Inspection of Figure 4.10 in the previous section demonstrates that as the flow oscillation progresses, coherent structures in the developing region of the jet are nominally positioned between the alternating bands of positive and negative transverse fluctuating velocity as they convect from the nozzle outlet towards the impingement surface. By examining the transverse fluctuating velocity component along the lip-line (y/h=0.5) for a series of phase angles, the approximate position of the structure at each phase angle can be inferred, and the convection velocity can be extracted. Part a) of Figure 4.20 shows a series of three profiles of the transverse fluctuating velocity component taken along the lip-line at three different phase angles of ϕ=0°, 45° & 90°, and part b) shows the structure positions extracted from the fluctuating velocity profiles over three repeated cycles.

Figure 4.21 shows the results of the dimensionless convection velocity (u_c) normalized by the flow velocity at the nozzle outlet, as a function of downstream position extracted using this technique. The plot shows a slight increase in the convection velocity from $u_c/U_o \approx 0.40$ to 0.45 over the developing region of the jet flow, with a decreasing trend becoming evident as the fluctuations approach the plate. This value of convection coefficient is significantly lower than those found for impinging *axisymmetric* jets, which is likely associated with the anti-symmetric form of the hydrodynamic mode for the planar jet as opposed to the axisymmetric modes excited in the case of round jets, as well as the larger size of coherent structures relative to the jet thickness. This convection velocity is similar to the value observed for the anti-symmetric flow oscillation in an acoustically excited planar jet at low Mach number (La Cuadra et al., 2007), for which a convection coefficient of κ=0.41 was observed for a flapping mode in the developing region of free planar jets. There are however, a number of potential shortcomings of this method arising from the fact that this method tracks the motion of disturbances within the flow and not necessarily the movement of the structures themselves, which can lead to misleading results regarding the convection speed, especially near the impingement surface. This is due to the complex distribution of the fluctuating velocity components in the impingement zone, where the paths of the coherent flow structures are highly two-dimensional. As a result, the use of a one-dimensional analysis technique to identify the motion of structures can result in significant error, especially in the region close to the plate.

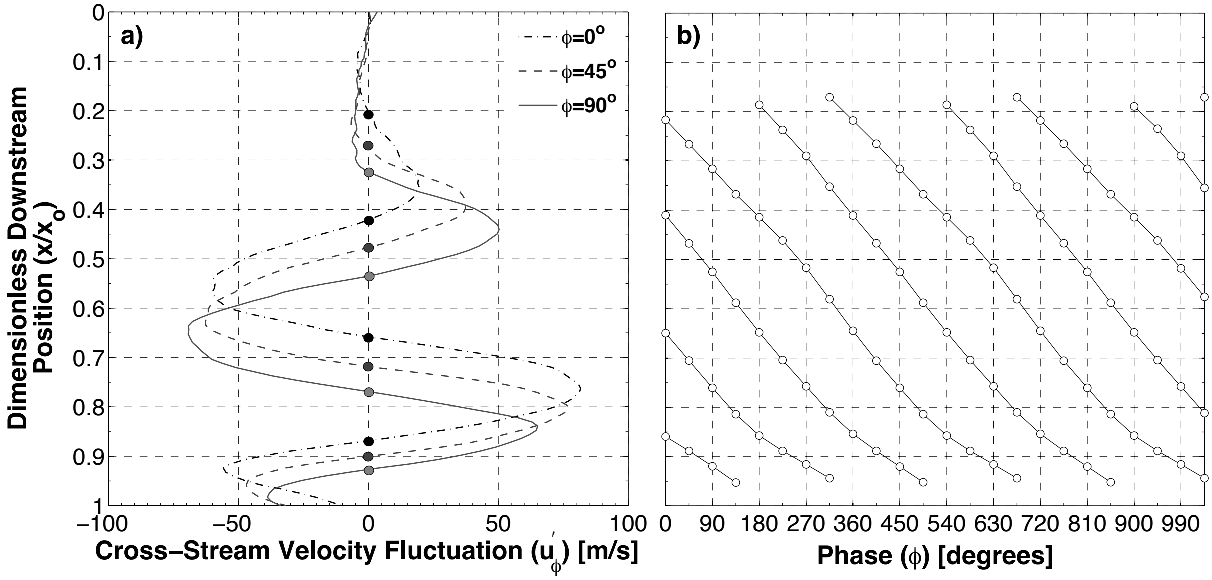

Figure 4.20: Profiles of the transverse fluctuating velocity component at the right lip-line (*y*/*h*=0.5) for three phase angles with points added to approximate the location of coherent structures along with the extracted structure position as a function of phase of the flow oscillation for three repeated cycles. x_o/h=10.5, M=0.9, *f*=10.6kHz.

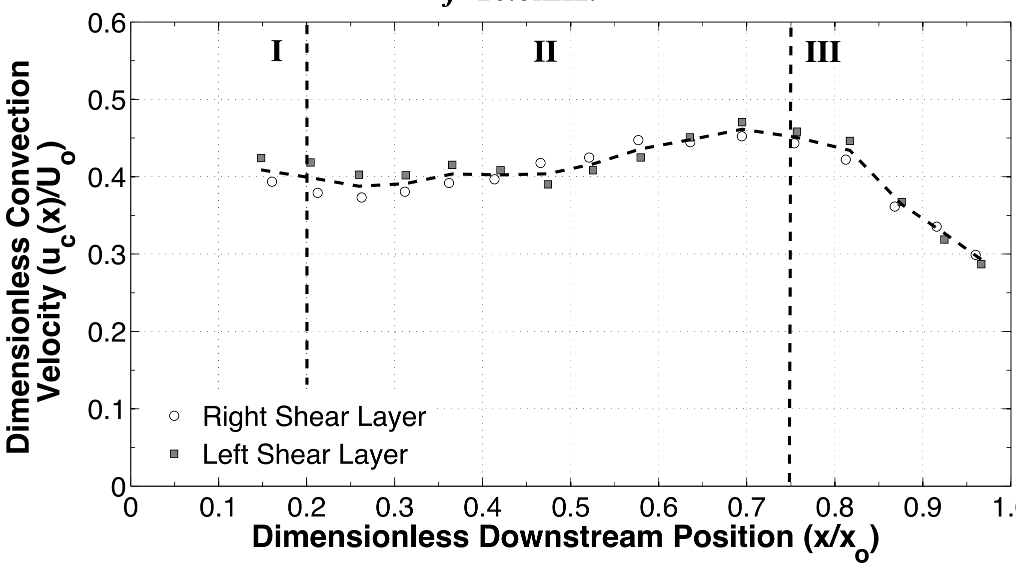

Figure 4.21: Convection coefficient as a function of dimensionless downstream position for a Mach numbers of M=0.9 and the *n*=3 anti-symmetric hydrodynamic mode.

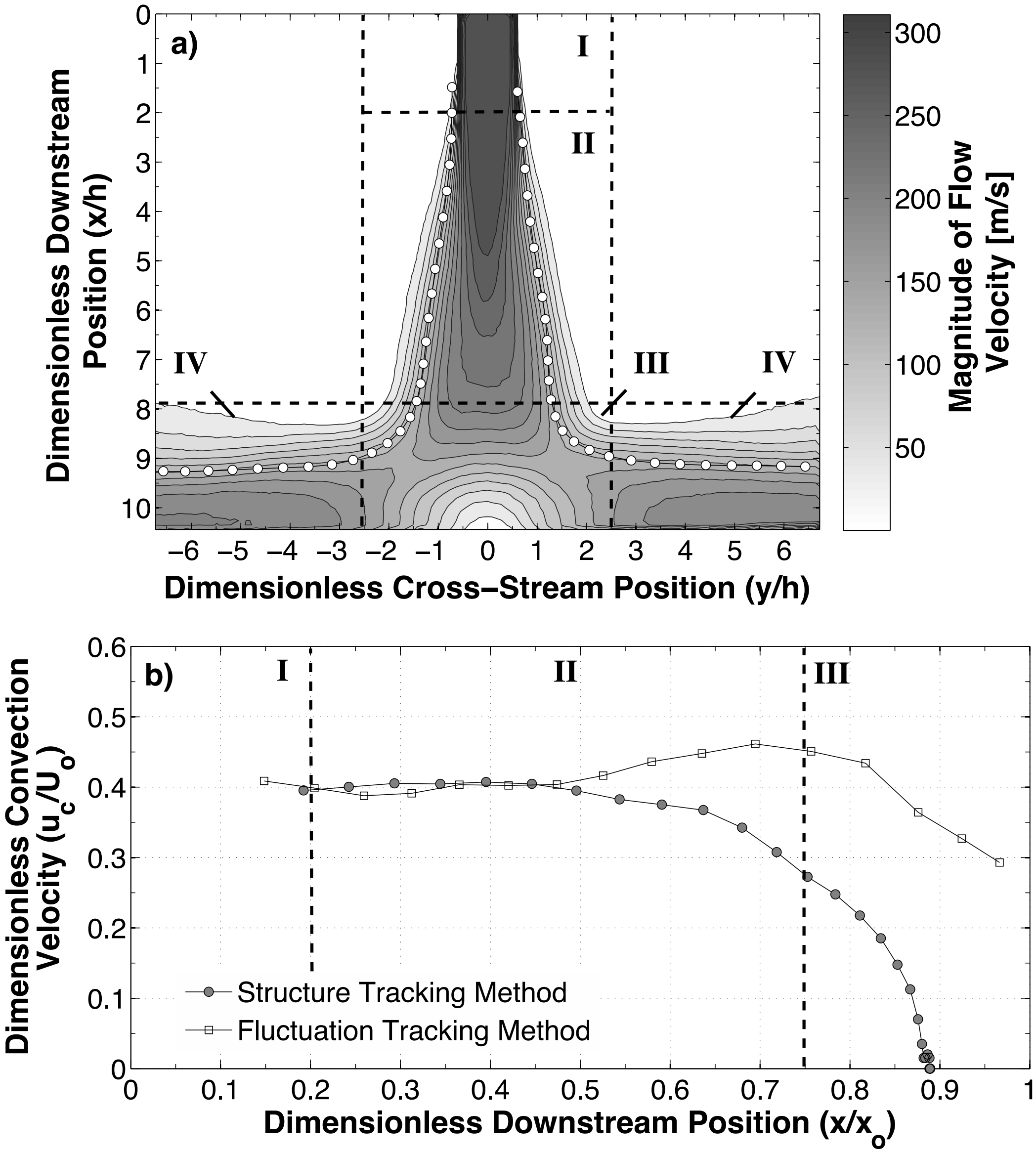

Figure 4.22: a) Plot of the time-averaged flow field of an impinging planar jet for x_o/h=10.5, M=0.9, along with the mean path of coherent flow structures and b) a comparison of the dimensionless convection velocities obtained by the structure and fluctuation tracking methods for a Mach number of M=0.9 for the n=3 anti-symmetric jet mode.

In order to obtain a more accurate measurement of the convection speed, a structure-tracking scheme has been developed, which uses the velocity discriminant parameter d_2 to identify and track the motion of coherent structures to measure not only their convection speed, but the convection path, size and strength, and to characterize the position at which the structures begin to impinge on the plate surface. The center of the coherent flow structures at each phase angle has been located by using Equations (4.8) and (4.9). Part a) of Figure 4.22 shows the path of the coherent flow structures produced in each shear layer extracted from the flow fields, which have been superimposed on the field of average velocity magnitude for measurements obtained over all phase angles. Inspection of the figure shows that the structures are first detected in the initial region of the jet, near $x/h\approx 1.5$ in each shear layer, and spread outward as they convect downstream, mirroring the spread rate of the impinging jet. As the structures progress towards the plate and enter the impingement zone at $x/h=7.9$ ($x/x_o=0.75$), they undergo a change of direction from being predominantly in the downstream direction, with some outward spread in the transverse direction, to entirely in the transverse direction, with the center of the structure reaching a maximum downstream distance of $x/x_o\approx 0.9$.

By extracting the differential structure displacement of the flow structure between the flow fields at each phase angle, and knowledge of the time increment being ⅛ of the period of the flow oscillation, the x and y-components of convection velocity can be obtained. Part b) of Figure 4.22 shows the results of the stream-wise convection velocity for the structure tracking technique, as well as the results of the fluctuation tracking technique as a comparison. Both techniques find similar values of dimensionless convection speeds of $u_c/U_o\approx 0.4$ early in the developing region of the jet, but the results of the structure tracking technique shows evidence of structure slowing as the flow progresses past the end of the jet potential core and enters the transition region. The differences between the two methods becomes more substantial as the flow approaches the plate, with a difference of nearly 45% at the edge of the impingement zone (x/x_o=0.75). Although tracking fluctuations within the flow has proved to be an adequate approach for estimating convection speed in simpler geometries where the mean flow and coherent flow structures travel predominantly in the downstream direction, such as in free jets, flow over cavities, and the jet-edge case, the present jet-plate configuration involves a more complex distribution of fluctuating components as a result of the two-dimensional structure path, a characteristic that can not be adequately modeled by a one-dimensional approach.

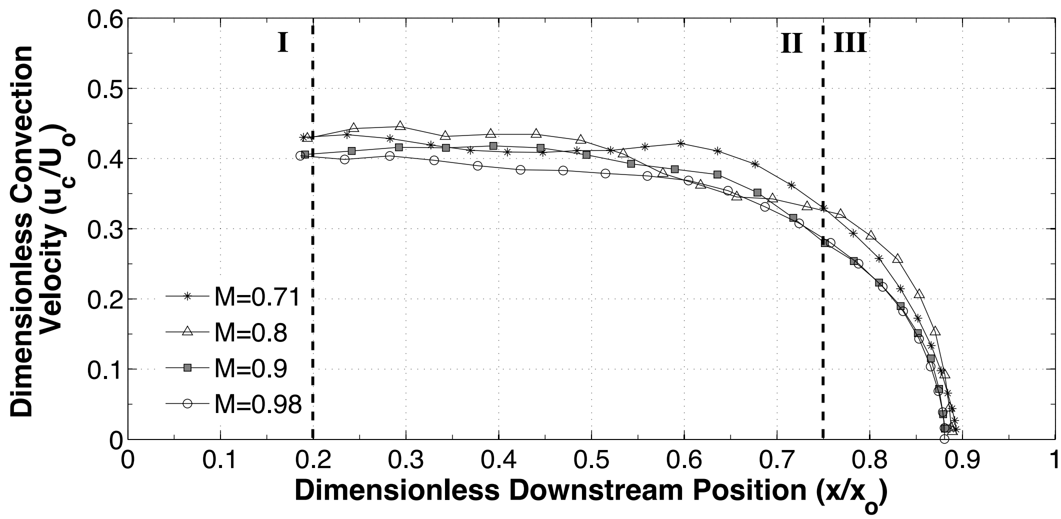

Figure 4.23: Normalized stream-wise convection velocity as a function of downstream position for an impinging planar jet with a fixed impingement ratio of x_o/h=10.5 and varying Mach number.

Figures 4.23 and 4.24 show result of the convection velocity for four cases with varying Mach number discussed in Section 4.4.2, as well as three of the seven cases with varying impingement ratio discussed in Section 4.4.3. Figure 4.23 shows that the results of the four Mach number cases display a reasonable collapse, with similar behavior in both the developing and impingement regions, and with nominally constant dimensionless convection velocities near $u_c/U_o \approx 0.4$ early in the developing region. As in the previous case, after the flow progresses past the end of the jet potential core, the mean value shows a decreasing trend associated with the bulk slowing of the jet in the transition regime, a trend which become more evident as the impingement ratio is increased, as will be the case in the subsequent figure. Similarly, the three cases for impingement ratios of x_o/h=9.15, 10.5 and 17.0 shown in Figure 4.24 display an analogous behavior, with the stream-wise dimensionless convection velocity having a value of $u_c/U_o \approx 0.4$ early in the developing region, but further evidence of decay in the convection speed occurring in the transition region. This decay is more evident for the x_o/h=17.0 case, which shows the onset of this decay occurring at smaller dimensionless downstream position, indicating that the larger transition region for this case is having a greater effect on the convection speed of the structure.

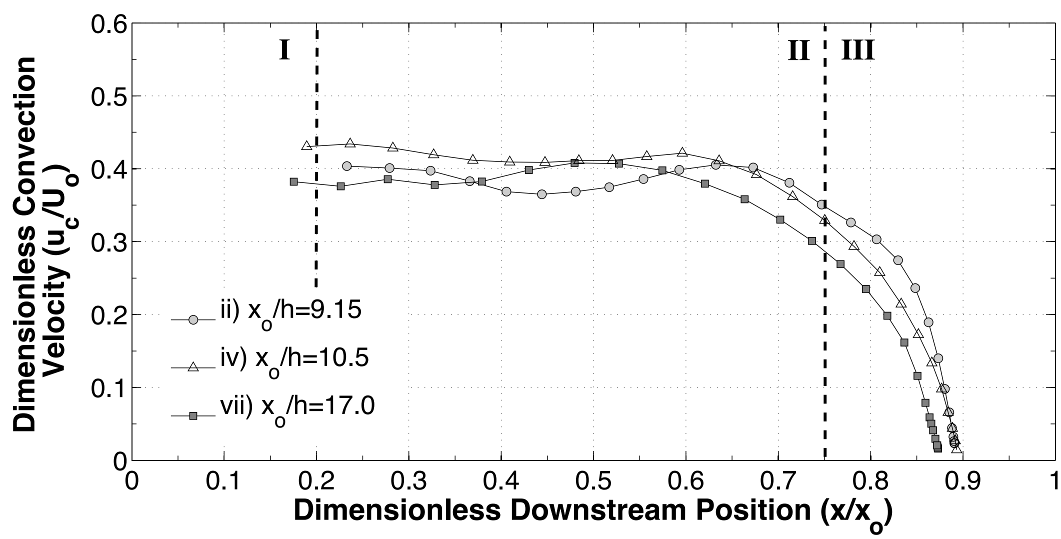

Figure 4.24: Normalized stream-wise convection velocity as a function of downstream position for a constant Mach number of M=0.71, but varying impingement ratio for the *n*=3 anti-symmetric hydrodynamic mode.

4.5.2 Effect of Mean Flow Velocity

One of the primary differences between the high-speed cavity flow, for which the Rossiter feedback model was originally developed (Rossiter, 1964), and the jet-plate case, is the variation in the mean flow structure. The cavity flow involves a uniform grazing velocity over the mouth of the cavity, whose mean velocity does not change appreciably as a function of downstream position, whereas the impinging jet flow involves a more complex flow structure, being comprised of an initial region with potential core with a uniform flow velocity, a transition region occurring downstream of the jet potential core where the flow speed decays as a function of downstream position, and an impingement region occurring close to the plate where the stream-wise flow velocity rapidly decays to zero. The relative effect of these different regions varies as the impingement ratio is varied, with the transition region making up a larger proportion of the flow for cases with larger impingement ratios. In the case of other impinging jet geometries producing self-excited flows, such as the impinging *axisymmetric* jet, the limited range of impingement ratio for which the flow exhibits self-excited behavior masks the effect of these structural differences, with the convecting flow structures being bound by the uniform high-speed inner flow of the jet potential core and the low-speed entrainment flow for virtually the entire impingement distance.

Measurements of the convection velocity in the previous section showed some evidence of structure slowing in the transition region, with this slowing ultimately affecting the frequency of self-excited flow oscillations. In order to quantify and account for the effect of the various flow regions in the planar impinging jet, PIV measurements have been performed on a series of six cases with varying impingement ratios between x_o/h=5.0 to 30.0, and at a constant Mach number of M=0.58 (U_o=200m/s). Figure 4.25 shows the results of these measurements, displaying the stream-wise mean velocity component along the jet centerline as a function of dimensionless downstream position for each of the six measured cases. The initial and impingement regions are clearly visible in each of the six profiles, with a constant flow speed being observed for all six impingement ratios within the jet potential core, a region of rapid velocity decay occurring close to the plate in the impingement region, and a transition region being evident for the impinging jet cases having an impingement ratio larger than x_o/h=5.

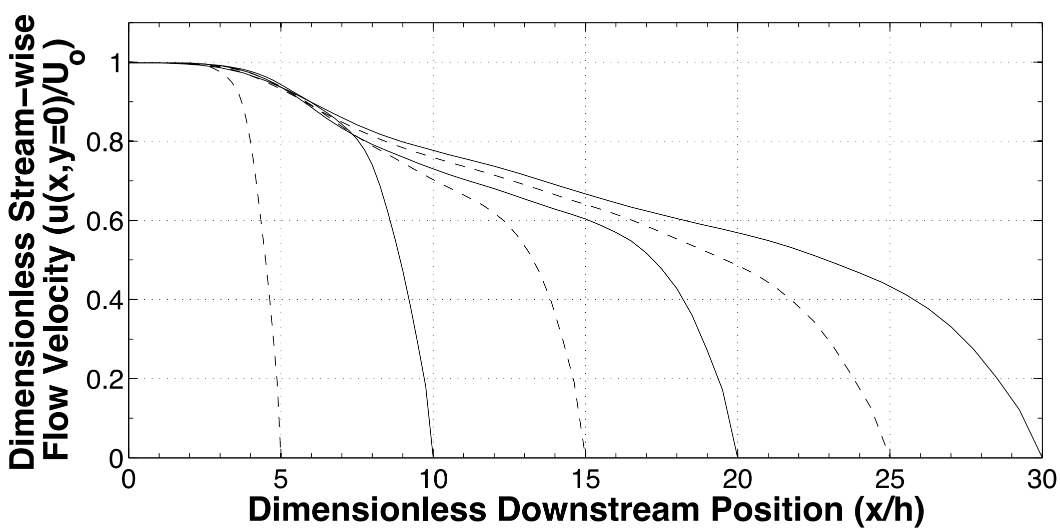

Figure 4.25: Dimensionless profiles of the time-averaged centerline flow velocity as a function of dimensionless downstream position of the impinging planar jet for six impingement ratios from x_o/h=5 to 30. U_o=200m/s (M=0.58) for all measurements.

In order to account for the effect of the changes in the mean flow pattern on the convection velocity of coherent structures, the following two expressions have been developed using the flow measurements shown in Figure 4.25 to estimate the convection speed as 40% the *average* centerline flow velocity in the developing region of the jet:

$$u_c \approx \kappa \cdot \left(\overline{u_{CL}}\right) \approx \kappa \cdot U_o \qquad \text{for } {x_o}/{h} \leq 8.5, \tag{4.11}$$

$$u_c \approx \kappa \cdot \left(\overline{u_{CL}}\right) \approx \kappa \cdot U_o \cdot 1.7 \cdot \left({x_o}/{h}\right)^{-1/4} \qquad \text{for } {x_o}/{h} > 8.5, \text{ and} \tag{4.12}$$

$$\overline{u_{CL}} = \frac{1}{0.75-0}\left(\int_{x/x_o=0}^{x/x_o=0.75} u(x,y=0)\,dx\right), \tag{4.13}$$

where $\overline{u_{CL}}$ is the mean centerline flow velocity over the developing region of the jet ($0 \leq x/x_o \leq 0.75$), U_o is the flow velocity at the nozzle outlet, and x_o/h is the impingement ratio. The two expressions are used to estimate the convection velocity over two separate ranges of impingement ratio, with the first expression being applied for relatively small impingement ratios of $x_o/h<8.5$, where the effects of the transition region are not significant, and the second expression being used for larger impingement ratios, where the effects of the transition region become substantial. The first expression, given in Equation (4.11), is of an identical form to those used by previous authors for the impinging axisymmetric case (Ho & Nosseir, 1981, Krothapalli et al., 1999 and Panickar & Raman, 2007) and is used over a similar range of impingement ratio, and estimates the convection velocity over the developing region as 40% of the flow velocity at the nozzle outlet. The second expression of Equation (4.12), is also of a similar form, but contains an additional term that accounts for the decay in centerline flow velocity occurring as the transition region becomes a significant fraction of the total impingement distance as the impingement ratio is increased.

4.5.3 Characterization of Vortex-Plate Interaction

The use of the impingement distance (x_o) as the relevant length scale in the feedback model of Equation 4.10 implies that the structure convects over the entire impingement distance before impinging on the plate surface. The use of this scale thus implicitly suggests that the size of the structures are small; that the structure does not impinge until the center of the vortex is at, or very close to, the impingement surface. Even a cursory inspection of the flow visualization images shown in Figure 4.5 or any of the PIV flow fields presented thus far shows that the structures do in fact have significant size, on the order of several times the jet thickness, that the center of the structure never reaches the plate, and that the structure begins to interact with the plate before it has travelled the complete impingement distance.

In order to better quantify the position at which the flow structure begins to interact with the plate, measurements of the circulation the coherent structures has been obtained as the structure progresses through the flow. The circulation has been obtained by integrating the vorticity of the individual flow structures for each phase-averaged vorticity field using the following expression:

$$\Gamma = \iint_A \omega_z \left(x, y\right) \cdot dA \quad , \qquad (4.13)$$

where ω_z is the vorticity, which is integrated over the extent of each flow structure whose bounds are defined by the onset negative values of the velocity discriminant parameter. Figure 4.26 shows the results of this analysis, with Part a) showing the dimensionless convection velocity components in the stream-wise and transverse flow directions, and Part b) plotting the structure circulation, with the parameters in both parts of the figure being plotted as a function of the dimensionless Lagrangian structure position, defined as the total distance travelled by the structure from the upstream edge of the nozzle (y/h=0.5, x=0), normalized by the impingement distance (x_o). The plot shows that the structure circulation increases continuously in the developing region, reaching a maximum strength near a downstream distance of $x/x_o \approx 0.75$, a position marking the onset of the impingement region. During the developing region, the y-component of convection velocity maintains a non-zero amplitude due to the spreading of the jet, and the downstream convection velocity component shows a slight decreasing trend as the flow progresses past the jet potential core due to the effect of the transition region. After reaching a maximum circulation near $x/x_o \approx 0.75$, the structure circulation enters a region of rapid decrease, marking the beginning of the impingement region (III), where the decrease in vorticity is associated with the interaction of the flow structure with the impingement surface and the generation of the resulting pressure perturbation. This downstream position also corresponds to the location of maximum transverse fluctuating velocity, as well as the onset of a region of secondary growth of the stream-wise component, both of which are shown in Figures 4.11, 4.14, 4.18 and 4.19.

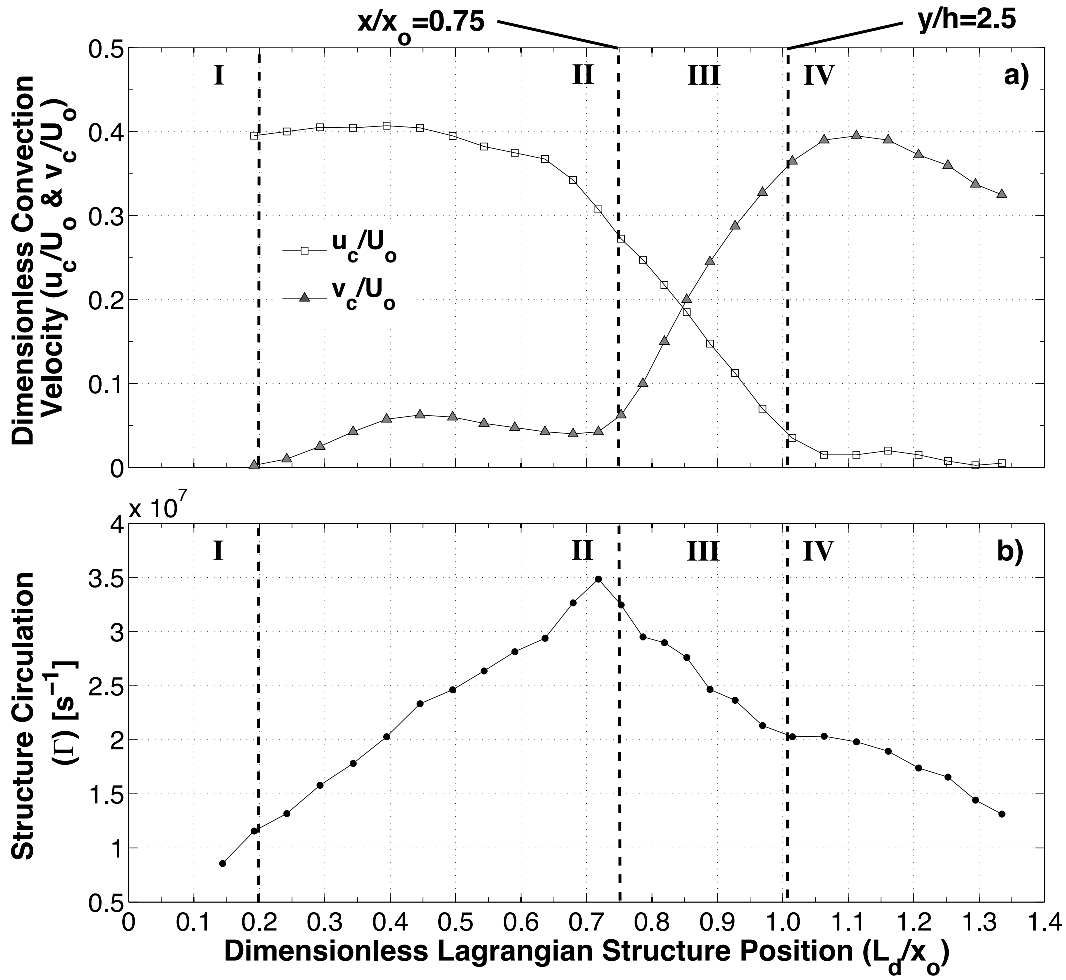

Figure 4.26: Plot of a) dimensionless convection velocity components and b) the circulation of the coherent structure as a function of the dimensionless Lagrangian structure position (L_d/x_o) in the initial (I), developing (II), impingement (III) and wall-jet regions (IV) of the flow for the M=0.9, x_o/h=10.5 case.

The circulation continues to decrease rapidly as the structure progresses through the impingement region, with the stream-wise convection velocity decreasing as the structure changes direction and begins to propagate in the cross-stream direction. After entering the wall-jet region at a cross-stream position of $y/h\approx 2.5$, the rate of decrease in circulation eases, with the structure continuing to lose strength as it convects parallel to the impingement surface. Results obtained for other Mach numbers and impingement ratios show similar trends in structure strength, with the structure circulation reaching a maximum near a dimensionless downstream position of $x/x_o \approx 0.75$, and with the location of the maximum structure circulation being correlated with the location of the maximum transverse velocity fluctuations.

4.5.4 Results of the Feedback Model

In this section the modified length and velocity scales developed in the previous sections are incorporated into the Rossiter feedback model for use with the impinging planar jet. The model is of the same basic form as Equation (4.10), but incorporates the results presented in the previous section to apply modifications to the downstream convection velocity (u_c) and the impingement length (x_o) scales. In Section 4.5.1, measurements of the convection speed were made for the impinging jet for a variety of Mach numbers and impingement ratios, and the coherent structures were found to convect relatively slowly at 40% of the jet velocity at the nozzle outlet in the initial and early developing regions, with evidence of structure slowing in the transition region due to the bulk slowing described in Section 4.5.2. As a result, the downstream convection velocity scale (u_c) is given in the form of two expressions given in Equations (4.11) and (4.12), with approximating the structure convection speed as 40% of the average stream-wise flow velocity along the jet centerline in the developing region. In Section 4.5.3, measurements of the structure circulation were performed to identify the onset of interaction between the structure and the plate, and to define an effective impingement length scale. The effective impingement length was found to be significantly shorter than the total impingement length at 75% of the total impingement length (x_o), a position that also corresponds to the maximum transverse fluctuating velocity component:

$$x_{eff} = 0.75 \cdot x_o \tag{4.14}$$

The resulting feedback model is given in the following equation:

$$f_{\mathrm{n}} = \frac{n \cdot u_{\mathrm{c}} \cdot c}{x_{\mathrm{eff}}\left(u_{\mathrm{c}} + c\right)}, \tag{4.15}$$

and is plotted in Parts a) through d) in Figure 4.27 for Mach numbers of M=0.58, 0.72, 0.87 and 0.98 respectively, as well as being shown earlier in Figures 4.5, 4.12 and 4.16, which all show excellent agreement with the experimental data. The model has been found to accurately predict acoustic tone frequencies over the complete range of impingement ratio and Mach number, with the majority of the discrepancy being accounted for by the effects of coupling with resonant acoustic modes, which produces a relatively flat frequency response as a function of varying impingement ratio and Mach number, and whose influence is not captured by the model.

In the past, many authors attempting to model self-excited flows have relied measurement of the convection speed performed in non-impinging flows as an initial estimate for the convection speed, and have either made minor adjustments to the convection coefficient, or added an adjustable parameter *d*, typically ranging for *d*=0 to −0.5, to obtain the best fit between their experimental measurements and the predictions of the model. A recent study by Arthurs & Ziada (2012b) used such an approach to apply the traditional Rossiter model to measurements of the self-excited impinging planar jet using the same experimental setup. This study used preliminary PIV measurements to determine the various hydrodynamic modes of the jet, and used estimates of convection speed obtained for similar free flows as a guideline to estimate the convection velocity for the impinging case. The resulting model used the entire impingement distance (x_o) as the relevant length scale, and applied a convection coefficient of κ=0.58 and an adjustable parameter d=0 in order to obtain the best fit between the model and the experimental measurements, a convection velocity which has been shown to be in error by nearly 50% in comparison with the present results. Krothapalli et al. (1999) examined the self-excited axisymmetric impinging jet using supersonic jets and performed measurements of the convection speed using a similar structure tracking technique, finding the structure convection coefficients to be in the range of $0.52 \leq \kappa \leq 0.6$, depending on flow speed and impingement ratio. They thus employed the measured phase speed in a feedback model of the same general form as Equation (4.10), but still obtained a relatively poor agreement, until changing the adjustable parameter to a value of $d=-0.4$. The addition of this adjustable parameter to the model has the same effect as *shortening* the overall impingement distance from x_o to an effective length of $x_{eff} \approx 0.85 \cdot x_o$, an effect that is likely produced by the large size and highly two-dimensional structure path of the coherent flow structures in this case. Flow visualization images provided by Krothapalli et al. (1999) show relatively large flow structures, with structure diameter being similar to the nozzle diameter, but smaller in size compared with the planar case, resulting in a longer effective impingement distance.

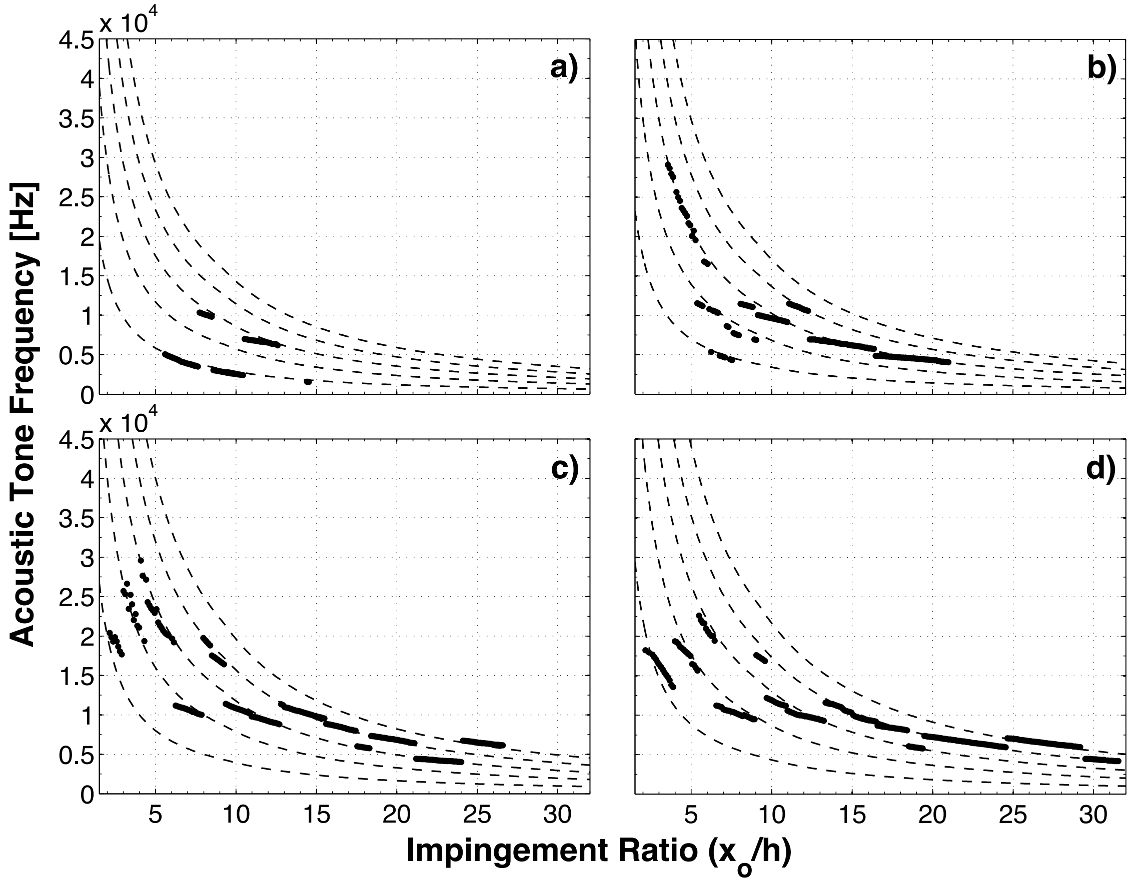

Figure 4.27: Predictions of the feedback model for acoustic tone frequency as a function of impingement ratio for a series of four flow velocities at the nozzle outlet. a) U_o=200m/s, b) 250m/s, c) 300m/s and d) 335m/s.

4.6 Conclusions

This work has used phase-locked PIV measurements to examine the flow evolution of the self-excited impinging planar jet in the fluid-resonant regime for a series of Mach numbers and impingement ratios. Fluctuations in the initial region of the jet have been found to be predominantly in the stream-wise direction, and the intense shearing in each shear layer being the primary mechanism initiating the formation of coherent flow structures. The formation and behavior of the fluctuating velocity components has been found to be intrinsically tied to the behavior of the coherent structures in the self-excited flow, with the maximum amplitude of these components being in excess of 30% of the flow velocity at the nozzle outlet. The distribution of fluctuating components has been found to be similar in all cases, with the amplitude of the fluctuating velocity components growing with increasing Mach number, and varying considerably as a function of varying impingement ratio, showing significantly stronger response for the larger impingement ratios within a particular resonant acoustic mode. In addition, a complex pattern of vortex merging and amalgamation was observed as the Mach number approached choked flow, a process thought to be tied to the increased prominence of harmonics in the acoustic spectrum.

Measurements have also been performed to examine the behavior of the coherent flow structures responsible for sustaining the self-excited flow, with measurements having been performed to quantify the convection velocity of the coherent flow structures, as well as the position at which the plate begins to affect the strength of the approaching structures. The results of these measurements have revealed that structures convect relatively slowly, at ~40% of the jet velocity in the initial and early developing regions of the jet, which slows as the flow progresses into the transition region for geometries with larger impingement ratios. In addition, measurements of the structure circulation have revealed that the plate starts to affect the structures at ~75% of the total impingement distance, a position which also corresponds to the maximum transverse fluctuating velocities. The results of these measurements have been incorporated into a feedback model that has been shown to accurately predict the response of the planar impinging jet over the complete range of Mach number and impingement ratios for which self-excited flows are observed.

4.7 References

Antonia, R., Browne, L., Rajagopalan, S., Chambers, A., 1983. On the organized motion of a turbulent plane jet. Journal of Fluid Mechanics. 134, 49–66.

Arthurs, D., Ziada, S., 2011. The planar jet-plate oscillator. Journal of Fluids and Structures. 27, 105–120.

Arthurs, D., Ziada, S., 2012a. Noise generation in the gas-wiping process, Journal of Fluids and Thermal Sciences. Accepted – In Press.

Arthurs, D., Ziada, S., 2012b. Self-excited oscillations of a high-speed impinging planar jet. Journal of Fluids and Structures. Accepted – In Press.

Billon, A. Valeau, V., Sakout, A., 2005. Two feedback paths for a jet-slot oscillator. Journal of Fluids and Structures. 21, 121– 132.

Camci, C., Herr, F., 2002. Forced convection heat transfer enhancement using a self-oscillating impinging planar jet. ASME Journal of Heat Transfer. 124(4), 770–782.

Chung, Y. M. & Luo, K. H., 2002. Unsteady heat transfer analysis of an impinging jet. Journal of Heat Transfer. 124, 1039–1048.

Elavarasan, R., Venkatakrishnan, L., Krothapalli, A., Lourenco, L., 2000. A PIV study of a supersonic impinging jet. Journal of Visualization. 2(3/4), 213–221.

Ferrari, J., Lior, N., Slycke, J., 2003. An evaluation of gas quenching of steel rings by multiple-jet impingement. Journal of Material Processing Technology. 136, 190–201.

Fleury, V., Bailly, C., Jondeau, E., Michard, M., Juve, D., 2008. Space–time correlations in two subsonic jets using dual particle image velocimetry measurements. AIAA Journal. 46, 2498–2509.

Glesser, M., Valeau, V., Sakout, A., 2008. Vortex sound in unconfined flows: Application to the coupling of a jet-slot oscillator with a resonator. Journal of Sound and Vibration. 314, 635–649.

Gutmark, E., Wolfshtein, M., 1978. The plane turbulent impinging jet. Journal of Fluid Mechanics. 88, 737–756.

Henderson, B., Bridges, J., Wernet, M., 2005. An experimental study of the oscillatory flow structure of tone-producing supersonic impinging jets. Journal of Fluid Mechanics. 542, 115–137.

Ho, C., Nosseir, N.S., 1981. Dynamics of an impinging jet. Part 1: The feedback mechanism. Journal of Fluid Mechanics. 105, 119–142.

Hsiao, F., Chou, Y., Huang, J., 1999.The study of self-sustained oscillating plane jet flow impinging upon a small cylinder. Experiments in Fluids. 27, 392–399.

Hsiao, F., Hsu, I., 2004. Evolution of coherent structures and feedback mechanism of the plane jet impinging on a small cylinder. Journal of Sound and Vibration. 278, 1163–1179.

Hussain, A., 1986. Coherent structures and turbulence. Journal of Fluid Mechanics. 173, 303–356.

Jeong, J., Hussain, F., 1995. On the identification of a vortex. Journal of Fluid Mechanics. 285, 69–94.

Kerhervé, F., Fitzpatrick, J., Jordan, P., 2006. The frequency dependence of jet turbulence for noise source modeling. Journal of Sound and Vibration. 296, 209–225.

Kerhervé, F., Fitzpatrick, J., Kennedy, J., 2010. Determination of two-dimensional space–time correlations in jet flows using simultaneous PIV and LDV measurements. Experimental Thermal and Fluid Science. 34, 788–797.

Krothapalli, A., 1985. Discrete tones generated by an impinging underexpanded rectangular jet. AIAA Journal. 23, 1910–1915.

Krothapalli, A., Hsia, Y., Baganoff, D., 1986. The role of screech tones in mixing of an underexpanded rectangular jet. Journal of Sound and Vibration. 106(1), 119–143.

Krothapalli, A., Rajkuperan, E., Alvi, F., 1999. Flow field and noise characteristics of a supersonic impinging jet. Journal of Fluid Mechanics. 392, 155–181.

Kwon, Y-P., 1998. Feedback mechanism of low-speed edge-tones. Journal of the Acoustical Society of America. 104(4), 2084–2089.

La Cuadra, De. P., Vergez, C., Fabre, B., 2007. Visualization and analysis of jet oscillation under transverse acoustic perturbation. Journal of Flow Visualization and Image Processing. 14(4), 355–374.

Lin, J., Rockwell, D., 2001. Oscillations of a turbulent jet incident upon an edge. Journal of Fluids and Structures. 15, 791–829.

Lucas, M., Rockwell, D., 1987. Effect of nozzle asymmetry on jet-edge oscillations. Journal of Sound and Vibration. 116, 355–369.

Maurel, S., Solliec, C., 2001. A turbulent plane jet impinging nearby and far from a flat plate. Experiments in Fluids. 31, 687–696.

Melling, A., 1997. Tracer particles and seeding for particle image velocimetry. Measurement Science Technology. 8, 1406–1416.

Narayanan, V., 2004. An experimental study of fluid mechanics and heat transfer in an impinging slot jet flow. International Journal of Heat and Mass Transfer. 47, 1827–1845.

Neuwerth, G., 1972. Acoustic feedback phenomena of the subsonic and hypersonic free jet impinging on a foreign body. NASA Technical Translation. TT F-15,719.

Norum, T., 1991. Supersonic rectangular jet impingement noise experiments. AIAA Journal. 14(4), 489–497.

Nosseir, N.S., Ho, C., 1982. Dynamics of an impinging jet. Part 2: The noise generation. Journal of Fluid Mechanics. 116, 379–391.

O'Donovan, T., Murray, D., 2007. Jet impingement heat transfer – Part II: A temporal investigation of heat transfer and local fluid velocities. International Journal of Heat and Mass Transfer. 50, 3302–3314.

Panickar, P., Raman, R., 2007. Criteria for the existence of helical instabilities in subsonic impinging jets. Physics of Fluids. 19, 106103–1.

Powell, A., 1961. On the edgetone. Journal of the Acoustical Society of America. 33, 395–409.

Raffel, M., Willert, C.E., Wereley, S.T., Kompenhans, J., 2007. Particle image velocimetry: a practical guide. 2nd edition. Springer Publishing, Berlin.

Raman, G., 1997. Cessation of screech in underexpanded jets. Journal of Fluid Mechanics. 336, 69–90.

Raman, G., 1999. Supersonic jet screech: Half-century from Powell to the present. Journal of Sound and Vibration. 225(3), 543–571.

Rockwell, D. & Naudascher, E., 1979. Self-sustained oscillations of impinging free shear layers. Annual Review of Fluid Mechanics. 11, 67–94.

Rossiter, J. E., 1964. Wind tunnel experiments on the flow over rectangular cavities at subsonic and transonic speeds. Royal Aircraft Establishment. TR No. 64307.

Scarano, F., Riethmuller, M., 2000. Advances in iterative multigrid PIV image processing. Experiments in Fluids. 29, 51–60.

Schram, C., 2003. Aeroacoustics of subsonic jets: prediction of the sound produced by vortex pairing based on particle image velocimetry. Ph.D. Thesis, Physics Department, Technical University of Eindhoven, The Netherlands.

Schram, C., Hirschberg, A., 2003. Application of vortex sound theory to vortex-pairing noise: sensitivity to errors in flow data. Journal of Sound and Vibration. 266, 1079–1098.

Schram C., Rambaud P., Riethmuller M.L., 2004. Wavelet based eddy structure eduction from a backward facing step flow investigated using particle image velocimetry. Experiments in Fluids. 36, 233–245.

Tam, K. W., 1988. The shock-cell structures and screech tone frequencies of rectangular and non-axisymmetric supersonic jets. Journal of Sound and Vibration. 121, 135-147.

Tam, C., Ahuja, K., 1990. Theoretical model of discrete tone generation by impinging jets. Journal of Fluid Mechanics. 214, 67–87.

Tam, C., Norum, T., 1992. Impingement tones of large aspect ratio supersonic rectangular jets. AIAA Journal. 30(2), 304–311.

Thomas, F., Chu, H., 1989. An experimental investigation of the transition of a planar jet-Subharmonic suppression and upstream feedback. Physics of Fluids A: Fluid Dynamics. 1, 1566–1587.

Thomas, F., Goldschmidt, V., 1986. Structural Characteristics of a Developing Turbulent Planar Jet. Journal of Fluid Mechanics. 163, 227–256.

Thomas, F., Prakash, K., 1991. An experimental investigation of the natural transition of an untuned planar jet. Physics of Fluids A: Fluid Dynamics. 3, 90–105.

Thurow, B. S., 2005. On the convective velocity of large-scale structures in compressible axisymmetric jets. Ph.D. Thesis, Department of Mechanical Engineering, The Ohio State University, United States of America.

Thurow, B. S., Jiang, N., Kim, J.-H., Lempert, W., Samimy, M., 2008. Issues with measurements of the convective velocity of large-scale structures in the compressible shear layer of a free jet. Physics of Fluids. 20, 066101.

Umeda, Y., Maeda, H., Ishii, R., 1987. Discrete tones generated by the impingement of a high-speed jet on a circular cylinder. Physics of Fluids. 30, 2380–2388.

Viskanta, R., 1993. Heat transfer to impinging isothermal gas and flame jets. Experimental Thermal and Fluid Science. 6, 111–134.

Vollmers, H., 2001. Detection of vortices and quantitative evaluation of their main parameters from experimental velocity data. Measurement Science Technology. 12, 1199–1207.

Walker, S., 1997. Experiments characterizing nonlinear shear layer dynamics in a supersonic rectangular jet undergoing screech. Physics of Fluids. 326, 2562–2579.

Wagner, F., 1971. The sound and flow field of an axially symmetric free jet upon impact on a wall. NASA Technical Translation. TT F–13,942.

Ziada, S., 1995. Feedback control of globally unstable flows: Impinging flows. Journal of Fluids and Structures. 9, 907–923.

Ziada, S., 2001. Interaction of a jet-slot oscillator with a deep cavity resonator and its control. Journal of Fluids and Structures. 15, 831–843.

Ziada, S., Rockwell, D., 1982. Oscillations of an unstable mixing layer impinging upon an edge. Journal of Fluid Mechanics. 124, 307–334.

CHAPTER 5

Effect of Nozzle Thickness on the Impinging Planar Jet

Complete Citation:

Arthurs, D., Ziada, S., 2012. Effect of Nozzle Thickness on the Impinging Planar Jet. Journal of Fluids and Structures. Submitted: 05/29/2012, Submission #: YJFLS-D-12-00195.

Copyright:

Preface

In this article, the effect of nozzle thickness on the response characteristics of the self-excited impinging planar jet are examined for a range of nozzle thicknesses between h=1mm to 4mm. Previous investigations involving similar geometries such as the impinging axisymmetric jet flow have suggested that the response of these systems is defined by a fluid-dynamic mechanism, where the particular hydrodynamic mode of the system is related to the structure of the impinging flow, i.e. responding with specific hydrodynamic modes of the jet over well-defined ranges of impingement ratio, regardless of the nozzle diameter, such as in Wagner (1971) and Neuwerth (1972). However, the present work outlined in the previous chapters of this thesis has shown that the planar impinging jet is excited by a fluid-resonant mechanism produced by a coupling between different hydrodynamic modes of the jet with a variety of trapped acoustic modes. The frequency of the resonant acoustic modes is defined by the speed of sound and a combination of length scales related to the three-dimensional acoustic volume between the nozzle and the impingement surface. As a result, the investigation presented in the article making up this chapter was undertaken to assess whether the present impinging planar jet is governed by a fluid-dynamic and/or fluid-resonant mechanism, and the degree to which these mechanisms affect the self-excited response of the system.

The present study presents the results of aeroacoustic measurements performed for a series of seven nozzle thicknesses between h=1mm and 4mm in increments of Δh=0.5mm, with all measurements having been performed for a single Mach number of M=0.9 for the flow exiting the nozzle. The response of all seven nozzle thickness cases were found to be qualitatively similar, with the frequency of the dominant acoustic tone being accurately predicted by the model developed in the previous article, and with the amplitude of acoustic tones being excited most strongly for intermediate impingement ratios near $x_o/h\approx10$. Dimensionless analysis using the Strouhal number based upon both nozzle thickness and the effective impingement distance revealed no significant collapse of the hydrodynamic modes of the jet based on the impingement ratio (i.e. the jet structure) with a variety of different modes being excited at any given impingement ratio for each of the seven cases tested.

Analysis of the acoustic tone frequency as a function of the impingement distance revealed a reasonable collapse, indicating that the system may be influenced by a fluid-resonant mechanism, with a fixed impingement distance resulting in the excitation of a given resonant acoustic mode between the nozzle and the plate. A more thorough analysis of the tone frequency data clusters appearing over a small range of impingement ratio revealed that acoustic tones of a constant frequency are excited at specific impingement distance regardless of the nozzle thickness under consideration, a conclusion which is at odds with previous research on related geometry cited earlier. Dimensionless analysis of these data clusters indicated that the tones excited within these clusters of nominally constant frequency were being excited by the same hydrodynamic mode of the jet regardless of impingement ratio, and subsequent flow visualization images confirmed this hypothesis. These trends indicate that the response of the planar impinging jet is strongly affected by a fluid-resonant mechanism, to such an extent that the formation of trapped acoustic modes completely dominates the response of the system, with the nozzle thickness having only a small effect related to the convection speed of the coherent flow structures.

Finally, evidence was presented that suggests that the present fluid-resonant mechanism may play a role in other geometries, specifically the axisymmetric nozzle employing lift-plates. These lift-plates may promote the formation of trapped modes in the acoustic volume between the plate and nozzle in a similar manner as the planar nozzle examined in this thesis, resulting in a collapse of tone frequency data as a function of impingement distance. Finally, knowledge of the aeroacoustic response within the fluid-resonant regime for a single nozzle thickness would likely serve as a reasonable guide to estimate the response at other nozzle thicknesses, provided that the acoustic air volume between the nozzle and the plate was not significantly changed in doing so.

All experimental measurements, analysis of the resulting data, and the writing of the published article were completed by the current author, under the supervision of my advisor: Professor Samir Ziada.

Effect of Nozzle Thickness on the Self-Excited Impinging Planar Jet

David Arthurs & Samir Ziada

McMaster University
1280 Main Street West
McMaster University – Dept. of Mech. Eng. JHE 316
Hamilton, ON, Canada
L8S 4L7

Abstract

The current study examines the effect of varying nozzle thickness on the self-excited oscillations of the impinging planar jet for a single transonic flow velocity. A series of experiments have been performed with varying nozzle thicknesses from h=1mm to 4mm in increments of Δh=0.5mm, where the flow velocity of the jet has been fixed and the impingement distance is varied over the complete range for which acoustic tones are generated. The measurements reveal that the jet oscillation is controlled by a fluid-dynamic mechanism for small impingement distances, where the hydrodynamic mode of the jet is excited as a function of the *impingement ratio*. At larger impingement distances, the response is dominated by a fluid-resonant mechanism, in which the various hydrodynamic modes of the jet couple with different resonant acoustic modes occurring between the nozzle and the impingement surface. Within the fluid-resonant regime the system produces acoustic tones that are excited predominantly as a function of the *impingement distance*, with the nozzle thickness and impingement ratio having only minor effects on the tone frequency. Flow visualization images show that the same hydrodynamic mode is excited for multiple nozzle thicknesses at a constant impingement distance, despite the wide range of associated impingement ratio. Finally, a feedback

model has been developed to predict the frequency of acoustic tones, and has been found to yield reasonable predictions over the complete range of impingement ratio and nozzle thickness tested.

5.1 Introduction

High-speed impinging planar jets are used in a wide variety of different industrial applications such as coating control applications (Arthurs & Ziada, 2012a, Arthurs & Ziada, 2012b), thermal processing of stock material during metal forming (Ferrari et al., 2003), the production of plate glass, polymer films (Camci & Herr, 2002) and paper products (Viskanta, 1993 and Chung & Luo, 2002). Although these flows produce very high rates of heat transfer and large shear stresses making them useful in many applications, they are also known to be liable to the excitation of very intense narrowband acoustic tones generated as a result of a feedback mechanism between instabilities in the jet free shear layers, and acoustic disturbances produced by the impingement of coherent structures at the downstream impingement surface. The generation of these acoustic tones can lead to issues with noise levels, and potential vibration and fatigue concerns if the aeroacoustic tones of the jet are allowed to couple with mechanical modes of surrounding structures. Some research has indicated that these self-excited flows may have beneficial effects in heat transfer applications, with a more than 70% increase in heat transfer rates being observed for self-excited planar impinging jet flows at low Mach numbers (Camci & Herr, 2002). PIV measurements by Arthurs & Ziada (2012c) have shown that the peak-to-peak fluctuation levels in the self-excited planar jet can reach as much as 70% of the initial jet velocity, which would undoubtedly increase heat transfer rates over an equivalent steady flow.

Of the geometries involving impinging jet flows examined in previous studies, geometries involving axisymmetric jets have received the bulk of attention in the literature, with Marsh (1961) first documenting an increase in overall sound pressure levels and discrete acoustic tones for the impinging axisymmetric jet, and the early works of Wagner (1971) and Neuwerth (1972) characterizing the range of impingement ratio and Mach number for which tones are generated, and the jet-staging phenomenon brought about by the excitation of tones by a series of different shear layer modes. Ho & Nosseir (1981) and Nosseir & Ho (1982) examined the noise generation and feedback mechanism in their two part study on the impinging axisymmetric jet, and attributed the generation of acoustic tones to a feedback mechanism between instabilities in the jet free shear layer which grow into large-scale coherent structures, and pressure fluctuations generated by the impingement of these structures at the downstream surface. Later works by Tam & Ahuja (1990) and Panickar & Raman (2007) investigated the presence of helical instabilities at transonic Mach numbers. In addition, a number of authors such as Krothapalli et al. (1999), Elavarasan et al. (2000) and Henderson et al. (2005) have investigated axisymmetric impinging jets using supersonic flow, however the behavior of these systems often involves more complex dynamics of shocks which are not present in the subsonic case.

Investigations of high-speed planar jets impinging on a flat plate have been far less common in the literature, with some recent research by Arthurs & Ziada (2012a, b &

c) performed to characterize the aeroacoustic response and shear layer modes of the impinging planar jet, but only for a single nozzle thickness of h=3mm. The impinging planar jet was found to generate acoustic tones over two specific regimes, a so-called linear regime occurring at moderate Mach numbers ($0.4<M<0.6$) where acoustic tones are generated by a Rossiter-type flow instability consisting of convecting disturbances in the shear layers and acoustic pressure fluctuations produced by impingement of the flow structures on the plate, and a fluid-resonant mechanism occurring at higher Mach numbers ($M>0.6$), where a Rossiter mode couples with a resonant acoustic mode occurring between the nozzle and the impingement surface. The tones were found to be excited over a large range of impingement ratio ($2.0 \leq x_o/h \leq 32.0$), with the tones generated at the largest impingement ratios being excited only for higher Mach numbers. Measurements of the flow field for a variety of conditions revealed that tones were generated by a series of five anti-symmetric hydrodynamic modes, along with a single symmetric mode occurring only for small impingement ratios. Other studies involving supersonic impinging planar jets have been performed by Krothapalli (1984), Norum (1989) and Tam & Norum (1990), each of which showed a qualitatively similar aeroacoustic response compared to the subsonic impinging planar jet.

There has been significant work performed on other related geometries utilizing impinging planar jets such as the jet-edge (Powell, 1961, Ziada, 1995 and Lin & Rockwell, 2001) and jet-slot (Ziada, 2001, Billon et al., 2005 and Glesser et al., 2008) systems which show a similar qualitative response. However, these cases involve jets with very low Mach numbers in the incompressible flow regime, limiting their applicability to the current case involving high Mach number flows. Other configurations involving higher Mach number jet flows are the cases of both planar (Hsiao et al., 1999 and Hsiao & Hsu, 2004) and axisymmetric jets (Umeda et al., 1987) impinging on a small cylinder at some distance downstream. These configurations have also shown strong tone generation attributed to a similar feedback mechanism.

The current study focuses on high-speed subsonic planar jet impinging normally on a flat, rigid surface at some distance downstream as shown in Figure 5.1. Experiments have been performed for a range of nozzle thicknesses for a single transonic flow velocity in order to investigate the effect of initial jet thickness on the feedback mechanism governing the frequency of generated tones.

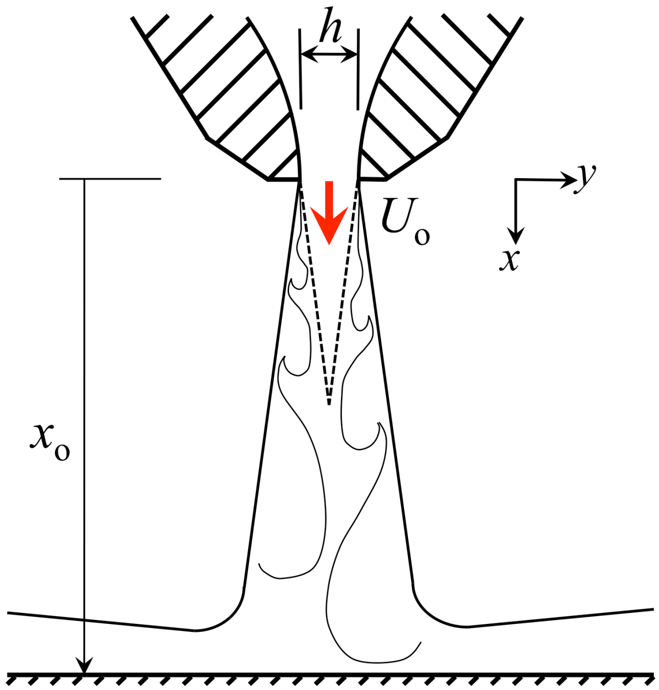

Figure 5.1: Basic schematic of the impinging planar jet geometry, showing the impingement distance (x_o), the nozzle thickness (h).

Table 5.1: Nomenclature of quantities and terms.

Nomenclature	
c	Speed of sound in air [m/s]
D	Nozzle diameter of an impinging axisymmetric jet [m]
f	Acoustic Tone frequency [Hz]
h	Nozzle thickness [m]
L	Length of the planar jet in the span-wise direction (100mm)
L/h	Nozzle aspect ratio
M	Mach number (U_o/c)
P_s	Supply pressure [Pa]
P_∞	Ambient pressure [Pa]
Re_h	Reynolds number based upon jet thickness ($U_o \cdot h/\nu$)
SPL	Sound pressure level in decibels [$20 \cdot \log_{10}(P_{RMS}/P_{ref})$ where P_{ref}=20μPa]
St_{xo}	Strouhal number based upon impingement distance ($f \cdot x_o/U_o$)
St_h	Strouhal number based upon nozzle thickness ($f \cdot h/U_o$)
St_D	Strouhal number based upon nozzle diameter ($f \cdot D/U_o$)
St_{eff}	Effective Strouhal number ($f \cdot x_o/U_{eff}$)
U_d	Downstream velocity of coherent structures [m/s]
U_{eff}	Effective velocity [$U_{eff} = 2 \cdot U_d \cdot c/(U_d + c)$] [m/s]
U_o	Jet velocity at the centerline of the nozzle outlet [m/s]
x_o	The impingement distance (distance from the nozzle lip to the impingement surface) [m/s]
x_o/h	Impingement ratio
δ	Disturbance thickness of the shear layer/boundary layer [m]
δ^*	Displacement thickness of the shear layer/boundary layer [m]
θ	Momentum thickness of the shear layer/boundary layer [m]

5.2 Experimental Apparatus

The current study consists of an experimental investigation of a high-speed planar gas jet with varying nozzle thickness impinging on a plate at some distance downstream. In order to allow the study of this geometry, the planar nozzle and plate geometry shown in Figure 5.2 was machined out of Aluminum. The nozzle has a span (L) of 100mm and the nozzle thickness has been varied from h=1.0mm to 4.0mm in increments of 0.5mm using a precision dowel system, for a range of aspect ratio of the nozzle in the range $100 \leq L/h \leq 25$. The nozzle is pressurized using compressed air, which enters the plenum through 25.4mm diameter hole on the top surface of a settling chamber, and at an angle perpendicular to the direction of the jet flow ultimately exiting the nozzle.

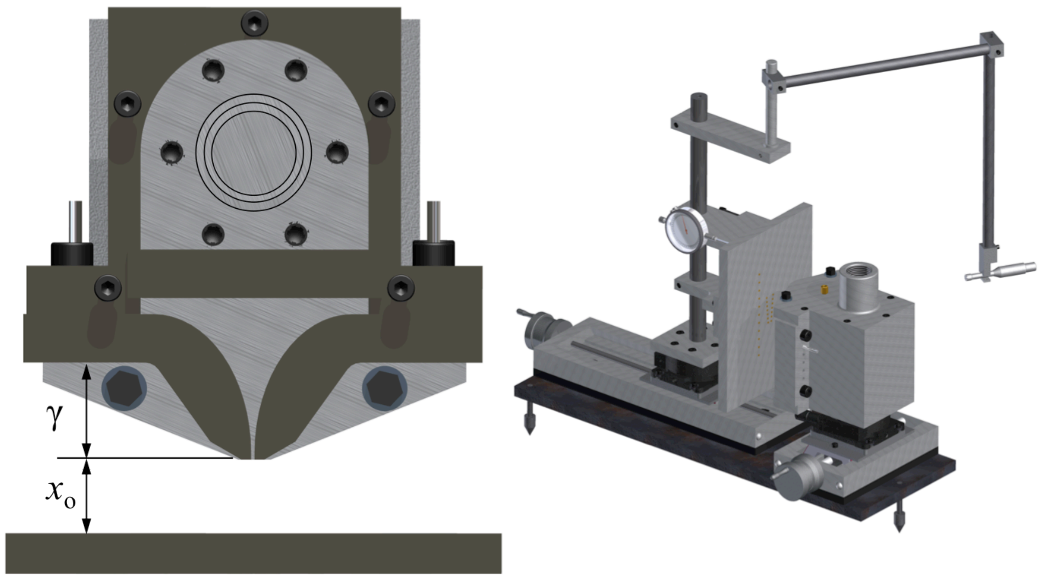

Figure 5.2: Sectioned view of the jet plenum and settling chamber and isometric view of planar jet-plate apparatus.

Air entering the plenum passes through a flow distribution tube, described in detail in Arthurs & Ziada (2012a), which is mounted in the plenum and has been designed to evenly distribute the flow along the jet-span. After entering the plenum through the flow distribution tube, the flow passes through a series of flow conditioning screens, consisting of a fine stainless steel cloth with a density of 70 wires per inch and an open area ratio of β=0.58 to break up any large turbulent structures (Mehta & Bradshaw, 1979). The jet nozzle uses an elliptical profile as shown in Figure 5.2, with dimensions of the major and minor axis of the ellipse of 45mm and 30mm respectively, providing a range of nozzle contraction ratios from 18.75 for the nozzle thickness of h=4mm, to 75 for h=1mm.

The supply pressure in the plenum was measured at a location immediately upstream of the nozzle contraction at the centerline, and this pressure was used to estimate the flow velocity of the jet exiting the nozzle using the following equation:

$$U_o = c \cdot \sqrt{\frac{2}{\gamma - 1}\left[\left(\frac{P_s + P_\infty}{P_\infty}\right)^{\left(\gamma-1/\gamma\right)} - 1\right]}, \tag{5.1}$$

where P_s and P_∞ are the static and ambient pressures, and γ and c are the ratio of specific heats and speed of sound in air, respectively. Subsequent PIV measurements were used to confirm the accuracy of this expression, which has been derived from equations of flow through a lossless nozzle, and was found to be accurate to within 2.5% for the conditions examined in this study.

Measurements of the initial velocity profile of the jet at the exit of the nozzle block were performed using a specially constructed stagnation pressure probe similar to that outlined in Arthurs & Ziada (2011), and a multi-axis traverse accurate to within ±0.01mm. Figure 5.3 shows the same velocity profiles using two different sets of scales. Part a) shows the velocity profiles in a dimensionless form, with the flow velocity being normalized by the free stream flow velocity at the jet centerline (U_o=300m/s), and the cross-stream position being normalized by the nozzle thickness. This portion of the figure shows that the shear layer thickness for each of the four cases shown makes up a different fraction of the initial jet thickness, with the shear layer of the thinner jet cases making up a greater portion of the width of the profile. However, the actual shear layer thickness, as shown in Part b) of Figure 5.3 and given in Table 5.2 in the form of the disturbance, displacement and momentum thicknesses, remains constant even as the nozzle thickness changes by a factor of four. Similar velocity measurements performed in the span-wise (z) direction such as those presented in Arthurs & Ziada (2012b) have shown that the flow is evenly distributed along the span of the jet, with a maximum variation of less than 1% across the nozzle span.

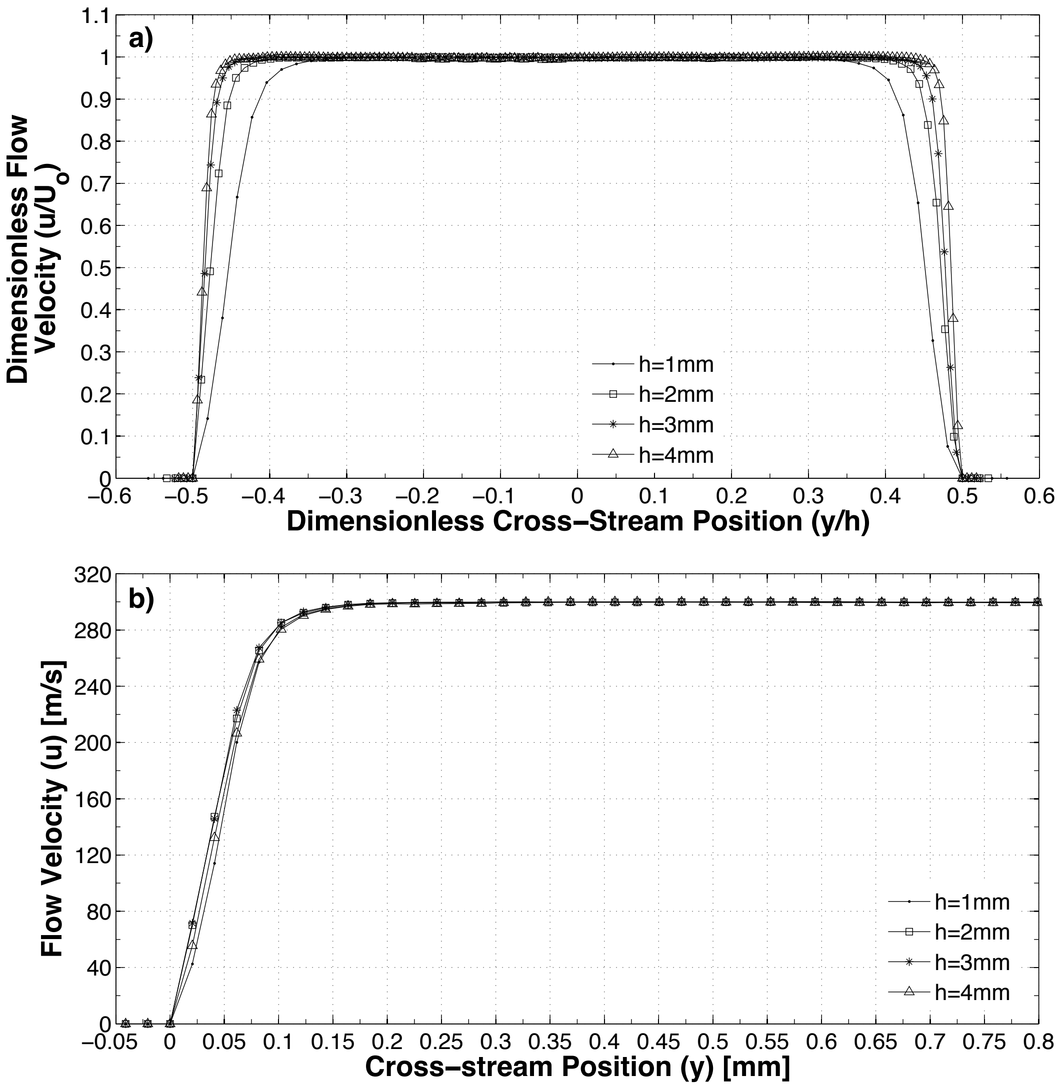

Figure 5.3: Velocity profiles at the nozzle exit for a range of nozzle thicknesses showing a) the overall profiles in dimensionless form and b) a close up of the shear layer thickness. Flow conditions: U_o=300m/s (M=0.87), $2.0\times10^4 \leq Re_h \leq 8.0\times10^4$.

Table 5.2: Shear layer disturbance thickness, displacement thickness and momentum thickness of the initial jet profile at the nozzle exit for a variety of nozzle thicknesses and a Mach number of M=0.9.

	Nozzle Thickness (*h*)			
	1mm	**2mm**	**3mm**	**4mm**
Disturbance Thickness (δ) [mm]	0.20	0.20	0.20	0.20
Displacement Thickness (δ*) [mm]	0.076	0.072	0.071	0.075
Momentum Thickness (θ) [mm]	0.021	0.021	0.021	0.022

The flat surface used for jet impingement consists of a large, rigid plate machined out of Aluminum measuring 150mm×200mm and a thickness of 10mm. The front and rear surfaces have been machined using a single point fly-cut milling operation to provide the flattest surface possible.

Measurements in the acoustic free-field were obtained using a GRAS 40BP 6.35mm high-level microphone combined with a GRAS 26AC preamplifier and a GRAS 12AA power supply module. The microphone has a flat frequency response of 2Hz-80kHz (±2dB) and was calibrated using a GRAS Type 42AB sound calibrator. The microphone was located using an adjustable microphone boom assembly shown in Figure 5.2, and the measurements presented in this paper have been recorded at an angle of θ=60° as measured from the jet plane, and at a microphone distance of d=200mm as measured from the plate surface at the jet centerline, and at the midpoint of the jet-span. Acoustic damping foam was placed on acoustically reflective surfaces in the immediate area of the experimental setup, and measurements were performed to confirm that all acoustic measurements were completed in the acoustic free-field under non-reverberant conditions.

Measurements were acquired using a National Instruments NI-4452 data acquisition card, which uses 4 simultaneously sampled channels, a maximum sample rate of 204.8kS/s, and hardware based anti-aliasing filters. Each acoustic measurement was obtained by recording the pressure-time signal using a sample rate of 204.8kHz for 15 seconds. Spectral analysis was performed by breaking the time signal into 60 equally sized blocks of 51,200 samples with no overlap, calculating the amplitude spectrum of RMS acoustic pressure for each block, and averaging the 60 spectra to produce an average acoustic spectrum. This results in an amplitude spectrum with a frequency range from 0Hz to 102.4kHz and a spectral resolution of 4Hz, which is truncated to a frequency range of 0Hz to 80kHz, corresponding to the linear response range of the microphone.

A standard 2D PIV system has been used to obtain flow visualization images of the impinging jet flow to confirm the form of the hydrodynamic modes for a variety of nozzle thicknesses. The PIV system has a single PowerView 4MP 12 bit digital camera with a resolution of 2048×2048 pixels. For flow field illumination, a 532nm New Wave Solo 120XT pulsed Nd:YAG laser with a maximum output of 120mJ per pulse was used. The beam was focused to a sheet using a plano-cylindrical and spherical lenses. Camera optics and lenses were determined by the required field of view for each flow field being captured, with a Sigma 105mm *f* 2.8 lens being used in combination with extension tubes for minor adjustment of the focal range and focusing distance. Synchronization of the laser pulses and camera images was performed using a TSI LaserPulse Model 610035 synchronizer with external triggering and software adjustable time delay. Seeding of the flow for PIV imaging was performed by means of a six-nozzle Laskin aerosol generator using olive oil as a seeding medium, producing 1μm mean diameter droplets. The Stokes number of seeding particles for all PIV cases shown in present work is below Sk=0.1 and falls within the range of $0.05 \leq Sk \leq 0.1$, which results in tracking error of less than 2% even for the relatively high frequency oscillations encountered in the present study (Melling, 1997). To avoid laser reflections from the machined Aluminum surfaces of the nozzle and the impingment surface from appearing in the images and/or damaging the camera sensor, a clear acrylic paint infused with laser fluorescing laser dye, Rhodamine Chloridewas applied to the exterior surfaces of the nozzle and to the impingement plate.

5.3 Typical Response of the Impinging Planar Jet

In order to examine the behavior of the impinging planar jet as a function of changing nozzle thickness, a series of experiments were performed at a single flow velocity of U_o=300m/s (M=0.87) for nozzle thicknesses from h=1mm to 4mm in increments of Δh=0.5mm. The selection of this single flow velocity provides conditions for which the impinging planar jet flow responds in a wide range of different hydrodynamic modes depending on the impingement distance, and removes much of the ambiguity associated with changing the mean flow conditions on any resonant acoustic modes. A single acoustic spectrum for a nozzle thickness of h=2.5mm, which falls in the middle of the range of those studied in this work, is shown in Figure 5.4. The mean flow velocity of the jet at the nozzle outlet is U_o=300m/s (M=0.87) and the impingement ratio is x_o/h=10.2. The spectrum shows a strong fundamental tone frequency of f=17.6kHz at an amplitude of over 140dB ($P_{RMS}\approx$215Pa), along with a series of three higher harmonics occurring at multiples of the fundamental frequency, and at progressively lower amplitudes. The spectrum also shows relatively high levels of broadband noise (~95dB) over a wide range of frequencies, as well as other minor peaks in the spectrum at a variety of locations. This spectrum is in general indicative of the type of aeroacoustic response that the planar jet-plate system generates, and the spectrum is also similar to those of other related geometries, such as the impinging axisymmetric jet flow involving both subsonic and supersonic flows, as well as supersonic planar impinging jet flows. Also shown on the figure for comparison is the acoustic spectrum of a free planar jet under identical conditions but without the presence of the downstream plate. The spectrum shows approximately 20dB lower broadband levels noise levels in the lower frequency range, and the absence of any narrowband spectral peaks, indicating that the presence of the plate is responsible for the generation of any narrow band acoustic tones due to the introduction of a flow-acoustic feedback mechanism, as well as for a significant increase in broadband noise due to increased turbulence levels.

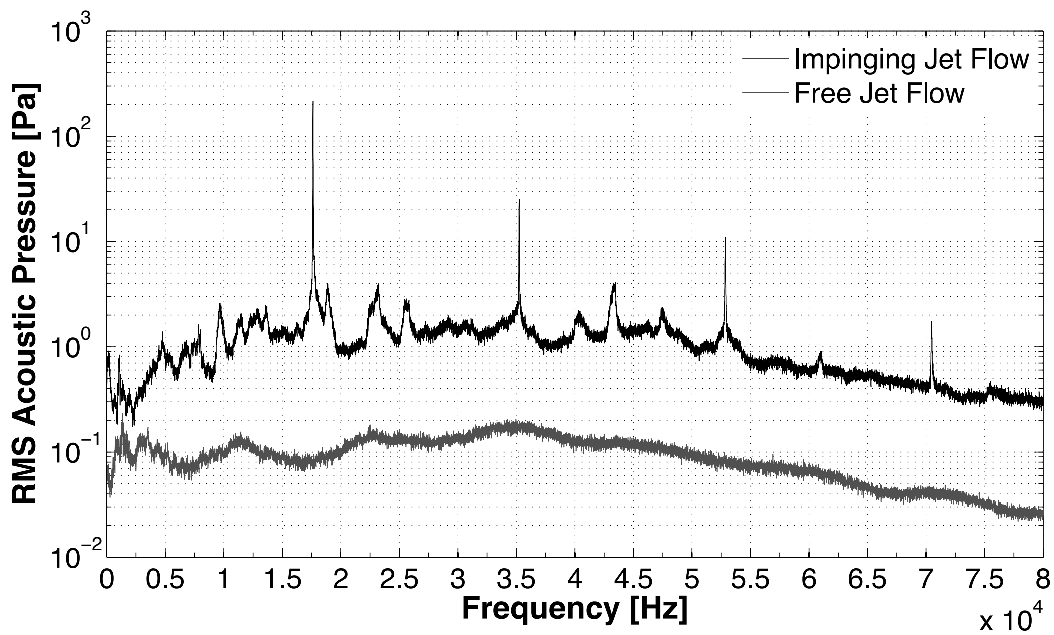

Figure 5.4: The aeroacoustic response of a free and an impinging planar jet with a nozzle thickness of h=2.5mm, an impingement ratio of x_o/h=10.2 and a Mach number at the nozzle exit of M=0.87 (U_o=300m/s).

Figure 5.5 shows a contour plot composed of acoustic spectra obtained as a function of impingement ratio, with a constant flow velocity of U_o=300m/s (M=0.87) and a nozzle thickness of h=2.5mm. The plot shows that the planar jet-plate system responds in series of different jet-stages over a relatively wide range of impingement ratios, with these stages produced by different hydrodynamic modes of the jet, and that the frequency of each of these hydrodynamic modes shows an approximately hyperbolic behavior, with their tone frequency being inversely proportional to the impingement distance. Also shown on the plot are the predictions of the first five stages of a feedback model first proposed in Arthurs & Ziada (2012b) and given by the following equations:

$$f_\mathrm{n} = \frac{n \cdot u_\mathrm{c} \cdot c}{x_\mathrm{eff}\left(u_\mathrm{c} + c\right)} , \qquad (5.2)$$

$$u_\mathrm{c} = \kappa \cdot U_\mathrm{o} \qquad \text{for } x_\mathrm{o}/h < 8.5 , \qquad (5.3)$$

$$u_\mathrm{c} = \kappa \cdot U_\mathrm{o} \cdot 1.7 \cdot \left(x_\mathrm{o}/h\right)^{-1/4} \qquad \text{for } x_\mathrm{o}/h \geq 8.5 \quad \text{and} \qquad (5.4)$$

$$x_\mathrm{eff} = 0.75 \cdot x_\mathrm{o} , \qquad (5.5)$$

where κ is the convection coefficient of coherent flow structures, defined as the convection speed (u_c), normalized by the jet velocity at the nozzle outlet, which was found to be $u_c/U_o \approx 0.4$ in previous work on this apparatus (Arthurs & Ziada, 2012c). Equation 5.2 is the expression for the feedback model, where n signifies the jet-stage or hydrodynamic mode of the jet, and is inversely related to the wavelength of the hydrodynamic mode of the jet, and Equations 5.3 and 5.4 are the relations for predicting the downstream velocity scale related to the convection of coherent flow structures over two separate ranges of impingement ratio. The effective impingement distance, defined as the downstream position at which the structure begins to impingement on the plate surface is given by Equation 5.5, as determined by Arthurs & Ziada (2012c) using phase-locked PIV measurements.

The predictions of the model fall close to the fundamental frequencies of the various hydrodynamic modes of the jet, with the myriad of tones occurring at higher frequencies being attributed to higher harmonics of the fundamental, as illustrated in Figure 5.4. The response of the planar jet-plate system shown in this figure is in many ways analogous to the impinging axisymmetric jet-plate system, with a similar range of frequencies being encountered in the axisymmetric case, as well as a similar hyperbolic behavior of the tones with respect to the impingement distance, and a similar jet-staging phenomenon (Nosseir & Ho, 1982 and Panickar & Raman, 2007). However, the range of impingement ratio for which tones are generated in the two geometries is quite different, with the planar case exciting tones over a relatively large range of impingement ratio from $1.5 \leq x_o/h \leq 32.0$, whereas the axisymmetric case is confined to impingement ratios on the order of the jet potential core in free jets ($1.5 \leq x_o/D \leq 7.0$). The acoustic pressure amplitude of the current planar case is lower than that of the axisymmetric case, being ~145dB compared to 170dB for the axisymmetric case, however the amplitudes are comparable when normalized for the differences in the mechanical stream power (or the flow area) for the two nozzles.

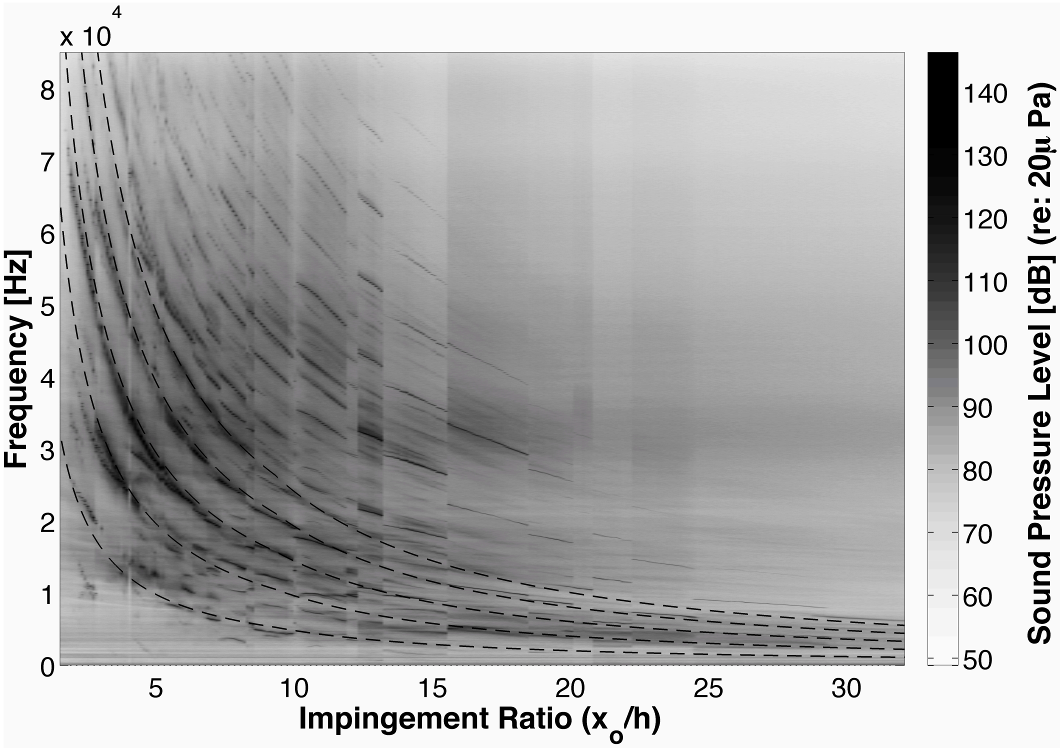

Figure 5.5: Contour plot of Sound Pressure Level (SPL) as a function of impingement ratio (x_o/h) for an impinging planar jet with a nozzle thickness of h=2.5mm and a jet velocity of U_o=300m/s (M=0.87). The dashed lines represent predictions of the feedback model given in Equation 5.2.

5.4 Effect of Nozzle Thickness on the Tone Frequency and Intensity

Figure 5.6 shows four plots showing the frequency of the fundamental acoustic tone as a function of impingement ratio for four separate nozzle thicknesses of h=1, 2, 3 and 4mm respectively. Also shown on each of the plots is the prediction of the same feedback model given by Equation 5.2 and shown in Figure 5.5. The four parts of the figure show that each of the four nozzle thickness cases display similar characteristics, with a large number of jet-stages being excited as the impingement ratio is varied, and a similar hyperbolic distribution of frequency as a function of impingement ratio shown earlier in Figure 5.5. The excited tone frequencies tend to vary inversely with nozzle thickness, with smaller nozzle thicknesses tending to excite higher frequencies at a given impingement ratio. In each case, the tone frequency data shows a good agreement with the predictions of the model.

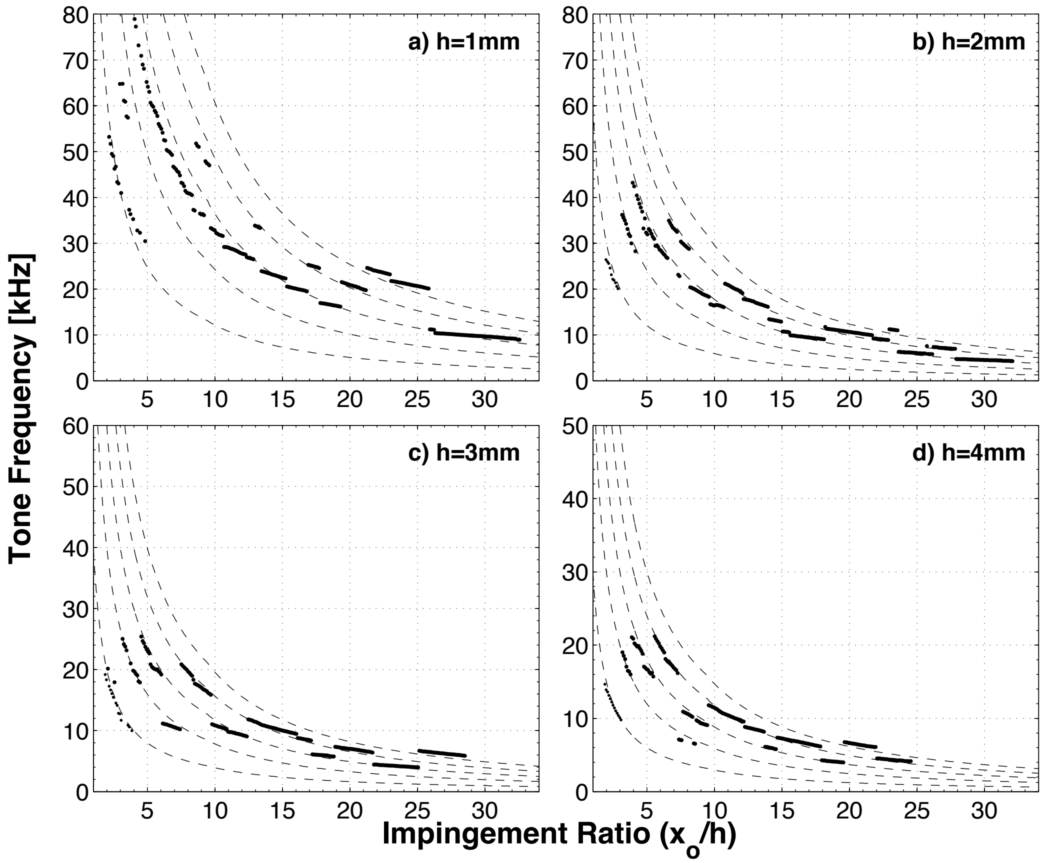

Figure 5.6: Acoustic tone frequency as a function of impingement ratio for a flow velocity of U_o=300m/s (M=0.87) and nozzle thicknesses of h = 1, 2, 3 & 4mm, along with the predictions of a feedback model developed by Arthurs & Ziada (2012c).

Previous work by Arthurs & Ziada (2012b) indicated that the acoustic tones produced by the planar impinging jet in this flow velocity range are produced by a coupling between the different anti-symmetric hydrodynamic modes of the jet, with a series of distinct resonant acoustic modes occurring between the nozzle and the plate. A number of major and minor discontinuities in the tone frequency can be observed in the data of all four nozzle thickness cases shown in Figure 5.6, with the major discontinuities, such as at impingement ratios of x_o/h=17, 18 and 19 (among many others) in Part a) of the figure being attributed to a change in the shear layer mode of the jet, and the minor discontinuities, such as at impingement ratios of x_o/h=15, 23 and 26 of the same part of the figure, resulting from a change in the resonant acoustic mode being excited, but for the same hydrodynamic mode of the jet. This fluid-resonant coupling is also responsible for the flatter frequency response of the data compared to the predictions of the model, as the frequency of the resonant acoustic modes depends not only on the distance between the nozzle flange and the plate (x_o+γ) which varies with the impingement distance, but also on a combination of length scales corresponding to the three-dimensional acoustic volume. The majority of the deviation between the model and actual system behavior can be accounted for by this flatter frequency response produced as a result of the fluid-resonant coupling.

Figure 5.7 shows four plots of the acoustic tone amplitude corresponding to the four nozzle thickness cases shown in Figure 5.6. This plot shows that each of the four nozzle thickness cases tend to excite tone most strongly at intermediate impingement ratios, near $x_o/h \approx 10$, as shown by the 4th order polynomial curve fitted to each data series, but that the tone amplitude varies significantly, depending on the combination of shear layer mode and resonant acoustic mode being excited. In general, within each resonant mode, the acoustic tone amplitude begins low and builds to a maximum amplitude near the center of the impingement ratio range for that particular mode, before the tone amplitude diminishes and a new hydrodynamic/resonant acoustic mode combination is excited.

Another trend that is clear from inspection of Figures 5.6 and 5.7 is that the maximum impingement ratio for which acoustic tones are produced tends to decrease as the nozzle thickness is increased. For instance, the h=1mm and 2mm cases shown in Parts a) and b) of the figures excite tones to impingement ratios of up to $x_o/h \approx 32$, however, the h=3mm and 4mm cases show a progressive reduction in this range, exciting tones up to $x_o/h \approx 28.5$ an $x_o/h \approx 25$ respectively. This reduction in the maximum impingement ratio is thought to be related to the ratio of the length of the jet span to the impingement distance. The span of the nozzle used in all testing is fixed at L=100mm, and for the smaller nozzle thickness cases tested in this work, the impingement distance remains small in comparison to the total jet-span even for relatively large impingement ratios, ensuring that the impinging jet flow remains two-dimensional. However, for the larger nozzle thicknesses, the impingement distance can approach the dimension of jet-span for larger impingement ratios, resulting in more three-dimensionality of the impinging jet flow, which is likely responsible for the suppression of otherwise well-correlated structures across the jet-span which may interrupt or weaken the feedback mechanism. This feature may explain one of the main differences between the planar and the axisymmetric impinging jet cases, namely that acoustic tones of axisymmetric jets are generated over a smaller range of impingement ratio than planar jets. In other words, as the aspect ratio of the planar jet decreases, the impingement ratio for tone generation may approach that of the axisymmetric case.

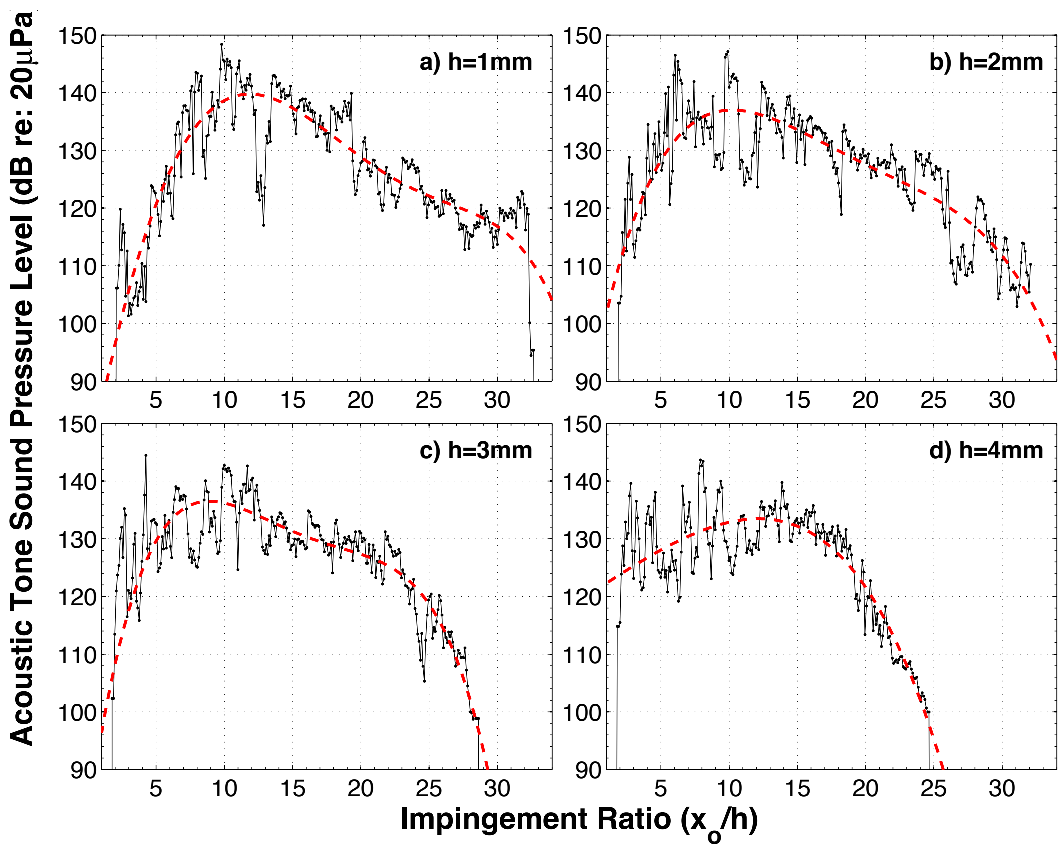

Figure 5.7: Acoustic tone amplitude as a function of impingement ratio for a flow velocity of U_o=300m/s (M=0.87) and nozzle thicknesses of h = 1, 2, 3 & 4mm.

5.5 Effect of Nozzle Thickness on the Strouhal Number

Figure 5.8 shows the acoustic tone frequency of all seven nozzle thicknesses, from h=1mm to 4mm in increments of Δh=0.5mm, non-dimensionalized in the form of an effective Strouhal number, which is given by:

$$\mathrm{St}_{\mathrm{eff}} = \frac{f \cdot x_{\mathrm{o}}}{U_{\mathrm{eff}}} \quad \text{and} \tag{5.6}$$

$$U_{\mathrm{eff}} = \frac{2 \cdot u_{\mathrm{c}} \cdot c}{u_{\mathrm{c}} + c} \,. \tag{5.7}$$

The effective Strouhal number makes some adjustments to both the length and velocity scales which have typically been used in the study of other related geometries (Nosseir & Ho, 1982, Krothapalli et al., 1999 and Panickar & Raman, 2007). First, the effective length scale, given earlier in Equation 5.5, has been defined as 75% of the total impingement distance and has been selected based on the work of Arthurs & Ziada (2012c), in which phased-locked PIV measurements were used to define the downstream position where the coherent vortex structures begin to impinge on the plate. Similarly, the effective velocity scale, given in Equation 5.7, has been modified to account for the velocities of both the upstream and downstream portion of the feedback cycle, and to account for the decrease in convection speed associated with the bulk slowing effect of the jet flow which occurs at larger impingement ratios. Finally, the convection coefficient (κ) has been measured directly in the previously mentioned study using phase-locked PIV measurements, and found to be relatively constant at 40% of the free stream velocity at the nozzle outlet over a wide range of Mach numbers and impingement ratios.

The plot shows a clear collapse of the seven data series to five well-defined hydrodynamic modes of the jet predicted by Equation 5.2, labeled n=1 through 5, with each hydrodynamic mode occurring over a range of impingement ratios. The lower modes, n=1 and n=2, occur primarily at smaller impingement ratios, with the higher modes (n=3, 4 & 5) occurring as the impingement ratios are increased. The upward sloping trend visible within each data set beginning at intermediate impingement ratios of $x_o/h \approx 10$ is indicative of the onset of fluid-resonant coupling, where the tone frequency begins to show less variation with changing impingement ratio. It is also observed that there is no discernable collapse in the behavior of the various shear layer modes as a function of impingement ratio, i.e. for a given impingement ratio any one of a number of different hydrodynamic modes can be excited.

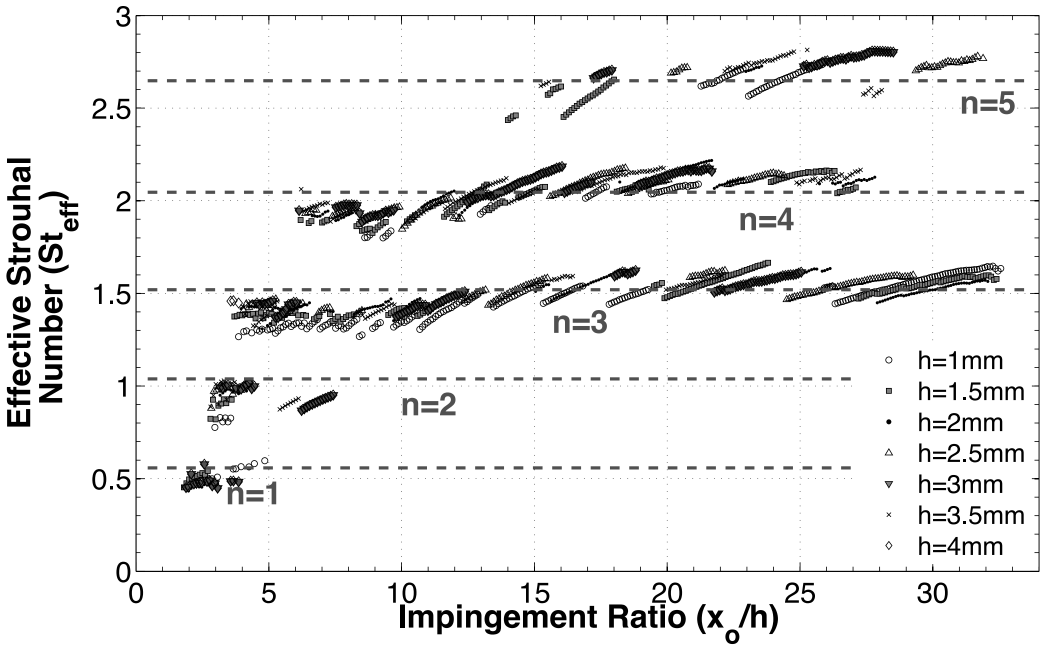

Figure 5.8: Effective Strouhal number (St_{eff}) as a function of impingement ratio for a range of nozzle thicknesses between 1mm≤*h*≤4mm and a flow velocity of U_o=300m/s (M=0.87).

The nozzle thickness (h) and the initial flow velocity at the nozzle exit (U_o) can also be used to normalize the acoustic tone frequency using the Strouhal number based upon nozzle thickness, give in the following equation:

$$\mathrm{St_h} = \frac{f \cdot h}{U_\mathrm{o}} \quad . \tag{5.9}$$

This Strouhal number scale is plotted in Figure 5.9 as a function of the impingement ratio, a form of the Strouhal number that has been commonly used in the study of other related geometries, such as jet screech in supersonic free jets, as well as instability in subsonic free jets. The data clearly collapse to the same hydrodynamic modes shown in the previous figure and described in Equation 5.2, and the distribution of each of the modes shows a clear linear collapse as shown on the log-log scale, as a result of the fixed length (h) and velocity scales (U_o) for each data series. The range of Strouhal number is similar to a number of related geometries involving planar jets, such as the flapping instability of a free subsonic jet, and jet screech in supersonic free planar jets. Flapping oscillations in free jets, often referred to as the preferred mode, tend to occur at dimensionless frequencies of $0.15<St_h<0.25$ for planar jets with relatively thick shear layers, and at a constant Strouhal number of $St_h=0.25$ as the shear layers become thin compared to the thickness of the jet, e.g. for $h/\theta\geq125$ as demonstrated by Ho & Hsiao (1983) and Ho & Huerre (1984). Jet screech has also been found to occur over a similar Strouhal number range of $0.1<St_h<0.4$ (Krothapalli et al., 1986 and Raman, 1999). These oscillations have been found to be excited by different hydrodynamic modes of the jet (Raman, 1997 and Alkislar et al., 2003). Flow visualization studies of both of these related flows have found a columnar flapping type flow of oscillation which is similar to that observed for the subsonic impinging planar jet in Arthurs & Ziada (2012b, 2012c), suggesting some similarity in the excitation mechanisms of these cases despite their disparate Mach number.

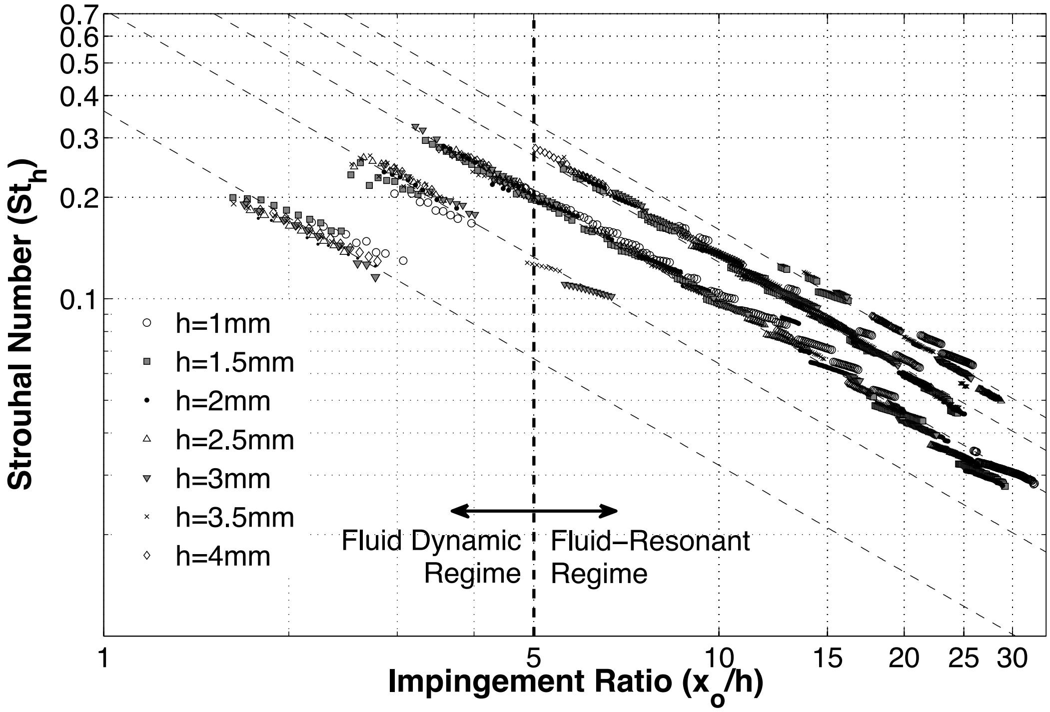

Figure 5.9: Strouhal number of tone frequency based upon nozzle thickness (St_h) as a function of impingement ratio for a range of nozzle thicknesses between 2mm≤*h*≤4mm and a flow velocity of U_o=300m/s (M=0.87).

The response of the current planar jet-plate system can be divided into two separate regimes: a fluid-dynamic regime occurring at low impingement ratios, and a fluid-resonant regime occurring for larger impingement ratios. The fluid-dynamic regime, which occurs for impingement ratios of $x_o/h \leq 5.0$, shows a collapse of the frequency response to specific hydrodynamic modes over well-defined ranges of impingement ratio and the average Strouhal number for this range remains approximately constant, indicating that the hydrodynamic modes of the jet excited within this range are related to the structure of the impinging jet flow. Similar behavior has been observed in the axisymmetric impinging jet flow, such as in the measurements of Wagner (1971) shown in Figure 5.10, which shows frequency response of three sharp-edged nozzles as a function of impingement distance for a constant Mach number of M=0.85. Part a) of the figure, which shows a re-plotting of the acoustic tone frequency as a function of impingement distance, indicates good correlation with the jet diameter. The oscillation frequency is seen to be lower for larger diameter jets, but for each diameter case, the frequency retains a mean value related to the jet diameter, by means of multiple frequency jumps as the impingement distance is increased. In Part b) of this figure, when the nozzle diameter is used to normalize the frequency and impingement distance, the Strouhal number data for all nozzle diameters collapse to specific hydrodynamic modes of the jet over specific ranges of impingement ratio. Note that the Strouhal number based upon the nozzle diameter remains in the range of St_D=0.3-0.5 over the complete range of impingement ratio for which tone are generated. These results indicate that the jet oscillation frequency is controlled not only by the impingement ratio, but also by the jet diameter.

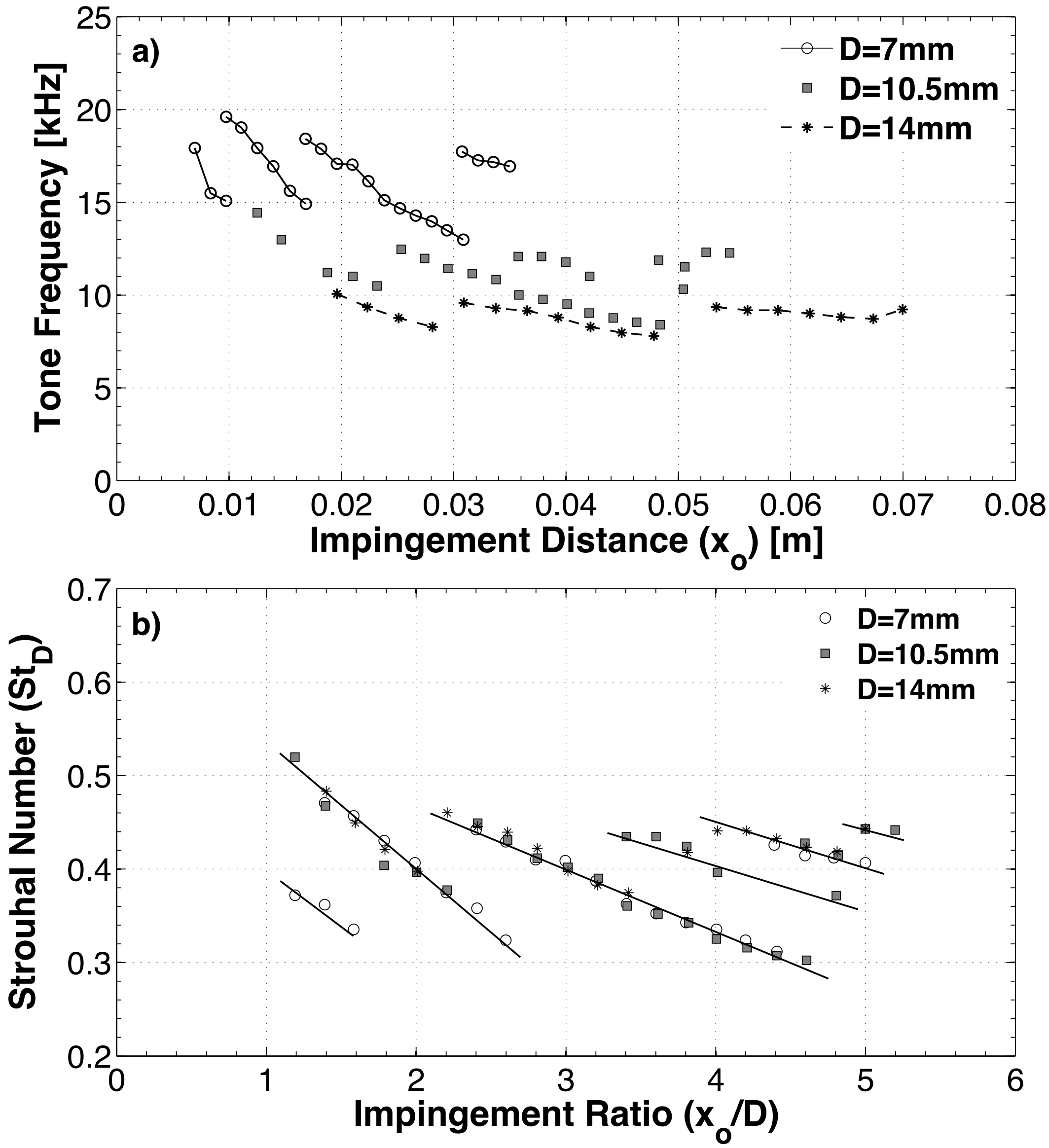

Figure 5.10: Data from Wagner (1971) re-plotted with a) tone frequency as a function of impingement distance and b) Strouhal number based upon diameter vs. impingement ratio.

The fluid-resonant regime, which occurs in the present case for impingement ratios larger than $x_o/h \approx 5.0$ in Figure 5.9, shows that for larger impingement ratios, any one of several hydrodynamic modes can be excited depending on the nozzle thickness being tested. In addition, the Strouhal number based upon nozzle thickness h, decreases continuously with increasing impingement ratio, i.e. it does not retain a mean value as observed in the data of Wagner (1971) shown in Figure 5.10b). These features suggest that the nozzle thickness does not seem to play a major role in selecting the oscillation frequency. Instead, it is the coupling between the instability of the jet shear layers and the trapped acoustic modes that determine the frequency of the oscillation. These trapped modes exist in the air volume between the nozzle flange and impingement surface (Koch, 1983 and Hien et al., 2003), and they modulate the high frequency shear layer oscillation, resulting in collective interaction of the of the shear layer instabilities and hydrodynamic modes of the jet at the resonance frequency. It follows that for a given impingement distance and jet velocity, changing the jet thickness does not result in a consummate frequency change because the resonant acoustic frequency and the shear layer thickness do not change when the jet thickness is changed (Figure 5.3b). The nature of this fluid-resonant interaction will be the subject of the remainder of this article.

5.6 The Fluid-Resonant Mechanism

Figure 5.11 shows the same data presented in Figure 5.9, but with the acoustic tone frequency plotted as a function of the impingement distance, for each of the seven nozzle thicknesses tested. The tone frequency shows some evidence of a collapse when plotted using these parameters, showing clusters of nominally constant frequency being excited by jets with different nozzle thicknesses over specific ranges of impingement distance. In order to more clearly illustrate this clustering effect, a series of three clusters labeled I, II and III, which will be discussed in greater depth momentarily, are highlighted on the figure. Cluster II, for example, shows very little change in tone frequency for a given impingement distance, although the nozzle thickness changes by a factor of four, from h=1mm to 4mm. It is also evident from inspection of cluster II that while the tone frequency remain virtually constant, the data show slight variation along the x-coordinate, with the acoustic tones of a nominally constant frequency being excited over slightly different ranges of impingement distance depending on the nozzle thickness being tested, a trend which obscures the collapse of the data. These trends are also exemplified in clusters I & III.

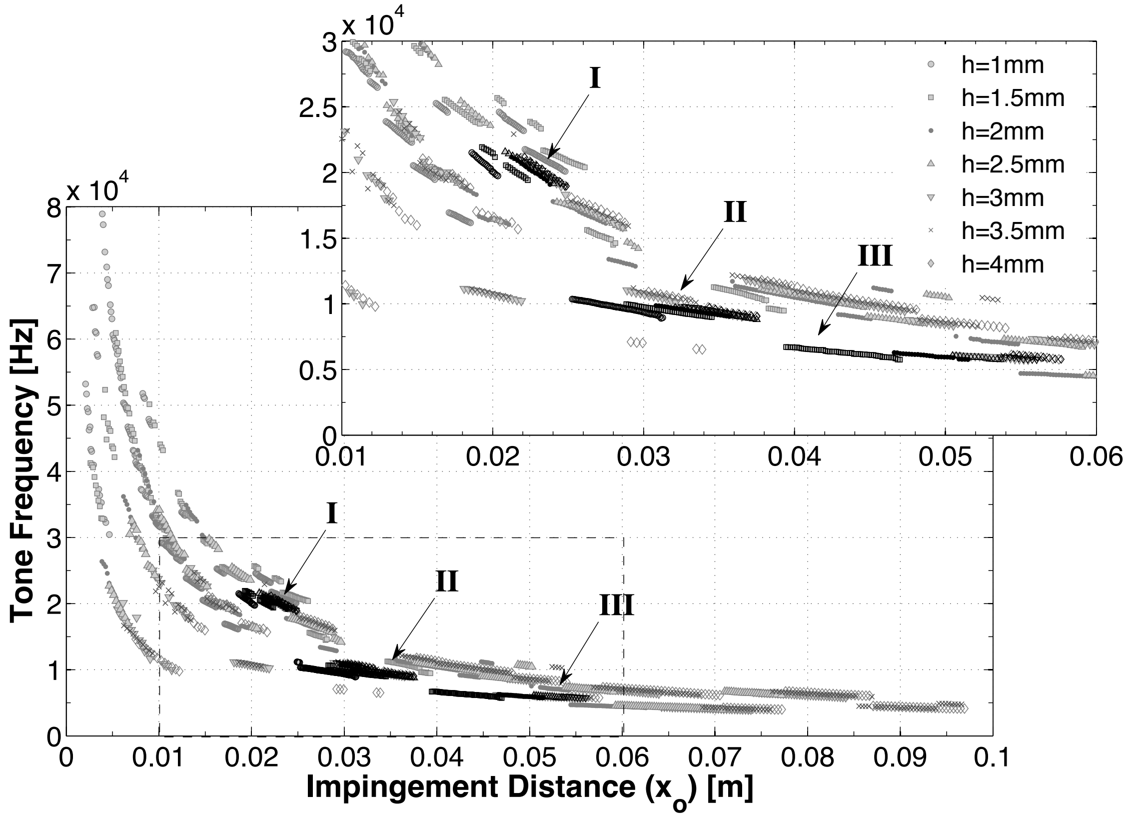

Figure 5.11: Acoustic tone frequency vs. impingement distance (x_0) for a range of nozzle thicknesses between 1mm≤h≤4mm, with inset figure showing cases I, II and III with an enlarged scale.

In order to gain more insight into the trends within these clusters, the data of cluster II has been plotted in Figure 5.12, with part a) of the figure showing the acoustic tone frequency as a function of impingement distance, and part b) showing the Strouhal number based upon nozzle thickness as a function of impingement ratio. Part a) of the figure shows that a nominally constant tone frequency of $f \approx 9.5$kHz is excited by each of the seven nozzle thicknesses as the impingement distance is varied within a relatively small range, with a decreasing trend in tone frequency as a function of impingement distance being apparent for each series. Increasing the nozzle thickness is seen to progressively increase the mean value of impingement distance for which the tone is excited. Part b) of Figure 5.12, which shows the Strouhal number based upon nozzle thickness as a function of impingement ratio, illustrates that unlike the trend found in Wagner's data (1971) shown in Figure 5.10b), the Strouhal number of the present case decreases substantially with decreasing nozzle thickness, and it corresponds to progressively larger values of impingement ratio. The h=4mm nozzle thickness case excites the tone at a relatively small impingement ratios from $7.5 \leq x_o/h \leq 8.5$, whereas the h=1mm nozzle thickness case excites the same tone at a much larger impingement ratios from $26.0 \leq x_o/h \leq 32.5$, with the intermediate cases falling in a well-defined trend between these extremes. This effect is produced as a result of the relatively constant tone frequency for a given impingement distance, but the large variation in nozzle thickness alters the impingement ratio substantially. These observations emphasize the relative independence of the tone frequency and nozzle thickness. All seven different nozzle thickness cases appear to excite the tones in the same n=3 anti-symmetric hydrodynamic mode of the jet, falling closely along the trend line for this mode.

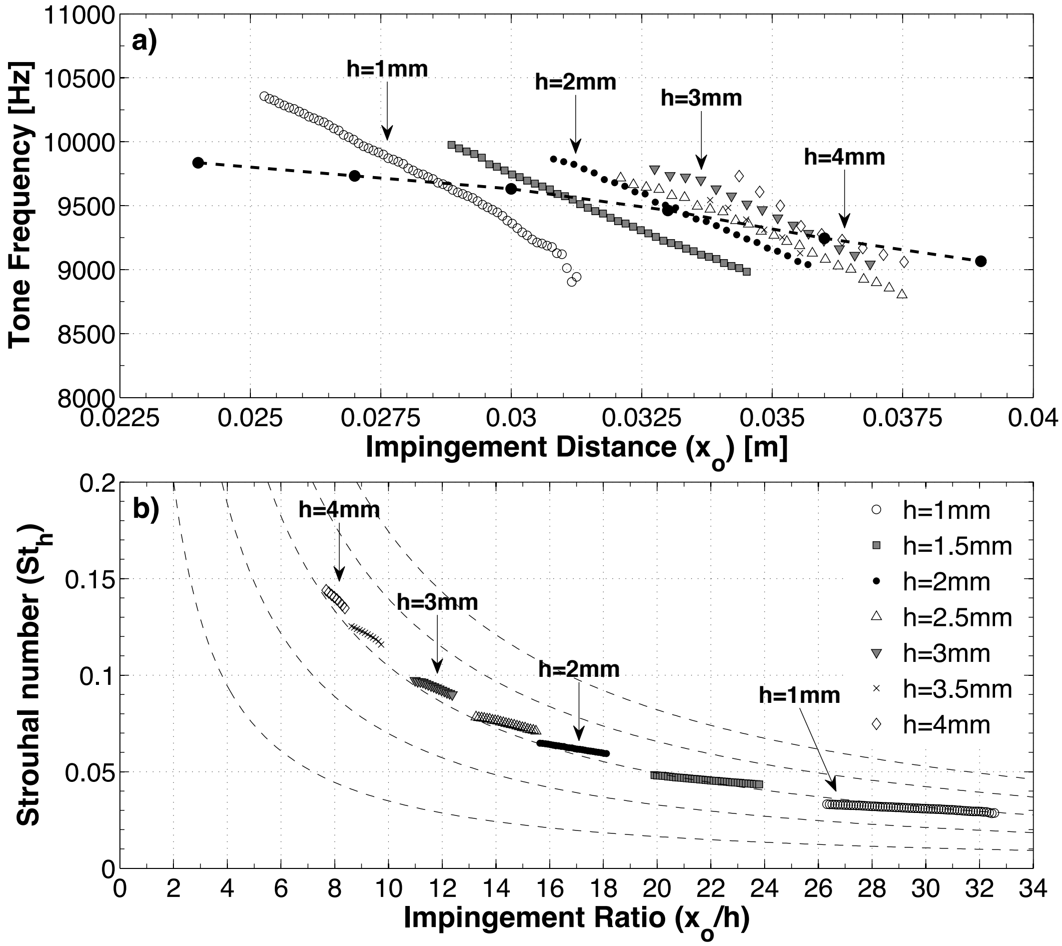

Figure 5.12: a) Acoustic tone frequency as a function of impingement distance (x_o) and b) Strouhal number based upon nozzle thickness as a function of impingement ratio for Case II shown in Figure 5.11.

Returning to Figure 5.12a), the observed decrease in the mean impingement distance as a function of decreasing nozzle thickness within the resonant mode is attributed to the variation of the convection speed of coherent flow structures that occurs as the impingement ratio is varied over a large range. To illustrate this effect, consider the case of an impinging planar jet flow with a fixed impingement distance and flow velocity, but with a varying nozzle thickness (and thus a varying impingement ratio). If the jet is self-excited in a constant hydrodynamic mode, as the nozzle thickness is decreased, the impingement ratio will increase. As the impingement ratio becomes significantly larger than the length of the jet potential core, a bulk slowing effect of the jet flow will occur downstream of the jet potential core, where the jet flow will slow as it spreads outward. This slowing effect will lower the convection speed of the downstream propagating coherent flow structures (u_c), and thus *lower the frequency* of the hydrodynamic jet oscillation. The condition of frequency coincidence between the resonant acoustic mode and the jet oscillation, which is necessary to maintain the fluid-resonant mechanism, will therefore be met at smaller impingement distances for thinner jets. The dotted line shown in Figure 5.12a) represents the predicted frequency of a resonant acoustic mode occurring between the nozzle flange and the impingement surface as a function of impingement distance obtained using the Finite Element Analysis (FEA) techniques outlined in Arthurs & Ziada (2012b). The decreasing trend in resonant frequency for this particular acoustic mode is associated with the increasing impingement distance, being one dimension of the three-dimensional acoustic resonator.

As discussed in relation to Figure 5.12b), the system oscillation appears to occur for the same n=3 hydrodynamic mode over a wide range of impingement ratio ($7.0 \leq x_o/h \leq 32.0$). In order to confirm that the same hydrodynamic mode is, in fact, being excited for all nozzle thicknesses over this relatively large range of impingement ratio, a series of flow visualization images shown in Figure 5.13 were obtained at a constant flow velocity of U_o=300m/s and a nominally constant impingement distance, but for a series of nozzle thicknesses between h=1mm and 4mm. The four images, which correspond to impingement ratios of x_o/h=28.0, 16.0, 10.5 and 8.4 for the h=1, 2, 3 and 4mm cases respectively, show the same general form of the n=3 anti-symmetric hydrodynamic mode, with a similar columnar displacement pattern from the centerline and the same number of coherent flow structures appearing on either side of the jet, indicating that at this impingement distance, the jet oscillates in the same hydrodynamic mode regardless of the jet thickness or impingement ratio. These flow visualization images, in conjunction with the frequency data, provide clear evidence that the fluid-dynamic mechanism observed by Wagner (1971) is not responsible for deciding the frequency or the oscillation mode. Instead, since the characteristics of the initial shear layers are virtually identical for all nozzle thickness cases, and the acoustic resonance frequency is determined by the impingement distance, the oscillation frequency and hydrodynamic mode must be selected by coupling between the shear layer instability and the resonant acoustic mode.

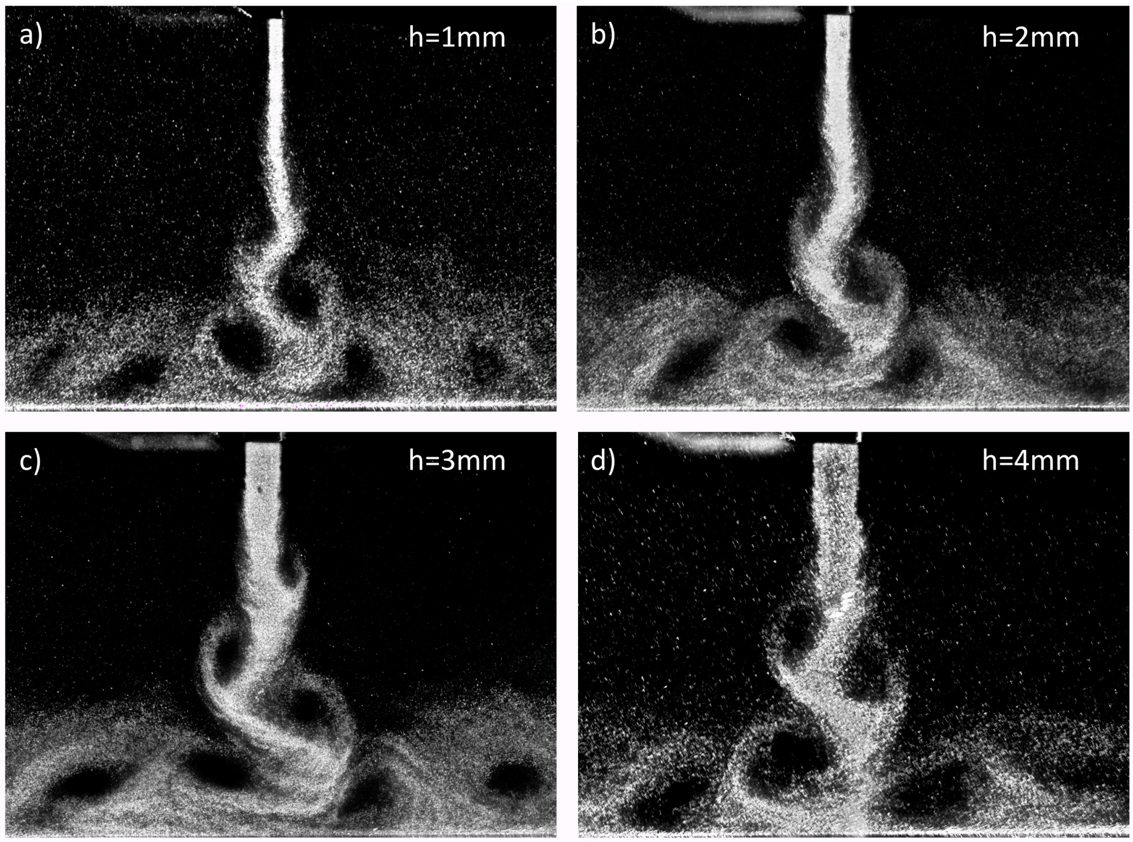

Figure 5.13: Flow visualization images of the planar impinging jet flow responding in the n=3 anti-symmetric hydrodynamic mode at $f\approx$9.5kHz (case II) for approximately constant impingement distance of $x_o\approx$0.03m and Mach number of M=0.87 for nozzle thicknesses of a) h=1mm, b) 2mm, c) 3mm and d) 4mm.

The present results suggest that some previous studies examining axisymmetric impinging jet flows, specifically those employing lift plates, may also be affected by this fluid-resonant interaction of hydrodynamic modes coupling with trapped acoustic modes. Lift plates are large circular baffles that are installed at the exit plane of the nozzle in order to examine lift-loss, the effect of strong negative pressures generated at the upstream surface due to entrainment effects. This effect is especially pronounced at small impingement distances where the effect of confinement is more significant. As a result of the acoustically reflective lift plates and significant confinement of the flow, these geometries may also be liable to the formation of trapped acoustic modes in the fluid volume between the plates and the impingement surface. Figure 5.14 shows the data of Panickar & Raman (2007) who investigated the impinging axisymmetric jet flow for a range of transonic Mach numbers, and a single nozzle diameter (*D*) with lift plates (lift plate diameter = 4·*D*). The original plotting of the data, which depicted the results for each of the four Mach numbers tested on separate plots, showed that all axisymmetric jet modes occurred at a constant mean Strouhal number for each Mach number. However, significant *variation* in these mean Strouhal numbers occurred as the Mach number was varied. As can be seen from Figure 5.14b), the values corresponding to axisymmetric modes varied by nearly 40% from $0.35 \leq St_D \leq 0.52$ over a relatively small range of Mach number from $0.8 \leq M \leq 0.95$. This observation is at odds with the data of Wagner (1971) shown earlier in Figure 5.10b). The same data of the axisymmetric mode are presented in Figure 5.14a), but re-plotted with the acoustic tone frequency as a function of impingement distance. This figure does show a clear collapse of frequency as a function of impingement distance, indicating that a fluid-resonant mechanism is likely responsible for acoustic tone generation for this case due to the acoustically reflective flange surface which is similar to a lift plate. This resonant acoustic coupling causes the trend of decreasing mean Strouhal numbers as a function of increasing Mach number, as tone frequencies tend to lock on to specific resonant acoustic modes corresponding to a given impingement distance, even as the flow velocity increases, resulting in a decrease in the mean value of Strouhal number. Further evidence of this resonant phenomenon can be observed in the shadowgraph images reported by Krothapalli et al. (1999), who performed a study on a similar apparatus using larger lift plates (lift plate diameter =

10·*D*). These images show a standing acoustic wave pattern between the lift plate and the impingement surface.

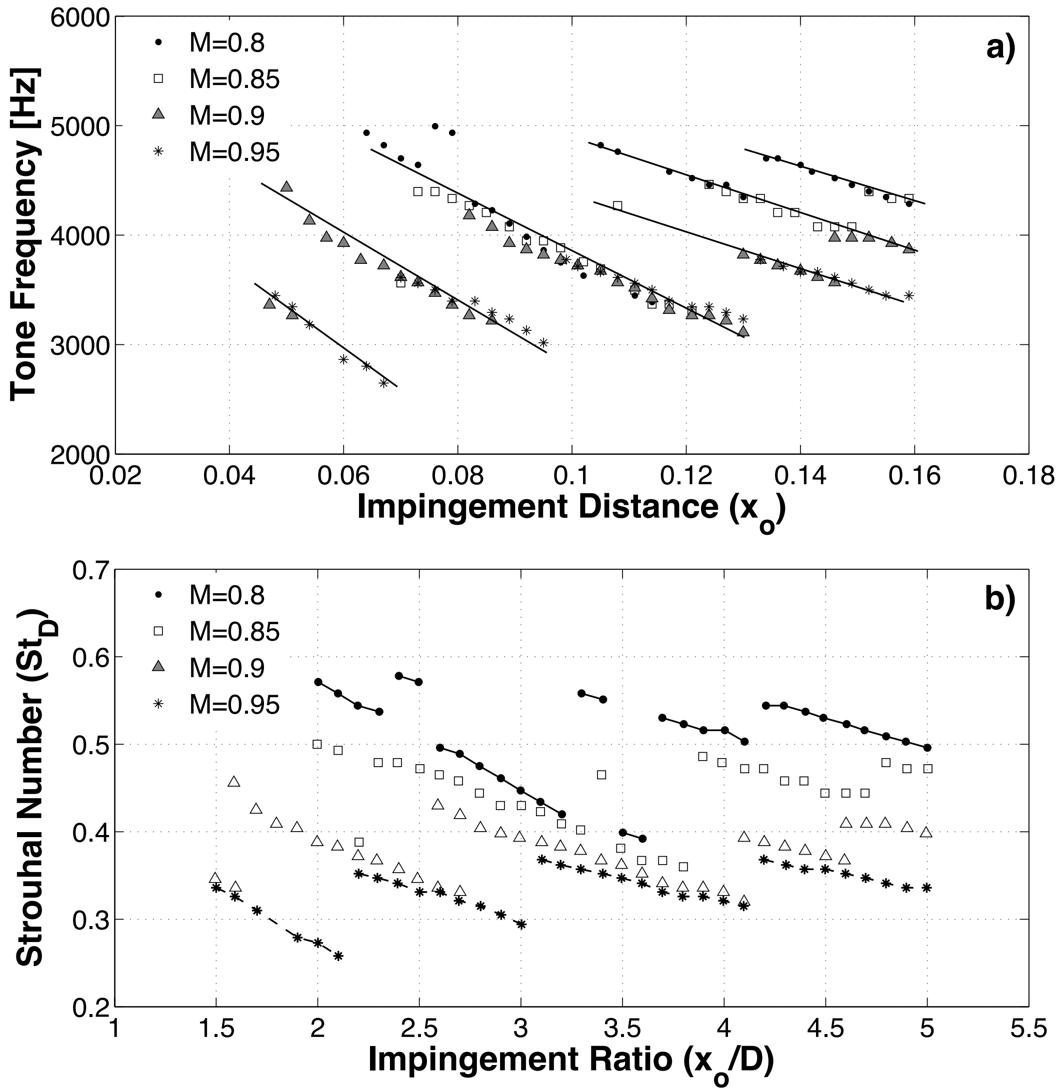

Figure 5.14: Data of Panickar and Raman (2007) for an impinging axisymmetric jet fitted with a 4·*D* diameter lift plate showing a) the Strouhal number based upon nozzle diameter as a function of impingement ratio and b) the acoustic tone frequency vs. impingement distance, each for a series of transonic Mach numbers.

Figures 5.15 and 5.16 show the same analysis as in Figure 5.12 for the other two highlighted cases (I & III) shown earlier in Figure 5.11. Each of these two cases shows similar trends as those observed for Case II, with resonant modes excited by larger nozzle thicknesses occurring at higher impingement distances as a result of the lower convection speeds associated with larger impingement ratios. Case I, which is shown in Figure 5.15, illustrates that the acoustic tone is excited by all seven nozzle thicknesses because the frequency coincidence occurs at relatively small impingement distances, however the resonant mode of Case III shown in Figure 5.16 is only excited by jets with nozzle thicknesses of h=1.5mm and larger, as the impingement ratio of the h=1mm case falls outside the maximum impingement ratio range of x_o/h=32.0 for the impinging planar jet. Each of these two plots shows virtually identical trends to those described in Figure 5.12, and with a single hydrodynamic mode being excited within each resonant mode at a constant frequency, and over a small range of impingement distance.

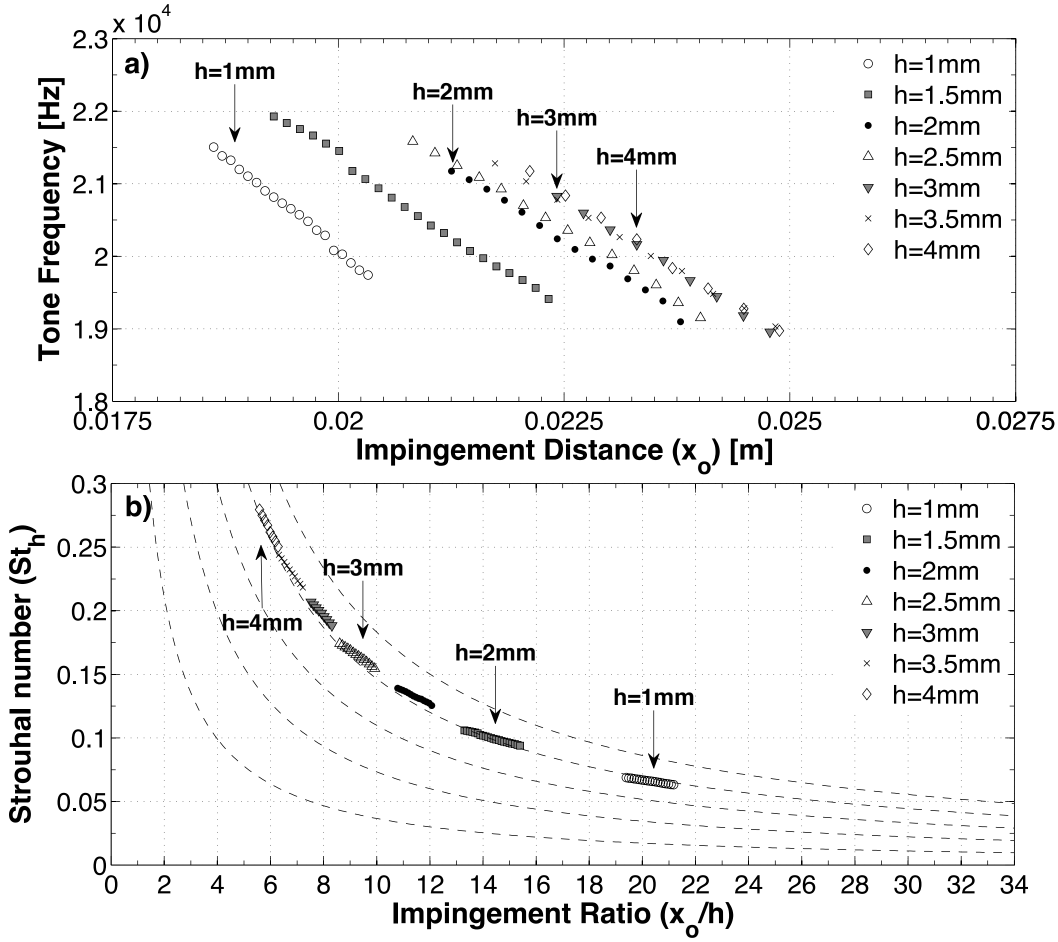

Figure 5.15: a) Acoustic tone frequency as a function of impingement distance (x_o) and b) Strouhal number based upon nozzle thickness as a function of impingement ratio for Case I shown in Figure 5.11.

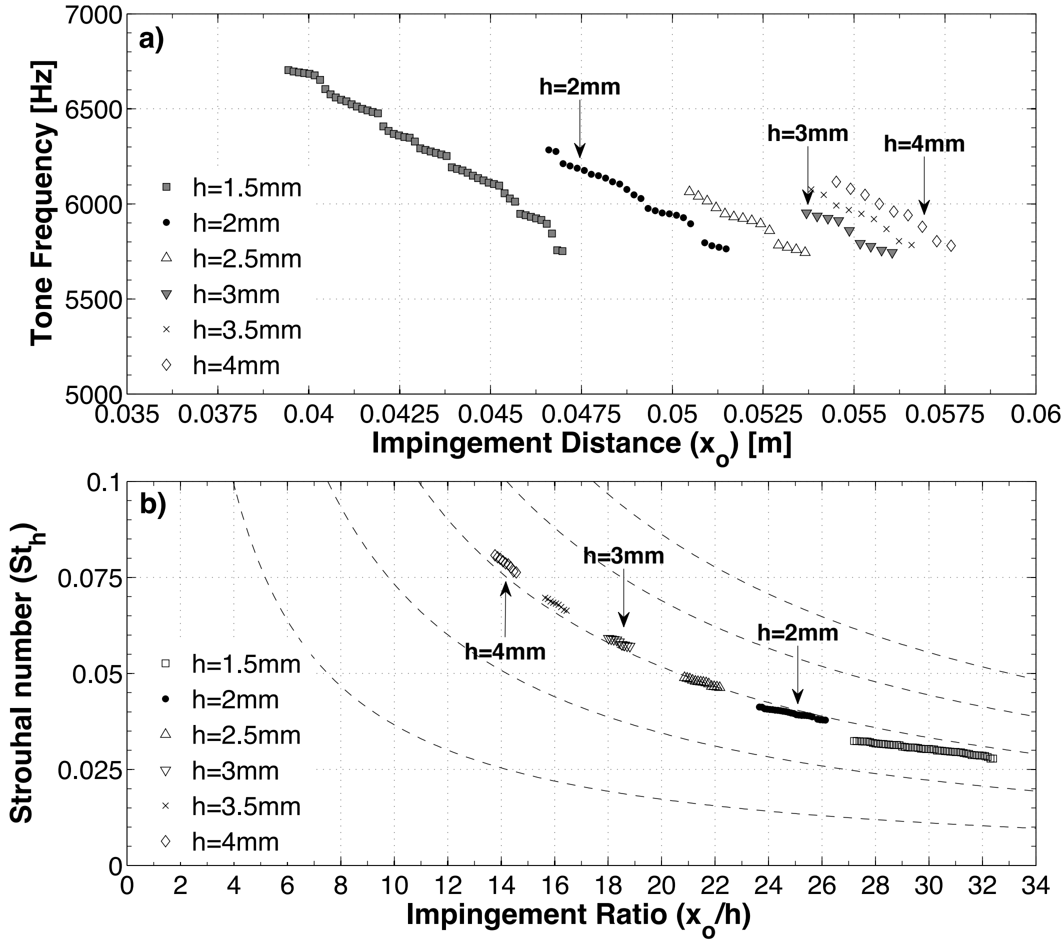

Figure 5.16: a) Acoustic tone frequency as a function of impingement distance (x_o) and b) Strouhal number based upon nozzle thickness as a function of impingement ratio for Case III shown in Figure 5.11.

5.7 Correction for Varying Phase Speed

Figure 5.17 shows the same data presented in Figure 5.11, but with a modified impingement distance scale on the *x*-axis which compensates for the effect of varying convection speed by applying a correction coefficient of the flow velocity at the nozzle outlet divided by the effective flow velocity given in Equations 5.3 and 5.4, with the resulting correction shifting each data point by an amount dependent on the impingement ratio. The resulting collapse of the data is improved dramatically by removing the effect of varying convection speed, with well-defined resonant frequencies being observed over discrete ranges of impingement distance, with no significant effect of varying nozzle thickness being apparent. Specific resonant modes are excited as a function of the impingement distance, with the nozzle thickness having only a slight effect due to variation in convection speed that occurs as a result of varying impingement ratio when the nozzle thickness is changed.

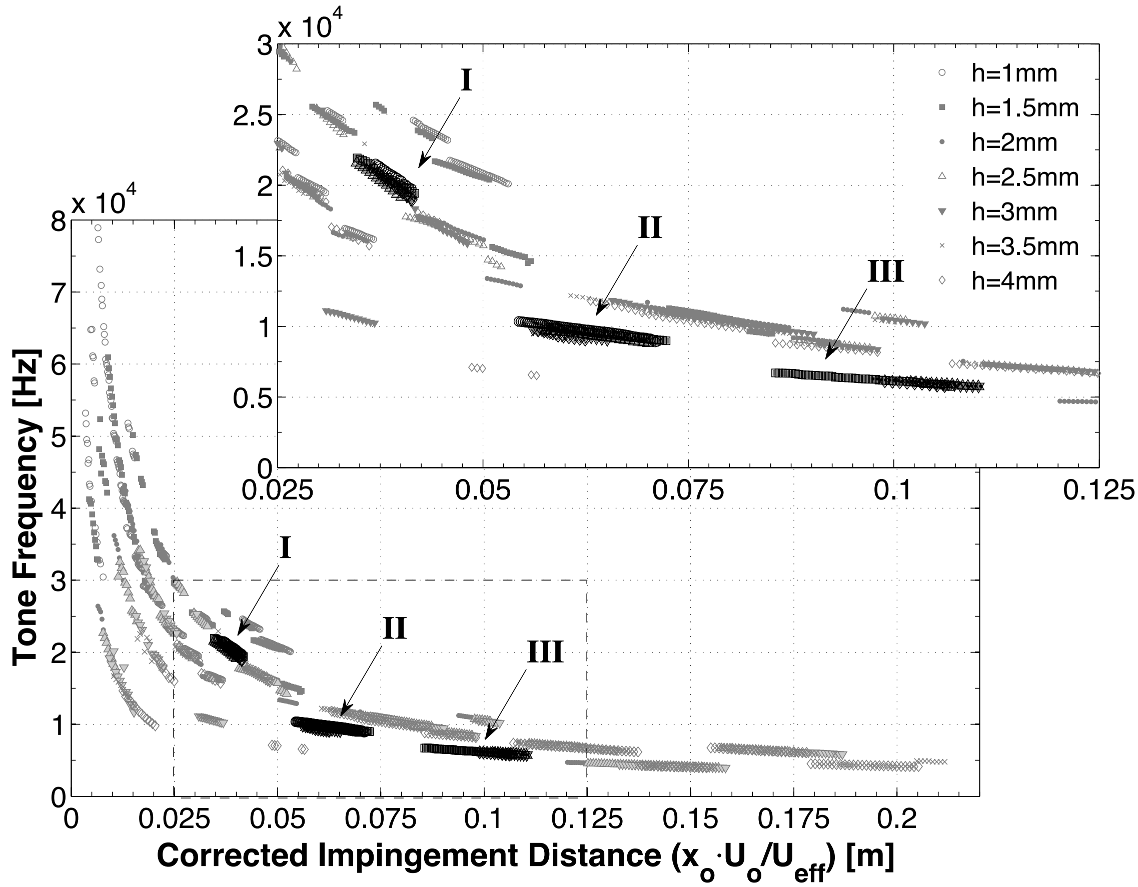

Figure 5.17: Acoustic tone frequency as a function of a modified impingement distance scale to account for variation in convection speed resulting from varying impingement ratio.

5.8 Conclusion

The effect of varying nozzle thickness in the high-speed impinging planar jet has been investigated. Acoustic tones where found to be excited by a series of anti-symmetric hydrodynamic modes of the jet over a large range of impingement ratio, and with tones being most intense at intermediate impingement ratios ($x_o/h \approx 10$) for all nozzle thicknesses tested. For cases where the impingement distance approaches the length of the jet-span, such as in the h=3mm and larger nozzle thicknesses at large impingement ratio, this tone generation range can be shortened due to increased three-dimensionality of the jet flow which weakens the effect of upstream feedback due to flow impingement and suppressing the formation of large-scale coherent flow structures. The frequency of the acoustic tones can be accurately predicted through the use of a feedback model which takes into account the relatively slow convection speed for anti-symmetric oscillation of the jet and the large size of the coherent structures, as well as the bulk slowing effect which occurs as the impingement ratio increases beyond the range of the jet potential core.

Comparison of the aeroacoustic response obtained for different nozzle thicknesses reveals that for small impingement ratios, the jet response is governed by a fluid-dynamic mechanism, in which the hydrodynamic mode of the jet is excited as a function of the impingement ratio. As the impingement ratio is increased, a fluid-resonant regime defines the response of the system, where the various hydrodynamic modes of the jet couple with different resonant acoustic modes occurring in the air volume between the nozzle and the impingement surface, resulting in tone frequencies that are largely a function of the impingement distance. The nozzle thickness has been found to have only minor effects on the oscillation frequency. This minor effect is caused by changes in the convection velocities due to the variation in the impingement ratio. Flow visualization images have been presented to show that a single hydrodynamic mode is excited within a resonant acoustic mode, despite large variation in the impingement ratio consequent upon increasing the nozzle thickness. Finally, some evidence was presented that high-speed impinging axisymmetric jet flows using acoustically reflective lift-plates at the upstream location may in fact also be excited by a similar fluid-resonant mechanism.

5.9 References

Alkislar, M. B., Krothapalli, A., Lourenco, L. M., 2003. Structure of a screeching rectangular jet: A stereoscopic particle image velocimetry study. Journal of Fluid Mechanics. 489, 121–154.

Arthurs, D., Ziada, S., 2011. The planar jet-plate oscillator. Journal of Fluids and Structures. 27, 105–120.

Arthurs, D., Ziada, S., 2012a. Noise generation in the gas-wiping process, Journal of Fluids and Thermal Sciences. Submission #: 4110905-FT18, Accepted, In-Press.

Arthurs, D., Ziada, S., 2012b. Self-excited oscillations of a high-speed impinging planar jet. Journal of Fluids and Structures. Submission #: YJFLS–1431, Accepted, In-Press.

Arthurs, D., Ziada, S., 2012c. Evolution of the self-excited impinging planar jet. Journal of Fluids and Structures. Submitted to the Journal of Fluid Mechanics, Submitted: 23/07/2012, Submission #: JFM–12–S–0698.

Billon, A., Valeau, V., Sakout, A., 2005. Two feedback paths for a jet-slot oscillator. Journal of Fluids and Structures. 21, 121–132.

Camci, C., Herr, F., 2002. Forced convection heat transfer enhancement using a self-oscillating impinging planar jet. ASME Journal of Heat Transfer. 124, 770–782.

Chung, Y. M., Luo, K. H., 2002. Unsteady heat transfer analysis of an impinging jet. Journal of Heat Transfer. 124, 1039–1048.

Elavarasan, R., Venkatakrishnan, L., Krothapalli, A., Lourenco, L., 2000. A PIV study of a supersonic impinging jet. Journal of Visualization. 2(3/4), 213–221.

Ferrari, J., Lior, N., Slycke, J., 2003. An evaluation of gas quenching of steel rings by multiple-jet impingement. Journal of Material Processing Technology. 136(1–3), 190–201.

Glesser, M., Valeau, V., Sakout, A., 2008. Vortex sound in unconfined flows: Application to the coupling of a jet-slot oscillator with a resonator. Journal of Sound and Vibration. 314, 635–649.

Hein, S., Hohage, T., Koch, W., 2004. On resonances in open systems. Journal of Fluid Mechanics. 506, 255–284.

Ho, C., Nosseir, N. S., 1981. Dynamics of an impinging jet. Part 1: The feedback mechanism. Journal of Fluid Mechanics. 105, 119–142.

Ho, C.M., Hsiao, F.B., 1983. Evolution of coherent structures in a lip jet. Structure of Complex Turbulent Shear Flow. 1, 121–136.

Ho, C., Huerre, P., 1984. Perturbed free shear layers. Annual Review Fluid Mechanics. 16, 365–424.

Henderson, B., Bridges, J., Wernet, M., 2005. An experimental study of the oscillatory flow structure of tone-producing supersonic impinging jets. Journal of Fluid Mechanics. 542, 115–137.

Hsiao, F., Chou, Y., Huang, J., 1999. The study of self-sustained oscillating plane jet flow impinging upon a small cylinder. Experiments in Fluids. 27, 392–399.

Hsiao, F., Hsu, I., 2004. Evolution of coherent structures and feedback mechanism of the plane jet impinging on a small cylinder. Journal of Sound and Vibration. 278, 1163–1179.

Koch, W., 1983. Resonant acoustic frequencies of flat plate cascades. Journal of Sound and Vibration. 88(2), 233–242.

Krothapalli, A., 1985. Discrete tones generated by an impinging underexpanded rectangular jet. AIAA Journal. 23, 1910–1915.

Krothapalli, A., Hsia, Y., Baganoff, D., 1986. The role of screech tones in mixing of an underexpanded rectangular jet. Journal of sound and Vibration. 106(1), 119–143.

Krothapalli, A., Rajkuperan, E., Alvi, F., 1999. Flow field and noise characteristics of a supersonic impinging jet. Journal of Fluid Mechanics. 392, 155–181.

Lin, J., Rockwell, D., 2001. Oscillations of a turbulent jet incident upon an edge. Journal of Fluids and Structures. 15, 791-829.

Marsh, A. H., 1961. Noise measurements around a subsonic air jet impinging on a plane, rigid surface. The Journal of the Acoustical Society of America. 33, 1065–1066.

Mehta, R., Bradshaw, P., 1979. Design rules for small low-speed wind tunnels. Aeronautical Journal of the Royal Aeronautical Society. 83, 443–449.

Melling, A., 1997. Tracer particles and seeding for particle image velocimetry. Measurement Science and Technology. 8, 1406–1416.

Narayanan, V., 2004. An experimental study of fluid mechanics and heat transfer in an impinging slot jet flow. International Journal of Heat and Mass Transfer. 47, 1827–1845.

Neuwerth, G., 1972. Acoustic feedback phenomena of the subsonic and hypersonic free jet impinging on a foreign body. NASA Technical Translation TT F–151-76.

Norum, T., 1991. Supersonic rectangular jet impingement noise experiments. AIAA Journal. 29(7), 1051–1055.

Nosseir, N.S., Ho, C., 1982. Dynamics of an impinging jet. Part 2: The noise generation. Journal of Fluid Mechanics. 116, 379–391.

O'Donovan, T., Murray, D., 2007. Jet impingement heat transfer – Part II: A temporal investigation of heat transfer and local fluid velocities. International Journal of Heat and Mass Transfer. 50, 3302–3314.

Panickar, P., Raman, R., 2007. Criteria for the existence of helical instabilities in subsonic impinging jets. Physics of Fluids. 19, 106103–1.

Powell, A., 1961. On the edgetone. The Journal of the Acoustical Society of America. 33, 395–409.

Raman, G., 1997. Cessation of screech in underexpanded jets. Journal of Fluid Mechanics. 336, 69–90.

Raman, G., 1999. Supersonic jet screech: Half-century from Powell to the present. Journal of Sound and Vibration. 225(3), 543–571.

Rossiter, J. E., 1964. Wind tunnel experiments on the flow over rectangular cavities at subsonic and transonic speeds. Royal Aircraft Establishment, TR No. 64307.

Tam, K. W., 1988. The shock-cell structures and screech tone frequencies of rectangular and non-axisymmetric supersonic jets. Journal of Sound and Vibration. 121, 135–147.

Tam, C., Ahuja, K., 1990. Theoretical model of discrete tone generation by impinging jets. Journal of Fluid Mechanics. 214, 67–87.

Tam, C., Norum, T., 1992. Impingement tones of large aspect ratio supersonic rectangular jets. AIAA Journal. 30(2), 304–311.

Thomas, F., 1991. An experimental investigation of the natural transition of an untuned planar jet. Physics of Fluids A: Fluid Dynamics. 3(1), 90–105.

Umeda, Y., Maeda, H., Ishii, R., 1987. Discrete tones generated by the impingement of a high- speed jet on a circular cylinder. Physics of Fluids. 30, 2380–2388.

Viskanta, R., 1993. Heat transfer to impinging isothermal gas and flame jets. Experimental Thermal and Fluid Science 6, 111–134.

Wagner, F., 1971. The sound and flow field of an axially symmetric free jet upon impact on a wall. NASA Technical Translation. TT F–131–32.

Ziada, S., 1995. Feedback control of globally unstable flows: Impinging flows. Journal of Fluids and Structures. 9, 907–923.

Ziada, S., 2001. Interaction of a jet-slot oscillator with a deep cavity resonator and its control. Journal of Fluids and Structures. 15, 831–843.

CHAPTER 6

Conclusion

6.1 Thesis Summary

This thesis has experimentally investigated the behavior of the self-excited planar jet impinging on a large rigid plate at some distance downstream. A planar nozzle and plate geometry was constructed, and a comprehensive set of experiments were performed for a range of subsonic Mach numbers, impingement ratios, and nozzle thickness to investigate the self-excited response of the system. The aeroacoustic response has been found to be significantly different from similar geometries, such as the impinging axisymmetric jet flow, showing a self-excited response over a much larger range of impingement ratio, and beginning at lower Mach numbers. Acoustic pressure fluctuations have been found to be large, with amplitudes of more than 170dB at the plate surface in the impingement zone, and in excess of 150dB in the acoustic far-field, with tones being largest for intermediate impingement ratios near x_o/h=10 for all nozzle thicknesses examined.

The impinging planar jet has been found to generate self-excited oscillations over two distinct flow regimes: a linear regime occurring at relatively low Mach number, where the acoustic tone frequency scales approximately linearly with increasing flow velocity, and a fluid-resonant regime occurring at higher Mach numbers, where hydrodynamic modes of the jet couple with trapped acoustic modes occurring between the nozzle and the impingement surface. Phase-locked PIV measurements and a thorough dimensionless analysis have been used to identify the various hydrodynamic modes of the jet, with acoustic tones in the linear regime being generated by a single flapping mode of the jet column, resulting in tones with relatively low acoustic pressure amplitudes. Self-excited behavior in the fluid-resonant regime is produced by a series of five anti-symmetric hydrodynamic modes of the jet, as well as a single symmetric mode occurring at low impingement ratio, and produce much more intense acoustic tones and flow oscillations. Anti-symmetric modes consist of a flapping motion of the jet column, along with an anti-symmetric distribution of large flow structures that form in the initial shear layers of the jet, convect downstream and impinge on the plate surface. A mode diagram, which illustrates the distribution of different hydrodynamic and resonant acoustic modes as a function of both Mach number and impingement ratio, has been created using the results of comprehensive set of measurements performed for a single nozzle thickness of h=3mm, and demonstrates the complex response of this system.

Coupling with trapped acoustic modes in the fluid-resonant regime, which has been demonstrated for impinging jet flows for the first time in this thesis, is found to dominate the self-excited response of the system, with the hydrodynamic mode of the jet and the oscillation frequency being selected by interaction with these resonant modes. The oscillation frequency has been found to scale almost exclusively with the stream-wise length scales associated with this acoustic volume, with the jet thickness having almost no effect on the behavior of the system, and the structure of the impinging jet flow having only minor effects due to variation in convection speed of the coherent flow structures. As a result of this behavior, the aeroacoustic response of an impinging jet with a given nozzle thickness can be used to predict the response of other jets using the same nozzle design, but different nozzle thicknesses. Similarly, the results of the mode diagram can be used to predict the system response for a variety of jet thicknesses.

A thorough investigation of the flow structure of the n=3 anti-symmetric mode of the impinging planar jet has been performed, and the impinging flow has been found to develop in three distinct regions. Coherent flow structures are formed in the initial region, comprising the first 20% of the total impingement length, and are produced as a result of fluctuating velocity components occurring principally in the stream-wise direction. After formation in the initial region, the coherent flow structures grow rapidly as they convect downstream in the developing region, with the rotation of the structures contributing to the development of the transverse fluctuating velocity component, and the resulting flapping motion of the jet column. The flow then enters the impingement region, which has been defined as the last 25% of the total impingement distance, with this region marking the onset of interaction between the coherent flow structures and the impingement surface. The amplitude of fluctuating velocity components has been found to be very large, with a peak-to-peak fluctuation level in excess of $0.7 \cdot U_o$ for cases at high Mach number in the fluid-resonant regime. Fluctuating velocity components show a similar stream-wise evolution as either the Mach number or impingement ratio are varied within a hydrodynamic mode, but with amplitudes tending to intensify with increasing

Mach number, as well as with increasing impingement ratio within a resonant acoustic mode.

A detailed examination of the behavior of the coherent flow structures has been completed, using the velocity discriminant parameter to identify coherent structures within the flow, and to develop a new structure tracking scheme to quantify their motion and behavior. Structures in the planar impinging jet case are found to convect relatively slowly compared to results of other related geometries, moving at 40% of the jet velocity in the initial region, with evidence of the structures slowing in the transition region for self-excited cases with larger impingement ratios. Measurements of the evolution of structure circulation reveal the vortices begin to impinge on the plate having travelled only 75% of the total impingement distance, as a result of the large size and the highly 2-dimensional path of the vortices.

Finally, a feedback model has been developed using the results of the flow field analysis, specifically information relating to the convection speed and impingement location of the coherent structures. The resulting model has been shown to accurately predict the oscillation frequency of the impinging planar jet system for the complete range of Mach number, impingement ratio and nozzle thickness examined in this work.

6.2 Conclusions

This thesis represents the first comprehensive examination of the self-excited planar jet impinging on a plate, and provides an overview of the self-excited response of the system, investigates the characteristics of the self-excited flow oscillations, and develops a feedback model that can be used to predict the response of the system. The main conclusions of this work are:

1. The characteristics of the self-excited response of the high-speed impinging planar jet has been investigated and quantified over a large range of flow and geometric parameters.
    - Self-excited oscillations are observed over a relatively large range of impingement ratio: $1.5 \leq x_o/h \leq 32.0$, for jets with a large aspect ratio.
    - Acoustic tones of significant amplitudes are generated at Mach numbers near $M \approx 0.4$, and are excited continuously in the subsonic flow regime up to a Mach number of $M \approx 1.0$ (*choked flow*).
    - Self-excited oscillations have been observed for the complete range of nozzle thicknesses examined, from h=1.0mm to 4.0mm, with the response of jets of different thicknesses showing similar characteristics as a function of Mach number and impingement ratio. The range of impingement ratio producing self-excited oscillations has been shown to decrease slightly at larger nozzle thicknesses, a trend which seems to be associated with decreasing aspect ratio of the nozzle and increased three-dimensionality of the impinging jet flow.
2. The impinging planar jet has been found to be self-excited over two distinct aeroacoustic regimes:
    - A linear regime, occurring at low Mach number, where the oscillation frequency is defined by a traditional feedback mechanism between downstream convecting flow instabilities, and upstream propagating acoustic disturbances.

- A fluid-resonant regime, occurring at higher Mach number, where self-excited flow oscillations and acoustic tones are generated by a traditional feedback mechanism coupled with trapped acoustic modes between the nozzle and the plate. Acoustic tones in this fluid-resonant regime exhibit less variation as a function of changing Mach number and impingement ratio, and are excited at much larger acoustic pressure amplitudes than those in the linear regime.

3. For the first time, unstable modes of the impinging jet have been shown to couple with trapped resonant acoustic modes on the exterior of the nozzle, with this fluid-resonant effect dominating the response of the system. The particular hydrodynamic mode of the jet excited and the oscillation frequency have both shown to be strongly related to the frequency of these trapped modes, with the structure of the impinging jet flow having only a minor effect on the tone frequency related to the convection speed of coherent flow structures.
4. The acoustic tone frequency has been shown to be unaffected by the jet thickness for an impinging planar jet with a fixed impingement length (x_o) responding in the fluid-resonant regime, as the frequency of the trapped acoustic modes are related to the impingement distance. As a result, the oscillation frequency within the fluid-resonant regime does not scale with the jet thickness, as it does within the linear regime.
5. Phase-locked PIV measurements have been used to identify the form of the various hydrodynamic modes of the jet participating in the feedback mechanism.

- Self-excited flow oscillations in the linear regime consist of a single flapping mode of the jet column producing relatively low fluctuating velocities and acoustic pressure amplitudes.
- Flow oscillations in the fluid-resonant regime consist of five anti-symmetric hydrodynamic modes of the jet, along with a single symmetric mode occurring for small impingement ratios. Anti-symmetric modes consist of a flapping motion of the jet column, along with an anti-symmetric distribution of large, coherent flow structures that form and convect in the jet shear layers.

6. The self-excited flow has been shown to develop in three distinct zones: the initial, developing and impingement regions, and the amplitude of fluctuating velocity components have been found to be very large, in excess of 35% of the initial jet flow velocity for the transverse component in some cases. These fluctuating velocity amplitudes have been found to intensify with increasing Mach number, as well as when the impingement ratio is increased within a given resonant acoustic mode.
7. The behavior of the large-scale coherent flow structures, which are integral to the feedback mechanism, have been examined and quantified, including the structure path, convection speed, size and circulation.
   - The structures have been found to convect relatively slowly, at 40% of the flow velocity in the initial region of the jet, with evidence of structure slowing occurring downstream of the jet potential core for large impingement ratios.

- Measurements of structure circulation shows that the vortices begin to interact with the downstream impingement surface having travelled an effective impingement length of only 75% of the total impingement distance.

8. A feedback model has been developed to predict oscillation frequency as a function of impingement ratio and Mach number. The model has been found to accurately predict acoustic tone frequency over the complete range of impingement ratio, Mach number and nozzle thickness tested in this work.

6.3 Contributions to the State of Knowledge

1. This thesis presents the first comprehensive experimental study of the self-excited subsonic impinging planar jet has been performed.
2. The planar impinging jet has been found to be self-excited over two distinct aeroacoustic regimes: a linear regime, occurring at low Mach number, and a fluid-resonant regime occurring at higher Mach number, observed for the first time in this work.
3. Self-excited response in the fluid-resonant regime has been found to be dominated by coupling between unstable hydrodynamic modes of the jet, and trapped acoustic modes between the nozzle and the impingement surface. The resonant coupling has been shown to be the principal mechanism that determines which hydrodynamic mode of the jet is excited for a given set of operating conditions.
4. The self-excited flow oscillations of the impinging planar jet have been investigated and quantified, and the form of the unstable hydrodynamic modes of the jet has been identified.

5. The behavior of the coherent flow structures has been investigated and quantified, including the convection speed, path, and evolution of structure strength throughout the impinging jet flow.
6. In the fluid-resonant regime, the oscillation frequency does not scale with the jet thickness, but rather with the impingement length.
7. A spatially dependent phase speed and an effective impingement length have been documented for a planar jet impinging on a plate.
8. A feedback model has been developed to predict the frequency of self-excited flow oscillations as a function of Mach number, impingement ratio and jet thickness.

6.4 Recommendations for Future Work

The subject of self-excited impinging planar jets has not received a great deal of attention in the literature, with this thesis being the first comprehensive investigation of this system. As a result, much work remains to be completed. The following is a brief list of potential research topics for further work in this area.

1. Develop techniques to enhance and attenuate the self-excited flow oscillations where required in industrial applications. In particular, nozzle designs could be optimized to minimize acoustic radiation to the surroundings, to maximize the self-excited response of the system, in order to enhance self-excited flow oscillations for use in heat transfer and mixing applications. Acoustic excitation within the jet air supply could be employed to excite the jet at off-resonant frequencies to attempt to attenuate self-excited flows and acoustic tones. In addition, acoustic baffles could be

investigated as a countermeasure to lower acoustic pressure amplitudes by preventing or altering the formation of trapped acoustic modes between the nozzle and the plate.

2. The self-excited response characteristics of other types of impinging planar jet geometries could be investigated. Examples include the co-planar impinging jet configuration, which is currently being investigated for use in coating control applications.
3. The effects of the inducing or enhancing self-excited flow oscillations on heat transfer rates could be investigated. It is anticipated that the very large fluctuating velocity components produced by these flows would dramatically enhance heat transfer compared to steady, non-oscillating flows, and that these geometries may prove useful in the development of high-performance thermal processing applications.

References

Akansu, Y.E., Sarioglu, M., Kuvvet, K., Yavuz, T., 2008. Flow field and heat transfer characteristics in an oblique slot jet impinging on a flat plate. International Communications in Heat and Mass Transfer. 35, 873–880.

Akiyama, T., Yamamoto, K., Squires, K.D., Hishida, K., 2005. Simulation and measurement of flow and heat transfer in two planar impinging jets. International Journal of Heat and Fluid Flow. 26, 244–255.

Alkislar, M.B., Krothapalli, A., Lourenco, L.M., 2003. Structure of a screeching rectangular jet: a stereoscopic particle image velocimetry study. Journal of Fluid Mechanics. 489, 121–154.

Angioletti, M., Di Tommaso, R., Nino, E., Ruocco, G., 2003. Simultaneous visualization of flow field and evaluation of local heat transfer by transitional impinging jets. International Journal of Heat and Mass Transfer. 46, 1703–1713.

Arthurs, D., Ziada, S., 2012. Noise generation in the gas-wiping process. Journal of Fluids and Thermal Sciences. Accepted – In Press.

Arthurs, D., Ziada, S., 2011. The planar jet-plate oscillator. Journal of Fluids and Structures. 27, 105–120.

Beaubert, F., Viazzo, S., 2003. Large eddy simulations of plane turbulent impinging jets at moderate Reynolds numbers. International Journal of Heat and Fluid Flow. 24, 512–519.

Billon, A., Valeau, V., Sakout, A., 2005. Two feedback paths for a jet-slot oscillator. Journal of Fluids and Structures. 21, 121–132.

Brown, G.L., Roshko, A., 1974. On density effects and large structure in turbulent mixing layers. Journal of Fluid Mechanics. 64, 775–816.

Camci, C., Herr, F., 2002. Forced convection heat transfer enhancement using a self-oscillating impinging planar jet. Journal of Heat Transfer. 124(4), 770–782.

Coleman, H.W., Steele, W.G., 1999. Experimentation and Uncertainty Analysis for Engineers, 2nd Edition. Wiley-Interscience.

Cooper, D., Jackson, D., Launder, B., 1993. Impinging jet studies for turbulence model assessment I: Flow- field experiments. International Journal of Heat and Mass Transfer. 36(18), 2675–2684.

Chung, Y.M., Luo, K.H., 2002. Unsteady Heat Transfer Analysis of an Impinging Jet. Journal of Heat Transfer. 124, 1039–1048.

Donaldson, C.D., Snedeker, R.S., 1971. A study of free jet impingement. Part 1. Mean properties of free and impinging jets. Journal of Fluid Mechanics. 45, 281–319.

Donaldson, C.D., Snedeker, R.S., Margolis, D., P. 1971. A study of free jet impingement.

Part 2. Free jet turbulent structure and impingement heat transfer. Journal of Fluid Mechanics. 45, 477–512.

Elavarasan, R., Venkatakrishnan, L., Krothapalli, A., Lourenco, L., 2000. A PIV study of a supersonic impinging jet. Journal of Visualization. 2, 213–221.

El-Sheikh, H., Garimella, S., 2000. Enhancement of air jet impingement heat transfer using pin-fin heat sinks. IEEE Transactions on Components and Packaging Technology. 23(2). 300–308.

Fairweather, M., Hargrave, G., 2002. Experimental investigation of an axisymmetric. impinging turbulent jet. 1. Velocity field. Experiments in Fluids. 33, 464– 47.

Fairweather, M. Hargrave, G., 2002. Experimental investigation of an axisymmetric, impinging turbulent jet. 2. Scalar field. Experiments in Fluids 33, 539–544.

Ferrari, J., Lior, N., Slycke, J., 2003. An evaluation of gas quenching of steel rings by multiple-jet impingement. Journal of Material Processing Technology. 136, 190–201.

Freymuth, P., 1966. On transition in a separated laminar boundary layer. Journal of Fluid Mechanics. 25, 683– 704.

Gärtner, F., Stoltenhoff, T., Schmidt, T., Kreye, H., 2006. The Cold Spray Process and Its Potential for Industrial Applications. Journal of Thermal Spray Technology. 15, 223–232.

Glesser, M., Valeau, V., Sakout, A., 2008. Vortex sound in unconfined flows: Application to the coupling of a jet-slot oscillator with a resonator. Journal of Sound and Vibration. 314, 635–649.

Guerra, D., Su, J., 2005. The near wall behavior of an impinging jet. International Journal of Heat and Mass Transfer. 48, 2829–2840.

Gutmark, E., Wolfshtein, M., Wygnanski, I., 1978. The plane turbulent impinging jet. Journal of Fluid Mechanics 88, 737–756.

Haneda, Y., Tsuchiya, Y., Nakabe, K., Suzuki, K., 1998. Enhancement of impinging jet heat transfer by making use of mechano–fluid interactive flow oscillation. International Journal of Heat and Fluid Flow. 19, 115–124.

Henderson, B., 2002. The connection between sound production and jet structure of the supersonic impinging jet. Journal of the Acoustical Society of America. 111, 735–747.

Henderson, B., Powell, A., 1993. Experiments concerning tones produced by an axisymmetric choked jet impinging on flat plates. Journal of Sound and Vibration. 168, 307–326.

Henderson, B., Bridges, J., Wernet, M., 2005. An experimental study of the oscillatory flow structure of tone-producing supersonic impinging jets. Journal of Fluid Mechanics. 542, 115–137.

Ho, C., Huang, L., 1982. Subharmonics and vortex merging in mixing layers. Journal of Fluid Mechanics. 119, 443–473.

Ho, C., Nosseir, N.S., 1981. Dynamics of an impinging jet. Part 1: The feedback mechanism. Journal of Fluid Mechanics. 105, 119–142.

Hourigan, K., Rudman, M., Brocher, E., 1996. The feedback loop in impinging two-dimensional high- subsonic and supersonic jets. Experimental Thermal Fluid Science. 12, 265–270.

Huang, L., El-Genk, M.S., 1994. Heat transfer of an impinging jet on a flat surface. International Journal of Heat and Mass Transfer. 37, 1915–1923.

Hwang, S.D., Cho, H.H., 2003. Effects of acoustic excitation positions on heat transfer and flow in axisymmetric impinging jet: main jet excitation and shear layer excitation. International Journal of Heat and Fluid Flow. 24, 199–209.

Hwang, S., Lee, C., Cho, H., 2001. Heat transfer and flow structures in axisymmetric impinging jet controlled by vortex pairing. International Journal of Heat and Fluid Flow. 22, 293–300.

Kennedy, C., Chen, J., 1998. Mean flow effects on the linear stability of compressible planar jets. Physics of Fluids. 10, 615–626.

Kopiev, V.F., Zaitsev, M.Y., Inshakov, S.I., Guriashkin, L.P., 2003. Visualization of the large-scale vortex structures in excited turbulent jets. Journal of visualization. 6, 303–311.

Krothapalli, A., 1985. Discrete tones generated by an impinging underexpanded rectangular jet. AIAA Journal. 23, 1910–1915.

Krothapalli, A., Rajkuperan, E., Alvi, F., Lourenco, L., 1999. Flow field and noise characteristics of a supersonic impinging jet. Journal of Fluid Mechanics. 392, 155–181.

Kwon, Y.P., 1998. Feedback mechanism of low-speed edgetones. The Journal of the Acoustical Society of America. 104, 2084–2089.

Li, H-L., Chiang, H-W. D., Hsu, C-N., 2011. Jet impingement and forced convection cooling experimental study in rotating turbine blades. International Journal of Turbo and Jet Engines. 28, 147–158.

Lin, J.C., Rockwell, D., 2001. Oscillations of a turbulent jet incident upon an edge. Journal of Fluids and Structures. 15, 791–829.

Liu, Y., Olsen, M.G., Fox, R.O., 2009. Turbulence in a microscale planar confined impinging-jet reactor. Lab on a Chip Journal, 9, 1110–1118.

Liu, T., Sullivan, J., 1996. Heat transfer and flow structures in an excited circular impinging jet. International Journal of Heat and Mass Transfer. 39, 3695–3706.

Looney, M., Walsh, J., 1984. Mean-Flow and Turbulent Characteristics of Free and

Impinging Jet Flows. Journal of Fluid Mechanics. 147, 397–429.

Lucas, M., Rockwell, D., 1984. Self- excited jet: upstream modulation and multiple frequencies. Journal of Fluid Mechanics. 147, 333–352.

Marsh, A.H., 1961. Noise measurements around a subsonic air jet impinging on a plane, rigid surface. The Journal of the Acoustical Society of America. 33, 1065–1066.

Maurel, S., Solliec, C., 2001. A turbulent plane jet impinging nearby and far from a flat plate. Experiments in Fluids. 31, 687–696.

Michalke, A., 1964. On the inviscid instability of the hyperbolic tangent velocity profile. Journal of Fluid Mechanics. 19, 543–556.

Michalke, A., 1965, On spatially growing disturbances in an inviscid shear layer. Journal of Fluid Mechanics. 23(3), 521–544.

Miksad, R.W., 1973. Experiments on nonlinear interactions in the transition of a free shear layer. Journal of Fluid Mechanics. 59, 1–21.

Neuwerth, G., 1972. Acoustic feedback phenomena of the subsonic and hypersonic free jet impinging on a foreign body. NASA Technical Translation. TT F-15,719.

Narayanan, V., Patil, V.A., 2007. Oscillatory thermal structures induced by unconfined slot jet impingement. Experimental Thermal and Fluid Science. 32, 682–695.

Narayanan, V., Seyed-Yagoobi, J., Page, R. H. 2004. An experimental study of fluid mechanics and heat transfer in an impinging slot jet flow. International Journal of Heat and Mass Transfer. 47, 1827–1845.

Nishino, K., Samada, M., Kasuya, K., 1996. Turbulence statistics in the stagnation region of an axisymmetric impinging jet flow. Journal of Heat and Fluid Flow. 17(3), 193–201.

Norum, T., 1991. Supersonic rectangular jet impingement noise experiments. AIAA Journal. 29, 1051–1055.

Nosseir, N.S., Ho, C., 1982. Dynamics of an impinging jet. Part 2: The noise generation. Journal of Fluid Mechanics. 116, 379–391.

Nyborg, W.L., 1954. Self-maintained oscillations of the jet in a jet-edge system. The Journal of the Acoustical Society of America. 26, 174–182.

O'Donovan, T., Murray, D., 2007a. Jet impingement heat transfer – Part I: Mean and root-mean-square heat transfer and velocity distributions. International Journal of Heat and Mass Transfer. 50, 3291–3301.

O'Donovan, T., Murray, D., 2007b. Jet impingement heat transfer – Part II: A temporal investigation of heat transfer and local fluid velocities. International Journal of Heat and Mass Transfer. 50, 3302–3314.

Ogawa, K., Seo, D., 2011. Repair of turbine blades using cold spray technique. Advances in Gas Turbine Technology, Chapter 21, InTech Publishing.

Panickar, P., Raman, R., 2007. Criteria for the existence of helical instabilities in subsonic impinging jets. Physics of Fluids. 19, 106103–1.

Powell, A., 1961. On the edgetone. The Journal of the Acoustical Society of America. 33, 395–409.

Rayleigh, L., 1880. On the stability or instability of certain fluid motions. Proceedings of the London Mathematical Society. 11, 57–70.

Roux, S., Fenot, M., Lalizel, G., Brizzi, L.E., Dorignac, E. 2011. Experimental investigation of the flow and heat transfer of an impinging jet under acoustic excitation. International Journal of Heat and Mass Transfer. 54, 3277–3290.

Sandham, N.D., Reynolds, W.C. 1991. Three-dimensional simulations of large eddies in the compressible mixing layer. Journal of Fluid Mechanics. 224, 133–158.

Schuller, T., Durox, D. Candel, S., 2002. Dynamics of and noise radiated by a perturbed impinging premixed jet flame. Combustion and Flame. 128, 88–110.

Steinberg, N. I., 1974. Apparatus for Quenching Polymer Films. US Patent 3853447, 1–6.

Tam, C., Ahuja, K., Theoretical-Model of Discrete Tone Generation by Impinging Jets. Journal of Fluid Mechanics. 214, 67–87.

Tam, C., Norum, T., 1992. Impingement tones of large aspect ratio supersonic rectangular jets. AIAA Journal. 30, 304–311.

Wagner, F., 1971. The sound and flow field of an axially symmetric free jet upon impact on a wall. NASA Technical Translation. TT F-13,942.

Yuceil, K., Otugen, M., 2002. Scaling parameters for underexpanded supersonic jets. Physics of Fluids. 14, 4206–4215.

Ziada, S., 1995. Feedback control of globally unstable flows: Impinging shear flows. Journal of Fluids and Structures. 9, 907–923.

Ziada, S., 2001. Interaction of a jet-slot oscillator with a deep cavity resonator and its control. Journal of Fluids and Structures. 15, 831–843.

Ziada, S., Rockwell, D., 1982. Oscillations of an unstable mixing layer impinging upon an edge. Journal of Fluid Mechanics. 124, 307–334.

Appendix A

Error Analysis

A.1 Analysis of Uncertainty

The uncertainties associated with the present measurements are discussed in this appendix. For a given variable (X). which is a function of a set of independent measured variables (Y_i), such that:

$$X = f\left(Y_1, Y_2, Y_3, \ldots, Y_i\right), \tag{A.1}$$

the uncertainty in (X) can be expressed in terms of the uncertainties of the independent measured values (Y_i) using the Kline and McClintock method (Coleman & Steels, 1998), given as:

$$\delta X = \sqrt{\sum_{i=1}^{N}\left(\frac{\partial X}{\partial Y_i}\delta Y_i\right)^2}, \tag{A.2}$$

where δY_i is the known uncertainty in each independent measured variable. The summation of the terms on the right hand side of Equation A.2 gives the overall uncertainty in the dependent variable (X). In the subsequent section, this analysis will be applied to the expression used to calculate the flow velocity of the jet exiting the nozzle.

A.2 Uncertainty in Flow Velocity

The flow velocity at the nozzle outlet was calculated using the following expression derived for compressible flow through an isentropic or lossless nozzle:

$$U_o = c \cdot \sqrt{\frac{2}{\gamma - 1}\left[\left(\frac{P_s + P_\infty}{P_\infty}\right)^{\gamma-1/\gamma} - 1\right]}, \tag{A.3}$$

where c is the speed of sound, γ is the ratio of specific heats of air, and P_s and P_∞ are the static and ambient pressure in the nozzle and of the surroundings respectively.

The speed of sound in air can be calculated as:

$$c = \sqrt{\gamma R T} \tag{A.4}$$

where R is the ideal gas constant for air [R=287.04 J/(kg·K)] and T is the absolute temperature of the ambient air in Kelvin. The ratio of specific heats for air is constant if the air is assumed to behave as an ideal gas, and changes very little as a function of variable temperature if a non-ideal assumption is made, with a total variation of ~0.01%/°K. For the purposes of this examination, air will be assumed to behave as an ideal gas and γ will be assumed to be constant at γ=1.400.

Therefore, the flow velocity at the nozzle outlet can be expressed as:

$$U_o = \sqrt{\frac{2\gamma RT}{\gamma - 1}\left[\left(\frac{P_s + P_\infty}{P_\infty}\right)^{\frac{\gamma-1}{\gamma}} - 1\right]}. \tag{A.5}$$

A total of three independent variables used in Equation A.5 are subject to uncertainty: the temperature of ambient conditions (T), the ambient pressure (P_∞), and the static pressure in the plenum (P_s). Expanding Equation A.2 using these uncertain variables, we obtain:

$$\frac{\partial U}{U} = \sqrt{\left(\frac{\partial U}{\partial T}\delta T\right)^2 + \left(\frac{\partial U}{\partial P_s}\delta P_s\right)^2 + \left(\frac{\partial U}{\partial P_\infty}\delta P_\infty\right)^2} \tag{A.6}$$

Substituting Equation A.5 into Equation A.6 and simplifying, the relative uncertainty in flow velocity measurements can be written as:

$$\frac{\partial U}{U}=\sqrt{\left(\frac{1}{2T}\right)^2\delta(T)^2+\left(\frac{\left(\frac{(\gamma-1)}{2\gamma P_\infty}\right)^2\delta(P_s)^2}{\left[\left(\frac{P_s+P_\infty}{P_\infty}\right)-\left(\frac{P_s+P_\infty}{P_\infty}\right)^{-1/\gamma}\right]^2}\right)+\left(\frac{\left(\frac{(\gamma-1)P_s}{2\gamma P_\infty^{\,2}}\right)^2\delta(P_\infty)^2}{\left[\left(\frac{P_s+P_\infty}{P_\infty}\right)-\left(\frac{P_s+P_\infty}{P_\infty}\right)^{-1/\gamma}\right]^2}\right)} \tag{A.7}$$

The nozzle is supplied with air via a 2” diameter compressed air line at a supply pressure of 85psi, which passes through a regulator, two porous bronze filters, and several full port gate valves before entering the plenum of the nozzle. As a result of the rapid expansion of the air exiting the compressed air line, the flow exiting the nozzle is 2−5K° cooler than the air in the room, depending on the season. However, as a result of the nozzle and plate assembly being enclosed by both laser safety curtains and acoustic insulation, and the high flow rates of the flow exiting the nozzle, the temperature of the ambient conditions surrounding the nozzle and plate are identical to those of the exiting flow. Temperature within the enclosure was monitored with a thermocouple, and variation during any given experiment was found to be $\delta T=\pm 2$K. The ambient air pressure was measured using a digital barometer, and the variations in ambient air pressure during an experiment were found to be $\delta P_\infty=\pm 0.15$kPa. The static pressure within the plenum was measured using a Validyne DP15 pressure transducer with a -40 12.5psi diaphragm that has an accuracy ±0.25% over the full scale. The pressure transducer was calibrated to a known pressure source at twelve points over the operating range of the sensor, and monitors the pressure within the plenum at a point just upstream of the nozzle contraction, after the flow conditioning screens, and at the centerline of the nozzle outlet.

The pressure transducer was used over a range of pressure from 14.2kPa$\leq P_s \leq$88.5kPa which results in an uncertainty of static pressure in the plenum is δP_s= ±0.22kPa. Using Equation A.7 and the absolute uncertainties given earlier, the relative uncertainty in flow velocity ($\delta U/U$) was found to be ~2.9%.

Other sources of uncertainty in flow velocity measurements include variation in the pressure of the supply line, and fluctuating pressures in the plenum due to turbulence of the incoming flow. Figure A.1 shows a plot of the flow velocity at the nozzle exit as a function of time for a series of ~500 distinct measurements over a period of approximately 4 hours, as calculated by Equation A.3. The solid data points represent the mean value of velocity for each measurement, and the error bars show +/- one standard deviation of the velocity due to pressure fluctuation in the plenum over each measurement period, which has been obtained using a dynamic pressure transducer mounted in the plenum. It is clear from inspection of the figure that the mean value of velocity changes very little, even over an extended period of time, and that the mean values show relatively little variation, less than 0.5%, over this extended period. The standard deviation of fluctuating velocity remains relatively low as well, with an average value of ±0.34m/s, or a relative deviation of only 0.11%.

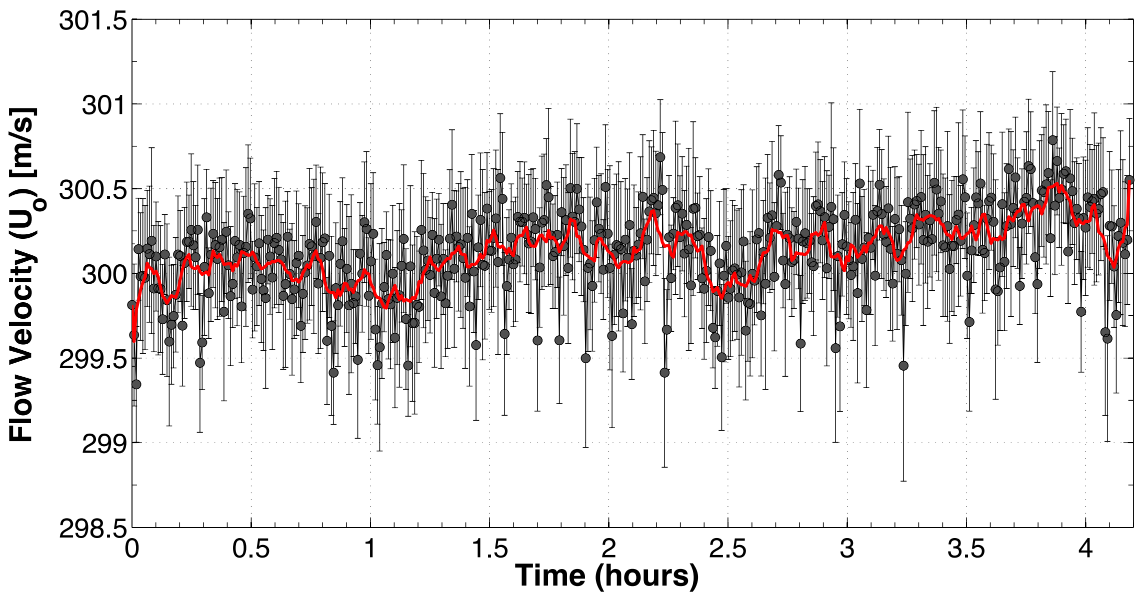

Figure A.1: Flow velocity at the nozzle outlet as a function of time in hours. Error bars set at ±1σ for each measurement point.

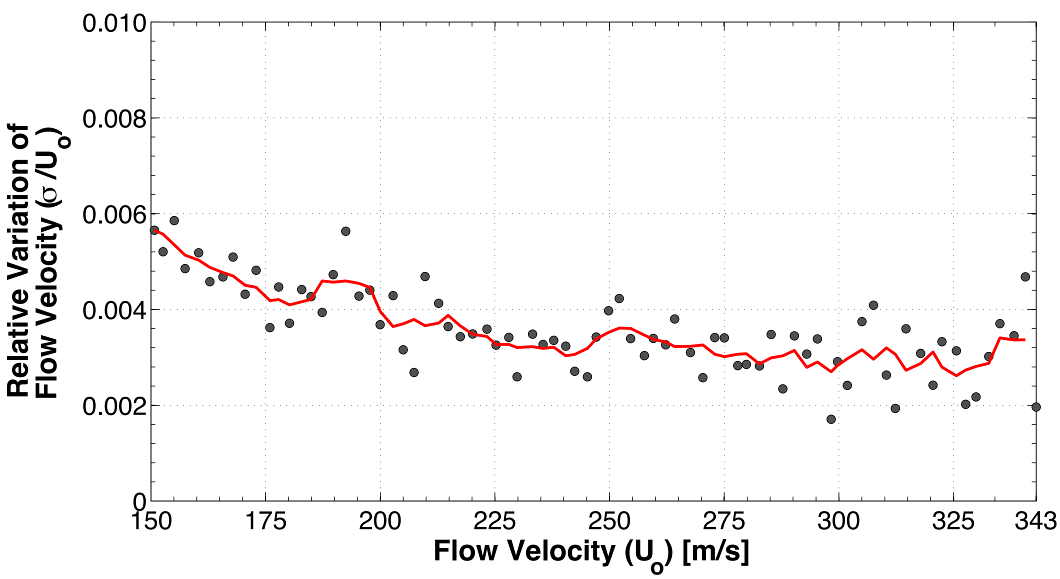

Figure A.2: Relative variation in flow velocity at the nozzle outlet (σ/U_o) as a function of flow velocity.

Figure A.2 shows a plot of the relative variation in flow velocity at the nozzle outlet, taken to be one standard deviation of the fluctuating pressure signal in the plenum normalized by the nozzle outlet, plotted as a function of flow velocity at the nozzle outlet. The plot shows that velocity measurements performed at the lower end of the scale, near

U_o=150m/s, show greater variation than those near choked flow, but that the variation remains low, less than σ/U_o =0.006, over the complete range of flow velocity examined.

A.3 PIV Error Analysis

The error analysis of PIV measurements provided in this section has been performed for the most challenging experimental conditions examined in the course of this study: an impinging planar jet with a Mach number of M=0.98 and an impingement ratio of x_o/h=10.5, producing very strong self-excited flow oscillations in the n=3 anti-symmetric hydrodynamic mode of the jet as a frequency of f=10.6kHz. The error analysis provided here is similar to the analyses of Scarano & Riethmuller (2000), Schram & Riethmuller (2002) and Schram et al. (2004 & 2005), who each provide an excellent and thorough treatment of similar systems, with strong vortical structures and highly unsteady flows. Figure A.3 shows a quiver plot of the vectors obtained from the PIV analysis, which have been obtained using a first-order deformation based correlation scheme with one multi-grid refinement step. The final window size of 24 pixels×24 pixels and an overlap of 75% were employed in the analysis, and vector validation rates in excess of 99% were obtained for each instantaneous field, with spurious vectors being replaced using a standard vector interpolation scheme. The deformation-based scheme was employed for its tolerance for larger displacement gradients than standard displacement schemes, with a maximum displacement gradient of 0.5 pixels/pixel with no truncation.

The largest displacement gradients encountered in this case occur in the initial shear layer of the jet exiting the nozzle, with gradients in excess of 0.5 pixels/pixel occurring for very small downstream distances, leading some gradient truncation at these locations. However, these regions are relatively small as the shear layers tend to thicken quickly as the flow progresses downstream, with displacement gradients falling below the 0.5 pixels/pixel threshold at a downstream distance of x/h>0.25. A pair of velocity profiles showing the stream-wise velocity component at two downstream positions of x/h=0.5 and 2.5 are shown in Figure A.3 along with the maximum displacement gradients at these locations. The profile taken at x/h=0.5 shows a larger displacement gradient of 0.343 pixels/pixel, corresponding to an uncertainty in particle displacement of 0.11 pixels, and a relative uncertainty of 1.9% (Scarano & Riethmuller, 2000). The subsequent profile, obtained a downstream position of the small intense coherent flow structure in the initial shear layer, shows a significantly lower gradient and thus a lower error.

A single profile of the transverse velocity component is shown for a cross-stream position of y/h=-0.9, with displacement gradients at downstream positions of x/h=2.5 and 6.0 having been highlighted for ease of inspection, with these locations corresponding to a small intense structure near the initial region of the jet, and a larger more developed structure in the developing region. The maximum gradient is observed at the downstream location, with a gradient of 0.051 pixels/pixel, corresponding to an uncertainty in particle displacement of 0.02 pixels, and a relative uncertainty of ~1.0%.

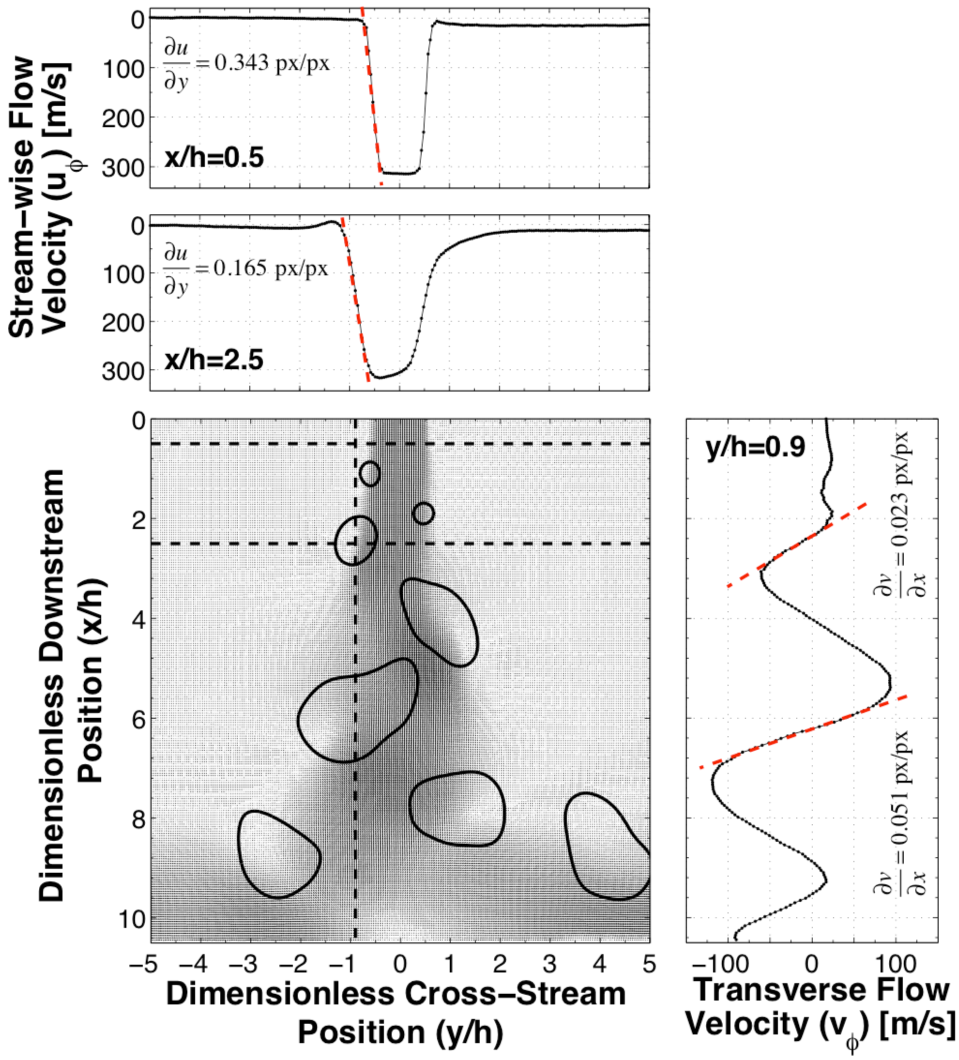

Figure A.3: Quiver plot showing the results of the PIV measurements for a Mach number of M=0.98 and an impingement ratio of x_0/h=10.5, responding at a frequency of f=10.6kHz.

The absolute uncertainty of the velocity gradient terms used to determine vorticity are given by the following expressions:

$$\varepsilon_{\left(\frac{\partial u}{\partial y}\right)} = \frac{0.7 \cdot \varepsilon_u}{\Delta X} \quad \text{and} \tag{A.8}$$

$$\varepsilon_{\left(\frac{\partial v}{\partial x}\right)} = \frac{0.7 \cdot \varepsilon_v}{\Delta Y}, \tag{A.9}$$

where the factor 0.7 is related to the uncertainty of the central difference scheme used to calculate the velocity gradients (Raffel et al., 2007). Absolute uncertainties of 0.009 pixels and 0.002 pixels are obtained for the *x* and *y*-components respectively, corresponding to relative uncertainties of 2.8% and 3.4% for these two gradient terms.

Table A.1: Results of the PIV error analysis for an impinging planar jet with M=0.98 and x_0/h=10.5.

Acquisition parameters		
Field of View (Masked Area)		29.7mm × 34.2mm
Total Sensor Size		2048 pixels × 2048 pixels
Total Image Size		1416 pixels × 1630 pixels
Spatial Calibration		20.97 μm/pixel
Pulse Seperation		350 ns
Number of Acquisitions		800 total, 100 per phase angle
Processing Parameters		
Initial Window Size		64 pixels × 64 pixels
Subpixel Interpolation Scheme		Guassian
Window Distortion Scheme		1st Order Deformation Scheme
Number of Grid Refinements		2 refinements
Final Window Size		24 pixels × 24 pixels
Final Overlap		75%
Number of Vectors	$[x \times y]$	[236 × 270] 63,700 per field
Spatial Resolution	$(\Delta x = \Delta y)$	126 μm
Validation Rate		>99%
Error Analysis		**(x=0.5·h, y=−0.9·h)**
Maximum Displacement Gradient	$(\partial u/\partial y)_{max}$	0.343 pixels/pixel
	$(\partial v/\partial x)_{max}$	0.051 pixels/pixel
Uncertainty in Particle Displacement	ε_u	0.11 pixel
	ε_v	0.02 pixel
Relative Uncertainty of Particle Displacement	ε_u/δ_u	1.9%
	ε_v/δ_v	1.0%
Uncertainty of Vorticity	$\varepsilon_{(\partial u/\partial y)} = 0.7 \cdot \varepsilon_u/\Delta X$	0.009 pixels/pixel
	$\varepsilon_{(\partial v/\partial x)} = 0.7 \cdot \varepsilon_u/\Delta X$	0.002 pixels/pixel
Relative Uncertainty of Vorticity	$\varepsilon_{(\partial u/\partial y)}/(\partial u/\partial y)_{max}$	2.80%
	$\varepsilon_{(\partial v/\partial x)}/(\partial v/\partial x)_{max}$	3.43%

Finally, the ratio of the interrogation region size (W_s) to the size of the smallest structure in the initial shear layer (Λ) is quite low at $W_s/\Lambda \approx 0.05$. This yields a truncation error of ~2% of the peak azimuthal velocity found around the vortex core (Scarano & Riethmuller, 2000). Because of the intense circulation of the coherent structures found in this geometry, significant rarefication of the seeding particles within the structures is evident in the raw images. This rarefaction is evidence of an induced outward radial component of the particles with respect to the surrounding air due to their higher density, resulting in an error in the radial velocity component of the structure, but relatively little error in the azimuthal component (Raffel et al., 2007). As a result, measurement of vorticity and structure circulation remains unaffected, as the radial component does not contribute to these quantities. This rarefication was overcome by using increased seeding density and through the use of a 12-bit camera to provide particle detection in the core of vortices.

A.4 Acoustic Measurements

Acoustic tones produced by the impinging jet flow have been found to be are inherently steady in nature, showing relatively small levels of amplitude modulation, especially for intermediate impingement ratios in the fluid-resonant regime, where acoustic tones and self-excited flow oscillations are strongest. A thorough analysis of the nature of the noise produced by this system revealed that the acoustic tone frequencies show very little variation, less than ±1Hz, and amplitudes showing relatively little variation for strongly self-excited flow conditions. As a result, convergence of the acoustic tone frequency and amplitude occurs rapidly, with little change in the mean values of either parameter being observed for more than 10 spectral averages.

All acoustic measurements were acquired using a National Instruments NI-4452 4 channel data acquisition card with a maximum sample rate of 204.8kS/s, and hardware based anti-aliasing filters. Each acoustic measurement was obtained by recording the pressure-time signal using a sample rate of 204.8kHz for 15 seconds. Spectral analysis was performed by breaking the time signal into 60 equally sized blocks of 51,200 samples with no overlap, calculating the amplitude spectrum of RMS acoustic pressure for each block, and averaging the 60 spectra to produce an average acoustic spectrum. This results in an amplitude spectrum with a frequency range from 0Hz to 102.4kHz and a spectral resolution of 4Hz, which have been truncated to a frequency range of 0Hz to 70-80kHz, corresponding to the linear response range of the microphone.

The spectral resolution of 4Hz and an average spectrum produced using 60 individual spectra were selected principally to allow for a collapse of the broadband noise of the spectrum in a realtively short period of time, in this case a total of 15 seconds per measurement, in order to allow for efficient measurement of the system. For self-excited flows occuring at larger impingement ratios, which tend to exhibit greater degree of intermittancy and amplitude modulation are also captured well using these measurement parameters, obtaining RMS acoustic presssure amplitudes to within 10% of those measured using a much larger number of spectral averages.

A.5 Setup of the Experimental Apparatus

Because of the relatively small scale of the flow geometry, and the sensitive nature of the system to the various geometric parameters such as inclination of the plate relative to the jet, a complete set of procedures were developed to align and set the geometry of the jet-plate system. This included the manufacture of a series of jigs and special tooling in order to set the inclination angle of the plate with respect to the jet in stream-wise and span-wise directions, as well as determining the distance between the nozzle and the plate to the nearest ±0.01mm. The resulting procedures resulted in a high level of experimental repeatability and accuracy in setting the apparatus to a particular geometric configuration, with the results of this procedure being illustrated in Figure A.4. The figure shows the acoustic response for two identical cases of a planar impinging jet with an impingement ratio of x_o/h=9.5 and a nozzle thickness of h=3mm, but with the results of each test having been obtained after a complete disassembly, reassembly and realignment using said procedures. The figure clearly shows that the use of these procedures result in highly repeatable self-excited response of the system, with the two independent tests showing nearly identical tone frequencies and amplitudes over the complete range of flow velocity.

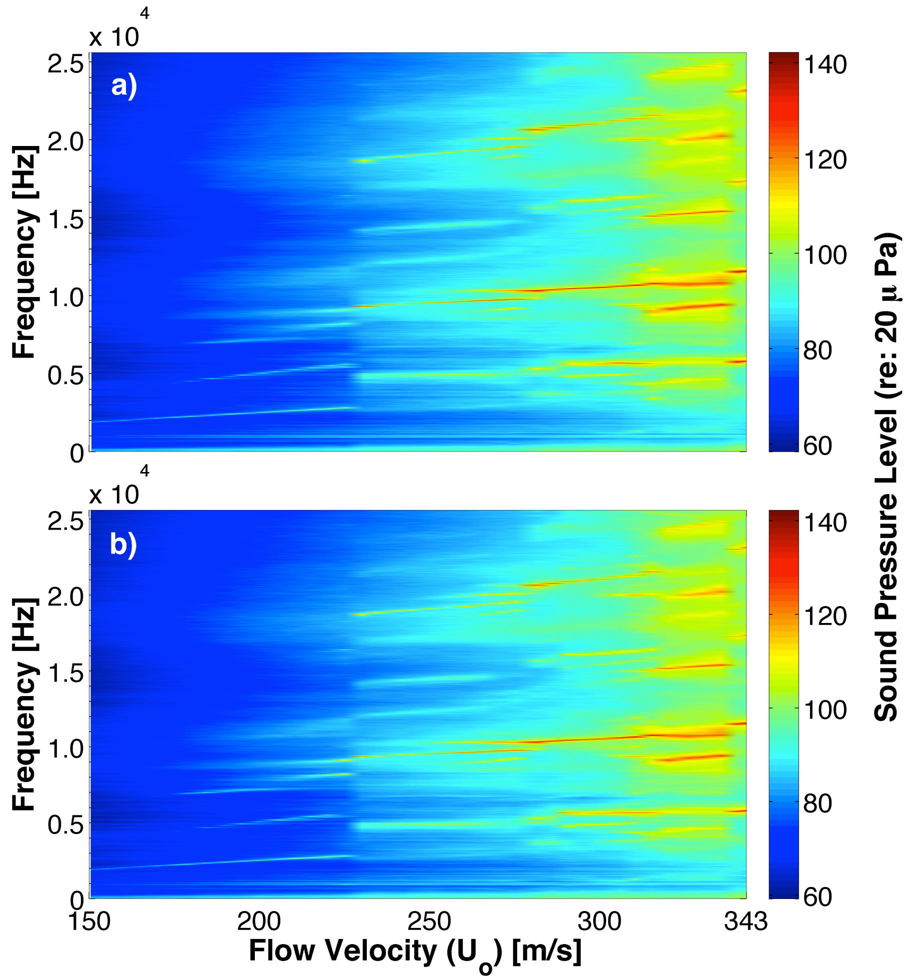

Figure A.4: Two contour plots showing the acoustic response of an identical jet plate system with impingement ratio of x_o/h=10 and a jet thickness of h=3mm. Test results of part b) were obtained following a complete disassembly, reassembly, and realignment of the experimental apparatus.

Appendix B

PIV Trigger Circuit

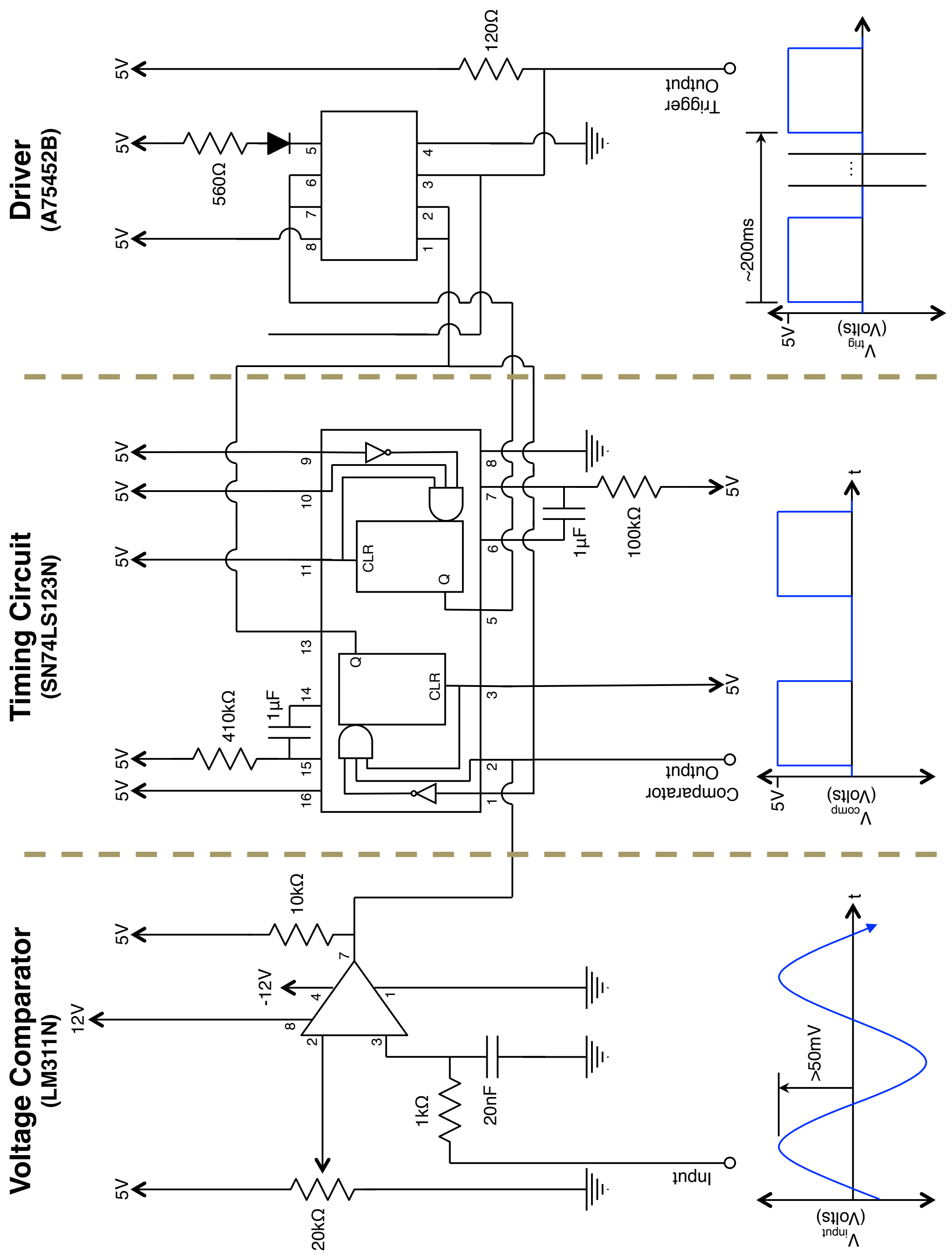

Figure B.1: Trigger generator circuit designed for generation of the trigger used in phase-locked PIV measurements.

Appendix C

Related Acoustic & Phase Measurements

C.1 Span-wise Correlation & Phase Measurements

In order to confirm that the self-excited flow oscillations are well correlated along the jet-span, a series of measurements were performed using two miniature dynamic pressure transducers flush mounted to the plate surface at varying distances along the jet span. One transducer was fixed at the midpoint of the jet span, and the other was moved through a series of ten locations along the jet span (L) in increments of z/L=0.1. Figure C.1 shows a series of three plots illustrating the character of the results obtained in these measurements showing a) the RMS acoustic pressure amplitude of the center mounted transducer, b) the coherence between the center mounted transducer and a transducer mounted at one end of the nozzle span (z/L=0.5), and c) the relative phase between these transducers. The results clearly show a strong coherence at the dominant and secondary acoustic tone frequencies, and phase of ϕ=0° at the dominant tone frequency of f=14.7kHz. Pressure measurements were performed at a cross-stream position corresponding to the maximum fluctuating pressure at the plate surface, for this case y/h≈2.5.

Figure C.2 shows the results of the set of ten measurements performed at increments of $\Delta z/L$=0.1, and illustrates that the coherence of measurements remains at ~1.0 and a phase angle of nominally ϕ=0° regardless of transducer spacing, indicating that the self-excited phenomenon is strongly correlated along the jet span. These measurements were repeated for a series of different flow and geometric conditions, and all measurements were found to be in agreement with measurements presented here.

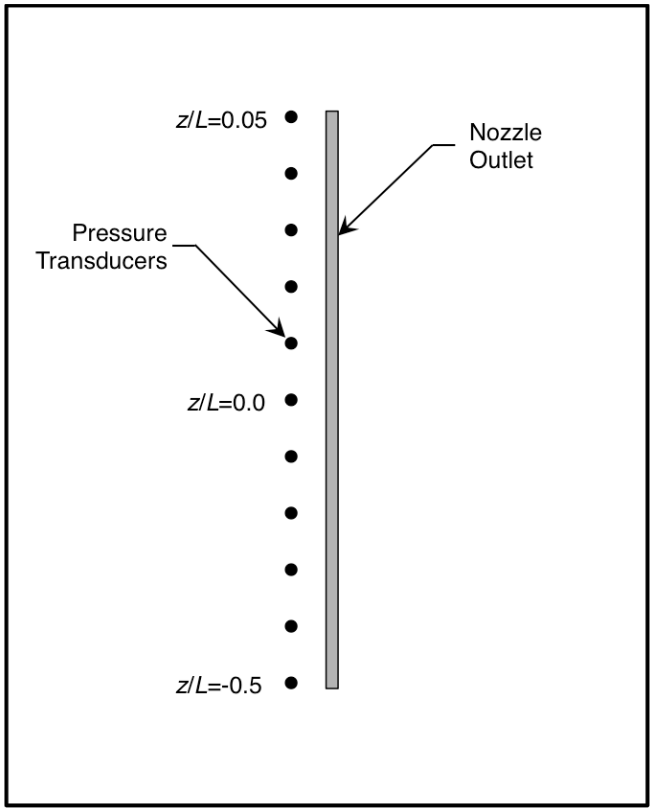

Figure C.1: Plan view of the impingement plate and the *projected* outlet of the nozzle showing the eleven mounting positions for the dynamic pressure transducers along the jet-span.

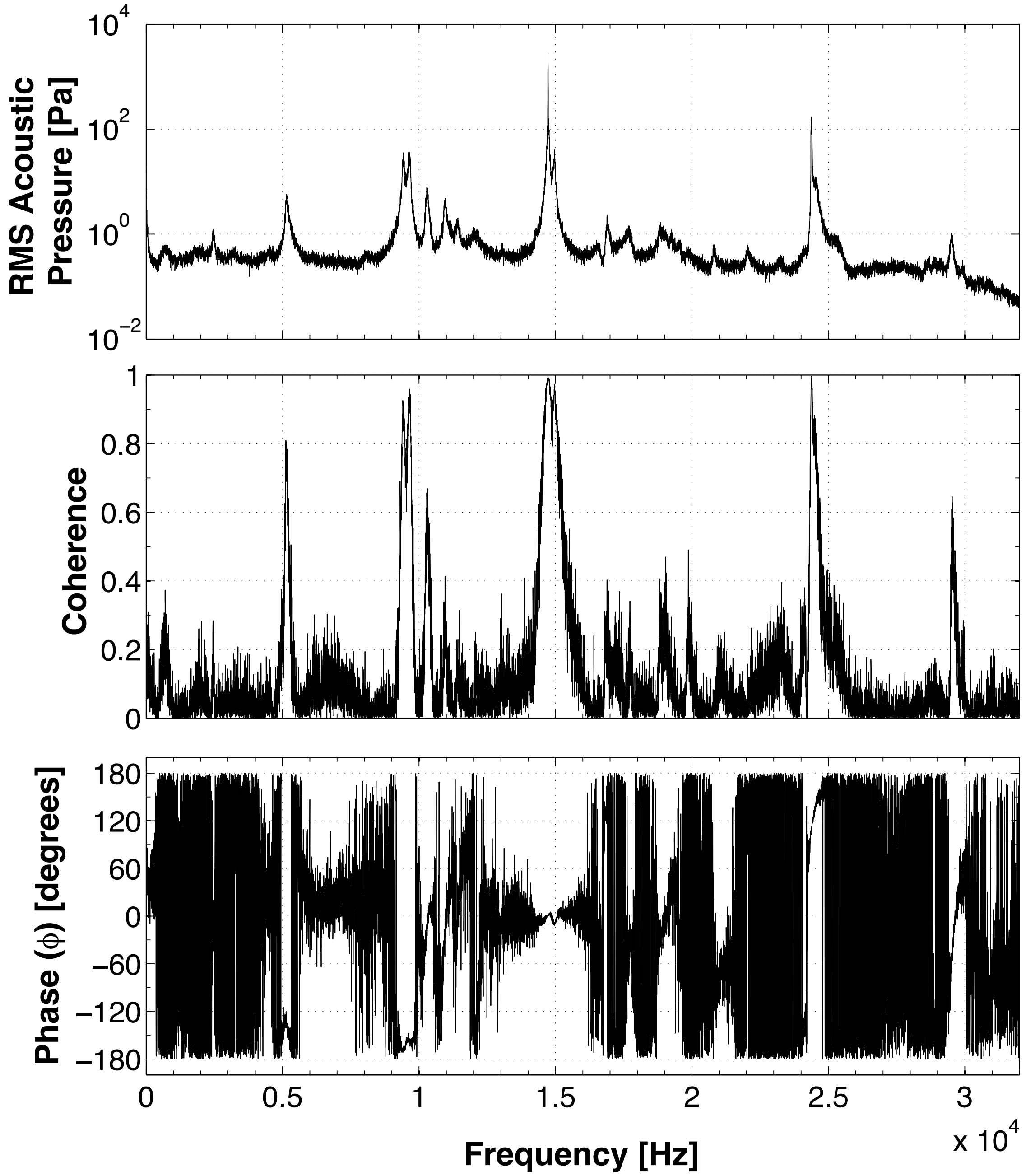

Figure C.2: a) RMS acoustic pressure, b) coherence and c) relative phase between two pressure transducers mounted at the plate surface at a distance of $\Delta z/L$=0.5 (phase & coherence between pressure measurements at z/L=0.0 and 0.5, spectrum from z/L=0.0). M=0.9, x_o/h=9.0, h=3mm.

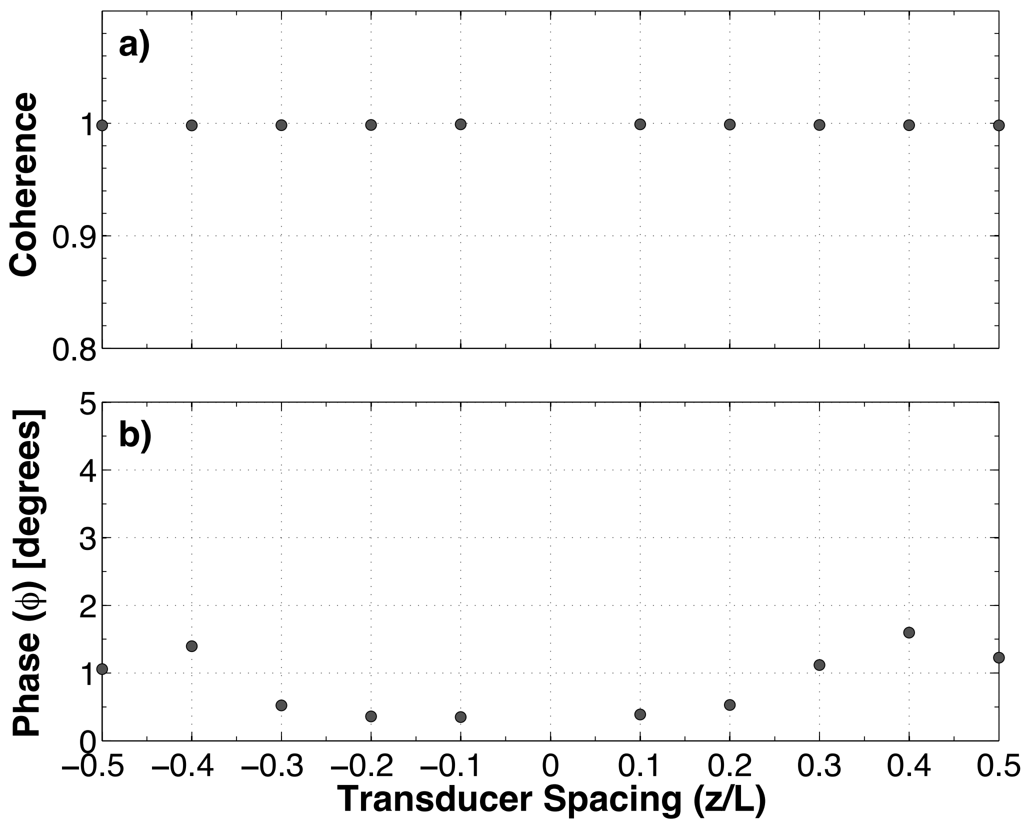

Figure C.3: a) Coherence and b) relative phase between two pressure transducers mounted at the plate surface at varying distances along the jet-span. M=0.9, x_0/h=9.0, h=3mm.

C.2 Characterization of the Sound Field

Measurements have been performed to assess the nature of the sound field produced by the self-excited oscillations, including tests to ensure measuremetns were performed in non-reverberant conditions, and to determine the directinvity of the sound field. Figure C.4 shows a plot of the sound pressure as a function of measurement distance with the x-axis shown in a logarithmic scale. The data shows a well-defined linear trend when plotted on these axis, indicating that the sound field throughout this range is in the acoustic free-field free of reverbaration. All acoustic measurements presented in this work were obtained within this reange at a measurement distance of d=0.3m.

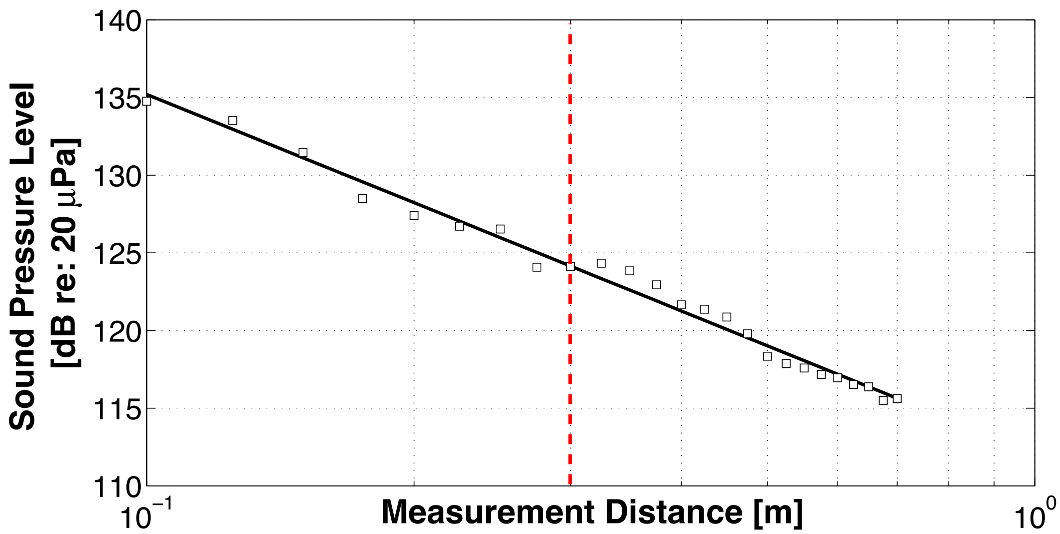

Figure C.4: Amplitude of the dominant acoustic tone as a function of measurement distance from the the jet impingement point for a measurement angle of θ=30°. Red line at 0.3m shows chosen measurement location.

Figure C.5 shows a pair of plots illustarting the dirrectivity of the sound field for a planar impinging jet as a function of the microphone location for varying measurements angle, but for a fixed microphone distance of d=0.3m. Part a) of the figure shows a contour plot of the self-excited response measured at different angles from the jet plane, which illustrates that at large angles noise measurements are subject to large amounts of low frequency noise due to the proximity of the microphone to the wall-jet flow. Part b) of the figure shows the amplitude of the dominant acoustic tone as a function of the measurement angle, which illustrates that the the acoustic tone is radiated most strongly at angles in the range between θ=50° and 70°, with tone amplitudes decreasing as the microphone approaches the plate at large angles, or as direct acoustic radiation is obstructed by the nozzle at angles less than θ=45°. All measurements performed in this work have been obtained at an angle of θ=60° to avoid the low frequencies associated with aerodynamic noise near the plate in the wall-jet region of the flow, and to measure the tones where they are most strongly radiated.

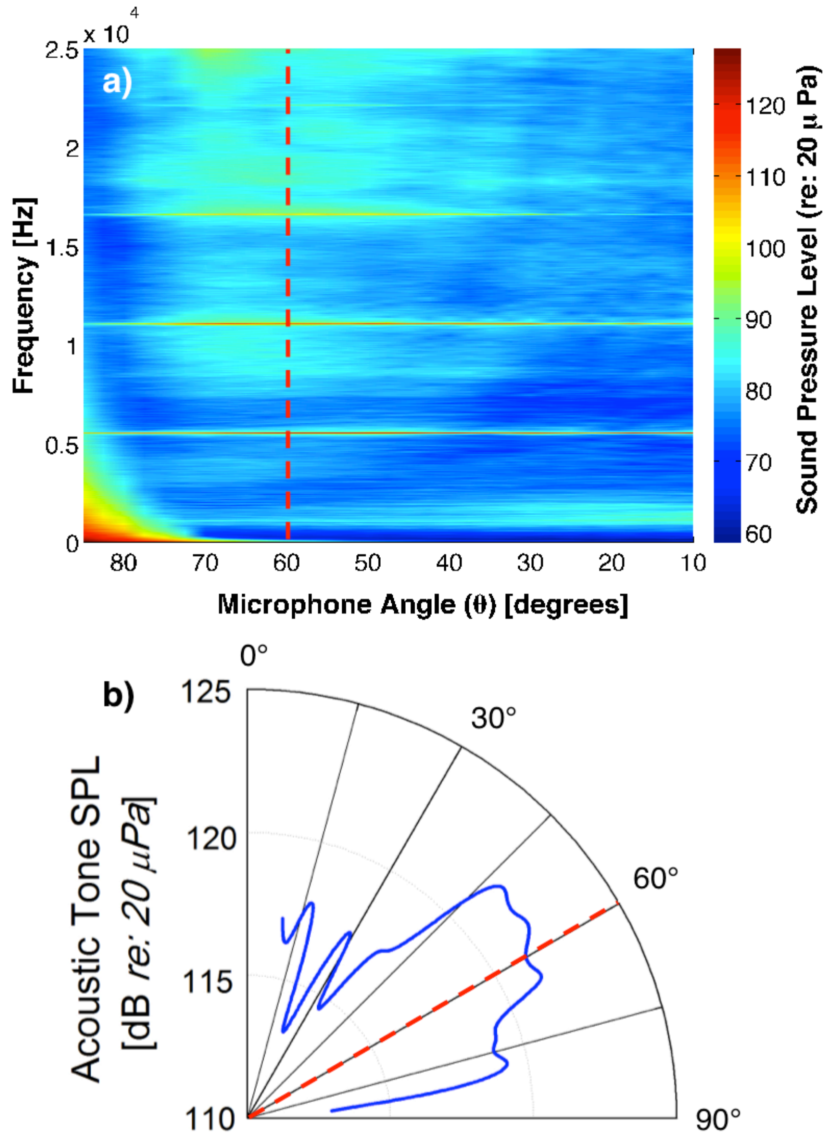

Figure C.5: a) Spectral response and b) amplitude of the dominant acoustic tone of the planar impinging jet as a function of measurement angle from the jet plane. Red lines at θ=30° show the chosen measurement angle.